Chemicals from Glycerol Bifunctional Catalysts for the Conversion of Biomass Components

ten Dam, Jeroen

DOI
10.4233/uuid:c4b72e7a-47a0-45b2-8b82-f50ae91888ab

Publication date
2016

Document Version
Final published version

Citation (APA)
ten Dam, J. (2016). *Chemicals from Glycerol Bifunctional Catalysts for the Conversion of Biomass Components*. [Dissertation (TU Delft), Delft University of Technology].
https://doi.org/10.4233/uuid:c4b72e7a-47a0-45b2-8b82-f50ae91888ab

Chemicals from Glycerol
Bifunctional Catalysts for the Conversion of Biomass Components

Proefschrift

ter verkrijging van de graad van doctor
aan de Technische Universiteit Delft,
op gezag van de Rector Magnificus prof.ir. K.Ch.A.M. Luyben;
voorzitter van het College voor Promoties,
in het openbaar te verdedigen op

Vrijdag 9 december 2016 om 10:00 uur

door

Jeroen ten Dam
doctorandus in de scheikunde,
Radboud Universiteit Nijmegen, Nederland
geboren te Deurne, Nederland

Dit proefschrift is goedgekeurd door de
promotoren: Prof.dr. U. Hanefeld en Prof.dr. F. Kapteijn

Samenstelling promotiecommissie:

Rector Magnificus	voorzitter
Prof.dr. U. Hanefeld	Technische Universiteit Delft, promotor
Prof.dr. F. Kapteijn	Technische Universiteit Delft, promotor
dr. K. Djanashvili	Technische Universiteit Delft, copromotor

Onafhankelijke leden:

Prof.dr. J.H. van Esch	Technische Universiteit Delft
Prof.dr.ir. H.J. Heeres	Rijksuniversiteit Groningen
Prof.dr.ir. B.F. Sels	Katholieke Universiteit Leuven
Prof.dr. G. Rothenberg	Universiteit van Amsterdam
Prof.dr. G.J. Witkamp	Technische Universiteit Delft, reservelid

The research reported in this thesis was carried out at the Department of Biotechnology and Department of Chemical Engineering, Faculty of Applied Sciences, Delft University of Technology (Julianalaan 136, 2628 BL Delft), with financial support of the Advanced Sustainable Processes by Engaging Catalytic Technologies (ASPECT) programme, part of the Advanced Chemical Technologies for Sustainability (ACTS) platform of the Netherlands Organisation for Scientific Research (NWO).

ISBN/EAN 9789462955332

Printed by Proefschriftmaken.nl || Uitgeverij BOXPress

Cover design by Jeroen ten Dam and Leon van de Water

CONTENTS

INTRODUCTION

RENEWABLE CHEMICALS: DEHYDROXYLATION OF GLYCEROL AND POLYOLS

This chapter is based on the publication "J. ten Dam and U. Hanefeld, ChemSusChem 4 (2011) 1017-1034."

ABSTRACT

The production of renewable chemicals is gaining attention over the past few years. The natural resources from which they can be derived in a sustainable way are most abundant in sugars, cellulose and hemi cellulose. These highly functionalized molecules need to be de-functionalized in order to be feedstocks for the chemical industry. A fundamentally different approach to chemistry thus becomes necessary, since the traditionally employed oil-based chemicals normally lack functionality. This new chemical toolbox needs to be designed to guarantee the demands of future generations at a reasonable price.

The surplus of functionality in sugars and glycerol consists of alcohol groups. To yield suitable renewable chemicals these natural products need to be defunctionalized by means of dehydroxylation. Here we review the possible approaches and evaluate them from a fundamental chemical aspect.

The chapter closes with an outline of the research described in this thesis.

Keywords: Renewable Chemicals; Polyols; Glycerol; Hydrogenolysis; Dehydroxylation

1 INTRODUCTION

The concept of producing materials from renewable biomass is not new. People have been wearing woollen clothing and building wooden houses for thousands of years. Even the first artificial fibers were made from wood-derived cellulose.

However, research was diverted to completely synthetic materials and chemicals due to the discovery of copious amounts of oil. Consequently, the processing of oil into chemicals has become incredibly efficient after 100 years of research and one can reasonably argue that today's society is not only addicted to oil as a fuel, but also to its products.

However, the plentiful supply of cheap oil will diminish due to depleting reserves, while the demand for these chemicals will only grow, which will result in an increasing oil price. A revival of chemicals from abundantly available biomass will therefore become competitive with chemicals from fossil sources once more and could potentially even replace oil-derived chemicals altogether.

The switch from oil-derived chemicals to bio-renewable chemicals calls for a considerable research effort, due to the fundamentally different nature of the feedstock used. While the catalysts that convert oil into chemicals focus on selectively functionalizing hydrocarbons, biomass is already highly functionalized. Therefore, the catalysts that were developed over the last 100 years are not directly applicable to a biomass feedstock. Instead, catalysts that can selectively remove some of the functionalities are desired. [1]

Ideally, one should take advantage of functional groups already present in different classes of biomass. Use fatty acids for detergents, benefit from the nitrogen already present in amino acids and treasure the hydroxy groups in sugars and polyols. In particular the conversion of carbohydrates rather than hydrocarbons is of great interest since they are so abundantly present in the form of cellulose and hemicellulose.

This review concerns the selective conversion of polyols. These highly oxygenated compounds can be transformed into a plethora of useful chemicals. The focus will be on the dehydration of the polyols and the possible hydrogenation of the resulting double bonds. Particular attention will be paid to inducing selectivity into these processes.

2 SELECTIVE DEHYDROXYLATION OF BIOMASS

The bulk of all materials from biomass are highly oxygenated, while most of the man-made chemicals are functionalized to a much lower degree. Biomass feedstock therefore needs to be deoxygenated in order to arrive at the same platform chemicals and final products that we currently utilize. For this essential deoxygenation six avenues of approach can be used: [2,3]

1 Dehydration of vicinal diols and hydrogenation of carbonyl groups

2 Dehydration of alcohols and hydrogenation of carbon-carbon double bonds

3 Condensation of alcohols and hydrogenolysis of the resulting cyclic ethers

4 Hydrogenolysis of ethers

5 Ketonization of carboxylic acids

6 Hydrogenation of carboxylic acids

This review focuses on the selective dehydroxylation of polyols and therefore the first three groups will be addressed in more detail. These three methods all involve the elimination of a hydroxyl group. [4] This dehydration can proceed via elimination or through homolytic cleavage of the C-O bond on a metallic surface. The elimination reaction can either proceed via E_1 or E_2 mechanism.

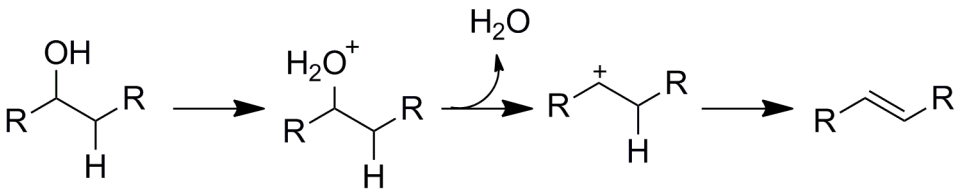

Scheme 1. E_1 mechanism.

The E_1 mechanism (Scheme 1) proceeds through protonation of a hydroxyl group, which is then expelled as water. The resulting carbocation is subsequently neutralized by the elimination of a neighbouring proton. The intermediate carbocation can be stabilized by the use of polar protic solvents, which can therefore enhance reaction rates.

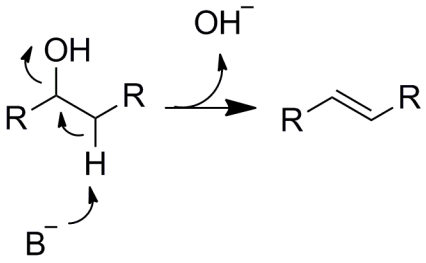

Scheme 2. E_2 mechanism.

Base is needed for the E_2 mechanism (Scheme 2), whereas E_1 is acid catalyzed. The presence of a carbonyl group (formed by dehydrogenation on a metallic surface) results in some acidic α-protons, which can be removed by base, resulting in E_2 elimination.

Homolytic cleavage of a C-O bond can be achieved on a metallic surface (Scheme 3). Joining the two fragments with homolytically cleaved hydrogen will result in water and a dehydroxylated species. This

reaction sequence is true hydrogenolysis, while this term is often used in cases where actually a sequential elimination-hydrogenation process is occurring.

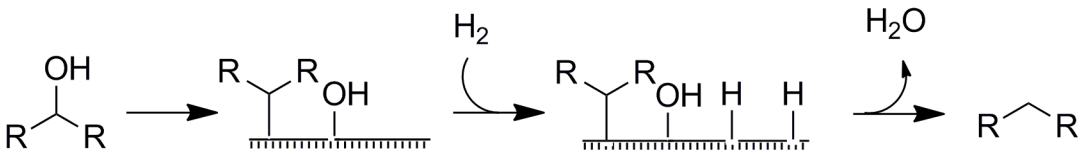

Scheme 3. Hydrogenolysis mechanism.

One method to introduce selectivity into the overall process is to direct the reaction in such a manner that it occurs only via one specific dehydration pathway. Since each of the three above-mentioned pathways requires different reaction conditions, this is relatively straightforward.

Another point of consideration is the endothermic character of a dehydration versus the exothermic nature of a hydrogenation (Scheme 4). These opposing needs for heat can be detrimental for product selectivity. The relatively high temperature needed for initial dehydration can cause degradation of glycerol, reaction intermediates or reaction product. The selectivity of deoxygenation can also be influenced by using additives in the catalytic system, regardless of the mechanism via which dehydroxylation occurs. These additives can coordinate available hydroxyl groups, thereby either activating or protecting the C-O bond. [5]

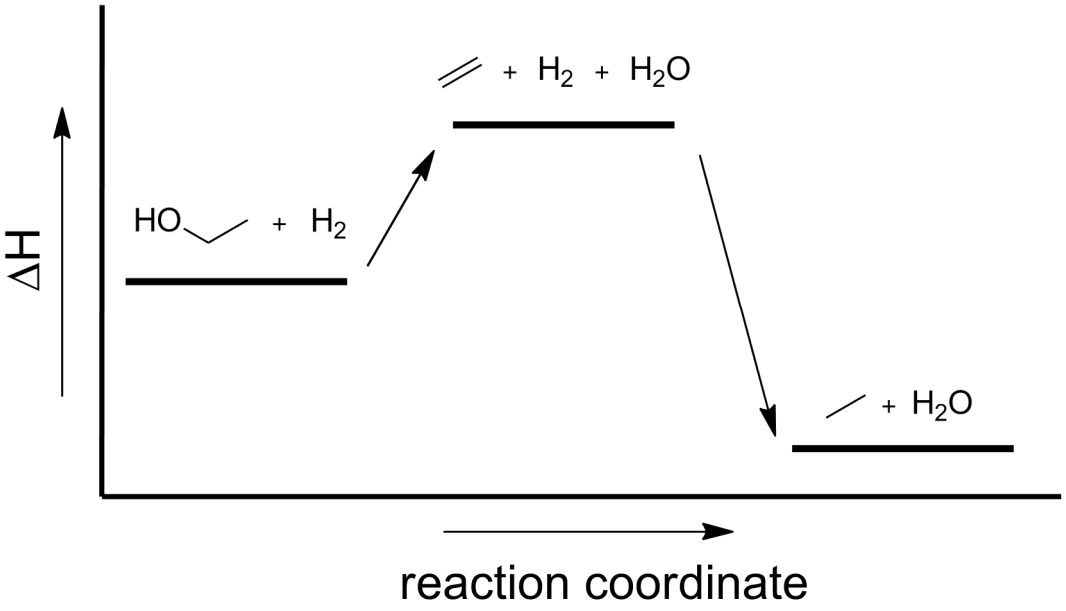

Scheme 4. Dehydration versus hydrogenation; endotherm versus exotherm.

An example is the use of boric acid to stabilize intermediates, thereby enabling the isomerization of glucose into fructose. [6] The initial formation of a borate ester lowers the overall activation energy, thereby making intermediates readily accessible.

2.1 DEHYDRATION OF VICINAL DIOLS AND HYDROGENATION OF CARBONYL GROUPS

The dehydration of vicinal diols results in an enol. This readily tautomerizes into a keton or aldehyde, which is subsequently hydrogenated (Scheme 5). The keto-enol tautomerization stabilizes the system, which makes the dehydration of diols relatively easy.

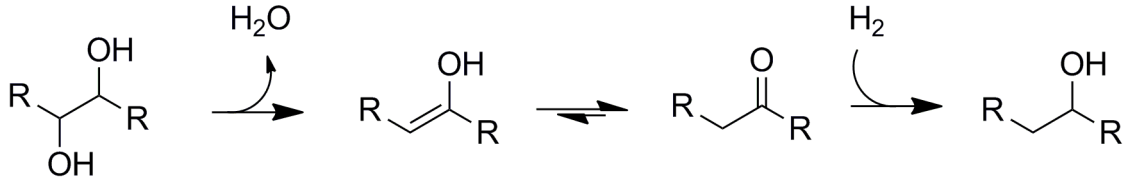

Scheme 5. Dehydration of vicinal diols and hydrogenation of carbonyl group.

The challenge is to selectively eliminate either a primary or a secondary alcohol. This is for example the basis for 1,2-propanediol and 1,3-propanediol selectivity in the transformation of glycerol. It is easier to eliminate a secondary alcohol via an acid catalyzed E_1 mechanism, since the intermediate secondary carbocation is more stable. However, the resulting aldehyde is less stable than the ketone formed after elimination of a primary alcohol.

A Brønsted acid will help in eliminating a secondary alcohol, whereas a Lewis acid can more easily coordinate to a primary alcohol, thereby weakening the C-O bond. [7] Indeed, primary alcohols are more reactive than secondary ones; this implies also a different order of reactivity if non acidic conditions are applied.

2.2 DEHYDRATION OF ALCOHOLS AND HYDROGENATION OF CARBON-CARBON DOUBLE BONDS

Isolated alcohols can be eliminated as well, which can be either acid or base catalyzed. However, lack of isomerization possibilities makes this process more difficult than the dehydration of vicinal diols (Scheme 6). The proximity of a double bond will offer some stabilization through a π-conjugated system, as is the case in acrolein formation.

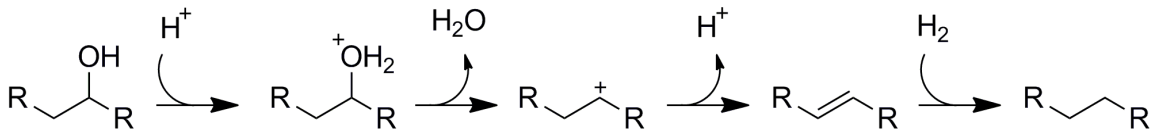

Scheme 6. Dehydration of alcohols and hydrogenation of carbon double bond.

2.3 CONDENSATION OF ALCOHOLS AND HYDROGENOLYSIS OF THE RESULTING CYCLIC ETHERS

This reaction sequence starts with the condensation of two alcohols by forming a cyclic ether (Scheme 7), which can then be cleaved by hydrogenolysis. However, often the rehydration and subsequent elimination (which is discussed in Section 1.1 and 1.2) is faster than a subsequent hydrogenolysis.

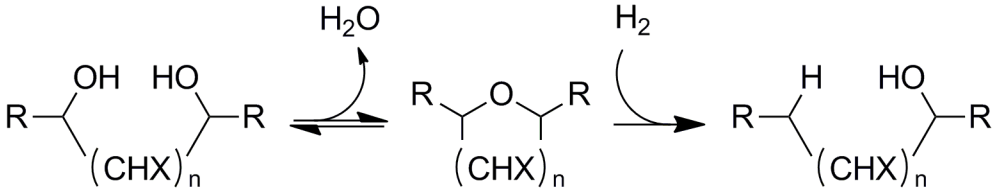

Scheme 7. Condensation of alcohols and hydrogenolysis of cyclic ether.

Nevertheless, the hydrogenolysis of the ether bond offers a good opportunity to introduce selectivity into the system, as studied by Koso *et al.*. [8,9] This group specifically studied the hydrogenolysis of tetrahydrofurfuryl alcohol and tetrahydropyran methanol using rhodium catalysts.

They found that the addition of tungsten, rhenium and molybdenum increased both the activity and the selectivity of the hydrogenolysis. [8] This higher selectivity is explained by both a smaller rhodium ensemble on a MO_x-Re catalyst and coordination of the free alcohol towards the MO_x. [8] This forms an alkoxide and the neighbouring C-O bond is then cleaved by hydroxides present on the adjacent rhodium surface.

The same bimetallic system is also highly selective in the hydrogenolysis of tetrahydropyran methanol into 1,6-hexanediol. A XANES and EXAFS study shows that the RhO_x and ReO_x particles have a direct interaction and it is indicated that the RhO_x surface is covered by small ReO_x species. [9]

This reaction sequence is not applicable to glycerol, since the condensation of alcohols in order to form cyclic ethers is limited to 5 membered or larger ring systems.

3 GLYCEROL

Glycerol is the smallest polyol readily available from biomass. It functions as the backbone of triglycerides, which constitute approximately 10% of total biomass. Glycerol is released as a byproduct from biodiesel production. For every ton of biodiesel produced, 100 kg of glycerol is generated. Consequently, glycerol constitutes 1% of total biomass. Glycerol is a popular starting material for further chemical derivatization. Although this review focuses on catalytic dehydration and reduction a range of products can be obtained through oxidation, esterification and etherification, stressing the versatility of this building block. [10,11]

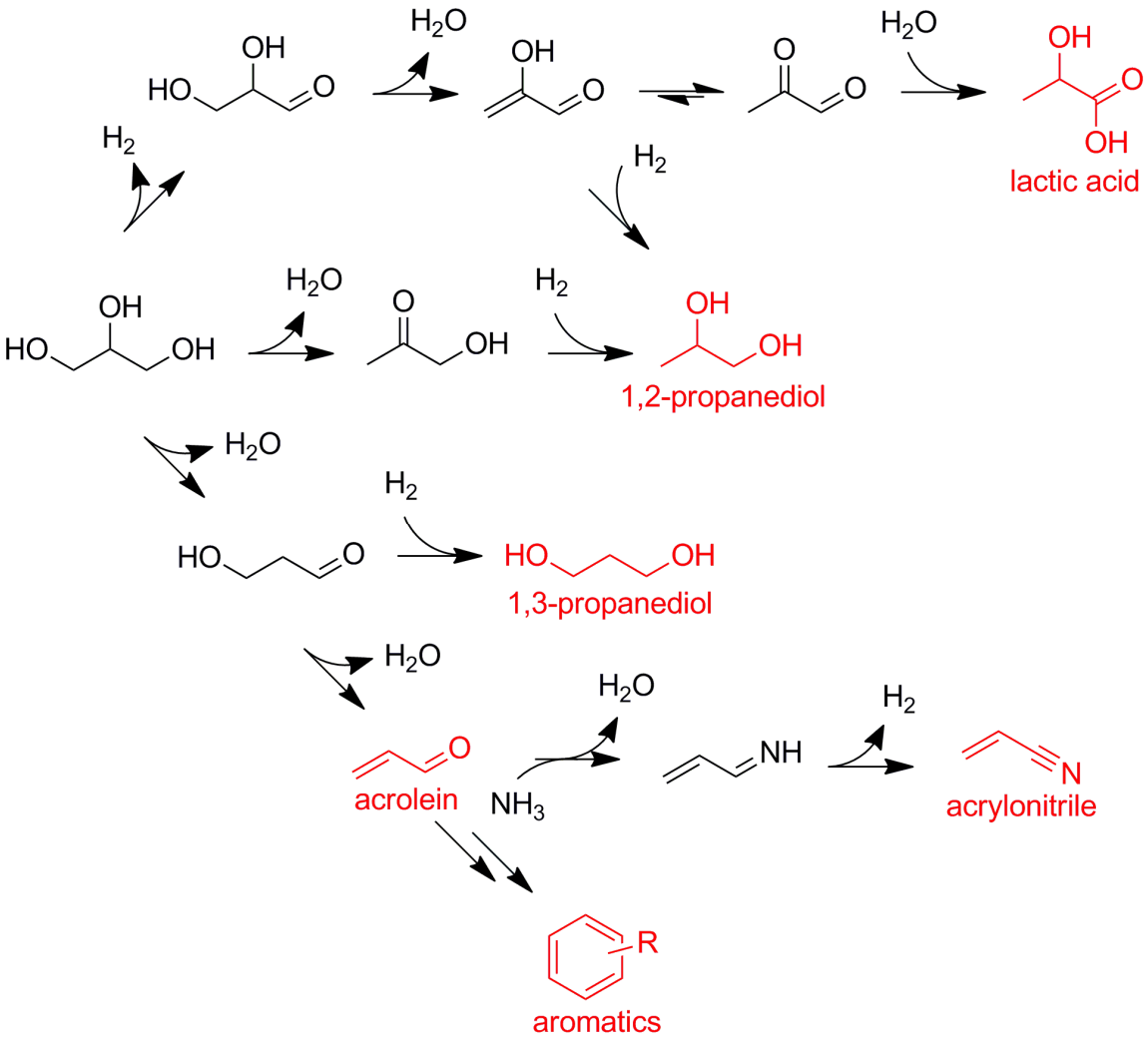

Scheme 8. Dehydrated products from glycerol.

Scheme 8 shows the dehydration and dehydroxylation routes leading to different products. It can be observed that some of the intermediates are branching points. By choosing the appropriate catalysts and conditions, selectivities can be directed towards either of these products. The processes that lead to the molecules depicted in red will be discussed in more detail in the following chapters. Scheme 9 shows that the initial dehydration to form acetol is thermodynamically favoured over the formation of 3-hydroxypropanal. Moreover, whenever 3-hydroxypropanal is formed, the subsequent dehydration to form acrolein is thermodynamically more likely than hydrogenation to 1,3-propanediol. This exemplifies the difficulties in achieving high 1,3-propanediol selectivities and it can be deduced that the formation of 1,3-propanediol is kinetically controlled.

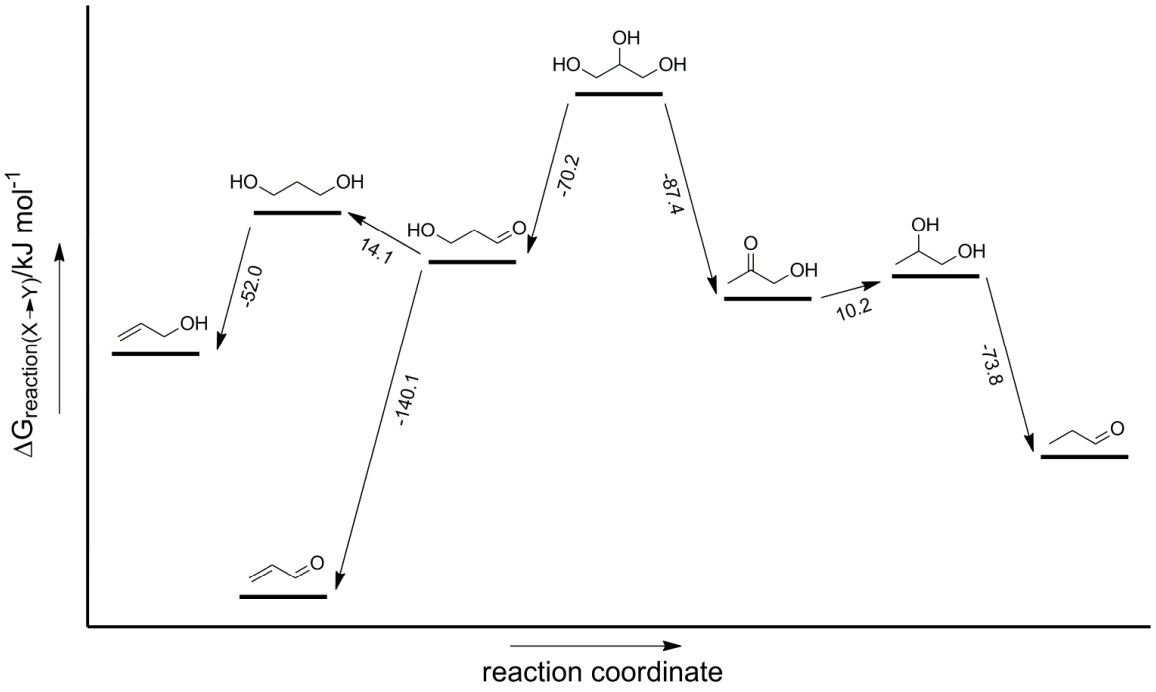

Scheme 9. Reaction energies for glycerol to 1,2-propanediol, 1,3-propanediol, acrolein, their intermediates and degradation products. [56]

3.1 Glycerol to 1,2-propanediol

Most of the propylene glycol, or 1,2-propanediol (12PD), is produced by the hydration of propylene oxide. This is produced via either the chlorohydrin process or the hydroperoxide process from oil-derived propylene. [12] 12PD is primarily used as a monomer in polyesters and as an anti-freeze or cooling liquid. A sustainable production starting from glycerol would involve a reduction step rather than an oxidation, exemplifying the challenge sketched in Figure 1.

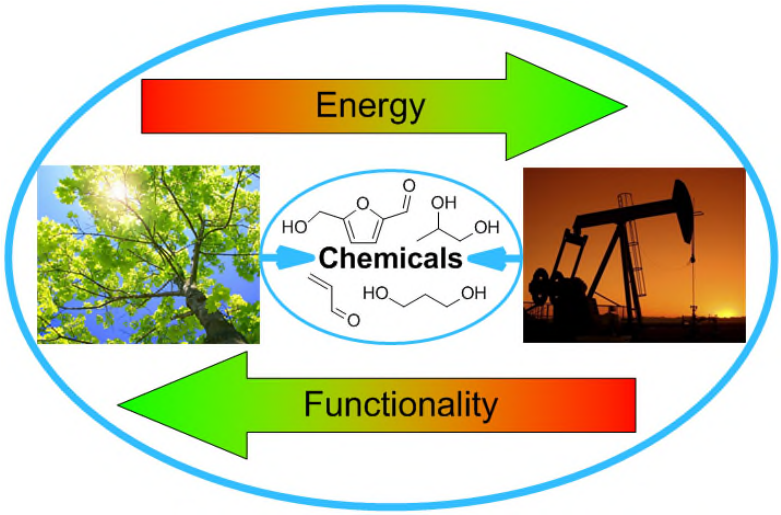

Figure 1. Defunctionalisation of biomass vs. functionalisation of oil.

3.1.1 REACTION MECHANISM

Understanding the reaction mechanism is a first step in rationally designing functional catalysts. Several reaction mechanisms have been proposed for a glycerol reduction to 12PD. Although most contributions mention hydrogenolysis, suggesting a direct C-O bond cleavage by hydrogen on a metallic surface, the actual mechanism involves an elimination followed by a reduction step, as described above (Section 1.1).

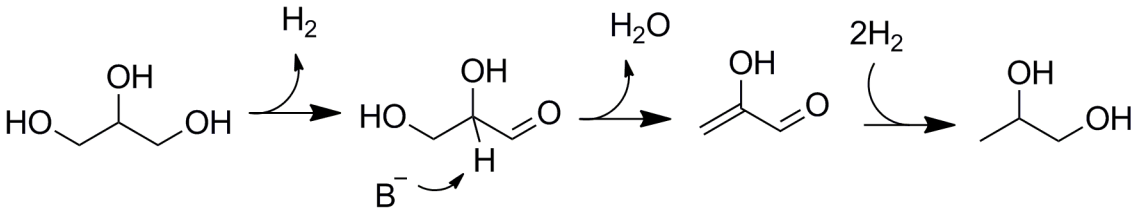

Scheme 10. 12PD formation from glycerol under alkaline conditions.

Under alkaline conditions, 12PD is being formed via glyceraldehyde, through an initial dehydrogenation, followed by water elimination and finally two reduction steps (Scheme 10). [13] The dehydrogenation as an oxidation seems surprising at first glance. It does however greatly ease the elimination step, since a conjugated system is obtained.

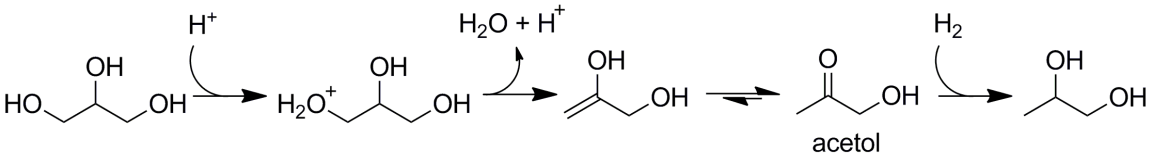

Scheme 11. 12PD formation from glycerol under acidic conditions.

Under acidic conditions, acetol is generally accepted as the key intermediate in 12PD formation (Scheme 11). [14,15] It can be formed via direct dehydration of glycerol and subsequent keto-enol tautomerization. Then it is reduced to 12PD. In principle, the acid catalyzed elimination can eliminate either a secondary or a primary alcohol, which leads to 3-hydroxypropanal or acetol, respectively. The elimination of a secondary alcohol proceeds via a relatively stable intermediate secondary carbocation and is therefore kinetically controlled. The elimination of a primary alcohol forms acetol, which is the thermodynamically more stable compared to 3-hydroxypropanal (Scheme 9). This consideration is the basis for 1,2-propanediol selectivity versus 1,3-propanediol selectivity. [16]

A complete hydrogenolysis reaction scheme is modelled for a Ru-Re/C catalyst in a batch slurry reactor. This shows that the reaction is kinetically controlled. This justifies the conclusion that hydrogenolysis can be improved by altering transition energies, by developing the appropriate catalytic system. [17]

Zhou *et al.* derived a kinetic model for a Cu-ZnO-Al_2O_3 catalyst. They showed that the reaction proceeds over two different catalytic sites. Glycerol, acetol and 12PD are adsorbed on one catalytic site and dissociative hydrogen adsorption occurs on the other. The model showed that dehydration of adsorbed

glycerol to acetol is slower than hydrogenation of acetol to 12PD and is therefore the rate-limiting step. This fact will prove helpful in developing more active catalysts. [18]

3.1.2 ALKALINE CONDITIONS

Under alkaline conditions selectivities towards 12PD are generally quite high, however, the objective is to obtain high conversions as well. Vasiliadou *et al.* show that the copper particle size plays a key role in silica supported copper catalyst activity. [19] Similarly, Bienholz *et al.* explain the essential role of copper surface area for catalyst activity for both the dehydration and hydrogenation step in the 12PD formation scheme, which makes the development of stable copper catalysts with high surface area highly desirable. Their Cu/SiO_2 catalyst is a good example, showing excellent conversion and high 12PD selectivity (Table 1, entry 1). [20]

The sintering of CuO in a CuO-ZnO catalyst during reaction was recently described by the same group. It is caused by reaction water and this has a far larger effect than increasing reaction temperature (Table 1, entry 2). [21] They were able to counteract the detrimental effect water by the co-precipitation of gallium with their CuO-ZnO catalyst. The stabilizing effect of gallium is attributed to a physical separation of the Cu-particles by Ga_2O_3 or $ZnGa_2O_4$-particles. The resulting $Cu/ZnO/Ga_2O_3$ catalyst is stable for several catalytic runs and shows high conversion and 12PD selectivity (Table 1, entry 3). [22]

In a preliminary study, Liu *et al.* demonstrated that the performance of a co-precipitated CuO-ZnO catalyst depended on the Cu particle size. Smaller particles led to higher selectivity and activity and the sintering of these particles has to be avoided. [23] They showed that it was possible to stabilize the Cu by a pre-reduction step, yielding a Cu-ZnO catalyst, thereby preventing the adverse effect of water. The reduction of the Cu before the reaction increased 12PD selectivity from 29% to 84%, while maintaining a similar conversion (Table 1, entry 4). [23]

In a follow-up paper the catalyst was described in more detail and an increase in selectivity to 94% was reported by increasing the hydrogen pressure from 4.2 MPa to 6.0 MPa. [15] Activity of the catalyst could be increased using higher glycerol concentrations, temperatures and pressure. However, these activities are reported as turnover frequencies, recorded at ca. 25% conversion, which makes it difficult to compare it with other studies. 75% conversion could be reached in 6 hours, with retention of 12PD selectivity, by increasing the catalyst loading to 2.2 g (Table 1, entry 5). Interestingly, the same authors reported that 12PD was formed via the glyceraldehyde mechanism, which involves the initial dehydrogenation of glycerol. The increased TOF by elevated pressures indicates that this dehydrogenation step is not rate-limiting. Therefore, a more alkaline support (to provide subsequent dehydration) or more active hydrogenation catalyst can improve the activity.

Table 1. 1,2-propanediol from glycerol.

Entry	Catalyst	Additive	Additive/ Metal ratio	*P* (bar)	*T* (K)	TOF[c] (h^{-1})	Conversion (%)	Selectivity 12PD (%)	Selectivity EG (%)	Yield 12PD (%)
Alkaline catalysts										
1[20]	Cu/SiO_2[e]	-	-	15	528	13.2	100	87.0	4.0	87.0
2[21]	CuO/ZnO	Zn	2[a]	50	473	9.0	46.0	90.0	1.0	41.4
3[22]	$Cu/ZnO/Ga_2O_3$	-	-	50	493	18.4	96.0	82.0	2.0	78.7
4[23]	Cu-ZnO	Zn	1 [a]	42	473	0.3	22.5	83.6	10.7	18.8
5[15]	Cu-ZnO	Zn	1[a]	60	473	0.9	75.0	93.9	5.5	70.4
6[24]	Pt/hydrotalcite	-	-	30	493	37.2	92.1	93.0	3.9	85.7
7[25]	Cu/MgO	-	-	30	453	1.0	72.0	97.6	1.3	70.3
8[26]	Cu/MgAlO	-	-	30	453	2.7	80.0	98.2	1.0	78.6
9[27]	CuO/SiO_2	-	-	90	473	2.6	73.4	94.3	3.6	69.2
Acidic catalysts										
10[28]	Ru/C	Amberlyst 15	2[b]	80	393	16.8	12.9	55.4	12.9	7.1
11[29]	Ru/C	Amberlyst 70	19[a]	80	453	804	48.8	70.2	8.3	34.3
12[30]	Ru/C	Amberlyst 15	2[b]	80	393	38.3	21.3	76.7	-	16.3
13[31]	Ru/C	Nb_2O_5	2[b]	60	453	20.0	62.8	66.5	21.2	41.8
14[32]	Ru/TiO_2	-	-	60	453	33.1	46.0	63.0	19.0	29.0
15[33]	Cu/Al_2O_3	-	-	15	473	9.2	41.9	93.3	-	39.1
16[34]	$CuAg/Al_2O_3$	Ag	0.4[a]	15	473	6.1	27.0	96.0	-	25.9
17[35]	Cu-STA/Al_2O_3[e]	STA	1[b]	60	513	64.0	90.1	89.7	4.2	80.8
18[36]	$CuCr_2O_4$	Cr	2[a]	80	493	6.3	80.0	84.0	-	67.2
19[37]	Cu:Al	Al	1[a]	70	513	4.9	76.0	89.0	-	67.6
20[38]	Ru-Cu/TMG-bentonite	Cu	0.3[a]	80	503	9.5	100	85.4	7.6	85.4
21[39]	Ru/Al_2O_3	$Re_2(CO)_{10}$	0.5[a]	80	433	21.5	53.4	50.1	7.8	26.8
22[40]	$RuRe/SiO_2$	Re	1[b]	80	433	20.5	51.7	44.8	6.4	23.2
23[40]	$RuRe/ZrO_2$	Re	1[b]	80	433	23.7	56.9	47.2	4.0	26.9
Miscellaneous catalysts										
24[41,42]	Cu/Al_2O_3[e]	-	-	1	473-393	0.4	100	96.7	1.9	96.7
25[43]	Pt/NaY	-	-	1[d]	503	15.0	85.4	64.0	-	54.7
26[44]	Ru/Al_2O_3 and Pt/Al_2O_3	-	-	14[d]	493	13.7	50.1	47.2	6.3	23.6
27[45]	Raney Ni	-	-	1[d]	453	1.0	100	25.0	32.0	25.0

[a] on a molar basis [b] on a weight basis [c] Turnover Frequency ($mmol_{12PD} \cdot mmol_{metal}^{-1} \cdot h^{-1}$) [d] N_2 pressure and *in situ* hydrogen formation [e] continuous reaction.

Hou *et al.* investigated Pt catalysts on various supports. It showed that the more alkaline supports were most active. Pt on hydrotalcite showed a conversion of 92% and a 12PD selectivity of 93%. It was superior to MgO > Al_2O_3 > HBeta ~ HZSM-5 (Table 1, entry 6). [24]

Since Pt on MgO showed reasonable conversion (50%), this group also tried immobilization of the more economical Cu on MgO. Here they showed that co-precipitation proved more successful than impregnation. This was attributed to the higher dispersion of Cu particles on a co-precipitated catalyst. The catalyst showed high selectivity towards 12PD (97.6%) and a conversion of 72% could be reached in 20 hours. The addition of NaOH promoted the dehydration step and this increased the conversion to 82% (Table 1, entry 7). [25]

A hydrotalcite-like material (Cu/MgAlO) showed to be both active and selective for 12PD production (Table 1, entry 8). The high activity was ensured by a homogeneous dispersion of copper in the solid base matrix. Here, the addition of NaOH could increase the conversion of glycerol to 91%, while only slightly decreasing the 12PD selectivity. [26]

Xia *et al.* prepared a CuO/SiO_2 catalyst by precipitation-gel technique. This catalyst showed a similar selectivity towards 12PD (94%) as the impregnated CuO/SiO_2 catalyst. However, the precipitation-gel catalyst is more stable due to strong Cu-support interaction and much more active (73% conversion) due to high Cu dispersion and smaller metal particle size (Table 1, entry 9). When the PG catalyst was run in a fixed-bed flow reactor, the conversion was increased to ~80% and the catalyst was stable for 200 hours. Even the selectivity was increased (98%), due to limited degradation possibilities in a continuous flow reactor. [27] This extraordinary stability is partly due to the presence of some sodium on the catalyst. This artefact of the precipitation-gel technique (which involves the addition of 4M NaOH to a solution of $Cu(NO_3)_2$ to form a precipitate) retards the leaching of copper. [14]

3.1.3 Acidic conditions

As discussed above the elimination step can be acid or base catalyzed. In an exploratory study Tomishige *et al.* showed that the sulfonic acid resin Amberlyst 15 is a more effective additive promoting 12PD formation than homogeneous sulfuric acid and hydrochloric acid. Moreover, hydrochloric acid inhibited catalyst activity by poisoning the Ru surface of the Ru/C catalyst. Activity of the Ru/C and Amberlyst 15 system was limited to 13% conversion (giving 55% 12PD selectivity) for a 20 wt% aqueous glycerol solution at 393 K and could not be increased by applying higher temperatures, because of the low thermal stability of the Amberlyst 15 (Table 1, entry 10). [28] This limitation could be overcome by using the more thermo-stable resin Amberlyst 70. Temperatures up to 453 K could be applied. This, in combination with a pre-reduction step of the ruthenium particles, increased conversion to 49% and 12PD selectivity to 70%, with a remarkable turnover frequency of 804 per hour (Table 1, entry 11 and 12). [29,30]

Lingaiah *et al.* used Ru/C in combination with several thermally stable solid acids. They showed that conversion could be linearly correlated to the amount of acid sites on the solid acid. Nb_2O_5 and ZrO_2 supported phosphotungstic acid, possessing moderate acid sites, proved to be the most active additives, whereas the type of additive does not influence the selectivity. The reaction conditions for Ru/C and Nb_2O_5 could be optimized to 63% conversion and 67% 12PD selectivity (Table 1, entry 13). [31]

In another paper by the same authors, Ru was immobilized on Lewis acidic TiO_2 support through a deposition-precipitation method. In this way, the acid sites are in close proximity of the hydrogenating metallic particles. This approach resulted in a very stable catalyst that gives 46% glycerol conversion and 63% 12PD selectivity in only 8 hours (Table 1, entry 14). [32]

The activity and selectivity of copper immobilized on various aluminium containing acidic supports was investigated by Zhang *et al.*. Pure alumina was more active than the more acidic zeolitic supports (HBeta, HY, HZSM-5 and 13X), which showed minimal or no activity at all. This could be due to the zeolites preferred selectivity towards acrolein, or because of the strong CuO-support interaction due to the high acidity of the zeolites. This interaction might prevent the pre-reduction of CuO to active metallic Cu. The Cu/Al_2O_3 catalyst was able to convert pure glycerol into 12PD at a conversion of 42%. Interestingly, no glycerol condensation products were formed using pure glycerol and 12PD selectivity was as high as 93% (Table 1, entry 15). [33] By co-impregnation of Cu/Al_2O_3 with silver, the copper could be reduced at reaction temperature, thereby rendering the pre-reduction step obsolete. Although the bimetallic catalyst showed improved 12PD selectivity, the activity of the $CuAg/Al_2O_3$ catalyst was lower compared to the parent pre-reduced Cu/Al_2O_3 (Table 1, entry 16). [34]

3.1.4 CATALYST PROMOTION

A commonly used strategy to improve catalyst activity is to co-immobilize a second metal or acid with the hydrogenating metal. Sun *et al.* impregnated silicotungstic acid and copper on alumina. The resulting catalyst was tested in a fixed-bed reactor. The co-impregnated acid in combination with the continuous reactor resulted in good glycerol conversion (90%) and 12PD selectivity (90%). Moreover, the catalyst was shown to be stable with regard to activity and selectivity for 250 h (Table 1, entry 17). [35]

Yi *et al.* used chromium to promote the activity of copper. Chromium itself showed minimal catalytic activity, [36] and impregnation of Cr_2O_3 with copper does not improve catalytic properties significantly. [46] However, by co-precipitating chromium with copper both activity and selectivity were increased tremendously. Using this method of preparation, an acidic $CuCr_2O_4$ spinel was formed. These spinels are known for storing hydrogen within their structure, thereby increasing their hydrogenation activity. This resulted, in combination with the improved acidity, in a hydrogenolysis catalyst that converts 80% of glycerol into 12PD at 84% selectivity (Table 1, entry 18). [36]

Chromium however, is not an environmentally friendly metal. Therefore, efforts were directed towards its replacement with a more benign alternative, such as aluminium. A co-precipitation Al:Cu catalyst showed higher acidity compared to two commercial copper chromate catalysts, which is translated into higher glycerol conversion. The conversion could be increased up to 76% at 513 K, while maintaining a high 12PD selectivity of 89%, showing only a small amount of degradation of glycerol into EG at this temperature (Table 1, entry 19). [37]

A very active and stable bimetallic catalyst was prepared by depositing ruthenium and subsequently copper on a bentonite carrier. Before the deposition of the metal, the sodium cations on the carrier were exchanged by the cations of the ionic liquid tetramethylguanidiniumlactate. These cations (tetramethylguanidinium TMG) proved to stabilize the metal particles by strong coordination. Aggregation of the particles was prevented by strong electrostatic interactions of TMG with the negative charge in the silicate layers of the bentonite.

TMG not only stabilized the metal particles, but also increased the amount of liquid product. The ruthenium in this bimetallic catalyst provides the activity (100% conversion), while Cu suppresses the degradation of glycerol into EG, thereby accommodating high 12PD selectivity (85%) (Table 1, entry 20). [38]

The influence of rhenium on the activity of several heterogeneous ruthenium catalysts was investigated by He *et al.*. The addition of heterogeneous $Re_2(CO)_{10}$ was most effective in combination with Ru/Al_2O_3. Together with this catalyst it not only increased the conversion of glycerol, it also improved 12PD and 13PD selectivity, by preventing the degradation of glycerol into EG. In combination with Ru/C the rhenium improved both conversion and selectivity, but to a somewhat lesser extent. The mix of Ru/ZrO_2 and $Re_2(CO)_{10}$ mainly improved the selectivity towards propanediols, while the effect on the conversion of glycerol was less pronounced (Table 1, entry 21). Interestingly, reasonable conversions were established at a relatively low temperature of 433 K and rhenium showed some increase in 13PD selectivity, a more valuable diol. [39]

This promising lead was followed up by impregnating the rhenium and ruthenium directly on different acidic supports. Conversions between 52 and 57% were reached using bimetallic SiO_2, ZrO_2, H-ZSM5 and HBeta catalysts, which was higher than using rhenium as an additive. However, the selectivity towards 12PD was only improved for $RuRe/SiO_2$ and was not improved for the other catalysts (Table 1, entry 22 and 23). [40]

The pre-treatment of the $RuRe/SiO_2$ catalyst was also investigated. High pre-reduction temperatures were unnecessary and even decreased the glycerol conversion, because these high temperatures caused the metals to sinter. However, pre-reduction at 473 K did show higher 12PD selectivity compared to the calcined catalyst. This means that for an active and selective catalyst, the rhenium could be in a ReO_x form, while ruthenium should be in its metallic form. [47]

An explanation for the promoting effect of rhenium is the surface acidity of ReO_x. This would promote the dehydration step in the hydrogenolysis of glycerol. Interestingly, it also showed some enhancement in 13PD selectivity, a more valuable diol than 12PD. This effect will be discussed in more detail in the chapter concerning the formation of 13PD.

3.1.5 TEMPERATURE GRADIENT

Hydrogenolysis is not only optimized by developing the most active and selective catalysts. Reaction engineering can also contribute substantially. This is already apparent from the contradicting temperature needs for dehydration and hydrogenation. Dehydration is endothermic and proceeds more rapidly at higher temperatures, while exothermic hydrogenation can be performed at milder temperatures, thereby avoiding degradation of glycerol or reaction products. Sato *et al.* were able to improve the hydrogenolysis of glycerol by making use of this fact. They applied Cu/Al_2O_3 in a fixed-bed down-flow reactor, which had different temperatures at the top and the bottom. At the top, the dehydration took place at 473 K and the subsequent hydrogenation at the bottom was performed at 393 K (Scheme 12). In this way, glycerol was completely converted and 12PD selectivity was 97% (Table 1, entry 24). [41,42] This is a significant increase in 12PD formation, since using Cu/Al2O3 at a constant 463 K yielded only 80% 12PD. [41]

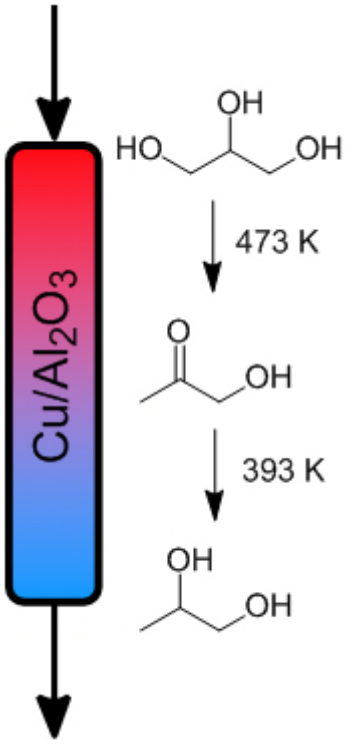

Scheme 12. Temperature gradient reduction of glycerol.

3.1.6 Absence of H_2

Externally added hydrogen is necessary for all previously mentioned processes to form 12PD. Normally, this hydrogen is derived from fossil fuels. However, the aqueous phase reforming of glycerol over Pt catalysts is also known. The hydrogen generated by this process can be directly used for the formation of 12PD. This was shown for the first time by D'Hondt *et al.*. They impregnated NaY zeolite with Pt, which was able to convert 85% glycerol with 64% 12PD selectivity (Table 1, entry 25). [43]

Roy *et al.* investigated the idea of *in situ* generation of hydrogen in more detail. A combination of both Ru/Al_2O_3 and Pt/Al_2O_3 was more active than the individual catalysts for *in situ* hydrogen formation and subsequent 12PD formation. An optimal temperature of 493 K was found (conversion 50%, 12PD selectivity 47%) (Table 1, entry 26). Increasing the temperature would further increase glycerol conversion. However, this would result in more gaseous products at the expense of 12PD selectivity. Counterintuitively, addition of external hydrogen was detrimental to 12PD selectivity and far more methane was formed, through methanation of carbon dioxide. [44]

An interesting development was reported by Yin *et al.*. They used Raney Ni for *in situ* hydrogen formation, thereby preventing the use of precious and scarce Pt and Ru. Raney Ni was able to catalyze the complete conversion of glycerol in 1 hour at 453 K. However, it was also very active in C-C bond cleavage, resulting in substantial EG selectivity (32%) on top of 12PD selectivity (25%) (Table 1, entry 27). [45]

To conclude, 12PD can generally be formed with good to very good selectivities, while in many examples the conversion needs improvement. It was shown that the abundantly available copper can achieve both. By utilizing the advantages of a continuous reactor, the initial dehydration of glycerol and subsequent hydrogenation of the formed acetal can be achieved at their respective optimum temperatures. This streamlines the overall reaction and yields almost 100% 12PD.

3.2 Glycerol to 1,3-propanediol

3.2.1 Introduction

1,3-propanediol (13PD) is the commercially most interesting hydrogenolysis product from glycerol. It is used in resins, engine coolants, dry-set mortars, water-based inks, but most of it is used in the production of polytrimethylene terephthalate (PTT), which is a polyester synthesized from 13PD and terephthalic acid. PTT is marketed by DuPont as SORONA® and used in the manufacture of fabrics.

Current production methods of 13PD are catalytic routes using oil derivatives such as ethylene oxide or acrolein as starting material. Ethylene oxide is converted to 13PD by subsequent hydroformylation and hydrogenation, whereas acrolein is subsequently hydrated and hydrogenated. [48]

It is also possible to convert glycerol, or glucose, into 13PD using a fermentation process. [48,49] It is even possible to combine 13PD and hydrogen production from crude biomass-derived glycerol, by using a mixed culture. In this way, optimal use is made of glycerol biomass, without the need for prior purification. [50]

In this review we will concentrate on the formation of 13PD from glycerol, using heterogeneous catalytic systems. The fact that the number of papers reporting on selective formation of 13PD is greatly outnumbered by the amount of papers reporting on selective 12PD formation is a clear sign that the formation of 13PD is more challenging. However, especially over the last two years, the factors that are important to influence 13PD formation are slowly being unravelled. An overview is given in the following section. It will become clear that, whilst for the conversion of glycerol into 12PD activity is the main challenge, for 13PD formation the main issue is to achieve high selectivity.

3.2.2 Reaction mechanism

The formation of 13PD proceeds via 3-hydroxypropanal as an intermediate. This aldehyde is formed after an initial elimination of the secondary alcohol group of glycerol. The formed C-C double bond undergoes a tautomerization, which yields the more stable aldehyde. Subsequent hydrogenation yields 13PD (Scheme 13).

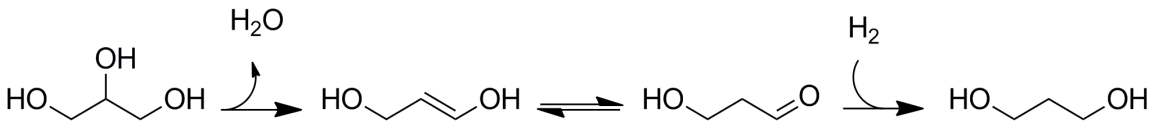

Scheme 13. Reaction mechanism 13PD formation via dehydration hydrogenation.

The initial alcohol elimination is endothermic and a relatively high temperature is needed for this elimination to proceed. The subsequent hydrogenation is exothermic and prefers lower reaction temperatures. Lower temperatures will also prevent further degradation of 13PD.

Recently, it has been reported that 13PD is formed at lowered temperatures, using rhenium oxide as an additive. This lower temperature indicates that the dehydration hydrogenation sequence is no longer active and points in the direction of energetically more favourable direct hydrogenolysis (*vide infra*).

3.2.3 Solvent

In 2004, Chaminand *et al.* were the first to report a hydrogenolysis reaction that produced more 13PD than 12PD (13PD/12PD ratio of 2). Using a slurry of Rh/C and tungstic acid in sulfolane, they were able to convert 32% glycerol. 13PD selectivity was 12% and a start towards 13PD was made (Table 2, entry 1). [5] This paper set the example for others to follow.

Table 2. 1,3-propanediol from glycerol.

Entry	Catalyst	Additive	Additive/ Metal (mol/mol)	Solvent	Reactor type	P (bar)	T (K)	TOF[a] (h^{-1})	Conversion (%)	Selectivity 13PD (%)	Selectivity 12PD (%)	Yield 13PD (%)	13PD/12PD ratio
1[5]	Rh/C	H_2WO_4	10	Sulfolane	batch	80	453	0.1	32.0	12.0	6.0	3.8	2.0
2[51]	$Pt/WO_3/TiO_2$	WO_3	2.9	DMI	batch	80	443	1.1	16.9	38.5	42.0	6.5	0.9
3[51]	$Pt/WO_3/HY$	WO_3	8.6	DMI	batch	80	443	1.2	25.9	27.8	34.4	7.2	0.8
4[51]	Pt/WO_3/ Al-MCM-41	WO_3	8.6	DMI	batch	80	443	1.3	27.8	27.0	25.2	7.5	1.1
5[51]	Pt/WO_3/ SiO_2-Al_2O_3	WO_3	8.6	DMI	batch	80	443	1.8	42.2	26.1	27.5	11.0	0.9
6[51]	$Pt/WO_3/Al_2O_3$	WO_3	8.6	DMI	batch	80	443	2.2	43.9	30.1	25.1	13.2	1.2
7[51]	$Pt/WO_3/ZrO_2$	WO_3	8.6	DMI	batch	80	443	4.0	85.8	28.2	14.6	24.2	1.9
8[51]	$Pd/WO_3/ZrO_2$	WO_3	8.6	DMI	batch	80	443	0.8	24.0	19.6	27.5	4.7	0.7
9[51]	$Ir/WO_3/ZrO_2$	WO_3	8.6	DMI	batch	80	443	0.5	21.8	14.2	30.7	3.1	0.5
10[51]	$Ru/WO_3/ZrO_2$	WO_3	8.6	DMI	batch	80	443	0.6	46.7	7.3	19.5	3.4	0.4
11[51]	$Rh/WO_3/ZrO_2$	WO_3	8.6	DMI	batch	80	443	0.7	86.4	4.7	32.6	4.1	0.1
12[52]	$Pt/WO_3/ZrO_2$	WO_3	8.6	DMI	batch	55	443	1.9	32.5	15.2	18.2	4.9	0.8
13[52]	$Pt/WO_3/ZrO_2$	WO_3	8.6	Sulfolane	batch	55	443	0.8	33.8	5.3	14.6	1.8	0.4
14[52]	$Pt/WO_3/ZrO_2$	WO_3	8.6	EtOH	batch	55	443	2.6	38.2	23.0	13.6	8.8	1.7
15[52]	$Pt/WO_3/ZrO_2$	WO_3	8.6	H_2O	batch	55	443	2.3	24.7	25.7	15.0	6.3	1.7
16[52]	$Pt/WO_3/ZrO_2$	WO_3	8.6	DMI-H_2O	batch	55	443	4.2	31.6	34.9	8.7	1.0	4.0
17[52]	$Pt/WO_3/ZrO_2$	WO_3	8.6	DMI-EtOH	batch	55	443	4.6	45.6	29.3	18.9	13.4	1.6
18[52]	$Pt/WO_3/ZrO_2$	WO_3	8.6	EtOH-H_2O	batch	55	443	3.3	45.7	21.2	8.0	9.7	2.7
19[54]	$Pt/WO_3/ZrO_2$	WO_3	8.6	H_2O	continuous	40	403	4.0	70.2	45.6	2.6	32.0	17.8
20[55]	$Pt/WO_3/TiO_2$/ SiO_2	WO_3/ TiO_2	2.1[b]	H_2O	batch	55	453	2.8	15.3	50.5	9.2	7.7	5.5
21[56]	$Cu\text{-}STA/SiO_2$	STA	0.033	-	continuous	5.4	483	0.2	83.4	32.1	22.2	26.8	1.4
22[57]	Rh/SiO_2	Amberlyst 15	-	H_2O	batch	80	393	1.1	14.3	9.8	26.0	1.4	0.4
23[58,59]	$Rh\text{-}ReO_x/SiO_2$	ReO_x	0.5	H_2O	batch	80	393	17.3	79.0	14.0	41.5	11.9	0.3
24[58]	$Rh\text{-}MoO_x/SiO_2$	MoO_x	0.0625	H_2O	batch	80	393	4.3	46.0	6.0	32.1	2.8	0.2
25[58]	$Rh\text{-}WO_x/SiO_2$	WO_x	0.125	H_2O	batch	80	393	6.0	34.0	11.3	43.2	3.8	0.3
26[60]	$Ir\text{-}ReO_x/SiO_2$	ReO_x and H_2SO_4	1	H_2O	batch	80	393	12.0	50.0	49.0	10.0	24.5	4.9
27[61]	Pt-Re/C	Re	1	H_2O	batch	40	443	11.9	20.0	34.0	33.0	6.8	1.0
28[61]	Pt-Re/C	Re	1	H_2O	batch	40	443	5.7	45.0	29.0	27.0	13.1	1.1

[a] Turnover Frequency ($mmol_{13PD} \cdot mmol_{metal}^{-1} \cdot h^{-1}$) [b] WO_3/ platinum.

The novelty of Chaminand *et al.*'s report was both the use of tungstic acid as an additive and sulfolane as a solvent. Kurosaka *et al.* adopted these ideas and realized a breakthrough by impregnating several acidic supports with tungsten oxide and platinum (Table 2, entries 2 to 7). These catalysts were tested using 1,3-dimethyl-2-imidazolidinone (DMI) as solvent, which is considered to be more stable, polar and aprotic than sulfolane. These acidic supports all yielded 13PD with selectivities between 26 and 39%. TiO_2 gave the highest selectivity (but only 17% glycerol conversion), while ZrO_2 stood out with a glycerol conversion of 86%, thereby showing impressive conversion and selectivity compared to Chaminand *et al.*'s results. [51]

This promising lead was followed up by adding different hydrogenation metals to a WO_3/ZrO_2 support by impregnation. 13PD selectivities ranged from 5 to 28% in the order Pt > Pd > Ir > Ru > Rh, while both Pt and Rh excelled with a glycerol conversion of 86% (Table 2, entries 7 to 11). [51]

Gong *et al.* used the same $Pt/WO_3/ZrO_2$ catalyst and examined the effect of the solvent (Table 2, entries 12 to 15). Sulfolane and DMI were used as polar aprotic solvents and EtOH and H_2O were used as polar protic solvents. It was demonstrated that aprotic solvents were not necessary for high 13PD selectivity. On the contrary, the aprotic solvents produced more 12PD than 13PD, while the protic solvents produced 13PD at higher selectivities (23 and 26%). The aprotic solvents showed comparable conversions (33-34%) but were outperformed by EtOH (38%). Conversion of glycerol in water was lagging (25%), which can be explained by the formation of H_2O during the reaction. [52]

EtOH-H_2O, DMI-EtOH and DMI-H_2O were tested as binary solvents (Table 2, entries 16 to 18). Interestingly, the solvents containing DMI showed a synergistic effect for 13PD selectivity. It could be increased to 29 and 35% using EtOH and H_2O as the second solvent, respectively. On the other hand, the conversion increased (to 46%) whenever EtOH was present in the binary solvent. Another interesting finding was the decrease of 12PD selectivity upon the presence of H_2O in the binary solvent. This could increase the 13PD/12PD ratio up to 4. [52]

It seems that the initial finding of Chaminand *et al.* that sulfolane, or another aprotic polar solvent, is necessary for high 13PD/12PD ratio is not general, since high ratios are also obtained in the absence of these solvents. The absence of H_2O can increase glycerol conversion due to beneficial equilibrium conditions, but high 13PD selectivities have been shown using H_2O or EtOH. It is likely that use of sulfolane was inspired by Bullock *et al.* They used sulfolane because their homogeneous catalysts were not stable in H_2O. [53] However, this is no longer important when the switch to heterogeneous catalysts is made.

Instead, results suggest that a protic solvent improves the reaction towards 13PD. This might be caused by facilitating a proton transfer from the (solid) acid to the secondary alcohol, which can then be eliminated. The polar character of the solvents is useful in stabilizing a charged intermediate. Using aqueous glycerol needs the initial elimination to work against equilibrium, which can be overcome by swift

reduction of the formed double bond. This can be achieved by active catalysts and using favourable hydrogenation conditions, i.e. moderate temperatures, since hydrogenation is an exothermic reaction.

3.2.4 ADDITIVES

3.2.4.1 TUNGSTEN

Qin *et al.* also used $Pt/WO_3/ZrO_2$ as a catalyst. Using a fixed-bed reactor they were able to obtain both high conversion (70%) and good 13PD selectivity (46%) using aqueous glycerol at only 403 K (Table 2, entry 19). [54] The authors ascribe the low reaction temperature to the ability of the catalyst to activate hydrogen as proton and hydride. First, hydrogen is homolytically split into hydrogen atoms (1, Figure 2), which can spill-over onto the WO_3/ZrO_2 surface (2, Figure 2). Here the hydrogen atom can donate an electron to a Lewis acidic site, generating a proton (3, Figure 2). This proton can be transferred to the substrate alcohol and a second hydrogen atom, acting as an acid, combines with the electron to form a hydride (4, Figure 2), stabilized on the Lewis acid site. This hydride is then finally used as a reductant. [62,63]

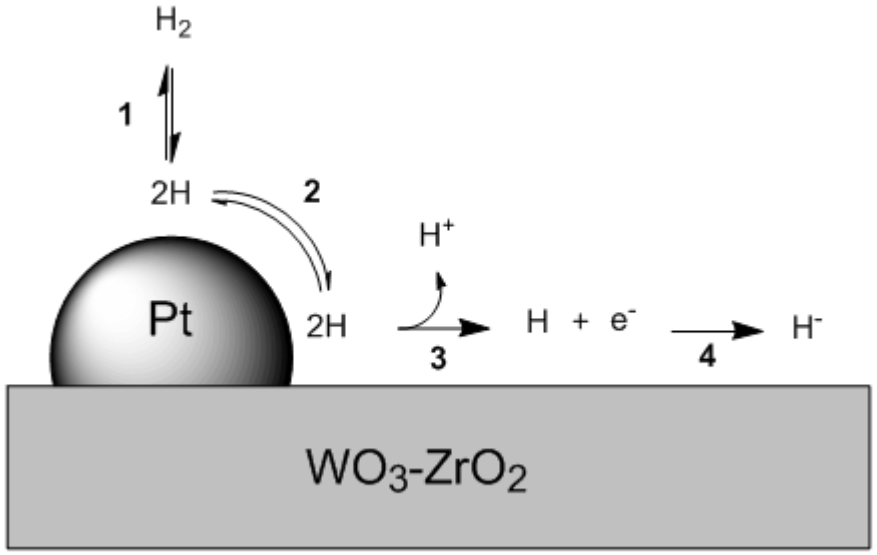

Figure 2. Homolytic cleavage of hydrogen on platinum and subsequent spillover.

This hypothesis is supported by NH_3 chemisorption measurements using supports that were calcined at different temperatures. Increasing the calcination temperature leads to higher acidity, resulting in higher conversion. [54]

The high 13PD selectivity can also be explained by this proton and hydride transfer mechanism over $Pt/WO_3/ZrO_2$, since protonation of secondary alcohols is preferred over primary ones. This results in an excellent 13PD/12PD ratio (Table 2, entry 19). [54]

Another reason for the high 13PD selectivity could be the use of a continuous-flow reactor. This will limit the degradation of 13PD formed, thereby increasing the yield.

Gong *et al.* found that a $Pt/WO_3/TiO_2$ catalyst showed good selectivity towards 13PD (44%). However, activity was lagging due to the non-porous character of the TiO_2 support. The porosity was increased by subsequently impregnating TiO_2, WO_3 and platinum on SiO_2. This increased the 13PD selectivity (51%) and doubled catalyst activity (conversion 15%) (Table 2, entry 20). [55] It was found that TiO_2 was responsible for a good dispersity of the platinum particles while the WO_3 provided the Brønsted acidic sites, necessary for 13PD selectivity.

Huang *et al.* used the heteropoly acid silicotungstic acid (STA) as the tungsten source for their hydrogenolysis catalyst. This superacid was impregnated onto SiO_2 to give STA/SiO_2. In a subsequent step, copper was impregnated, to introduce the hydrogenation metal. A vapour phase reaction is necessary since STA is soluble in H_2O and would wash out of the catalyst if aqueous glycerol was used. This $Cu\text{-}STA/SiO_2$ catalyst was tested in a vapour phase fixed-bed reactor and gave high conversion (83%) and good 13PD selectivity (32%). [56] However, the 13PD/12PD ratio was much lower (1.4) compared to the previous catalyst, but is still very impressive for the abundantly available copper catalyst (Table 2, entry 21).

3.2.4.2 RHENIUM

In an initial screening by Furikado *et al.*, Rh/SiO_2 was found to give most hydrogenolysis products from 12 catalysts tested (Rh, Ru, Pt and Pd on SiO_2, Al_2O_3 and C) at a relatively low temperature (393 K). Al_2O_3 was not effective under the conditions used. This was due to more demanding pre-reducing conditions of Al_2O_3 supported catalysts. [57]

The addition of Amberlyst 15 improved the catalytic activity of Rh/SiO_2. Earlier, the same group established this enhancing effect of the sulfonic acid resin for Ru/C. [28] However, so far both the Ru/C and Rh/SiO_2 catalyst are more selective for 12PD, even though Rh/SiO_2 showed 10% 13PD selectivity (Table 2, entry 22). [57] Interestingly, a degradation study showed that 13PD is dehydrated over Ru/C, whilst this is limited over Rh/SiO_2, opening up new opportunities for a selective 13PD catalyst. [57]

To study the effect of tungsten, molybdenum and rhenium as additives, these metals were impregnated onto Rh/SiO_2. All three additives increase activity, but this is most pronounced for rhenium. Both rhenium and tungsten increase 13PD selectivity, while this effect is not observed for molybdenum containing catalysts (Table 2, entries 23 to 25). [58,59]

Due to both activity and selectivity enhancement of the catalyst by ReO_x, the $Rh\text{-}ReO_x/SiO_2$ catalyst was characterized in more detail. EXAFS analysis revealed that Re is present as Re^{7+} on the calcined catalyst, while the reductive pre-treatment reduced rhenium to an oxidation state of Re^{2+} to $Re^{2.5+}$. This pre-treatment also resulted in a direct contact between Re and Rh and it is suggested that ReO_x clusters are in close contact to Rh particles. [58]

The authors were able to increase the 13PD selectivity tremendously by impregnating rhenium on Ir/SiO_2. However, some additional sulfuric acid was needed, possibly because of the lower hydrogenation activity of iridium. This is unexpected, since the relatively low operating temperature suggests a direct hydrogenolysis involving the ReO_x species, while the sulfuric acid induces an elimination mechanism, which does not show 13PD selectivity. [64] Upon addition of sulfuric acid the conversion of glycerol was increased to 80% at a 13PD selectivity of 48%. Initial 13PD selectivity was as high as 68% and a satisfying 13PD/12PD ratio of 5 was reached (Table 2, entry 26). [60]

Daniel *et al.* prepared a co-impregnated Pt-Re/C catalyst. High temperature catalyst treatment led to higher rhenium incorporation into the platinum particle with minimal metal sintering, which resulted in high 13PD selectivity (34% selectivity at 20% conversion) (Table 2, entry 27 and 28). [61]

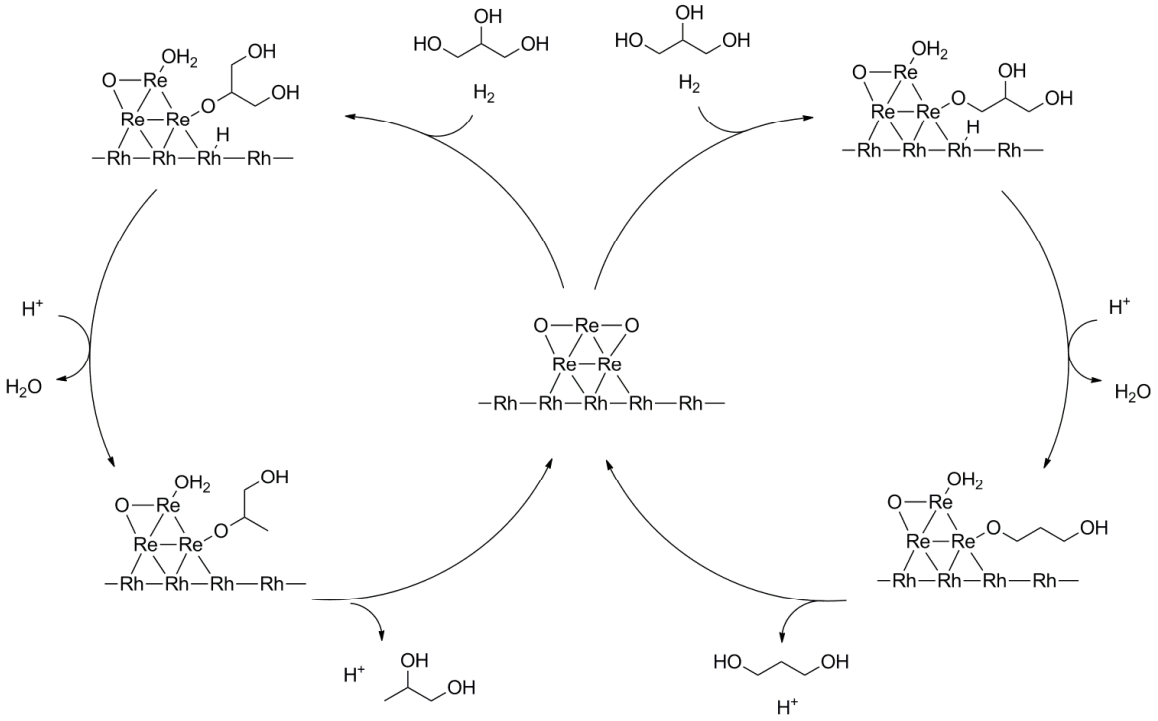

Scheme 14. Proposed mechanism for ReO_x enhanced glycerol conversion and 13PD selectivity.

Tomishige *et al.* proposed a mechanism how rhenium oxide can promote activity and 13PD selectivity (Scheme 14). [58-60,65] Initially, glycerol is adsorbed as an alkoxide species. Subsequently, an acidic proton transforms a hydroxyl group in a leaving group and a hydride, originating from adsorbed hydrogen, expels a water molecule. Finally, propanediol is desorbed and the initial catalyst is recovered. At this point it is not clear which factor determines either 12PD or 13PD selectivity, but it is suggested that the size of the ReO_x particle plays a role in steric selection. [60] It must be noted that in most examples where Re was used as an additive, 12PD selectivity is still higher than 13PD selectivity, while switching to iridium the formation of 13PD was favoured over 12PD formation, depicted in the 13PD to 12PD ratio.

The formation of 13PD is not as straightforward as it seems. It is only formed under acidic conditions and in all cases 12PD formation is observed as a byproduct. In fact, in most examples where 13PD is formed, 12PD is the major product. There are a few examples where 13PD is formed as the major product and most of these processes use platinum as the hydrogenation metal and tungsten as additive. When this combination was used in a continuous reactor a 13PD yield of 32% could be reached, while only a minimal 12PD formation was observed. Another interesting additive with respect to 13PD selectivity is ReO_x. Using this oxide, the reaction temperature could be lowered to 393K, suggesting a direct hydrogenolysis mechanism.

3.3 GLYCEROL TO ACROLEIN

Current industrial acrolein production is based on the oxidation of propene over $BiMoO_x$-based catalysts. [66] Acrolein itself is mainly used as a precursor for *DL*-methionine synthesis. This essential amino acid cannot be synthesized by mammals and is therefore added to animal feed to accelerate growth. Acrolein production from glycerol is a promising alternative route and involves total dehydration of glycerol. Acrolein can be formed either in the liquid phase or in the gas phase. Generally, the gas phase gives higher acrolein yields. The process is normally performed in a continuous reactor, which can prevent further reactions of the reactive acrolein. An excellent recent review on acrolein from glycerol shows that high conversions and selectivities are already obtained using various catalysts, reactor types and reaction phases (Table 3, entries 1 to 8). [67] However, a general challenge for efficient catalysts is to decrease coke formation or circumvent catalyst deactivation in another way. By tuning the pore sizes of the catalyst, the catalyst lifetime can be extended. [68]

3.3.1 REACTION MECHANISM

The acrolein formation pathway closely resembles the dehydration-hydrogenation pathway of 13PD formation. Instead of hydrogenating the 3-hydroxypropanal, another hydroxyl group is eliminated, resulting in the stable π-system of acrolein (Scheme 15). Therefore it is not surprising that acidity is the key in catalyst activity and selectivity. Strong acidity will lead to higher activity. However, acrolein selectivity can decrease due to coke formation.

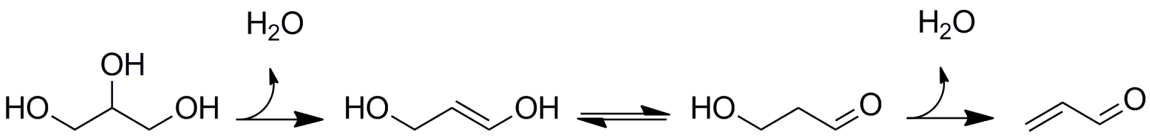

Scheme 15. Acrolein formation mechanism.

Chai *et al.* published a guiding article in which they tested numerous materials, ranging from alkaline to highly acidic catalysts. They concluded that catalysts having a Hammett acidity function (H_0) between -8.2 ≤ H_0 ≤ -3.0 were most effective in selective glycerol dehydration, giving acrolein selectivities between 60

and 70%. Catalysts with stronger acid sites ($H_0 \leq -8.2$) or weaker acid sites ($-3.0 \leq H_0 \leq 6.8$) gave lower acrolein selectivities due to coke deposition during the reaction. Their data also implied that Brønsted acidic catalysts were more effective than Lewis acidic catalysts. Alkaline catalysts were found to be ineffective for acrolein formation. Interestingly, their most successful catalyst (WO_3/ZrO_2) is the support material of the most successful 13PD catalyst (Table 3, entry 9). [69] This is not surprising, since the first step is identical to the 13PD formation (Scheme 13).

Table 3. Acrolein from glycerol

Entry	Catalyst	Additive	Time on stream (h)	WHSV[a] (h^{-1})	*P* (bar)	*T* (K)	Reactor type	Phase	Conversion (%)	Selectivity Acrolein (%)	Yield Acrolein (%)
1[67]	STA/SiO_2	-	5	n.a.	1	548	Continuous	Gas	100	87.0	87.0
2[67]	$Nd_4(P_2O_7)_3$	-	8	227[b]	1	593	Continuous	Gas	87.2	79.9	69.7
3[67]	$Gd_4(P_2O_7)_3$	-	8	227[b]	1	593	Continuous	Gas	88.2	78.9	69.6
4[67]	$Sm_4(P_2O_7)_3$	-	8	227[b]	1	593	Continuous	Gas	89.7	77.8	69.8
5[67]	ZSM-5	-	n.a.	n.a.	1	588	Continuous	Gas	98.3	74.9	73.6
6[67]	H_2SO_4	-	n.a.	n.a.	345	673	Continuous	Supercritical	92.0	80.4	74.0
7[67]	H_2SO_4	-	n.a.	n.a.	345	623	Batch	Liquid	55.0	86.0	47.3
8[67]	$ZnSO_4$	-	n.a	n.a.	250	633	Continuous	Liquid	50.0	75.0	37.5
9[69]	WO_3/ZrO_2	-	10	80[b]	1	588	Continuous	Gas	100	65.0	65.0
10[70]	Nb_2O_5	-	10	80[b]	1	588	Continuous	Gas	88.0	51.0	44.9
11[71]	Nb_2O_5-SiO_2	-	2	80	1	593	Continuous	Gas	100	65.0	65.0
12[72]	ZSM-5	-	2	7.2	1	588	Continuous	Gas	93.7	57.4	53.8
13[73]	TiAl	-	10	400[b]	1	588	Continuous	Gas	67.0	52.0	34.8
14[73]	TiZr	-	10	400[b]	1	588	Continuous	Gas	60.0	45.0	27.0
15[74]	STA/SiO_2	-	5	0.6	1	548	Continuous	Gas	98.3	86.2	84.7
26[75,76]	PTA/ZrO_2	-	10	400[b]	1	588	Continuous	Gas	76.0	71.0	54.0
17[7]	CsPTA	-	1	2.8	1	548	Continuous	Gas	100	98.0	98.0
18[7]	CsPTA	-	5	2.8	1	548	Continuous	Gas	41.0	94.0	38.5
19[7]	Pd/CsPTA	H_2	5	2.8	1	548	Continuous	Gas	79.0	96.0	75.8
20[77]	ZrNbO	-	48	0.5	1	573	Continuous	Gas	99.0	72.0	71.3
21[78]	$VOHPO_4$	O_2	10	0.5	1	573	Continuous	Gas	100	66.0	66.0
22[79]	VPO	O_2	10	0.5	1	573	Continuous	Gas	100	64.0	64.0
23[80]	ZSM-5	-	n.a.	335	1	623	Continuous	Gas	100	62.1	62.1

[a] Weight Hourly Space Volume ($mass_{glycerol} \cdot mass_{catalyst}^{-1} \cdot h^{-1}$) [b] Gas Hourly Space Volume ($V_{feed} \cdot V_{catalyst}^{-1} \cdot h^{-1}$).

3.3.2 ACIDITY AND PORE SIZE MANIPULATION TO IMPROVE CATALYST PERFORMANCE

Niobium oxide is a suitable material to show the effect of the acidity of the material on acrolein formation. The acidity of the material can be controlled by choosing an appropriate calcination temperature. A relatively low calcination temperature gives the highest amount of relevant acidic sites ($-8.2 \leq H_0 \leq -3.0$). And indeed, these catalysts gave the highest acrolein selectivity (51% selectivity at 88% glycerol conversion) (Table 3, entry 10). [70] Another group was able to improve the niobium based catalyst, through impregnation on SiO_2. Initially, the catalyst reached 65% selectivity, at 100% conversion, but this dropped to 50% conversion after 10 hours of operation (Table 3, entry 11). [71]

The number and strength of acidic sites can also be tuned by changing the Si/Al ratio in H-ZSM-5. Na-ZSM-5, effectively blocking the Brønsted acidic sites, gave less than 1% acrolein, proving the importance of this acid type.

Of the H-ZSM-5 with Si/Al ratios 30, 60, 150, 500 and 1000, the ZSM-5 150 was most effective. This implies again an optimum in acidity for acrolein formation. The best catalyst reached 94% conversion and 57% acrolein selectivity during the initial two hours of reaction, and after 12 hours a selectivity of 46% at 39% glycerol conversion remained. This strong deactivation is caused by pore blocking due to coke formation (Table 3, entry 12). [72]

Obviously, tuning of acidity is not the only relevant parameter. This was demonstrated by the synthesis of bimetallic catalysts, consisting of combinations of Sn, Ti, Zr, Al, Si and Zn oxides, with different acidities. Some of the catalysts with the appropriate acidity between $-8.2 \leq H_0 \leq -3.0$ did not perform as well as expected. This could be explained by the micro pores present in these catalysts. These small pores were easily blocked by coke formation and could retain the formed acrolein to facilitate secondary reactions (Table 3, entries 13 and 14). [73]

This effect was also noticed by Tsukuda *et al.*. A series of SiO_2 supported silicotungstic acids (STA) showed improved performance, both in activity and selectivity, when the pore sizes where increased from 3 to 10 nm. Their STA/SiO_2 with an average pore size of 10 nm showed an excellent conversion (98%) and very high acrolein selectivity (86%) during the first 5 hours of reaction (Table 3, entry 15). [74]

In another paper by Chai *et al.*, the performance of phosphotungstic acid (PTA) on SiO_2 and ZrO_2 was compared. PTA on ZrO_2 showed superior activity and selectivity and was able to produce a 54% yield, even after 10 hours on stream. This is explained by the higher stability and dispersion of the PTA on the ZrO_2 surface, compared to the SiO_2 carrier (Table 3, entry 16). [75,76]

PTA can be used as a heterogeneous catalyst by preparing its insoluble caesium salt. Its initial performance is outstanding: 98% yield during the first hour of reaction (Table 3, entry 17). However, the catalyst is prone to severe deactivation due to coking. Selectivity, on the other hand, could be maintained (Table 3,

entry 18). Coking could be delayed by impregnation of the CsPTA with a small amount of palladium and co-feeding with hydrogen. In this way a conversion of 79% accompanied by a selectivity of 96% could be reached (Table 3, entry 19). [7]

3.3.3 CATALYST DEACTIVATION

All catalysts mentioned previously suffer from deactivation due to coke formation which is unavoidable due to the acidic nature of the catalysts and the elevated temperature. Interestingly, the deactivation of a co-precipitated ZrNbO catalyst was very limited compared to impregnated NbO_x/ZrO_2 catalyst. A high glycerol conversion and acrolein selectivity could be maintained for over 48 hours (Table 3, entry 20), which was explained by the formation of a solid solution of Nb into the ZrO_2 due to the ZrNbO synthesis method. [77]

Loading CsPTA with a platinum group metal and co-feeding hydrogen, as demonstrated in a previous example, is one possibility to readily remove the formed coke from the catalyst. However, adding precious metal and the introduction of a reductive atmosphere is not ideal.

Another possibility is to oxidize the formed coke, by adding oxygen. This was done by Wang *et al.* over a vanadium phosphate oxide (VPO) and a vanadium oxide hydrophosphate ($VOHPO_4$) catalyst. In this case, the oxygen present in the feed can also re-oxidize vanadium to its active form. By adding oxygen, the conversion was increased from 43% to 100% and selectivity from 35% to 66% (Table 3, entry 21 and 22). In theory, acrolein could also be oxidized to acrylic acid, an important monomer in polymer chemistry. However, in this case only small amounts of acrylic acid were formed. [78,79]

A technological solution for the coking problem would be an FCC type reactor. In these reactors both catalyst and substrate are continuously fed to the reactor and separated afterwards. This allows for catalyst regeneration outside process conditions. This opens up the opportunity to burn off the coke and then feed the regenerated catalyst to the reactor. This type of operation was simulated by Corma *et al.* using a moving bed reactor. In this reactor catalyst and substrate are fed simultaneously, however the catalyst regeneration unit and re-feeding unit is absent. This resulted in 62% selectivity at 100% conversion, using H-ZSM-5 as a catalyst (Table 3, entry 23). The advantage of this type of operation is that while the catalyst is regenerated by burning off the coke, the produced heat is used to maintain the process temperate. [80]

Acidity and porosity are the main parameters that influence activity and selectivity of the catalyst. These can be effectively controlled and high acrolein yields can be obtained. However, the catalysts have only a limited lifetime due to coke formation during the reaction. Interestingly, highly selective acrolein catalysts often consist of a tungsten containing heteropolyacid. These materials show 13PD selectivity in combination with a hydrogenation catalyst. This can be explained by the identical initial steps in both acrolein and 13PD formation.

3.4 GLYCEROL TO OTHER PRODUCTS

3.4.1 LACTIC ACID

Most papers on deoxygenation of glycerol concern the formation of either 1,2-propanediol, 1,3-propanediol or acrolein. However, there are some other interesting possibilities. For instance, in case 1,2-propanediol is produced under alkaline conditions, lactic acid is often found as a side product. [81,82]

Lactic acid is a widely used chemical in the food, pharmaceutical and chemical industries. The demand for lactic acid increases, mainly due to the use of polylactic acid as a biodegradable polymer. Currently, lactic acid is produced through the fermentation of carbohydrates. However, this process can be more efficient and other, alternative routes should be investigated.

The fact that lactic acid, having an oxidized carbon, is formed under reductive conditions seems somewhat strange at first, but the observation that this only occurs under alkaline conditions is a clue to its formation process. This resembles the 1,2-propanediol formation (Scheme 10), but instead of being reduced after dehydration, the intermediate is subjected to a disproportionation via an intramolecular Cannizzaro reaction. [83] The metallic catalyst is necessary for the initial dehydrogenation, which allows lower reaction temperatures compared to the hydrothermal formation of lactic acid (Scheme 16). [84]

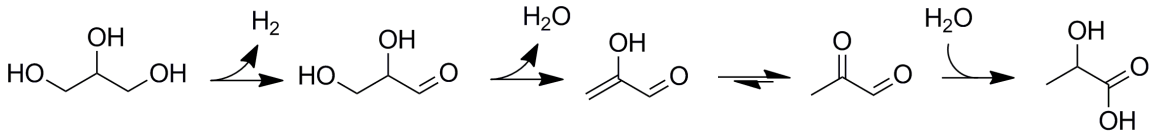

Scheme 16. Lactic acid formation from glycerol via base catalyzed intramolecular Cannizzaro reaction.

However, lactic acid is normally formed under oxidative conditions, which do not need high temperatures for dehydrogenation. [85] Under oxidative conditions, glycerol is readily oxidized to glyceraldehyde. The art lies in facilitating the subsequent dehydration, which will yield lactic acid, instead of oxidation, to yield glyceric acid (Scheme 17). [85]

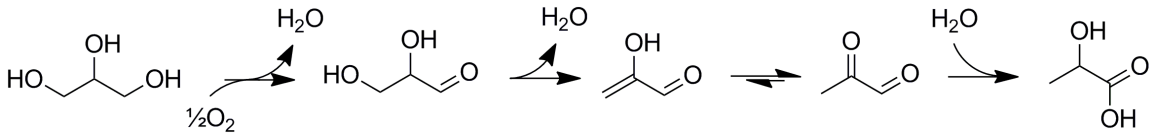

Scheme 17. Lactic acid formation under oxidative conditions.

3.4.2 AROMATICS

In case aromatics are mentioned in combination with biomass, one immediately thinks of lignin. Lignin is abundant in wood and its amount is only surpassed by cellulose. However, lignin consists of a mix of methoxylated monolignols and needs to be degraded into a multitude of chemicals, before it can be processed further. Such a complex feed will hinder the selective formation of useful products.

Therefore, it is an interesting development that propanal can be converted into aromatics over zeolitic catalysts. [86-88] Aromatics are supposedly formed via a series of subsequent aldol and elimination reactions. The resulting unsaturated aldehyde is then ring-closed and elimination of the final hydroxyl yields the aromatic ring system. [87] The catalyst stability can be influenced by adjusting the pore size of the H-ZSM-5 by desilication. Mildly desilicated catalyst performed best in terms of inhibiting coke formation and showed satisfying selectivity towards aromatic compounds.

Aromatics can also be formed directly from glycerol, by initial dehydroxylation or dehydration followed by the aldol condensation sequence mentioned above. Three dimensional HY and H-ZSM-5 showed aromatics formation, indicating that the pore intersections are important in aromatics formation. The aromatics yield was improved by using a dual bed Pd/ZnO-H-ZSM-5 catalytic system, by partially deoxygenating glycerol over Pd/ZnO before it is fed to H-ZSM-5. [89]

This method leads to a mixture of aromatics, which need to be purified when used as chemicals but can directly be applied as fuels, representing an interesting lead towards aromatics from biomass, without using lignin.

3.4.3 ACRYLONITRILE

Obviously, conversion of glycerol and carbohydrates leads to compounds consisting of hydrogen, carbon and oxygen. Bio-based molecules that have nitrogen containing functional groups normally originate from amino acids. The formation of acrylonitrile from glycerol is not only an interesting reaction because a nitrogen functionality is introduced, but also because acrylonitrile is a monomer for polyacrylonitrile and starting material for acrylamide and acrylic acid.

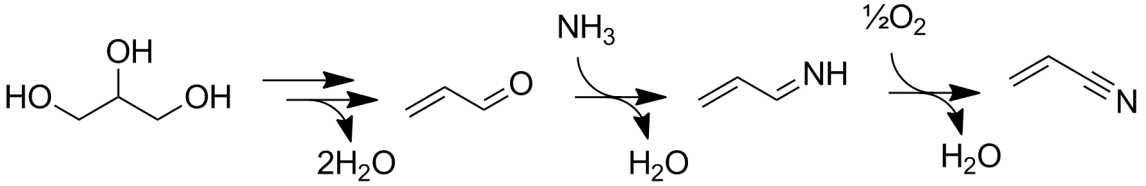

Scheme 18. Ammoxidation of glycerol.

Glycerol can be converted (83% conversion) into acrylonitrile (58% selectivity) in vapour phase over a VSbNb/Al catalyst while co-fed with ammonia and oxygen. The reaction occurs in two stages. First,

acrolein is formed, after which ammonia is inserted in a condensation and oxidation (Scheme 18). The vanadium provides activity in the reaction, while the antimony and niobium are important for acrylonitrile selectivity. [90]

Glycerol ammoxidation can be performed in liquid phase when promoted by microwave irradiation. In this case ammoniumhydroxide is used as the nitrogen source and hydrogen peroxide is used as a soluble oxidizing agent. An acrylonitrile selectivity of 84% can be reached at 47% glycerol conversion. [91]

3.4.4 EPICHLOROHYDRIN

Before glycerol became abundantly available through the transesterification of fats, it was chemically produced via epichlorohydrin. Illustrative is the fact that nowadays epichlorohydrin is available from glycerol and is used as a component in epoxy resins. Glycerol can be selectively converted into α,γ-dichlorohydrin, using gaseous hydrochloric acid and a carboxylic acid catalyst (Scheme 19). Epichlorohydrin can be obtained by treating the dichlorohydrin with base. [92]

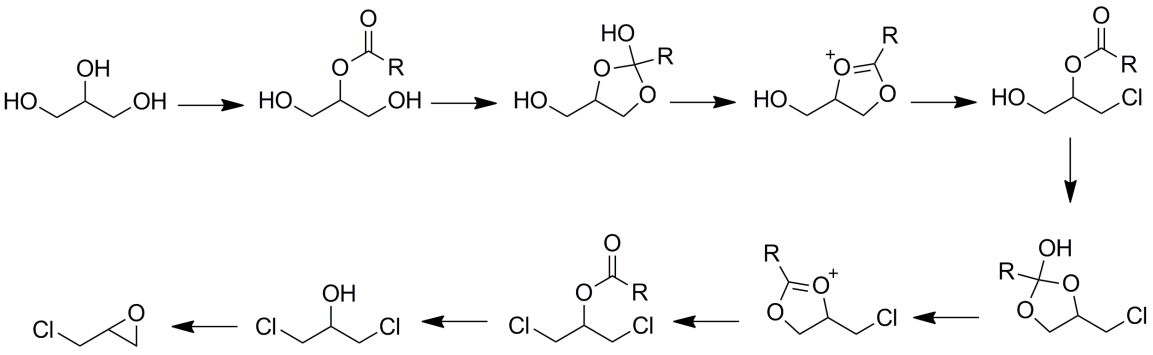

Scheme 19. α,γ-Dichlorohydrin formation from glycerol.

The selectivity towards α,γ-dichlorohydrin is a result of the carboxylic acid catalyst. This is an advantage over the less selective formation from allylchloride, since the α,γ-dichlorohydrin is 10 times more reactive in epichlorohydrin formation than its α,β-counterpart. [93,94]

3.4.5 ETHYLENE GLYCOL

Ethylene glycol is often observed as a byproduct in propanediol formation from glycerol. It is used in high quantities as a starting material for PET, a polyester used in the manufacturing of drinking bottles. However, the formation of ethylene glycol is a result of a C-C bond cleavage, which is an inefficient use of glycerol feedstock and its formation has to be suppressed to allow for higher propanediol selectivities.

The formation of ethylene glycol proceeds via a retro-aldol condensation, followed by a hydrogenation (Scheme 20). [13] The formation of ethylene glycol is influenced by the type of metal that is used. For instance, higher amounts of ethylene glycol are formed upon addition of platinum to a Ni/Al_2O_3 catalyst. [95] Ethylene glycol formation is also more pronounced on ruthenium catalysts, while copper catalysts are

normally very selective towards 12PD. These are indications that ethylene glycol can also be formed by a deformylation pathway.

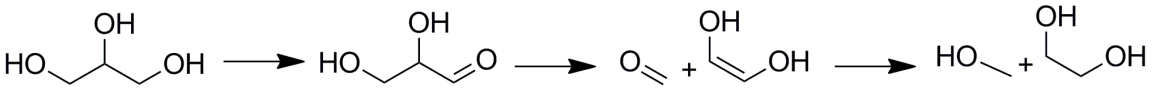

Scheme 20. Ethylene glycol formation via retro aldol.

4 LONGER CHAIN POLYOLS

A considerable research effort has been directed to the conversion of glycerol. It is the smallest polyol readily available from biomass. Despite its limited size it already offers a plethora of possible products. Compared to cellulose, constituting 35 - 50% of total biomass, glycerol is only a minor component. Before cellulose can be used as a starting material for chemicals, it has to be broken down into its glucose monomers. Current research focuses on heterogeneous acidic catalysts for the hydrolysis of cellulose. [96-98] One of the encountered problems is the crystallinity of cellulose. This order in the cellulose fiber hinders the accessibility of the 1,4-glucosidic bond for hydrolysis.

However, its abundance in biomass is not proportional to the amount of research focusing on the conversion of cellulose derived glucose to chemicals. This is a result of the complexity of glucose compared to glycerol. Besides its additional hydroxyl groups, it also has an aldehyde functionality, which significantly increases the challenge of selective glucose conversion. This challenge is often met by hydrogenating glucose to sorbitol, thereby greatly reducing the reaction possibilities.

Employing an acidic catalyst, sorbitol can be converted into isosorbide via a stepwise dehydration via 1,4-anhydrosorbitol.[99] However, the protons needed for acid catalyzed dehydration can also be directly provided by high temperature water, thereby avoiding the addition of a separate acidic catalyst.[100] By combining a reduction catalyst with an acidic catalyst, cellulose can also directly be converted into isosorbide, merging the cellulose hydrolysis, glucose reduction and sorbitol dehydration into one process. [101]

A strategy employed by the group of Dumesic is to reduce the functionality of sorbitol and glucose through hydrodeoxygenation over a PtRe/C catalyst. PtRe/C is both a deoxygenating and reforming catalyst, providing the hydrogen for hydrogenation reactions. This combination of reactivity yields alkanes and a scale of mono-functional chemicals, like mono-alcohols, heterocycles, ketones and acids. Due to their extensive deoxygenation (80% of initial oxygen removed) they phase separate from water, which facilitates the subsequent upgrading to fuel and chemicals. [102,103]

For instance, a dual-bed catalytic system was used to convert the mono-functional chemical stream from the PtRe/C catalyst into C_7 to C_{12+} molecules. A $CeZrO_x$ catalyst was used for ketonization of the

carboxylic acid feed, while Pd/ZrO_2 was used as an aldol condensation and hydrogenation catalyst. The resulting C-C coupled products were finally dehydrated and hydrogenated over Pt/SiO_2-Al_2O_3 to give diesel-like alkanes. [104]

C-O bond cleavage and hydrogenation are the reactions that form the basis of aqueous phase hydrodeoxygenation. Often, sometimes unwanted, C-C bond scission is also observed. Li and Huber sought to clarify the reaction pathways in aqueous phase hydrodeoxygenation over a Pt/SiO_2-Al_2O_3 catalyst by studying these three reaction types. They found that C-O bond cleavage mainly occurs via dehydration over Brønsted acidic sites while C-C bond scissions involve a retro-aldol condensation or decarbonylation over Pt metallic surface. By using these three reactions they were able to construct a degradation pathway for sorbitol and they foresee that the product selectivity can be altered by tuning the activity of individual reactions. [105]

In case sorbitol is treated under alkaline hydrogenating conditions it is subjected to C-C bond scission through a retro-aldol reaction and subsequent hydrogenation (Scheme 21) similar to the formation of ethylene glycol. [13] In 1958 Clark reported the formation of 12PD, ethylene glycol and glycerol using a Ni/kieselguhr catalyst and $Ca(OH)_2$ as an additive. [106] Back then, the formation of glycerol was the main objective, while nowadays the formation of both 12PD and ethylene glycol is preferred.

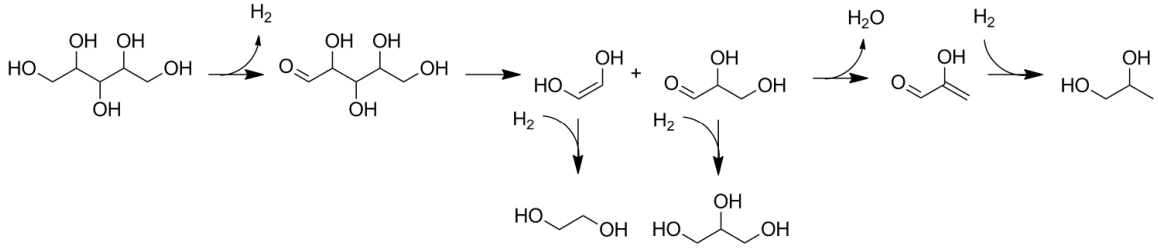

Scheme 21. Xylitol hydrogenolysis under alkaline conditions.

Sorbitol can be converted into mainly 12PD using Ni/NaY as a catalyst (66% conversion, 62% 12PD selectivity), while Pt/NaY yields primarily glycerol (43% conversion, 62% glycerol selectivity). The addition of $Ca(OH)_2$ increases the conversion of sorbitol in both cases (to 75% and 60% conversion, respectively). It is postulated that the difference in product selectivity is a result from other modes of adsorbtion of sorbitol over the two metals. [107]

Employing a Ru/CNF catalyst (CNF = carbon nanofiber) with $Ca(OH)_2$ as a promoter, Zhou *et al.* were able to form ethylene glycol, 12PD and glycerol. The benefits of using CNF instead of normal carbonaceous support are the higher dispersity of metal on the carbon surface and the limited amount of micropores in CNF, which cause mass transfer limitations. [108,109] Similar conditions can be applied using xylitol as a starting material. This will also yield mainly 12PD, ethylene glycol and glycerol. However, lactic acid is observed as a major product as well. Sun *et al.* found that the activity increased using the following metals: Rh > Pd > Ru > Pt. The support of ruthenium catalysts influenced activity as well (TiO_2

> ZrO_2 > $Mg_2Al_2O_x$ > Al_2O_3 > C) and lactic acid selectivity increased upon increased basicity of the support. [110]

Another interesting process is the formation of 5-hydroxymethylfurfural (HMF) by dehydration of fructose. [111] Riisager demonstrated the conversion of aqueous solutions of fructose and hydrochloric acid by microwave irradiation. The advantage of microwave irradiation lies in swift and precise heating and could thereby increase the formation rate of HMF, compared to thermal heating. The product distribution was comparable for the two heating methods, which proved microwave irradiation to be an efficient alternative heating method. [112]

In another paper by the same group, fructose was converted into HMF using boric acid as an additive. Boric acid is not sufficiently acidic in itself for fructose dehydration. However, by forming borate esters with fructose, the reaction mixture is acidified through a shift in equilibrium and HMF is readily formed. The addition of sodium chloride further improved HMF yield. This was ascribed to a salting-out effect in the two-phase system. By increasing the extraction of the formed HMF it is no longer prone to rehydration due to a shift of the equilibrium. [113]

Obviously, formation of HMF from glucose instead of fructose would be preferred from an availability point of view, since glucose can be generated from cellulose. However, this calls for the isomerization of glucose into fructose, prior to dehydration. This isomerization is catalyzed by alkaline sites, while the formed fructose is dehydrated to HMF on acidic sites. Yan *et al.* synthesized a SO_4^{2-}/ZrO_2-Al_2O_3 catalyst that bears both alkaline and acidic sites, and were thereby able to directly convert glucose into HMF in a 48% yield, using DMSO as a solvent. [114]

Zhao *et al.* were able to generate a remarkable HMF yield of 68% from glucose, by using chromium dichloride as a catalyst and an imidazolium-based ionic liquid as a solvent. The benefit of using an ionic liquid as a solvent is twofold. Firstly, HMF degradation is minimized by minimizing water interactions. Secondly, and more importantly, the imidazolium ionic liquid takes part in the reaction mechanism (Scheme 22). [115]

Despite extensive catalyst testing, only chromium showed high HMF yields. This metal is thought to form a trichloride anion, with the ionic liquid cation as a counterion. This anion facilitates the conversion of glucose into fructose which is then dehydrated to HMF. [115,116]

Yong *et al.* showed that the addition of sterically hindered carbene ligands, similar to the imidazolium anion of the ionic liquid, could improve the reaction yield even more. These ligands prevent over-coordination, thereby leaving the chromium centre in its most active state, yielding 81% HMF from glucose. [117]

In a communication Binder *et al.* described the formation of HMF from glucose using dimethyl acetamide together with a halide salt as a solvent, thereby circumventing the use of an ionic liquid. They found that

the halide played an important role in the reaction mechanism as a nucleophile, by quenching an intermediate oxonium ion in HMF formation (Scheme 21). Bromide proved to be most efficient and chromium tribromide gave a HMF yield of 80%. [118]

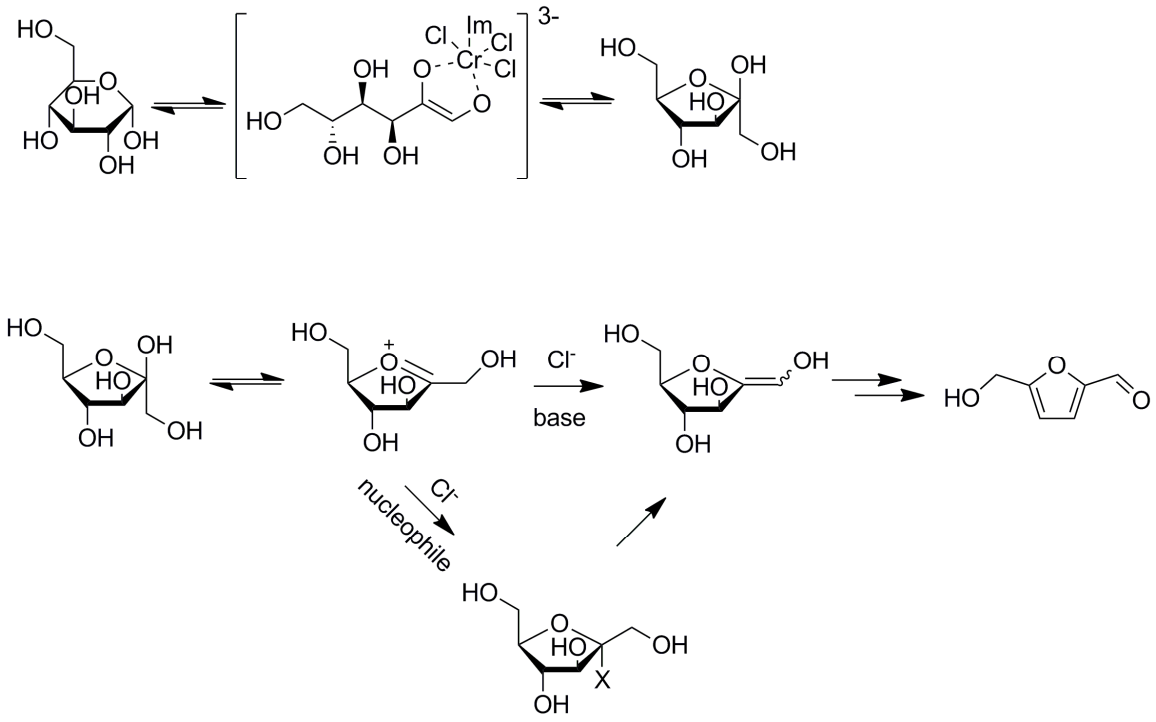

Scheme 22. HMF formation from glucose.

Interestingly, they were also able to convert cellulose directly into HMF. Here, they used additional ionic liquid, to dissolve cellulose. Hydrochloride was added for the hydrolysis of the glucoside bonds. Overall, an impressive yield of 54% HMF from cellulose was obtained. [118]

Another group reported the direct conversion of cellulose into HMF through the addition of $RuCl_3$. The $RuCl_3$ is able to efficiently hydrolyse cellulose to glucose, while $CrCl_2$ is essential for a smooth conversion of glucose into fructose, which is then dehydrated to form HMF. [119]

By substituting toxic chromium dichloride with non-toxic boric acid, Ståhlberg *et al.* were able to convert glucose into HMF. Boric acid lowered the transition state for glucose isomerization through formation of a borate ester. The resulting fructose is subsequently converted into HMF. An HMF yield of 42% could be obtained by using one equivalent of boric acid. Using more boric acid results in the formation of more esters, which are too stable, thereby hindering the HMF formation. [6]

5 CONCLUSION

The majority of research in deoxygenation of polyols has been invested in the conversion of glycerol. This smallest naturally available polyol can be converted into a range of useful chemicals through dehydration, direct hydrogenolysis or a dehydration-hydrogenation sequence.

The major deoxygenation products from glycerol are 12PD, 13PD and acrolein. The formation of these products all have their individual challenges. Acrolein can be formed at both high conversion and selectivity, but the catalysts used for this process suffer from deactivation through coke formation. 12PD can be formed at high selectivities using abundantly available copper as a hydrogenating catalyst and the aim is to increase the conversion. For 13PD it is still the selective formation itself that is a main concern. In this respect the catalysts used for acrolein formation might be a good lead for new catalyst developments, since both acrolein and 13PD share the same initial intermediates.

In principle, these processes can also be applied to longer chain polyols like erithritol and xylitol. However, the wide research field that exists for glycerol is missing. This could be due to the larger challenge to obtain products in a selective way, since the complexity of these C_4 and C_5 polyols is increased by the extension of their carbon backbone. Another reason could be the lower availability of these polyols from biomass. Erithritol is produced from glucose by fermentation and is as such not present in large quantities of biomass. However, xylose is a main constitute of hemicellulose and can be readily converted into xylitol through hydrogenation. But unlike cellulose, hemicellulose is composed of a mix of sugars, which makes purification of these sugars before derivatization desirable.

Sorbitol, on the other hand is readily available from the hydrolysis and subsequent hydrogenation of the formed glucose. The main products from glucose and sorbitol dehydration are hydroxymethylfurfural and isosorbide, respectively. Hydrogenolysis of sorbitol yields ethylene glycol, 12PD and glycerol. One might expect that a broader range of chemicals would be available from these starting materials, obviously the potential of these feedstocks has not yet been realized.

OUTLINE OF THIS THESIS

The work presented in this thesis was focussed on the conversion of glycerol to form 1,3-propanediol and the associated development of bifunctional catalysts. The hydrodeoxygenation of glycerol can yield different isomers and 1,3-propanediol was targeted, as this is more valuable than 1,2-propanediol.

The introductory chapter starts with a general overview of the reactions that lead to the deoxygenation of biomass. It then focuses on glycerol and the different products that can be formed through deoxygenation.

The initial idea of this thesis was to produce 1,3-propanediol by using a boric acid co-catalyst. Boric acid forms borate esters in combination with diols and polyols. It was hypothesised that through the use of a hydrogenation catalyst in combination with boric acid, the selectivity in glycerol borate ester formation could lead to increased 1,3-propanediol selectivity. The determination of the association constants of borate and boronate esters with various diols and glycerol is described in the appendix of Chapter 1. The use of boric acid as a co-catalyst is described in Chapter 1. Design of Experiment methodology allowed an efficient probing of the reaction conditions and showed that 1,2-propanediol and lactic acid could be formed selectively, depending on reaction conditions. However, no 1,3-propanediol was formed.

Chapter 2 uses a Design of Experiment approach to assess the use of tungstic acid as a co-catalyst in the hydrodeoxygenation of glycerol. The tungsten additives that were used in this chapter were tungstic acid and the homogeneous heteropolyacids silicotungstic acid and phosphotungstic acid. The next logical step in the development of a heterogeneous catalyst system for the production of 1,3-propanediol from glycerol was the development of a heterogeneous tungsten catalyst.

Chapter 3 describes the synthesis of two types of such a catalyst. WO_3/TUD-1 is a TUD-1 support that is impregnated with different amounts of WO_3. W-TUD-1 is a heterogeneous catalyst where tungsten is introduced during the TUD-1 synthesis. This yielded a catalyst with increased acidity, due to the high WO_3 dispersion. The catalytic activity of this catalyst was evaluated using the acid catalysed Prins cyclisation of citronellal.

The catalysts that are described in Chapter 3 were used as a catalyst support for a Pt based hydrogenation catalyst, thereby generating a bifunctional catalyst. The synthesis, characterization and catalytic activity of these catalysts are described in Chapter 4. The performance of the bifunctional catalysts was evaluated using the synthesis of menthol from citronellal. A first order rate approximation allowed the comparison of initial reaction rates of these catalysts.

The Summary and Conclusion briefly restates the most important findings in this thesis.

REFERENCES

[1] B. H. Shanks, Ind. Eng. Chem. Res. 2010, 49, 10212.

[2] M. Schlaf, M. E. Thibault, D. DiMondo, D. Taher, E. Karimi, D. Ashok, Int. J. Chem. React. Eng. 2009, 7, A34.

[3] M. Schlaf, Dalton Trans. 2006, 4645.

[4] M. R. Nimlos, S. J. Blanksby, X. H. Qian, M. E. Himmel, D. K. Johnson, J. Phys. Chem. A 2006, 110, 6145.

[5] J. Chaminand, L. Djakovitch, P. Gallezot, P. Marion, C. Pinel, C. Rosier, Green Chem. 2004, 6, 359.

[6] T. Ståhlberg, S. Rodriguez-Rodriguez, P. Fristrup, A. Riisager, Chem. Eur. J. 2011, 17, 1456.

[7] A. Alhanash, E. F. Kozhevnikova, I. V. Kozhevnikov, Appl. Catal. A 2010, 378, 11.

[8] S. Koso, N. Ueda, Y. Shinmi, K. Okumura, T. Kizuka, K. Tomishige, J. Catal. 2009, 267, 89.

[9] K. Y. Chen, S. Koso, T. Kubota, Y. Nakagawa, K. Tomishige, ChemCatChem 2010, 2, 547.

[10] A. Behr, J. Eilting, K. Irawadi, J. Leschinski, F. Lindner, Green Chem. 2008, 10, 13.

[11] J. J. Bozell, G. R. Petersen, Green Chem. 2010, 12, 539.

[12] D. L. Trent in Kirk-Othmer Encyclopedia of chemical technology, Vol. 20 (Ed.: J. I. Kroschwitz), Wiley-Interscience, New York, 1996, pp. 271-302.

[13] C. Montassier, J. C. Ménézo, L. C. Hoang, C. Renaud, J. Barbier, J. Mol. Catal. 1991, 70, 99.

[14] Z. W. Huang, F. Cui, H. X. Kang, J. Chen, C. G. Xia, Appl. Catal.A 2009, 366, 288.

[15] S. A. Wang, Y. C. Zhang, H. C. Liu, Chem. Asian J. 2010, 5, 1100.

[16] D. Coll, F. Delbecq, Y. Aray, P. Sautet, Phys. Chem. Chem. Phys. 2011, 13, 1448.

[17] A. Torres, D. Roy, B. Subramaniam, R. V. Chaudhari, Ind. Eng. Chem. Res. 2010, 49, 10826.

[18] Z. M. Zhou, X. Li, T. Y. Zeng, W. B. Hong, Z. M. Cheng, W. K. Yuan, Chin. J. Chem. Eng. 2010, 18, 384.

[19] E. S. Vasiliadou, A. A. Lemonidou, Appl. Catal. A 2011, 396, 177.

[20] A. Bienholz, H. Hofmann, P. Claus, Appl. Catal. A 2011, 391, 153.

[21] A. Bienholz, F. Schwab, P. Claus, Green Chem. 2010, 12, 290.

[22] A. Bienholz, R. Blume, A. Knop-Gericke, F. Girgsdies, M. Behrens, P. Claus, J. Phys. Chem. C 2011, 115, 999.

[23] S. Wang, H. C. Liu, Catal. Lett. 2007, 117, 62.

[24] Z. L. Yuan, P. Wu, J. Gao, X. Y. Lu, Z. Y. Hou, X. M. Zheng, Catal. Lett. 2009, 130, 261.

[25] Z. L. Yuan, J. H. Wang, L. N. Wang, W. H. Xie, P. Chen, Z. Y. Hou, X. M. Zheng, Bioresour. Technol. 2010, 101, 7088.

[26] Z. L. Yuan, L. N. Wang, J. H. Wang, S. X. Xia, P. Chen, Z. Y. Hou, X. M. Zheng, Appl. Catal. B 2011, 101, 431.

[27] Z. W. Huang, F. Cui, H. X. Kang, J. Chen, X. Z. Zhang, C. G. Xia, Chem. Mater. 2008, 20, 5090.

[28] T. Miyazawa, Y. Kusunoki, K. Kunimori, K. Tomishige, J. Catal. 2006, 240, 213.

[29] T. Miyazawa, S. Koso, K. Kunimori, K. Tomishige, Appl. Catal. A 2007, 329, 30.

[30] T. Miyazawa, S. Koso, K. Kunimori, K. Tomishige, Appl. Catal. A 2007, 318, 244.

[31] M. Balaraju, V. Rekha, P. S. S. Prasad, B. L. A. P. Devi, R. B. N. Prasad, N. Lingaiah, Appl. Catal. A 2009, 354, 82.

[32] M. Balaraju, V. Rekha, B. L. A. P. Devi, R. B. N. Prasad, P. S. S. Prasad, N. Lingaiah, Appl. Catal. A 2010, 384, 107.

[33] L. Y. Guo, J. X. Zhou, J. B. Mao, X. W. Guo, S. G. Zhang, Appl. Catal. A 2009, 367, 93.

[34] J. X. Zhou, L. Y. Guo, X. W. Guo, J. B. Mao, S. G. Zhang, Green Chem. 2010, 12, 1835.

[35] S. L. Hao, W. C. Peng, N. Zhao, F. K. Xiao, W. Wei, Y. H. Sun, J. Chem. Technol. Biotechnol. 2010, 85, 1499.

[36] N. D. Kim, S. Oh, J. B. Joo, K. S. Jung, J. Yi, Top. Catal., 2010, 53, 517.

[37] R. B. Mane, A. M. Hengne, A. A. Ghalwadkar, S. Vijayanand, P. H. Mohite, H. S. Potdar, C. V. Rode, Catal. Lett. 2010, 135, 141.

[38] T. Jiang, Y. X. Zhou, S. G. Liang, H. Z. Liu, B. X. Han, Green Chem. 2009, 11, 1000.

[39] L. Ma, D. H. He, Z. P. Li, Catal. Commun. 2008, 9, 2489.

[40] L. Ma, D. H. He, Top. Catal. 2009, 52, 834.

[41] M. Akiyama, S. Sato, R. Takahashi, K. Inui, M. Yokota, Appl. Catal. A 2009, 371, 60.

[42] S. Sato, M. Akiyama, K. Inui, M. Yokota, Chem. Lett. 2009, 38, 560.

[43] E. D'Hondt, S. Van de Vyver, B. F. Sels, P. A. Jacobs, Chem. Commun. 2008, 6011.

[44] D. Roy, B. Subramaniam, R. V. Chaudhari, Catal. Today 2010, 156, 31.

[45] A. Y. Yin, X. Y. Guo, W. L. Dai, K. N. Fan, Green Chem., 2009, 11, 1514.

[46] N. D. Kim, S. Oh, J. B. Joo, K. S. Jung, J. Yi, Korean J. Chem. Eng. 2010, 27, 431.

[47] L. Ma, D. H. He, Catal. Today 2010, 149, 148.

[48] G. A. Kraus, Clean 2008, 36, 648.

[49] R. K. Saxena, P. Anand, S. Saran, J. Isar, Biotechnol. Adv. 2009, 27, 895.

[50] P. A. Selembo, J. M. Perez, W. A. Lloyd, B. E. Logan, Biotechnol. Bioeng. 2009, 104, 1098.

[51] T. Kurosaka, H. Maruyama, I. Naribayashi, Y. Sasaki, Catal. Commun. 2008, 9, 1360.

[52] L. F. Gong, Y. Lü, Y. J. Ding, R. H. Lin, J. W. Li, W. D. Dong, T. Wang, W. M. Chen, Chin. J. Catal. 2009, 30, 1189.

[53] M. Schlaf, P. Ghosh, P. J. Fagan, E. Hauptman, R. M. Bullock, Angew. Chem., Int. Ed. 2001, 40, 3887.

[54] L. Z. Qin, M. J. Song, C. L. Chen, Green Chem. 2010, 12, 1466.

[55] L. F. Gong, Y. A. Lu, Y. J. Ding, R. H. Lin, J. W. Li, W. D. Dong, T. Wang, W. M. Chen, Appl. Catal A 2010, 390, 119.

[56] L. Huang, Y. L. Zhu, H. Y. Zheng, G. Q. Ding, Y. W. Li, Catal. Lett. 2009, 131, 312.

[57] I. Furikado, T. Miyazawa, S. Koso, A. Shimao, K. Kunimori, K. Tomishige, Green Chem. 2007, 9, 582.

[58] Y. Shinmi, S. Koso, T. Kubota, Y. Nakagawa, K. Tomishige, Appl. Catal. B 2010, 94, 318.

[59] A. Shimao, S. Koso, N. Ueda, Y. Shinmi, I. Furikado, K. Tomishige, Chem. Lett. 2009, 38, 540.

[60] Y. Nakagawa, Y. Shinmi, S. Koso, K. Tomishige, J. Catal. 2010, 272, 191.

[61] O. M. Daniel, A. DeLaRiva, E. L. Kunkes, A. K. Datye, J. A. Dumesic, R. J. Davis, ChemCatChem, 2010, 2, 1107.

[62] S. Triwahyono, A. A. Jalil, H. Hattori, J. Nat. Gas Chem. 2007, 16, 252.

[63] S. Triwahyono, T. Yamada, H. Hattori, Appl. Cat. A 2003, 242, 101.

[64] S. Koso, I. Furikado, A. Shimao, T. Miyazawa, K. Kunimori, K. Tomishige, Chem. Commun. 2009, 2035.

[65] Y. Amada, S. Koso, Y. Nakagawa, K. Tomishige, ChemSusChem 2010, 3, 728.

[66] G. W. Keulks, L. D. Krenzke, T. M. Notermann in Advances in Catalysis, Vol. 27 (Eds.: D. D. Eley, H. Pines, P. B. Weisz), Academic Press, New York, 1979, pp. 183-225.

[67] B. Katryniok, S. Paul, M. Capron, F. Dumeignil, ChemSusChem 2009, 2, 719.

[68] W. Suprun, M. Lutecki, T. Haber, H. Papp, J. Mol. Cat. A: Chem. 2009, 309, 71.

[69] S. H. Chai, H. P. Wang, Y. Liang, B. Q. Xu, Green Chem. 2007, 9, 1130.

[70] S. H. Chai, H. P. Wang, Y. Liang, B. Q. Xu, J. Catal. 2007, 250, 342.

[71] N. R. Shiju, D. R. Brown, K. Wilson, G. Rothenberg, Top. Catal. 2010, 53, 1217.

[72] Y. T. Kim, K. D. Jung, E. D. Park, Microporous Mesoporous Mater. 2010, 131, 28.

[73] L. Z. Tao, S. H. Chai, Y. Zuo, W. T. Zheng, Y. Liang, B. Q. Xu, Catal. Today 2010, 158, 310.

[74] E. Tsukuda, S. Sato, R. Takahashi, T. Sodesawa, Catal. Commun. 2007, 8, 1349.

[75] S. H. Chai, H. P. Wang, Y. Liang, B. Q. Xu, Green Chem. 2008, 10, 1087.

[76] S. H. Chai, H. P. Wang, Y. Liang, B. Q. Xu, Appl. Catal. A 2009, 353, 213.

[77] P. Lauriol-Garbay, J. M. M. Millet, S. Loridant, V. Bellière-Baca, P. Rey, J. Catal. 2011, 280, 68.

[78] F. Wang, J. L. Dubois, W. Ueda, J. Catal. 2009, 268, 260.

[79] F. Wang, J. L. Dubois, W. Ueda, Appl. Catal. A 2010, 376, 25.

[80] A. Corma, G. W. Huber, L. Sauvanaud, P. O'Connor, J. Catal. 2008, 257, 163.

[81] E. P. Maris, R. J. Davis, J. Catal., 2007, 249, 328.

[82] E. P. Maris, W. C. Ketchie, M. Murayama, R. J. Davis, J. Catal. 2007, 251, 281.

[83] P. P. Pescarmona, K. P. F. Janssen, C. Delaet, C. Stroobants, K. Houthoofd, A. Philippaerts, C. D. Jonghe, J. S. Paul, P. A. Jacobs, B. F. Sels, Green Chem. 2010, 12, 1083.

[84] Z. Shen, F. M. Jin, Y. L. Zhang, B. Wu, A. Kishita, K. Tohji, H. Kishida, Ind. Eng. Chem. Res. 2009, 48, 8920.

[85] Y. H. Shen, S. H. Zhang, H. J. Li, Y. Ren, H. C. Liu, Chem. Eur. J. 2010, 16, 7368.

[86] T. Q. Hoang, X. L. Zhu, L. L. Lobban, D. E. Resasco, R. G. Mallinson, Catal. Commun. 2010, 11, 977.

[87] T. Q. Hoang, X. L. Zhu, T. Sooknoi, D. E. Resasco, R. G. Mallinson, J. Catal. 2010, 271, 201.

[88] X. L. Zhu, L. L. Lobban, R. G. Mallinson, D. E. Resasco, J. Catal. 2010, 271, 88.

[89] T. Q. Hoang, X. L. Zhu, T. Danuthai, L. L. Lobban, D. E. Resasco, R. G. Mallinson, Energy Fuels 2010, 24, 3804.

[90] M. O. Guerrero-Pérez, M. A. Bañares, ChemSusChem 2008, 1, 511.

[91] V. Calvino-Casilda, M. O. Guerrero-Pérez, M. A. Bañares, Green Chem. 2009, 11, 939.

[92] B. M. Bell, J. R. Briggs, R. M. Campbell, S. M. Chambers, P. D. Gaarenstroom, J. G. Hippler, B. D. Hook, K. Kearns, J. M. Kenney, W. J. Kruper, D. J. Schreck, C. N. Theriault, C. P. Wolfe, Clean 2008, 36, 657.

[93] E. Santacesaria, R. Tesser, M. Di Serio, L. Casale, D. Verde, Ind. Eng. Chem. Res. 2010, 49, 964.

[94] R. Tesser, E. Santacesaria, M. Di Serio, G. Di Nuzzi, V. Fiandra, Ind. Eng. Chem. Res. 2007, 46, 6456.

[95] N. Ueda, Y. Nakagawa, K. Tomishige, Chem. Lett. 2010, 39, 506.

[96] P. L. Dhepe, A. Fukuoka, ChemSusChem 2008, 1, 969.

[97] R. Rinaldi, F. Schüth, Energy Environm. Sci. 2009, 2, 610.

[98] R. Rinaldi, F. Schüth, ChemSusChem 2009, 2, 1096.

[99] P. Sun, D. H. Yu, Y. Hu, Z. C. Tang, J. J. Xia, H. Li, H. Huang, Korean J. Chem. Eng. 2011, 28, 99.

[100] A. Yamaguchi, N. Hiyoshi, O. Sato, M. Shirai, Green Chem. 2011, 13, 873.

[101] G. F. Liang, C. Y. Wu, L. M. He, J. Ming, H. Y. Cheng, L. H. Zhuo, F. Y. Zhao, Green Chem. 2011, 13, 839.

[102] E. L. Kunkes, D. A. Simonetti, R. M. West, J. C. Serrano-Ruiz, C. A. Gärtner, J. A. Dumesic, Science 2008, 322, 417.

[103] R. M. West, E. L. Kunkes, D. A. Simonetti, J. A. Dumesic, Catal. Today 2009, 147, 115.

[104] E. I. Gürbüz, E. L. Kunkes, J. A. Dumesic, Green Chem. 2010, 12, 223.

[105] N. Li, G. W. Huber, J. Catal. 2010, 270, 48.

[106] I. T. Clark, Ind. Eng. Chem. 1958, 50, 1125.

[107] M. Banu, S. Sivasanker, T. M. Sankaranarayanan, P. Venuvanalingam, Catal. Commun. 2011, 12, 673.

[108] L. Zhao, J. H. Zhou, Z. J. Sui, X. G. Zhou, Chem. Eng. Sci. 2009, 65, 30.

[109] J. H. Zhou, M. G. Zhang, L. Zhao, P. Li, X. G. Zhou, W. K. Yuan, Catal. Today 2009, 147, S225.

[110] J. Y. Sun, H. C. Liu, Green Chem., 2011, 13, 135.

[111] A. A. Rosatella, S. P. Simeonov, R. F. M. Frade, C. A. M. Afonso, Green Chem. 2011, 13, 754.

[112] T. S. Hansen, J. M. Woodley, A. Riisager, Carbohydr. Res. 2009, 344, 2568.

[113] T. S. Hansen, J. Mielby, A. Riisager, Green Chem. 2011, 13, 109.

[114] H. P. Yan, Y. Yang, D. M. Tong, X. Xiang, C. W. Hu, Catal. Commun. 2009, 10, 1558.

[115] H. B. Zhao, J. E. Holladay, H. Brown, Z. C. Zhang, Science 2007, 316, 1597.

[116] T. Ståhlberg, M. G. Sørensen, A. Riisager, Green Chem. 2010, 12, 321.

[117] G. Yong, Y. G. Zhang, J. Y. Ying, Angew. Chem., Int. Ed. 2008, 47, 9345.

[118] J. B. Binder, R. T. Raines, J. Am. Chem. Soc. 2009, 131, 1979.

[119] B. Kim, J. Jeong, D. Lee, S. Kim, H. J. Yoon, Y. S. Lee, J. K. Cho, Green Chem., DOI: 10.1039/c1gc15152e.

CHAPTER 1

TUNING SELECTIVITY OF Pt/$CaCO_3$ IN GLYCEROL HYDROGENOLYSIS – A DESIGN OF EXPERIMENTS APPROACH

This chapter is based on the publication "J. ten Dam, F. Kapteijn, K. Djanashvili and U. Hanefeld, Catalysis Communications 14 (2011) 1-5."

ABSTRACT

19 commercially available catalysts have been effectively screened in only 30 experiments for the hydrogenolysis of glycerol using a D-optimal design. $Pt/CaCO_3$ emerged as both an active and selective catalyst and was studied in greater detail using a Central Composite Design. Upon addition of boric acid, the $Pt/CaCO_3$ product selectivity could be changed from 1,2-propanediol towards lactic acid. The formation of 1,2-propanediol and lactic acid could be optimized by considering the Response Surface Model plots and formation pathways.

Keywords: Design of Experiment; Heterogeneous Catalysis; Glycerol; Boric Acid; 1,2-Propanediol; Lactic Acid.

1 INTRODUCTION

The production of chemicals from biomass is an essential feature of a sustainable future. [1,2] Polyols and sugars constitute a considerable fraction of the available biomass and are therefore an attractive feedstock for bio-based chemicals. [3,4] These oxygen rich starting materials need to be defunctionalized to produce appropriate building blocks for the chemical industry. Hydrogenolysis is a key process to achieve this goal. [5]

Glycerol is an attractive starting material for hydrogenolysis, since it can serve as a model compound for larger polyols and sugars. [6] The added advantage is the economical relevance of its conversion into 1,2-propanediol (12PD) and 1,3-propanediol (13PD), both used in polymer synthesis. [7] Interestingly, glycerol can also yield lactic acid (LA), an oxidation product, under hydrogenolysis conditions. [8,9] This base-induced reaction resembles an intra-molecular Cannizzaro reaction and needs to be taken into consideration in the overall process (Scheme 1). [10]

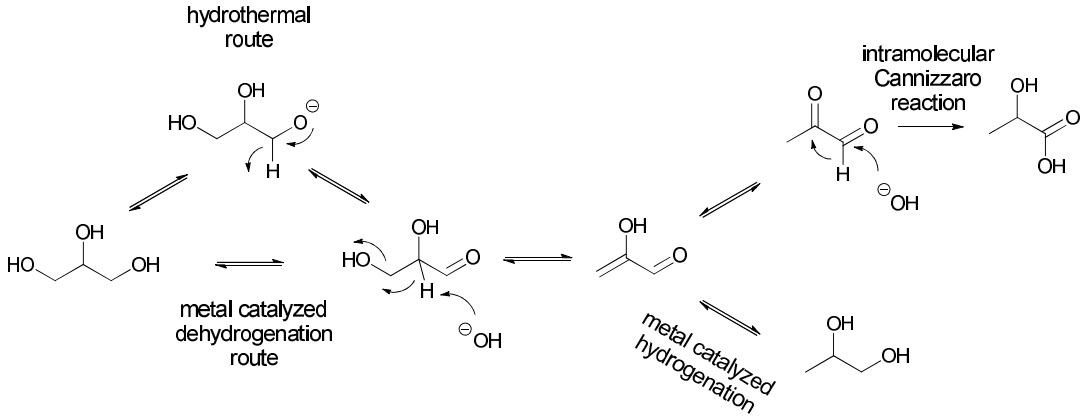

Scheme 1. The formation pathway of 12PD and LA from glycerol.

The aim of this research is to identify a selective catalyst for the hydrogenolysis of glycerol in water, and to achieve a better understanding of the variables influencing its activity and selectivity. Furthermore, we envision the influence of boric acid (BA) on selectivity of catalysts in the hydrogenolysis reaction of glycerol through formation of borate esters in solution, and thereby, leaving a single hydroxyl group accessible for dehydrogenation (Scheme 2). [11]

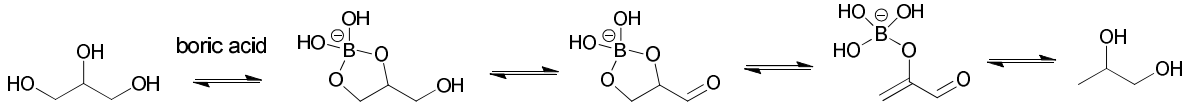

Scheme 2. BA as a hypothetical selectivity inducer through the formation of borate esters.

Numerous papers describe the formation of 12PD through hydrogenolysis of glycerol, employing different catalysts and conditions. [12-19] This led to a general picture of the formation of 12PD. Still, the effect of individual variables is not completely understood. This is where a method such as Design of

Experiments (DoE) can be very efficient to readily determine the influence of several variables on activity and selectivity of the catalysts, and elucidate the effects of BA. [20]

2. EXPERIMENTAL

2.1 MATERIALS

The catalysts used in this work were purchased from Acros Organics (50% Ni/Al_2O_3, 66% Ni/SiO_2, 5% Pd/Al_2O_3, 5% Pd/C, 5% Pt/Al_2O_3, 5% $Pt/CaCO_3$, 5% Rh/Al_2O_3, 5% Rh/C, Sigma Aldrich (5% $Pd/BaSO_4$, 1% Pt/SiO_2, 5% Ru/Al_2O_3, 5% Ru/C), Degussa (5% $Pd/CaCO_3$), Janssen Chimica (5% Pt/C) and Strem (75% Ni/C, 5% Pd/SiO_2), or prepared (5% Ir/C, 5% Rh/SiO_2, 5% Ru/SiO_2) according to the literature. [21]

12PD 99%, *n*-propanol 99.7% (PrOH), ethylene glycol 99.8% (EG), BA 99.99% and sulfolane 99% were purchased from Sigma Aldrich, glycerol 99+% and 1,3-propanediol 98% (13PD) were purchased from Acros Organics, sodium lactate was purchased from Fluka, ethanol 99.8% (EtOH) was purchased from Merck and methanol 99.8% (MeOH) was purchased from J.T. Baker. All chemicals were used as received. The pH was measured using a Metrohm 654 pH-meter. DoE was performed with DesignExpert 7.1.6 from Stat-Ease.

2.2 CATALYST CHARACTERIZATION

Porosity and surface area were determined by nitrogen sorption measurements (Table 1) on a Quantachrome Autosorb-6B at 77 K. Prior to the measurements, the samples were degassed overnight under vacuum at 230 °C using a Quantachrome Autosorb degasser.

2.3 PREPARATION OF STANDARD REACTION MIXTURES

Standard reaction mixtures were prepared by dissolving appropriate amounts of glycerol and BA in demineralized water in the volumetric flask adjusting the pH with 0.1 M aqueous sodium hydroxide (Table S1 and S2, Appendix 1).

2.4 REACTION PROCEDURE

The hydrogenolysis of glycerol was performed in a HEL PolyBLOCK 8, a parallel autoclave reactor system consisting of eight 16 mL vessels. The appropriate amount of catalyst (5 mol% active metal, relative to glycerol) was added to 5 mL of aqueous standard reaction mixture. Reactors were purged 3

Table 1. Loading, porosity and BET surface area of catalysts.

Catalyst	Metal loading (wt%)	V_{pore} (mL/g)	S_{BET} (m^2/g)
Ni/Al_2O_3[a]	50	0.52	209
Pd/Al_2O_3[a]	5	0.24	171
Pt/Al_2O_3[a]	5	0.44	212
Rh/Al_2O_3[a]	5	0.40	150
Ru/Al_2O_3[a]	5	0.38	100
Ni/C[a]	75	0.34	803
Pd/C[a]	5	0.70	951
Pt/C[a]	5	0.68	1010
Rh/C[a]	5	0.77	985
Ru/C[a]	5	0.54	839
Ir/C[b]	5	0.57	954
Ni/SiO_2[a]	66	0.17	104
Pd/SiO_2[a]	5	1.00	221
Pt/SiO_2[a]	1	1.03	236
Rh/SiO_2[a]	5	0.95	247
Ru/SiO_2[a]	5	0.99	324
Pd/$BaSO_4$[b]	5	0.03	10
Pd/$CaCO_3$[b]	5	0.03	8
Pt/$CaCO_3$[b]	5	0.04	11

[a] used in D-optimal design 1; [b] used in D-optimal design 2.

times with N_2 (20 bar) and 3 times with H_2 (40 bar). Then they were pressurized to 40 bar H_2, stirred at 800 rpm and and heated to the reaction temperature within 20 min. Stirring was stopped after 18 h and the reactors were allowed to cool down to room temperature. Then the reaction mixture was filtered over a nylon micro filter (Rotilabo, 0.2 μm). An HPLC sample was prepared by diluting 500 μL filtered reaction mixture using 500 μL 5 mM H_2SO_4. The liquid products were analyzed by HPLC.

2.5 CATALYST RECYCLING

After a standard reaction procedure, the reaction mixture was centrifuged at 900 G using a Heraeus Megafuge 2.0R centrifuge. The supernatant was removed for sampling and 5.5 mL fresh reaction mixture was added to the centrifuged catalyst. 0.5 mL reaction mixture was taken for t = 0 h HPLC sample and the remaining reaction mixture was submitted to a second run, using the standard reaction procedure.

2.6 TEM MEASUREMENTS

Transmission electron microscopy (TEM) was performed using a FEI Tecnai TF20 electron microscope with a field emission gun as the source of electrons operated at 200 kV. Samples were mounted on

Quantifoil® carbon polymer supported on a copper grid by placing a few droplets of a suspension of ground sample in ethanol on the grid, followed by drying at ambient conditions.

2.7 HPLC METHOD

Samples were analyzed on a CARBOSep COREGEL-87H3 column using a Waters 515 HPLC pump (0.8 mL·min^{-1}) equipped with a Shodex RI SE-61 detector, a Perkin Elmer Series 200 Autosampler (10 µL injection) and a Chrompack HPLC column thermostat SpH 99 (70 °C). 5 mM H_2SO_4 (pH 1.5) in demineralized water was used as eluens. This resulted in the following retention times: 8.3 (BA), 9.3 (LA), 9.9 (glycerol), 11.9 (EG), 12.7 (12PD), 13.0 (13PD), 14.2 (MeOH), 16.2 (EtOH) and 19.8 min (PrOH). [22] Calibration curves of these analytes were constructed to analyze the product concentrations. Products detected by HPLC were 12PD, LA, EG and EtOH. Conversion (*C*) and selectivity ($S_{analyte}$) were calculated by equations (1) and (2), respectively.

$$C = \frac{[\text{glycerol}]_0 - [\text{glycerol}]_x}{[\text{glycerol}]_0} \cdot 100 \qquad \textbf{(1)}$$

$$S_{\text{analyte}} = \frac{\left([\text{analyte}]_x \Big/ [\text{glycerol}]_0 \right) \cdot 100}{C} \cdot 100 \qquad \textbf{(2)}$$

where $[\text{glycerol}]_x$ and $[\text{analyte}]_x$ stand for glycerol and analyte concentration at reaction time *x* in hours. Degradation accounts for the formation of gaseous products and is calculated using equation (3). In this case it is assumed that

$$\text{degradation} = 100 - \sum_{\text{analyte}} S_{\text{analyte}} \qquad \textbf{(3)}$$

3. RESULTS AND DISCUSSION

3.1 D-OPTIMAL DESIGN

A series of variables (temperature, pH, additive) and 19 heterogeneous catalysts, with comparable porosity and surface area within each support class (Table 1), were screened for hydrogenolysis activity, using a DoE approach to optimize the experimental effort. Temperature was chosen for its expected influence on the conversion of glycerol, while the effect of pH influences the equilibrium reaction of glycerol with BA and can therefore affect the overall reaction as well. Sulfolane has been shown to have an influence on reaction selectivity and was therefore included in this initial screening.

Factorial designs or fractional factorial designs can be used in case of screening of continuous variables, such as pH and temperature. However, in this case some of the variables are discrete (active metal and support type), for which a D-optimal design is more efficient. This is due to the fact that a complete factorial is needed for every combination of discrete variables, which hugely increases the experimental effort. The aim of the initial D-optimal screenings was to evaluate the main influence of the individual variables, which results in a minimal amount of experiments. For this reason, the amount of continuous variables was limited to three. The design will result in a model by fitting the experimental data in a polynomial, which will only describe the main variables in the form of a first order polynomial (equation 4).

$$y = \beta_0 + \beta_1 x_1 + \beta_2 x_2 + \varepsilon \qquad \textbf{(4)}$$

Here, y is the response (in this case glycerol conversion), x_i is variable i, β_0 is the intercept and β_i is the coefficient of variable i and ε includes the experimental error and the effects of any uncontrolled variable present. This initial result allows for choosing an appropriate catalyst, which can be optimized in a subsequent, more detailed study.

We envisioned that BA could influence the selectivity of the hydrogenolysis by forming borate esters in solution. Borate esters are only formed at alkaline pH. [23] The formation of borate esters of diols at alkaline pH has also been studied by NMR titration experiments (Appendix 2). Therefore, the pH values were varied between 10 and 12. Preliminary experiments showed that hydrogenolysis occurs at temperatures between 150 and 200 °C. The effect of sulfolane as an additive was investigated, because earlier research had demonstrated that this polar, aprotic solvent could affect the selectivity of several catalysts. [11,24]

The catalysts were divided into two groups and a D-optimal design was constructed for both. Design 1 was used to screen 15 catalysts, considering the variables: active metal (Ni, Pd, Pt, Rh, Ru), support type (Al_2O_3, C, SiO_2), temperature (150 – 200 °C), pH (9 – 12) and additive (0 – 5% v/v sulfolane). Design 2 was employed to screen the remaining four catalysts (Ir/C, Pd/$BaSO_4$, Pd/$CaCO_3$, Pt/$CaCO_3$) and the same three continuous variables. The division of the catalysts in these two groups was done since not all the combinations of active metal and support type were available. Thus, using these two designs, 19 catalysts could be effectively screened in only 30, out of a total of 240, experiments (Table S1, Appendix 1).

It appeared that the Ru catalysts in D-optimal design 1 were especially active. However, they mainly degraded the glycerol and only small amounts of C3 products were detected. Due to the setup of our parallel autoclaves (no option for sampling over time) we could not compare catalyst selectivities at comparable conversions. The reaction products are prone to further degradation. Therefore, the performance of the Ru catalysts will probably be improved when the reaction is stopped before 18 h.

Therefore, the ruthenium catalysts were excluded from the dataset for polynomial fitting. This resulted in a statistical polynomial model, of which the significant coefficients are plotted in the coefficient plot regarding the glycerol conversion (Figure 1a). It shows that only the variables active metal, support type and temperature have a significant influence on glycerol conversion. In this case the additive and pH had no significant influence on glycerol conversion and are therefore not included in the coefficient plot.

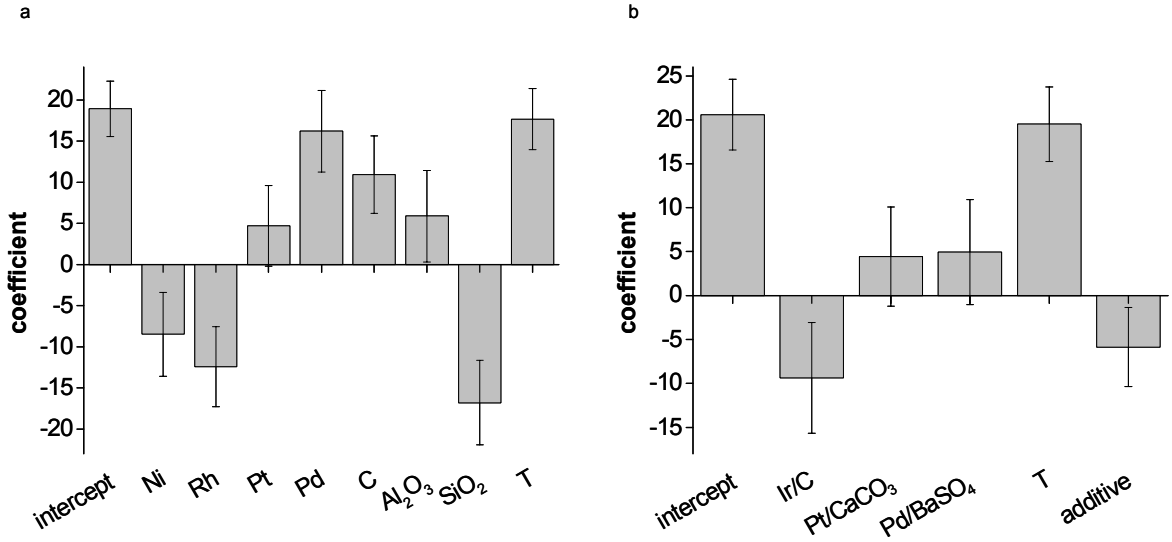

Figure 1. Coefficient plots of D-optimal designs regarding glycerol conversion (*y*); a) D-optimal design 1, $R^2 = 0.9680$; b) D-optimal design 2, $R^2 = 0.9807$.

In design 2, the $Pd/CaCO_3$ catalyst appeared to be not active at all. By excluding the three $Pd/CaCO_3$ experiments, the total number of catalysts was reduced from four to three and the results could be correlated by a polynomial model. The coefficients of this model are plotted in the coefficient plot regarding the glycerol conversion (Figure 1b). This model showed that in addition to the catalysts, temperature and the presence of sulfolane influence the conversion of glycerol, with a large positive and a small negative effect, respectively. pH had no significant effect on glycerol conversion and was therefore omitted from the coefficient plot.

3.2 LA FORMATION

It is remarkable that an oxidation product such as LA can be formed under reductive hydrogenolysis conditions. Its hydrothermal formation from glycerol in the absence of a metal (95% conversion, 90% selectivity, Scheme 1) was reported by Kishida *et al.*. [25] However, 300 °C was required to overcome the energy barrier raised by the hydride elimination. Maris *et al.* reported the formation of LA at a relatively reduced temperature (200 °C) in the presence of heterogeneous catalysts (Pt/C, Ru/C, AuRu/C or PtRu/C). [8] Apparently, the addition of a catalyst could lower the reaction temperature. This can be explained by the presence of a metallic surface, facilitating the dehydrogenation of a hydroxyl group. To

exclude that boric acid is sufficient to catalyze the LA formation, a blank experiment was performed in the absence of catalyst. This showed only 0.5% LA formation, confirming the catalytic role of the metal catalyst.

3.3 Influence of BA on activity and selectivity

Our initial hypothesis was that BA could influence the selectivity of the hydrogenolysis through formation of borate esters in solution, leaving one hydroxyl group available for reduction. The formation of these borate borate esters is described in more detail in Appendix 2. As a Lewis acid, BA can also activate the hydroxyl groups of glycerol and increase the activity.

The effect of BA on the activity and selectivity of the catalysts was investigated by repeating a set of six successful experiments from the two D-optimal designs, this time in the absence of BA (Figure 2). This showed that in most cases, the activity is increased upon addition of BA (Figure 2a); in the case of Pt/$CaCO_3$ the activity is even more than doubled.

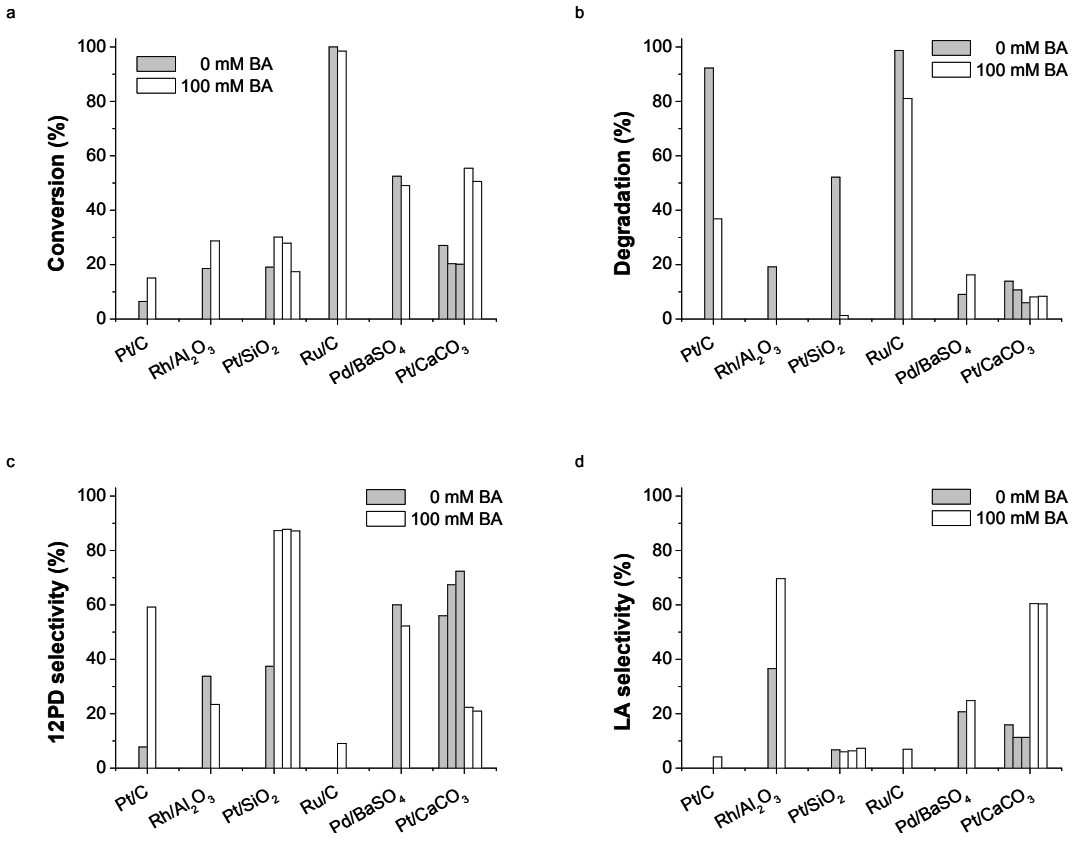

Figure 2. The influence of BA on a) conversion; b) degradation; c) 12PD-selectivity and d) LA selectivity. Some reactions were performed in duplicate or triplicate in order to establish the error margin. Reaction conditions for the respective catalysts are given in Table S1, Appendix 1.

Not only conversion of glycerol was increased (in most cases) in the presence of BA, also less glycerol was degraded (Figure 2b). Consequently, more glycerol is converted into desired products, best expressed for Rh/Al_2O_3 and Pt/SiO_2, where the degradation of glycerol is almost completely suppressed.

Interestingly, BA's influence on selectivity is not clear-cut. In some cases (Pt/C, Pt/SiO_2) 12PD-selectivity was substantially increased (Figure 2c), while in other cases (Rh/Al_2O_3, $Pt/CaCO_3$) LA formation was favoured upon the addition of BA (Figure 2d). In case of $Pt/CaCO_3$ the increase of LA-selectivity was accompanied by a decrease of 12PD-selectivity, resulting in a selectivity switch from 12PD to LA upon the addition of BA.

3.4 Response Surface Model design

A Central Composite Design (CCD) was set up to study the significant influence of BA on the selectivity of $Pt/CaCO_3$. A CCD consists of a full factorial design augmented with star points, which increase the variable space and allow the modeling of nonlinear effects. A CCD results in a Response Surface Model (RSM), which enables to draw insightfull RSM plots (Figure 3, raw data in Table S2, Appendix 1).

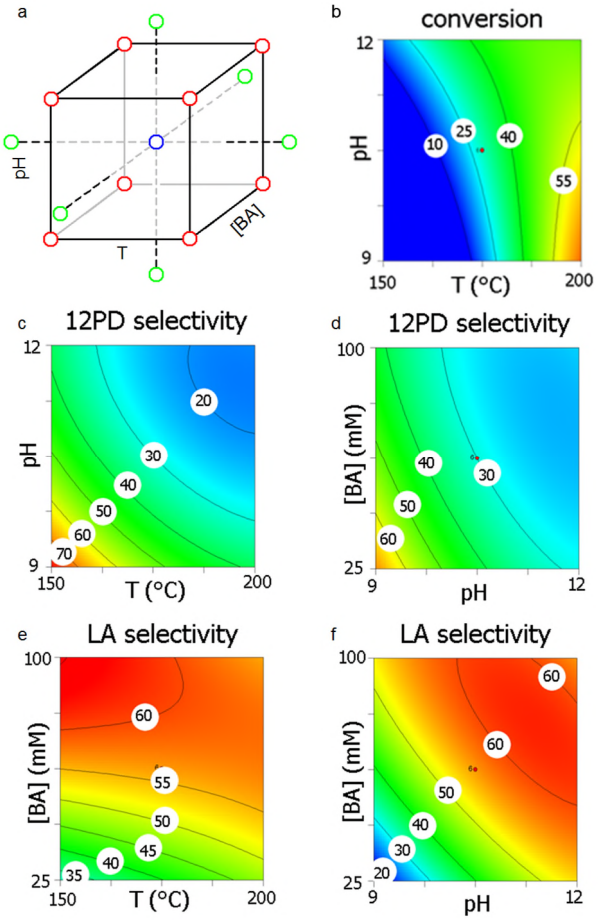

Figure 3. RSM-plots resulting from a Central Composite Design. Relevant cross sections through the centre points were chosen and the value of the remaining parameter is given in the respective footnote. a)

Central Composite Design, the circles represent experiments within parameter space, blue = 6× centre point, red = 8× factorial point, green = 6× star point; b) RSM-plot for glycerol conversion at 62.5 mM BA; c) RSM-plot for 12PD-selectivity at 62.5 mM BA; d) RSM-plot for 12PD-selectivity at 175 °C; e) RSM-plot for LA-selectivity at pH 10.5; f) RSM-plot for LA-selectivity at 175 °C.

In addition to BA concentration (0 – 125 mM), the influence of the variables temperature (130 – 220 °C) and pH (8 – 13) on activity and selectivity of the catalyst were investigated. These three variables could be effectively modeled using a CCD consisting of 20 experiments (8 factorial points, 6 star points and 6 centre points) (Figure 3a). The centre point is repeated six times in order to obtain a good estimate for the standard deviation of the system. The model for the conversion of glycerol indicated that the variable temperature and the interaction pH×temperature have a significant effect on the conversion of glycerol. These effects are visualized in the RSM plot in Figure 2b: pH has an influence on glycerol conversion, but it is mainly controlled by temperature.

The selectivity of Pt/$CaCO_3$ towards 12PD and LA was modeled by omitting the selectivity data at conversions below 5%. These data were excluded because the low conversion data contain a high uncertainty in the selectivity. The resulting selectivity models show an influence of all three variables, best visualized in RSM plots (Figure 3c-f).

The selectivity, within variable space, towards 12PD is highest at low BA concentration, low pH and low temperature (Figure 3c-d). However, at these conditions the conversion of glycerol is very low, resulting in the formation of a small amount of 12PD.

The LA-selectivity is the highest at high pH and BA concentration, while the effect of temperature is less significant (Figure 3e-f). This means that a high LA-selectivity is possible at a relatively high glycerol conversion. Interestingly, it is visualized that upon changing reaction variables, Pt/$CaCO_3$ can be either selective for 12PD or LA formation.

3.5 Increasing 12PD-selectivity

Based on the RSM plots in Figure 3 (c and d), it can be expected that decreasing pH below pH 9 at 200 °C should increase 12PD-selectivity, while maintaining a high conversion. Therefore, an additional reaction was run at 200 °C, 100 mM BA concentration and pH 5.6, i.e. without addition of sodium hydroxide (Figure 4a). Indeed, this resulted in a substantial increase of 12PD-selectivity, accompanied by a decimation of the LA-selectivity. The overall yield of 12PD was increased, even though the glycerol conversion was decreased. Mechanistically, the increase in 12PD-selectivity can be explained by the suppression of the LA formation pathway, since this is base-induced, [24] leaving more glycerol for hydrogenolysis in 12PD. A reason for the decrease of conversion rate could be that at pH 5.6 only one pathway is operational, instead of two pathways at pH 12.

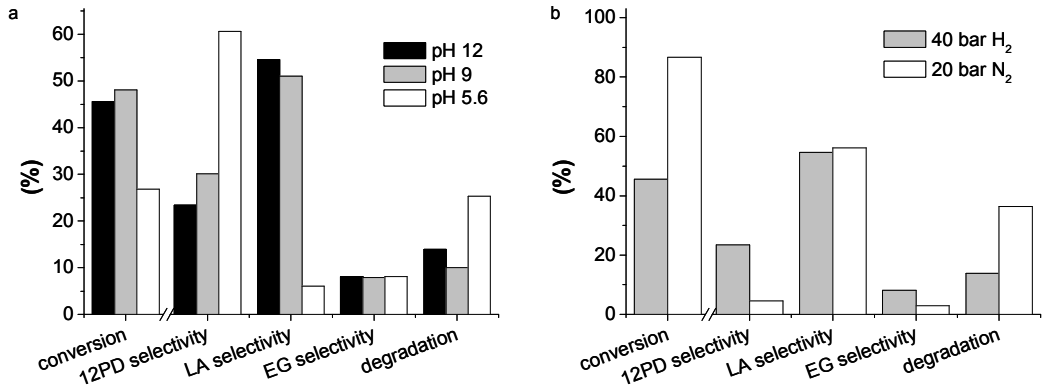

Figure 4. a**)** Effect of pH on glycerol conversion and selectivity. Reaction conditions: 5 mol% $Pt/CaCO_3$, 5 mL aqueous reaction mixture (100 mM glycerol, 100 mM BA, variable pH), 200 °C, 40 bar H_2, 18 h, 800 rpm; b) Effect of hydrogen pressure vs. inert atmosphere. Reaction conditions: 5 mol% $Pt/CaCO_3$, 5 mL aqueous reaction mixture (100 mM glycerol, 100 mM BA, pH 12), 200 °C, 40 bar H_2 or 20 bar N_2, 18 h, 800 rpm.

3.6 Increasing LA-formation

The RSM plots show that an optimum for LA-selectivity is close to, or within the chosen parameter space (Figure 3e-f). Therefore, changing these variables would not substantially increase the LA-selectivity. However, the selectivity could be increased by avoiding the 12PD formation pathway. This can be achieved by running the reaction in the absence of hydrogen, thereby prohibiting the formation of 12PD and leaving the dehydrogenated glycerol available for LA formation. Figure 4b shows that in the absence of hydrogen pressure, the LA-selectivity remains the same, while the conversion and, as a consequence, the LA-formation were substantially increased. The 12PD-selectivity had dropped considerably, but still small amounts of 12PD were formed. Obviously, hydrogen, necessary for 12PD formation, is produced during the reaction: one equivalent of hydrogen is formed for each LA and even more can be formed during the degradation of glycerol. [18]

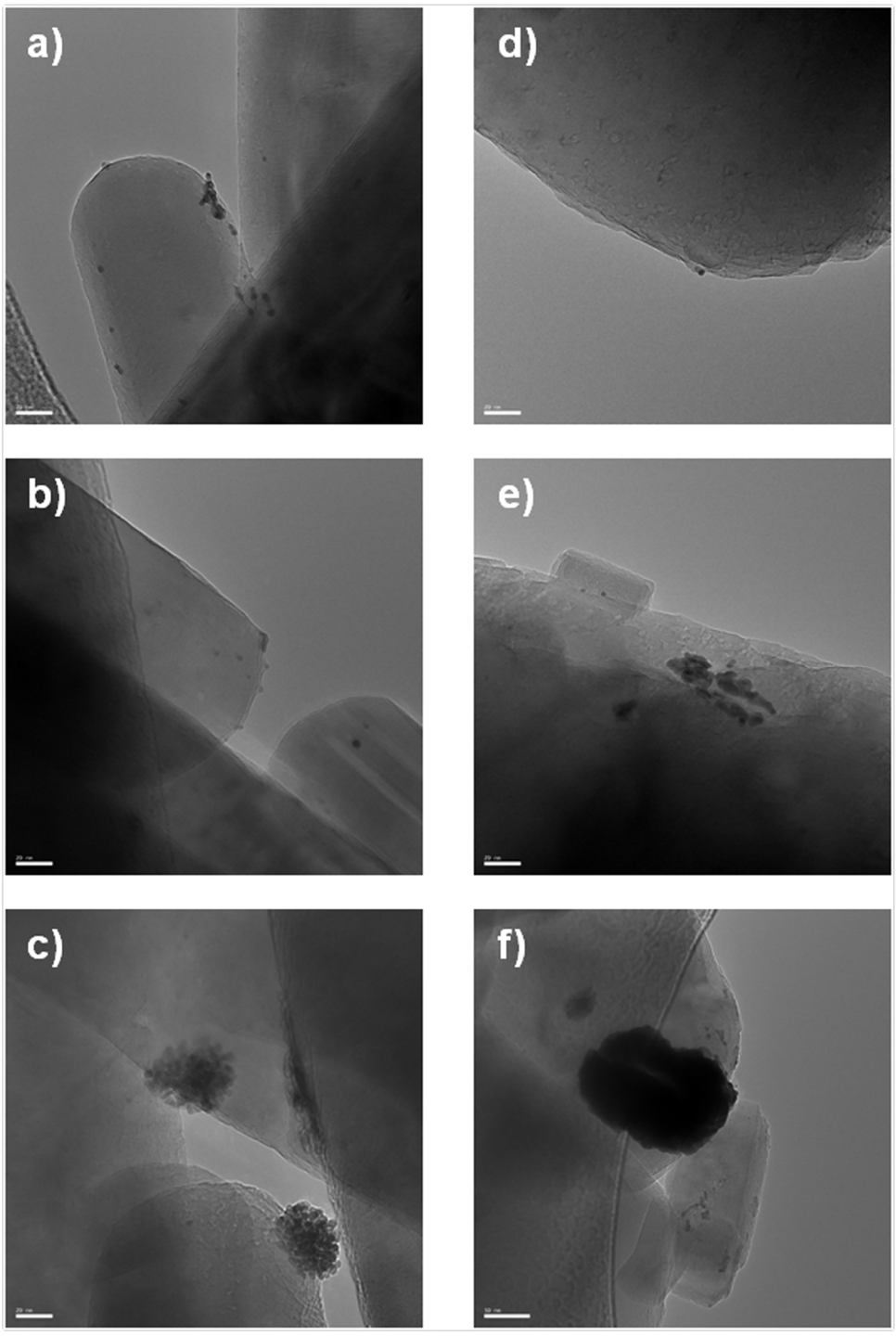

Figure 5. TEM data; a) fresh Pt/$CaCO_3$, bar is 20 nm; b) fresh Pt/$CaCO_3$, bar is 20 nm; c) fresh Pt/$CaCO_3$, bar is 20 nm; d) recycled Pt/$CaCO_3$, bar is 20 nm; e) recycled Pt/$CaCO_3$, bar is 20 nm; f) recycled Pt/$CaCO_3$, bar is 50 nm.

3.7 CATALYST RECYCLING

The carrier material of $Pt/CaCO_3$ should be stable under the alkaline conditions used in this study. However, the elevated temperatures and stirring might degrade the catalyst to some extent. Therefore, the stability of $Pt/CaCO_3$ was investigated by means of a catalyst recycling experiment (Figure 6).†

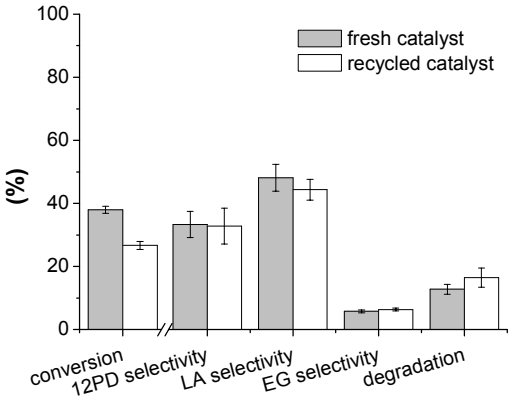

Figure 6. Recycling experiment. Reaction conditions: 5 mol% $Pt/CaCO_3$ (initial loading), 5 mL aqueous reaction mixture (100 mM glycerol, 62.5 mM boric acid, pH 10.5), 175 °C, 40 bar H_2, 18 h, 800 rpm.

The selectivity of recycled catalyst is comparable with the selectivity of fresh catalyst, but the activity decreased when using the recycled catalyst. TEM analysis before and after reaction (Figure 5) shows that the $CaCO_3$ surface is partly eroded and platinum particles have sintered. The resulting loss of active sites can explain the lower catalyst activity.

4. CONCLUSIONS

The D-optimal screening of 19 catalysts showed that active metal, catalyst support and temperature have the highest influence on glycerol hydrogenolysis activity. A preliminary study regarding the effect of BA indicated that it can increase glycerol conversion and influences selectivity of the catalysts. Upon addition of BA, the selectivity of $Pt/CaCO_3$ was switched from 12PD to LA. Among all catalysts screened in the D-optimal design, $Pt/CaCO_3$ was found to be the most active with little glycerol degradation. A central composite design revealed the strong relation between the pH and 12PD-selectivity. Decreasing the pH gave higher 12PD-selectivity by suppressing the base catalyzed LA formation pathway. Performing the reaction in the absence of hydrogen increased the LA formation due to interruption of the 12PD formation. Although LA-selectivity remained the same, conversion was considerably increased, while 12PD-selectivity was diminished. The catalyst could be recycled and maintained selectivity, but showed some deactivation.

This study shows that DoE was not only highly effective in identifying active catalysts, it also provided useful insights into the effects of pH, BA concentration and temperature on the activity and selectivity of

the selected Pt/$CaCO_3$. These insights were succesfully used to direct the selectivity of Pt/$CaCO_3$ to either 12PD or LA.

ACKNOWLEDGEMENTS

We are grateful to Dr. Silvia Pereira for assistance regarding DoE and to Dr. Catherine Pinel (IRCELYON) for helping us with the HPLC analysis. Jeroen ten Dam gratefully acknowledges financial support from NWO ASPECT (053.62.020)

NOTES AND REFERENCES

† For the recycling study a new batch of catalyst has been used. The new batch had higher activity and comparable selectivities.

[1] A. Corma, S. Iborra and A. Velty, Chem. Rev., 2007, 107, 2411-2502.

[2] C. H. Christensen, J. Rass-Hansen, C. C. Marsden, E. Taarning and K. Egeblad, ChemSusChem, 2008, 1, 283-289.

[3] A. Brandner, K. Lehnert, A. Bienholz, M. Lucas and P. Claus, Top. Catal., 2009, 52, 278-287.

[4] Y. G. Zheng, X. L. Chen and Y. C. Shen, Chem. Rev., 2008, 108, 5253-5277.

[5] C. H. C. Zhou, J. N. Beltramini, Y. X. Fan and G. Q. M. Lu, Chem. Soc. Rev., 2008, 37, 527-549.

[6] J. J. Bozell and G. R. Petersen, Green Chem., 2010, 12, 539-554.

[7] J. V. Kurian, J. Polym. Environ., 2005, 13, 159-167.

[8] E. P. Maris and R. J. Davis, J. Catal., 2007, 249, 328-337.

[9] E. P. Maris, W. C. Ketchie, M. Murayama and R. J. Davis, J. Catal., 2007, 251, 281-294.

[10] P. P. Pescarmona, K. P. F. Janssen, C. Delaet, C. Stroobants, K. Houthoofd, A. Philippaerts, C. D. Jonghe, J. S. Paul, P. A. Jacobs and B. F. Sels, Green Chem., 2010, 12, 1083-1089.

[11] J. Chaminand, L. Djakovitch, P. Gallezot, P. Marion, C. Pinel and C. Rosier, Green Chem., 2004, 6, 359-361.

[12] J. Wang, S. H. Shen, B. D. Li, H. Q. Lin and Y. Z. Yuan, Chem. Lett., 2009, 38, 572-573.

[13] A. Shimao, S. Koso, N. Ueda, Y. Shinmi, I. Furikado and K. Tomishige, Chem. Lett., 2009, 38, 540-541.

[14] S. Sato, M. Akiyama, K. Inui and M. Yokota, Chem. Lett., 2009, 38, 560-561.

[15] T. Jiang, Y. X. Zhou, S. G. Liang, H. Z. Liu and B. X. Han, Green Chem., 2009, 11, 1000-1006.

[16] L. Y. Guo, J. X. Zhou, J. B. Mao, X. W. Guo and S. G. Zhang, Appl. Catal. A-Gen., 2009, 367, 93-98.

[17] L. Ma, D. H. He and Z. P. Li, Catal. Commun., 2008, 9, 2489-2495.

[18] E. D'Hondt, S. V. de Vyver, B. F. Sels and P. A. Jacobs, Chem. Commun., 2008, 6011-6012.

[19] T. Miyazawa, S. Koso, K. Kunimori and K. Tomishige, Appl. Catal. A-Gen., 2007, 329, 30-35.

[20] O. W. Gooding, Curr. Opin. Chem. Biol., 2004, 8, 297-304.

[21] P. G. J. Koopman, A. P. G. Kieboom and H. van Bekkum, J. Catal., 1981, 69, 172-179.

[22] Catalytic hydrogenolysis of glycerol, M. Besson, L. Djakovitch, P. Gallezot, C. Pinel, A. Salameh and M. Vospernik, Chemical Industries (Boca Raton, FL, United States), 2009, 123 (Catalysis of Organic Reactions), 313-318.

[23] J. Yan, G. Springsteen, S. Deeter and B. H. Wang, Tetrahedron, 2004, 60, 11205-11209.

[24] M. Schlaf, P. Ghosh, P. J. Fagan, E. Hauptman and R. M. Bullock, Angew. Chem., Int. Ed., 2001, 40, 3887-3890.

[25] H. Kishida, F. M. Jin, Z. Y. Zhou, T. Moriya and H. Enomoto, Chem. Lett., 2005, 34, 1560-1561.

APPENDIX 1

Table S1. All results from two D-optimal designs, ordered by conversion.

Entry	Catalyst	*T* (°C)	pH	Sulfolane (v/v %)	Conversion (%)	Selectivity (%)				
						12PD	LA	EG	EtOH	Deg. [a]
1 [b]	Ru/Al_2O_3	200	10	0	100	3.0	0	0	0	97.0
2 [b]	Ru/C	150	10	0	98.4	9.0	6.9	1.5	1.6	81.0
3 [b]	Pd/C	200	12	0	64.4	25.4	43.0	5.8	6.8	19.0
4 [c]	$Pt/CaCO_3$	200	10	0	55.4	22.3	60.5	7.0	2.2	8.0
5 [c]	$Pt/CaCO_3$	200	10	0	50.6	20.9	60.3	8.3	2.3	8.3
6 [c]	$Pd/BaSO_4$	200	12	0	49.1	52.2	24.8	6.8	0	16.2
7 [b]	Pt/SiO_2	200	10	5	30.1	87.3	6.0	5.6	0	1.2
8 [b]	Rh/Al_2O_3	200	12	0	28.7	23.4	69.6	7.0	0	0
9 [b]	Pt/SiO_2	200	10	5	27.8	89.6	6.4	6.1	0	0
10 [c]	Ir/C	200	10	5	21.4	82.6	12.9	7.2	0	0
11 [b]	Pt/SiO_2	200	10	5	17.4	95.0	7.9	6.1	0	0
12 [b]	Pt/C	150	12	0	15.1	59.1	4.1	0	0	36.8
13 [b]	Ni/SiO_2	200	12	0	13.1	51.9	6.3	40.6	0	1.2
14 [b]	Rh/SiO_2	200	10	0	5.9	28.9	62.2	8.9	0	0
15 [b]	Rh/SiO_2	200	10	0	5.9	27.3	62.3	10.4	0	0
16 [c]	$Pt/CaCO_3$	150	12	0	4.5	39.5	60.5	0	0	0
17 [b]	Rh/C	150	10	5	4.0	69.0	17.2	13.8	0	0
18 [b]	Ni/C	150	12	5	2.4	0	0	0	0	100
19 [c]	$Pd/BaSO_4$	150	10	5	2.3	0	0	0	0	100
20 [c]	$Pd/CaCO_3$	150	10	0	2.1	0	0	0	0	100
21 [b]	Ni/C	150	12	5	1.9	0	0	0	0	100
22 [c]	$Pt/CaCO_3$	150	12	5	1.3	40	60	0	0	0
23 [c]	Ir/C	150	12	0	1.0	100	0	0	0	0
24 [c]	$Pd/BaSO_4$	150	10	5	0	0	0	0	0	100
25 [c]	$Pd/BaSO_4$	150	12	5	0	0	0	0	0	100
26 [b]	Ni/Al_2O_3	150	10	5	0	0	0	0	0	100
27 [b]	Pd/SiO_2	150	10	0	0	0	0	0	0	100
28 [b]	Ru/SiO_2	150	12	5	0	0	0	0	0	100
29 [c]	$Pd/CaCO_3$	200	10	0	0	0	0	0	0	100
30 [c]	$Pd/CaCO_3$	200	12	5	0	0	0	0	0	100

Reaction conditions: 5 mol% catalyst, 5 mL aqueous reaction mixture (100 mM glycerol, 100 mM BA, indicated pH), indicated *T*, 40 bar H_2, 18 h, 800 rpm; [a] degradation, products undetectable by HPLC; [b] D-optimal design 1; [c] D-optimal design 2.

Table S2. Central Composite Design using $Pt/CaCO_3$ as a catalyst.

Entry	*T* (°C)	pH	BA concentration (mM)	Conversion (%)	Selectivity (%)				
					12PD	LA	EG	EtOH	Deg. [a]
1	150	9	25	3.8	70.5	23.8	5.7	0	0
2	200	9	25	60.9	59.2	27.0	6.3	0	7.5
3	150	12	25	9.3	47.4	48.1	4.5	0	0
4	200	12	25	35.5	27.6	63.2	9.2	0	0
5	150	9	100	4.8	78.8	21.2	0	0	0
6	200	9	100	60.1	30.5	48.2	8.6	2.9	9.8
7	150	12	100	10.2	41.4	58.6	0	0	0
8	200	12	100	45.6	23.4	54.6	8.1	0	13.9
9	175	10.5	62.5	29.2	30.8	56.3	8.9	0	4.0
10	175	10.5	62.5	21.3	30.9	61.8	7.4	0	0
11	175	10.5	62.5	27.9	27.8	59.1	8.2	0	4.9
12	175	10.5	62.5	24.7	35.3	58.8	5.9	0	0
13	175	10.5	62.5	26.8	27.4	54.2	7.7	0	10.7
14	175	10.5	62.5	35.9	31.3	57.0	6.6	0	5.1
15	130	10.5	62.5	1.5	100	0	0	0	0
16	220	10.5	62.5	73.6	21.7	52.2	9.3	2.7	14.1
17	175	8	62.5	21.2	73.3	17.7	9.1	0	0
18	175	13	62.5	65.6	23.6	57.8	7.3	0	11.4
19	175	10.5	0	19.3	51.2	17.5	7.0	0	24.4
20	175	10.5	125	38.6	26.2	57.9	7.0	0	8.9

Reaction condition: 5 mol% $Pt/CaCO_3$, 5 mL aqueous reaction mixture (100 mM glycerol, indicated BA, indicated pH), indicated *T*, 40 bar H_2, 18 h, 800 rpm; [a] degradation, products undetectable by HPLC.

APPENDIX 2

EXPERIMENTAL SECTION

MATERIALS

Deuterated water (D_2O, 99.9 %) was purchased from Cambridge Isotope Laboratories. Boric acid (Sigma Aldrich, >99.5%); ethylene glycol (Sigma Aldrich, 99.8%); propane-1,2-diol (Sigma Aldrich, 99%); propane-1,3-diol (Acros, 98%); 3-fluoropropane-1,2-diol (Sigma Aldrich); butane-1,2-diol (Sigma Aldrich, 98%) and glycerol (Acros, >99%) were used as received.

^{1}H NMR SPECTROSCOPY

Spectra were recorded on a Bruker Avance 400 spectrometer at 400 MHz at room temperature. ^{1}H NMR spectra are reported in ppm (δ) relative to ^{t}BuOH (δ = 1.24 ppm).

^{11}B NMR SPECTROSCOPY

^{11}B NMR spectra were recorded on a Bruker Avance 400 spectrometer at 128.31 MHz at room temperature. ^{11}B NMR spectra are reported in ppm (δ) relative to 0.1 M boric acid in D_2O as external reference (δ = 0.0 ppm).

^{13}C NMR SPECTROSCOPY

^{13}C NMR spectra were recorded on a Bruker Avance 400 spectrometer at 100.56 MHz or on a Bruker 300 spectrometer at 75 MHz at room temperature. ^{13}C NMR spectra are reported in ppm (δ) relative to ^{t}BuOH (δ = 30.29 ppm).

pD MEASUREMENT

The pD of the NMR titration experiment samples were determined with a calibrated MI412 Micro-combination probe from Microelectrodes, Inc. by inserting the narrow probe into the NMR tube before measurement.

The pK_a^D that is derived from these pD titrations in D_2O measurements can be converted into pK_a^H values that are valid for H_2O solutions by using the following equation [2]:

$$pK_a^H = 0.929pK_a^D + 0.42$$

GENERAL PROCEDURES

STANDARD SOLUTIONS

Standard solutions were prepared by weighing the appropriate amount of material into a volumetric flask and filling the flask with 5 mL 0.5 M NaOH in D_2O. A drop of ^tBuOH in D_2O (1:1) was added to the standard solutions of the alcohols.

NMR TITRATION EXPERIMENTS

The initial NMR sample contained 600 μL 0.1 M bor(on)ic acid and 0.1 M alcohol in 0.5 M NaOH in D_2O (0.05 M boronic acid and equimolecular amounts of alcohol were used for the less soluble 3-nitrophenyl- and 1-naphthylboronic acid). The pD was measured and ^{11}B and ^1H NMR spectra were recorded. The pD of the sample was decreased using drops of 0.5 M DCl in D_2O. The new pD value was determined and another ^{11}B and ^1H NMR spectra were recorded. Proton signals resulting from the diol were used for product specification, unless stated otherwise. This procedure was repeated until only trigonal boron was present.

CURVE FITTINGS

Titration curves were fitted by using MicroMath Scientist software for Windows.

The pD values and normalized NMR integrals are used as an input for the Scientist fittings of the pK_a and K values of the titration. First, the pK_a of the bor(on)ic acid is determined by using the data from the titration of the bor(on)ic acid species in the absence of ligand. The Scientist method // pKa BOR(ON)IC ACID (appendix A1) was used for this purpose.

For boronic acid species both delBmin and delB0 were calculated, for boric acid delB0 was set on zero. The parameters obtained in this way were used in the fittings for the association constants K.

The association constants of boric acid with a diol were calculated using the Scientist method // 2 BORATEESTER (mono-ester & di-ester) (appendix A2). The values for pK1, delBmin and delB0 were taken from the pKa fitting.

The association constants of boric acid with a triol (glycerol) were calculated using the Scientist method // 4 BORATEESTERS (2 x mono-ester & 2 x di-ester) (appendix A3). The values for pK1, delBmin and delB0 were taken from the pKa fitting.

The models used for the fitting of association constants for boronate esters were different from the models used for borate esters, because the formation of diesters is impossible in this case.

The association constant of boronic acid with a diol was calculated using the Scientist method // 1 BORONATE ESTER (appendix A4). The values for pK1, delBmin and delB0 were taken from the pKa fitting.

The association constants of boronic acid with a triol (glycerol) was calculated using the Scientist method // 2 BORATEESTERS (1,2-ester & 1,3-ester) (appendix A5). The values for pK1, delBmin and delB0 were taken from the pKa fitting.

The association constants Kxy are defined as follows: K2 = [BL] / ([B-] * [L])

For diesters, x is 2, otherwise it is absent. For 1,2-esters y is 2, for 1,3-esters y is 3.

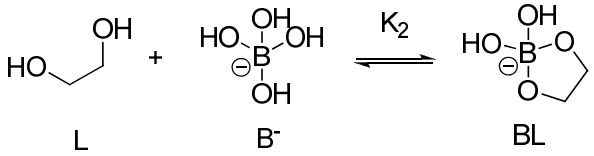

RESULTS AND DISCUSSION

BOR(ON)IC ACID TITRATIONS

pK_A DETERMINATION

To investigate the effect of the pK_a of bor(on)ic acid on bor(on)ate ester formation the pK_a's from boric acid and a series of substituted phenylboronic acids was determined by ^{11}B NMR titration experiments. The determination of the pK_a's is based on the relative shift of the ^{11}B signal, depending on the amount of B^- or B^0 present in aqueous solution. As the equilibrium between B^0 and B^- is very fast on the NMR timescale, the observed chemical shift for boron is an average for the B^0 and the B^- signal (equation 7). [1] This is defined in the following expressions, based on the equilibrium constant (equation 3), pD (equation 1) and mass balance (equation 2):

1 $$[D^+] = 10^{-pD}$$

2 $$[B_{tot}] = [B^-] + [B^0]$$

3 $$K_a = \frac{[B^-][D^+]}{[B^0]}$$

4 $$pK_a = 10^{-K_a}$$

5 $$[B^0] = \frac{[B^-][D^+]}{K_a}$$

6 $$fB^- = \frac{[B^-]}{[B_{tot}]}$$

7 $$\delta B = fB^- * \delta B^- + (1 - fB^-) * \delta B^0$$

Where $[H^+]$ is proton concentration, $[B_{tot}]$ is total boron concentration, $[B^-]$ is tetrahedral borate concentration, $[B^0]$ is trigonal boron concentration, K_a is the acidic constant, fB^- is the fraction of

tetrahedral borate, δB is the observed ^{11}B chemical shift, dB^- is the chemical shift for 100% tetrahedral borate and δB^0 is the chemical shift for 100% trigonal boron. Since pD and δB can be measured for individual samples, $[B_{tot}]$ is known due to standard preparation, and δB^- and δB^0 can be obtained by measuring ^{11}B chemical shift at high and low pH, respectively, there is enough information available to fit K_a value to the titration curve (Figure 1a-e). For this a Scientist fitting program was used (appendix A1).

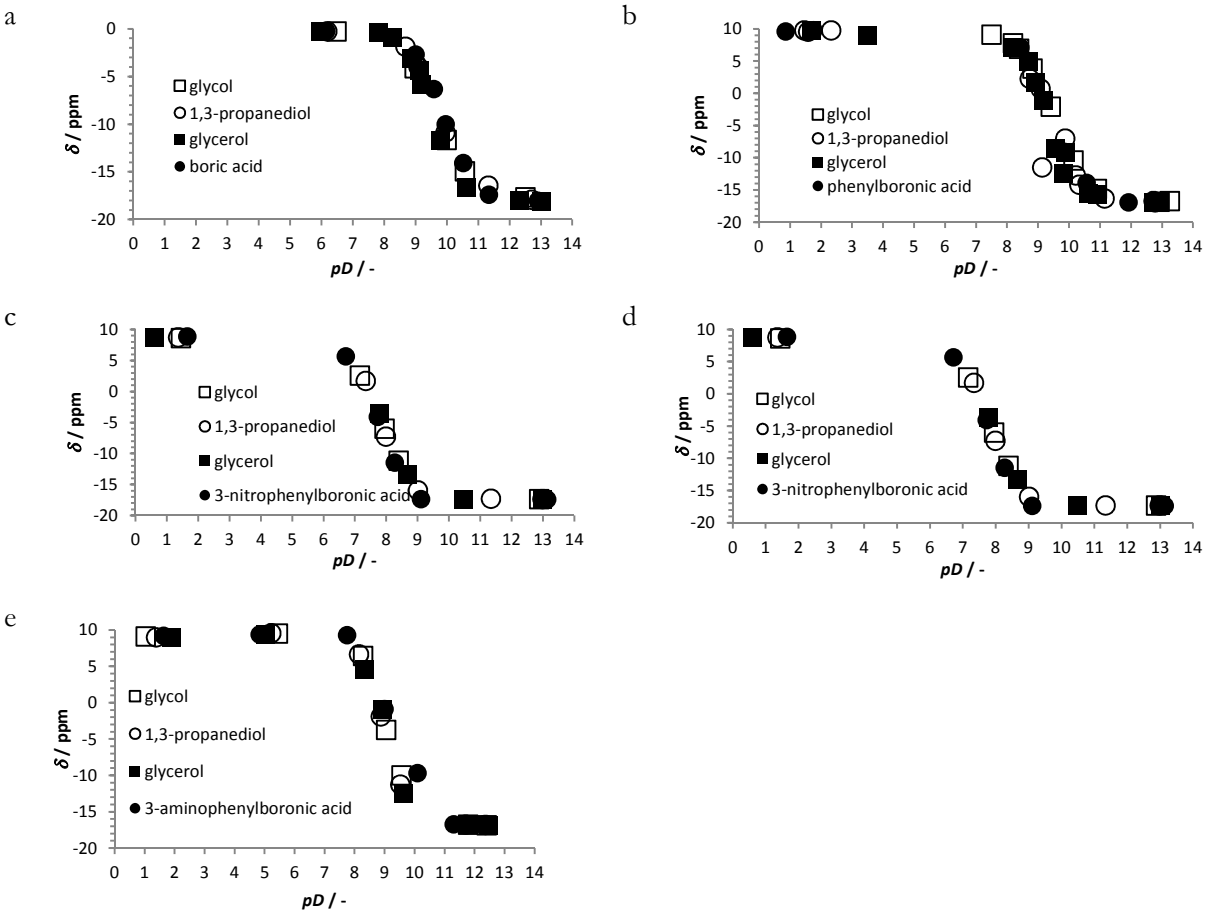

Figure 1. a) boric acid/borate titration curves pK_a^D 9.85 (^{11}B NMR); b) phenylboronic acid/phenylborate titration curves pK_a^D 9.46 (^{11}B NMR); c) 3-nitrophenylboronic acid/phenylborate titration curves (^{11}B NMR); d) pK_a^D determination of 3-aminophenylboronic acid (pK_a^D = 9.16); e) pK_a^D determination of 3-hydroxyphenylboronic acid (pK_a^D = 9.30).

The Scientist fittings resulted in the pK_a values displayed in Table 1. The pK_a determination of 1-naphthaleneboronic acid was attempted as well, but was discarded as the solubility is limited, it crystalizes out of water at pD 7.3. The solubility of 3-nitrophenylboronic acid was also limited, which forced us to establish the pK_a at lower concentrations (0.05 M instead of the standard 0.1 M).

The pK_a values determined in this way are not to be taken as absolute values, as they are measured in D_2O, which influences the pH measurement. This can be corrected by using equation 1. Even adjusting for this isotope effect using the equation below [2]:

$$pK_a^H = 0.929pK_a^D + 0.42$$

Table 1. Bor(on)ic acid pK_a's. [4]

	pK_a^H fitted*	pK_a literature value	Electron withdrawing/donating effect
Boric acid	9.57	9.24	n.a.
Phenylboronic acid	9.21	8.8	Donating
3-hydroxyphenylboronic acid	9.06		Donating?
3-aminophenylboronic acid	8.93	8.9	Donating/Withdrawing (NH_2/NH_3^+)
3-nitrophenylboronic acid	7.63	7.1	Withdrawing

* calculated using pD's, adjusted for pH using $pK_a^H = 0.929pK_a^D + 0.42$. [2]

The pK_a's are still consistently high (0.33-0.38). However, it is still possible to make a relative comparison between these 5 examples, as they have been determined using the same method.

BOR(ON)ATE ESTER ASSOCIATION CONSTANT DETERMINATION

The formation and hydrolysis of borate esters are key steps when boric acid is used as a temporary protecting group (Figure 2). These reversible reactions were quantified by determining the association constants (K_n, equation 8, not to be confused with the acid constant K_a of equation 3) of the bor(on)ate esters of glycerol, ethylene glycol, and 1,3-propanediol using boric acid and a series of phenylboronic acids (Table 2).

8 $$K_n = \frac{[B^-L]}{[B^-][L]}$$

Where n stands for 1,2-esters (n=2) or 1,3-esters (n=3).

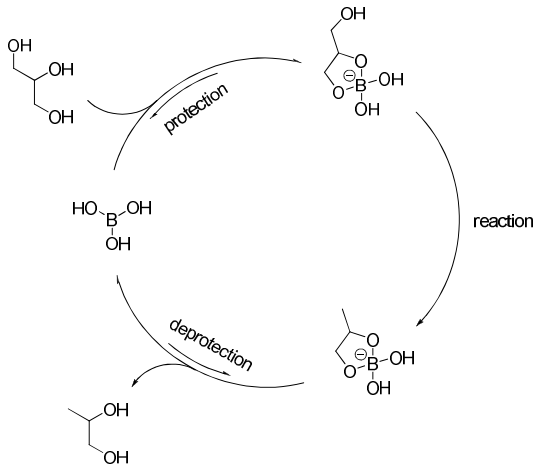

Figure 2. Boric acid as a potential temporary protecting group. First, boric acid forms a borate ester with glycerol, after which a reaction with a catalyst occurs. Finally, the boric acid is retrieved due to the lower formation constant of the borate ester of propane-1,2-diol, compared to glycerol.

Table 2. Bor(on)ate ester association constants. [4,5]

Bor(on)ic acid	pK_a^H *	Glycol	Glycerol	Glycerol	selectivity
		K_2	K_2	K_3	K_2/K_3
Boric acid	9.57	0.4	11.2	2.0	5.6
Phenyl boronic acid	9.21	1.4	6.5	3.0	2.2
3-hydroxyphenyl boronic acid	9.06	1.2	4.1	1.4	2.9
3-aminophenyl boronic acid	8.93	1.3	4.1	1.8	2.3
3-nitrophenyl boronic acid	7.63	0.8	1.8	0.8	2.3

* calculated using pD's, adjusted for pH using $pK_a^H = 0.929pK_a^D + 0.42$. [2]

When phenylboronic acids are used, the equation above is sufficient to quantify the ester formation. However, boric acid has the possibility to form di-esters (Figure 3). Therefore, the following equilibrium constants need to be considered as well.

9 $$K_{nm} = \frac{[B^-L_2]}{[B^-L][L]}$$

Where n and m stand for 1,2-esters (n or m = 2) or 1,3-esters (n or m = 3).

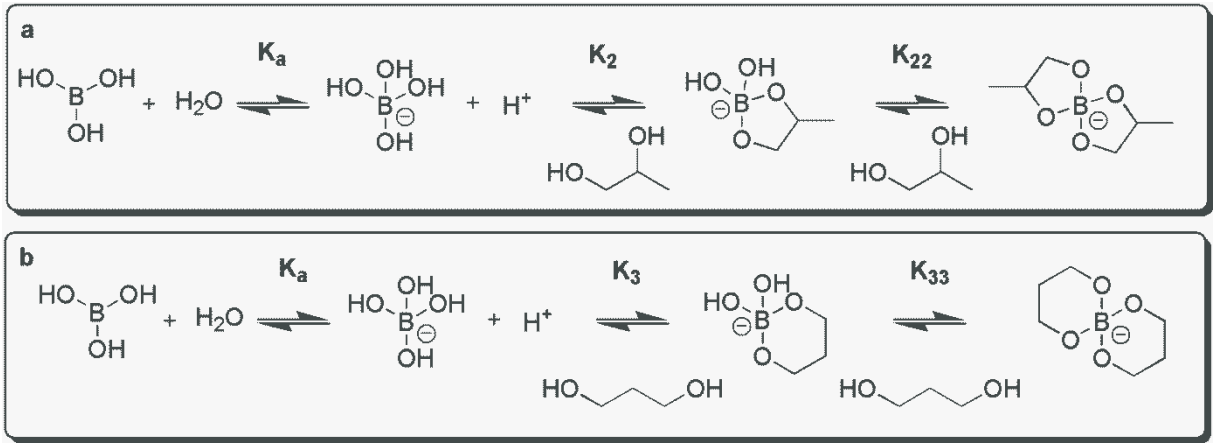

Figure 3. a) Formation of 1,2-propadiol borate ester and 1,2-propanediol borate di-ester, with the relevant association constants [3]; b) Formation of 1,3-propadiol borate ester and 1,3-propanediol borate di-ester, with the relevant association constants.

The respective association constants are determined through titration experiments. Aqueous boric acid is present in its trigonal form at acidic pH and in its tetrahedral form (borate) at alkaline pH. The equilibrium between these species is fast. [1] Therefore, only one boron signal (δB) is visible in 11B NMR spectra. The chemical shift of this signal is the sum of the contribution of tetrahedral (δB^-) and trigonal (δB^0) boron (equation 10):

10 $$\delta B = fB^- * \delta B^- + (1 - fB^-) * \delta B^0$$

11 $$[B_{tot}] = [B^-] + [B^0] + [B^-L]$$

This equation, together with the mass balance (equation 11) and equation 6 is used to determine the borate concentration ([B^-]), where [B_{tot}] is total free boron concentration, dB^- is the chemical shift of tetrahedral boric acid and dB^0 is the chemical shift of pure trigonal boric acid.

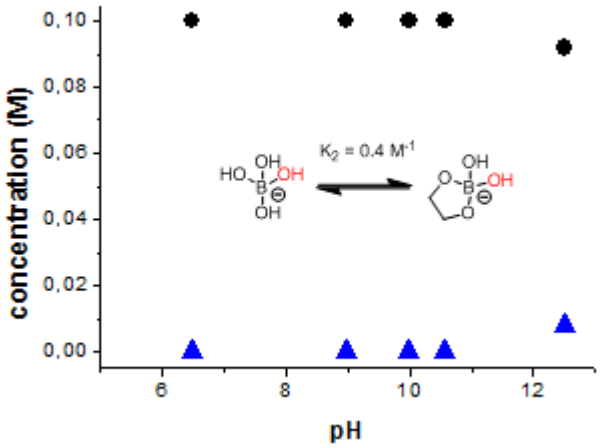

Figure 4. Example of a ^{11}B NMR titration experiment – titration of boric acid (black dot) in the presence of glycol to form glycol borate ester (blue triangle).

The concentrations of borate ester (B-L), borate (B^-) and diol (L) were determined using ^{11}B and ^1H NMR titration techniques (Figure 4). These concentrations were fitted according to a model which resulted in the association constants listed in Table 2.

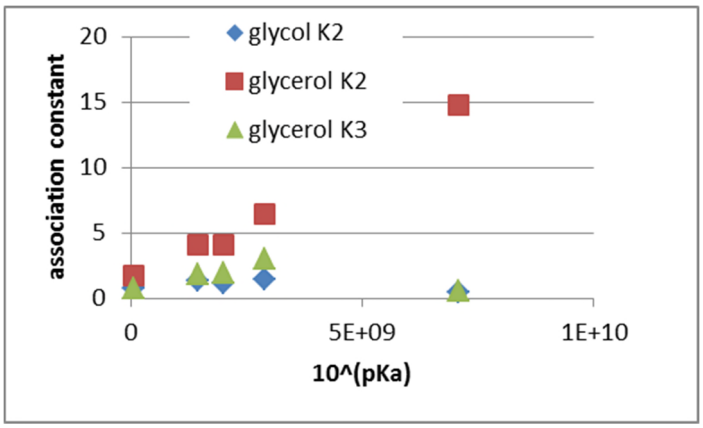

Figure 5. Exemplifying differences in K values and pK_a's from Table 2. (acidic boronic acids on the left, boric acid on right (forming most of the borate ester).

Table 2 and Figure 5 show a correlation between the pK_a of the bor(on)ic acid and the association constant of the diol bor(on)ate ester. A lower pK_a results in a lower association constant and thus in smaller amounts of diol bor(on)ate ester. Since the pK_a of boric acid is highest of the set of bor(on)ic acids in Table 2, it follows that this species forms highest levels of ester at a given pH. The acidity (lowering of pK_a) of boronic acids is increased by adding electron withdrawing groups. For this reason,

phenylboronic acid is more acidic than boric acid and 3-nitrophenyl boronic acid is most acidic as the nitro-group on the phenyl is highly electron withdrawing. [4]

Since boric acid showed the highest association constants of the series of bor(on)ic acids it was decided to use this species in further experiments. The association constants of glycerol and its hydrodeoxygenation products, i.e. ethylene glycol, 1,2-propadiol and 1,3-propadiol, were determined (Table 3). Conveniently, glycerol has the highest association constants of the different polyols. This is advantageous when glycerol is intended as a reaction substrate, as it will readily form glycerol borate esters in the reaction mixture. Moreover, when glycerol has been converted into something else, be it ethylene glycol, 1,2-propanediol or 1,3-propanediol, these newly formed esters will have a smaller association constant and will thus readily be displaced by fresh glycerol.

Table 3. Borate ester association constants. [5]

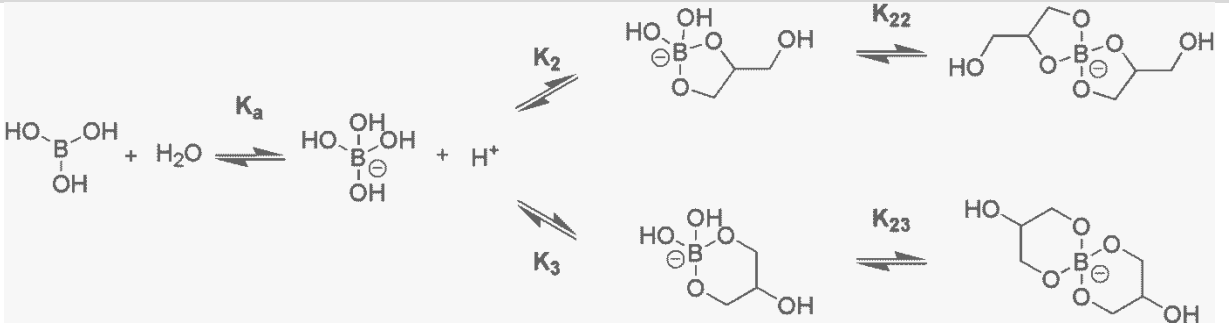

	K_2[a]	K_3[a]	K_{22}[a]	K_{23}[a]
Glycerol	11.2	1.7	2.0	0
Ethylene glycol	0.6	n.a.	0	n.a.
1,2-Propanediol	2.7	n.a.	0.6	n.a.
1,3-Propanediol	n.a.	0.9	n.a.	0

[a] ^{11}B NMR signals used for association constant determination

It is noted that from the glycerol hydrodeoxygenation products, 1,2-propanediol has the highest association constant, followed by 1,3-propanediol and ethylene glycol.

The phenylboronic acid ester association constants for glycerol and its hydrodeoxygenation products ethylene glycol, 1,2-propadiol and 1,3-propadiol were determined as well (Table 4). This showed the same trend as for when boric acid was used as the boron source. Glycerol forms most of the boronate ester, while 1,2-propanediol is the reaction product that has the highest association constant, followed by ethylene glycol and 1,3-propanediol.

So far it has been established that the amount of ester that can be formed can be controlled by choosing a bor(on)ic acid with a high pK_a. However, there is obviously a variable on the diol part of the equation that has an effect on bor(on)ate ester formation as well. For instance, the preference of glycerol to form 1,2-bor(on)ate esters can be partially explained by chance. There are two possibilities to form a glycerol-1,2-

bor(on)ate ester, while there is only one possibility to form a 1,3-glycerol bor(on)ate ester. However, this does not explain why 1,2-propanediol bor(on)ate ester is more readily formed than 1,3-propanediol bor(on)ate ester. The fact that relatively large amounts of 1,3-glycerol bor(on)ate esters are formed compared to 1,3-propanediol bor(on)ate esters suggests that this is not a result of ring strain, as this strain cannot be relieved by the presence of a secondary hydroxyl group. It is probable that 1,3-glycerol bor(on)ate ester is more readily formed because this product is better soluble in water compared to its 1,3-propanediol bor(on)ate ester counterparts and therefore benefits from an 'enthalpy bonus' due to the solvation by surrounding water molecules.

Table 4. Phenylboronate ester association constants. [5]

	K_2[a]	K_3[a]
Glycerol	6.5	3.0
Ethylene glycol	1.3	n.a.
1,2-Propanediol	4.1	n.a.
1,3-Propanediol	n.a.	0.2

[a] ^{1}H NMR diol signal data used for association constant determination

This leaves why 1,2-propanediol bor(on)ate ester is more readily formed than 1,3-propanediol bor(on)ate ester. An initial hint is given by (the lack of) ethylene glycol bor(on)ate ester formation. Why is the formation of 1,2-propanediol bor(on)ate ester favored over ethylene glycol bor(on)ate ester? Both are 1,2-bor(on)ate esters and the only difference is the presence of a mere methyl-group. Might this additional group have something to do with the increased amount of 1,2-propanediol bor(on)ate ester that is observed in the titration experiments? In order to investigate, a series of titration experiments with increasing tail-lengths were performed.

ENTROPY EFFECT OF INCREASING TAIL

The bor(on)ate ester association constants of ethylene glycol, 1,2-propanediol, 1,2-butanediol and 3-fluoro-1,2-propanediol were established using ^{11}B and ^{1}H NMR titrations and Scientist fittings (Table 5).

The results in this table show that the initial indication that an increasing substitution chain positively correlates with higher association constants. The hint of extra methyl group in 1,2-propanediol is responsible for increased ester formation is backed up by even higher ester formations for 1,2-butanediol and 3-fluoro-1,2-propanediol. The presence of the free moving substitution chain can have an effect on the entropy of the system, where a longer chain is responsible for a higher entropy and thus for higher ester formation due to the possibility to freely move around, while an ethylene glycol ester is rather rigid. This can be proven using Van 't Hoff plots, which can be obtained from temperature dependent titrations. The Van 't Hoff equation (equation 14) can be derived from equations 12 and 13.

12 $$\Delta G = \Delta H - T\Delta S$$

13 $$\Delta G = -RTlnK$$

14 $$lnK = -\frac{\Delta H}{R}\frac{1}{T} + \frac{\Delta S}{R}$$

Where ΔG is Gibbs energy, ΔH is enthalpy, T is temperature, ΔS is entropy, R is the gas constant (8.3145 $Jmol^{-1}K^{-1}$) and K is the equilibrium constant. The Van ´t Hoff equation can be plotted by assigning $1/T$ to the horizontal axis and lnK to the vertical axis. The datapoints can be measured by determining the association constant at different temperatures. These temperature dependent titrations have been performed for ethylene glycol, 1,2-propanediol, 1,2-butanediol and glycerol (Figure 6).

Table 5.

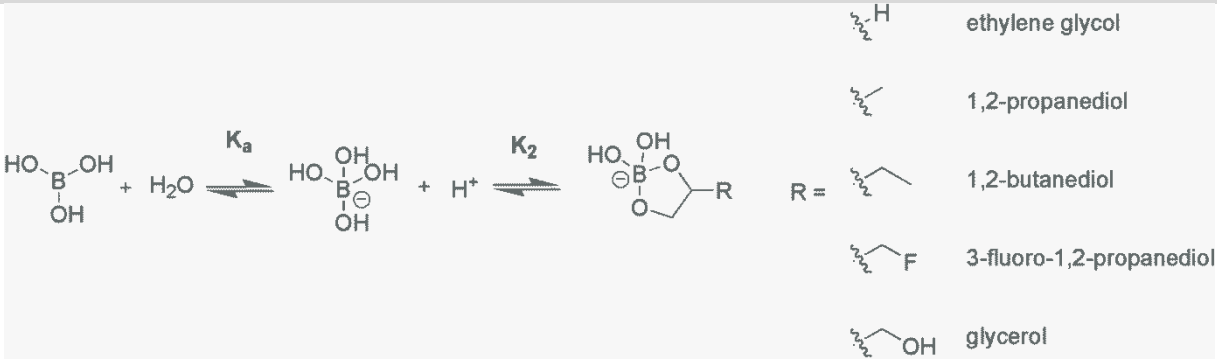

	Boronate ester[a]			Phenylboronic ester[b]	
	K_2	K_{22}	K_3	K_2	K_3
ethylene glycol	0.6	0	n.a.	1.3	n.a.
1,2-propanediol	2.7	0.6	n.a.	4.1	n.a.
1,2-butanediol	4.3	0.6	n.a.	6.1	n.a.
3-fluoro-1,2-propanediol	7.9	1.3	n.a.	6.6	n.a.
Glycerol	11.2	1.7	2.0	6.5	3.0
1,3-propanediol	n.a.	0	0.9	n.a.	0.2

[a] determined using the ^{11}B NMR signal; [b] determined using the ^{1}H NMR signal.

The enthalpy and entropy of the systems can be derived from these plots: the slope is equal to $-\Delta H/R$, while the intersection with the y-axis gives $\Delta S/R$. These thermodynamic quantities have been determined for 6 different borate esters, where the boric acid titration of glycerol resulted in the enthalpy and entropy of both 1,2- as 1,3-glycerol borate (Table 6).

The Gibbs energy for the 1,2-borate esters is decreasing in the series from ethylene glycol ester > 1,2-propanediol ester > 1,2-butanediol ester > 1,2-glycerol ester, which is in accordance with the observed equilibrium constants. Both the enthalpy and entropy are decreasing in the order 1,2-butanediol ester > 1,2-glycerol ester > 1,2-propanediol ester > ethylene glycol ester, which is the inverse trend of the Gibbs energy. However, since the entropy term ($-T\Delta S$) is inversely proportional to the temperature it will dominate the Gibbs energy at higher temperatures. As a result, a smaller entropy will result in a larger

entropy term (-*TΔS*) and therefore a higher Gibbs energy, associated with a smaller association constant (Figure 7).

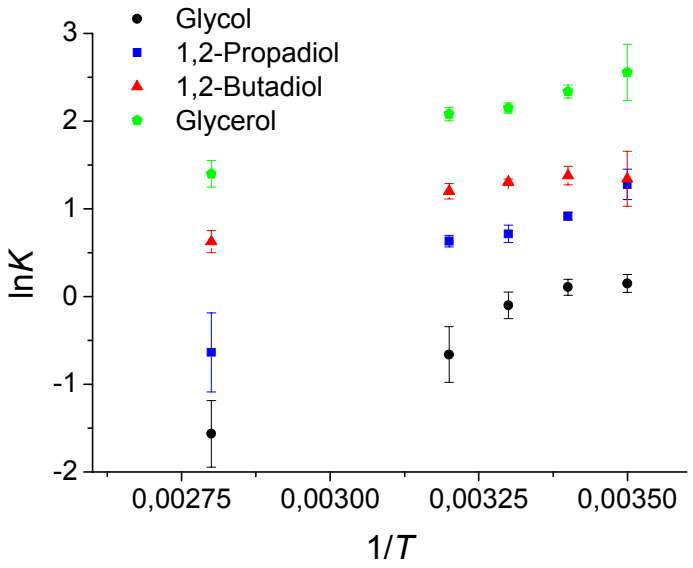

Figure 6. Van 't Hoff plots derived from temperature dependent titrations of boric acid and ethylene glycol, 1,2-propanediol, 1,2-butanediol and glycerol.

Table 6. Thermodynamic data derived from Van 't Hoff plots obtained by temperature dependent titration.

Borate ester	***ΔH*** **(kJ/mol)**	***ΔS*** **(J/mol·K)**	***ΔG*** **(kJ/mol) (293K)**
1,2-butanediol	-9.1	-20.0	-3.3
1,2-glycerol	-13.5	-26.3	-5.8
1,2-propanediol	-22.2	-67.4	-2.4
ethylene glycol	-21.9	-74.7	0.0
1,3-glycerol	-26.1	-85.0	-1.3
1,3-propanediol	-29.4	-99.5	-0.3

Figure 8 shows the Gibbs energies and their enthalpy and entropy terms for ethylene glycol borate ester and the 1,3-borate esters. These esters are compared as they have no free moving substitution chain, as defined in Table 5. The Gibbs energies for these esters is decreasing in the series from ethylene glycol ester > 1,3-propanediol ester > 1,3- glycerol ester, which is in accordance with the observed equilibrium constants. Both the enthalpy and entropy are decreasing in the order ethylene glycol > 1,3-glycerol ester > 1,3-propanediol ester. However, since the entropy term (-*TΔS*) is inversely proportional to the temperature it will dominate the Gibbs energy at higher temperatures. As a result, a smaller entropy will

result in a larger entropy term ($-T\Delta S$) and therefore a higher Gibbs energy, associated with a smaller association constant (Figure 8). In fact, even at room temperature only very small amounts of 1,3-borate esters are formed.

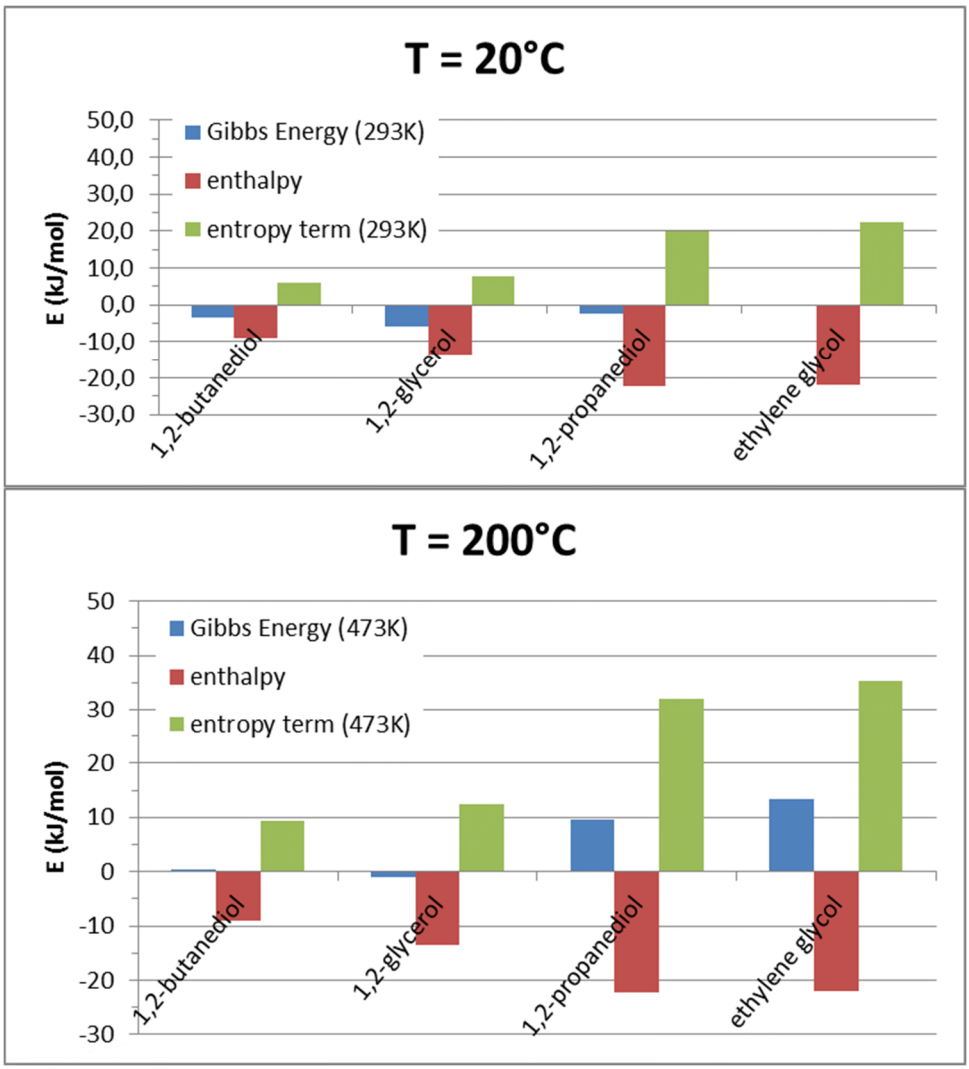

Figure 7. Gibbs energies, enthalpy and entropy terms at different temperatures for 1,2-borate esters; a) 20°C – borate ester formation at typical NMR experiment temperature; b) 200°C – borate ester formation at reaction temperature.

The entropy of 1,3-propanediol borate ester formation and 1,3-glycerol borate ester formation is smaller than ethylene glycol borate ester formation. This indicates that more entropy is lost upon 1,3-ester formation compared to 1,2-ester formation. This is in line with the entropy hypothesis, as the 1,3-propanediol and glycerol have more rotational axis than ethylene glycol, which are lost upon formation of the respective borate esters.

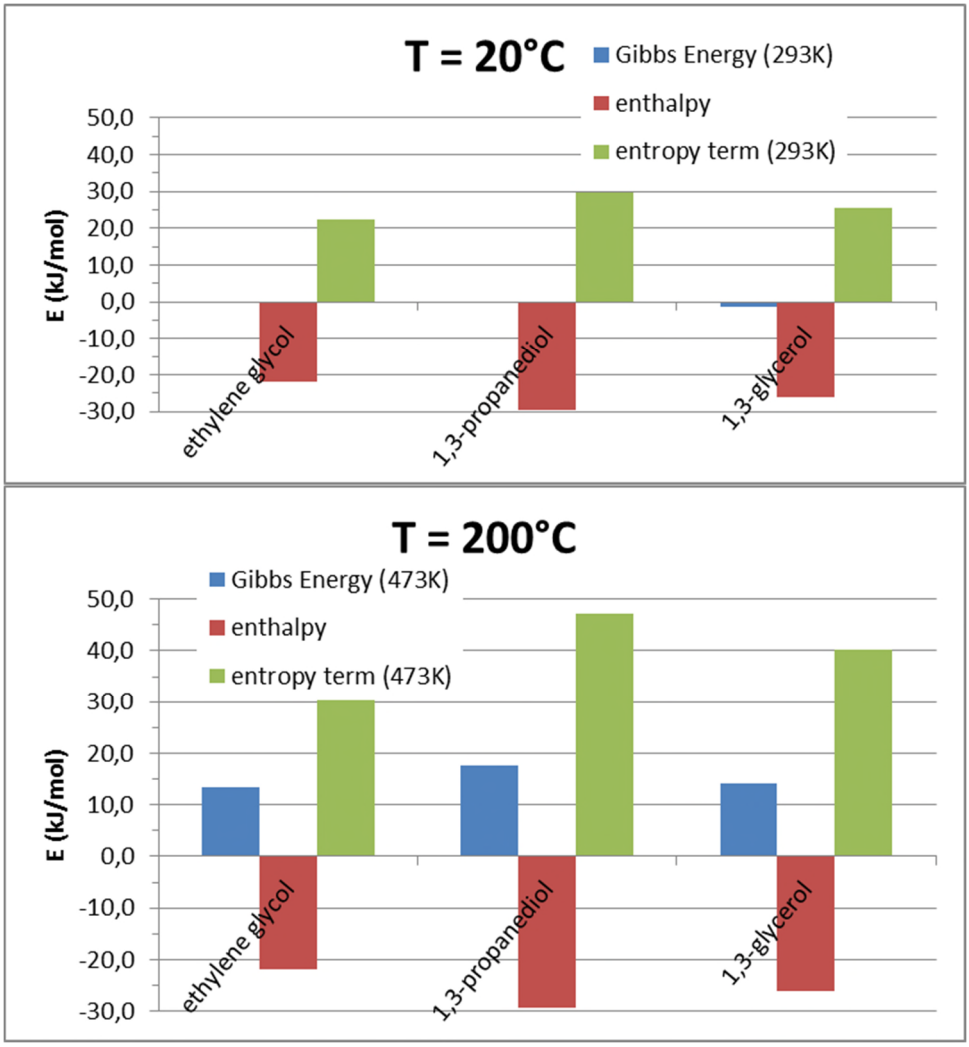

Figure 8. Gibbs energies, enthalpy and entropy terms at different temperatures for ethylene glycol borate and 1,3-borate esters; a) 20°C – borate ester formation at typical NMR experiment temperature; b) 200°C – borate ester formation at reaction temperature.

CONCLUSION

Borate ester and boronate ester formation are dependent on both the nature of the boron species and the the diol. The amount of bor(on)ate ester that is formed is a function of the pK_a of the respective boron species. The less acidic the boronic acid, the more ester is formed.

The diol has an influence as well. 1,2-bor(on)ate esters are preferred over 1,3-bor(on)ate esters and having diols with a longer tail yields more ester. It was shown using temperature dependent NMR titrations that this is due to an entropy effect. This effect can be rationalized as follows. The formation of a 1,3-boronate ester leads to a more rigid structure, thereby losing more degrees of freedom compared to a 1,2-boronate ester. This leads to an entropy penalty and results in a higher selectivity towards 1,2-boronate esters.

The effect of boric acid as a co-catalyst in the hydrogenolysis of glycerol is described in Chapter 1.

REFERENCES

[1] J.A. Peeters, Coord. Chem. Rev., 2014, 268, 1-22.

[2] A. Krężel and W. Bal, J. Inorg. Biochem., 2004, 98, 161-166.

[3] L.I. Bosch, T.M. Fyles and T.D. James, Tetrahedron, 2004, 60, 11175-11190.

[4] J. Yan, G. Springsteen, S. Deeter and B. Wang, Tetrahedron, 2004, 60, 11205-11209.

[5] J.P. Lorand and J.O. Edwards, J. Org. Chem., 1959, 24, 769-774.

APPENDIX A1

```
// pKa BOR(ON)IC ACID
IndVars: pH, Btot
DepVars: delB
Params: pK1, delBmin, delB0

H = 10^(-pH)
K1 = 10^(-pK1)
B0 = (Bmin*H) / K1
Btot = B0 + Bmin
fBmin = Bmin / (Bmin + B0)
delB = fBmin * delBmin + (1-fBmin) * delB0

0 < Bmin < Btot
0 < pH < 14

***
Where:
Btot        = total boron concentration
delB        = chemical shift B⁰/B⁻ signal
pK1         = pKa bor(on)ic acid species
delBmin     = chemical shift of a pure B⁻ signal
delB0       = chemical shift of a pure B⁰ signal
H           = proton concentration
K1          = Ka bor(on)ic acid species
B0          = B⁰ concentration
Bmin        = B⁻ concentration
fBmin       = B⁻ fraction
```

APPENDIX A2

```
// 2 BORATEESTER (mono-ester & di-ester)
IndVars: pH, Btot, Ltot
DepVars: IntB, IntBL, IntB2L, delB
Params: K2, K3

pK1 = 9.85282652
delBmin = -17.7849312
delB0 = 0

H = 10^(-pH)
K1 = 10^(-pK1)

B = (Bmin * H) / K1
BL = K2 * Bmin * L
B2L = K3 * BL * L
Btot = B0 + Bmin + BL + B2L
Ltot = L + BL + 2 * B2L
fBmin = Bmin / (Bmin + B0)
delB = fBmin * delBmin + (1 - fBmin) * delB0
fB = (B0 + Bmin) / Btot
intB = 100 * fB
fBL = BL / Btot
intBL = 100 * fBL
fB2L = B2L / Btot
intB2L = 100 * fB2L

0 < Bmin < Btot
0 < L < Ltot
0 < pH < 14

// B0 = boric acid
// Bmin = borate
// BL = borate ester
// B2L = borate diester

***
Where:
Ltot        = total ligand concentration
intB        = integral of B⁰/B⁻ signal
intBL       = integral of borate ester signal
intB2L      = integral of borate diester signal
K2          = association constant borate ester (K2)
K3          = association constant borate diester (K22 or 3)
BL          = borate ester concentration
B2L         = borate diester concentration
L           = ligand concentration
fB          = B⁰/B⁻ fraction
fBL         = borate ester fraction
fB2L        = borate diester fraction
```

APPENDIX A3

```
// 4 BORATEESTERS (2 x mono-ester & 2 x di-ester)
IndVars: pH, Btot, Ltot
DepVars: IntB, IntBL2, IntB2L2, IntBL3, IntB2L3
Params: K2, K3, K4, K5

pK1 = 9.85282652
delBmin = -17.7849312
delB0 = 0

H = 10^(-pH)
K1 = 10^(-pK1)

B0 = (Bmin * H) / K1
BL2 = K2 * Bmin * L
B2L2 = K3 * BL2 * L
BL3 = K4 * Bmin * L
B2L3 = K5 * BL3 * L
Btot = B0 + Bmin + BL2 + B2L2 + BL3 + B2L3
Ltot = L + BL2 + 2*B2L2 + BL3 + 2*B2L3
fBmin = Bmin / (Bmin + B0)
delB1 = fBmin * delBmin + (1 - fBmin) * delB0
fB = (B0 + Bmin) / Btot
intB = 100 * fB1
fBL2 = BL2 / Btot
intBL2 = 100 * fBL2
fB2L2 = B2L2 / Btot
intB2L2 = 100 * fB2L2
fBL3 = BL3 / Btot
intBL3 = 100 * fBL3
fB2L3 = B2L3 / Btot
intB2L3 = 100 * fB2L3

0 < Bmin < Btot
0 < L < Ltot
0 < pH < 14

// B0 = boric acid
// Bmin = borate
// BL2 = 1,2-ester
// B2L2 = 1,2-diester
// BL3 = 1,3-ester
// B2L3 = 1,3-diester

***
Where:
K2          = association constant borate 1,2-ester (K2)
K3          = association constant borate 1,2-diester (K22)
K4          = association constant borate 1,3-ester (K3)
K5          = association constant borate 1,3-diester (K23)
```

APPENDIX A4

```
// 1 BORONATE ESTER
IndVars: pH, Btot, Ltot
DepVars: IntB, IntBL, delB
Params: K2

pK1 = 9.30072742
delBmin = -16.1859394
delB0 = 9.33131056

H = 10^(-pH)
K1 = 10^(-pK1)

B0 = (Bmin * H) / K1
BL = K2 * Bmin * L
Btot = B0 + Bmin + BL
Ltot = L + BL
fBmin = Bmin / (Bmin + B0)
delB = fBmin * delBmin + (1 - fBmin) * delB0
fB = (B0 + Bmin) / Btot
intB = 100 * fB
fBL = BL / Btot
intBL = 100 * fBL

0 < Bmin < Btot
0 < L < Ltot
0 < pH < 14

// B0 = boronic acid
// Bmin = borate
// BL = borate ester

***
Where:
K2          = association constant boronate ester (K2 or 3)
```

APPENDIX A5

```
// 2 BORATEESTER (1,2-ester & 1,3-ester)
IndVars: pH, Btot, Ltot
DepVars: IntB, IntBL2, IntBL3, delB
Params: K2, K3

pK1=7.76231682
delBmin=-17.8162781
delB0=8.45640741

H = 10^(-pH)
K1 = 10^(-pK1)

B0 = (Bmin * H) / K1
BL2 = K2 * Bmin * L
BL3 = K3 * Bmin * L
Btot = B0 + Bmin + BL2 + BL3
Ltot = L + BL2 + BL3
fBmin = Bmin / (Bmin + B0)
delB = fBmin * delBmin + (1 - fBmin) * delB0
fB = (B0 + Bmin) / Btot
intB = 100 * fB
fBL2 = BL2 / Btot
intBL2 = 100 * fBL2
fBL3 = BL3 / Btot
intBL3 = 100 * fBL3

0 < Bmin < Btot
0 < L < Ltot
0 < pH < 14

// B0 = boronic acid
// Bmin = boronate
// BL2 = 1,2-boronate ester
// BL3 = 1,3-boronate ester

***
Where:
K2          = association constant boronate 1,2-ester (K2)
K3          = association constant boronate 1,3-ester (K3)
```

CHAPTER 2

Pt/Al_2O_3 CATALYZED 1,3-PROPANEDIOL FORMATION FROM GLYCEROL USING TUNGSTEN ADDITIVES

This chapter is based on the publication "J. ten Dam, K. Djanashvili, F. Kapteijn and U. Hanefeld, ChemCatChem 5 (2013) 497-505."

ABSTRACT

Screening of four commercial catalysts (Pt/Al_2O_3, Pt/SiO_2, Pd/Al_2O_3 and Pd/SiO_2) and four acidic additives (hydrochloric, tungstic, phosphotungstic and silicotungstic acid) showed that the combination of a platinum hydrogenation catalyst with tungsten containing acidic additives yields 1,3-propanediol from aqueous glycerol. The performance of the best catalytic system Pt/Al_2O_3 with silicotungstic acid as additive was optimized by experimental design, capturing the influence of reaction time, glycerol concentration, acid concentration, pressure and temperature on the formation of 1,3-propanediol from glycerol. State of the art 1,3-propanediol yield in an aqueous batch system could be achieved (49% conversion, 28% selectivity) with excellent 1,3-propanediol to 1,2-propanediol ratios. A mechanistic interpretation is given for this bifunctional system, supported by the relative stability of 1,3-propanediol in comparison with 1,2-propanediol under the chosen reaction conditions.

Keywords: Heterogeneous Catalysis; Glycerol; Elimination; Hydrogenation; Hydrogenolysis.

1 INTRODUCTION

Renewable glycerol is the starting material in a wide range of processes and can be converted into a plethora of products. [1] A product of particular interest is 1,3-propanediol (13PD), which is used in the polyester polypropylene terephthalate. 13PD can be produced via hydrogenolysis. While its regioisomer 1,2-propanediol (12PD) can be produced at both high conversion and selectivity, [2-4] this proves to be more challenging for 13PD (Table 1). [5-16]

Table 1. State of the art in selective hydrogenolysis of glycerol to 1,3-propanediol.

Catalyst	Solvent	Additive	Pressure[a] (bar)	Temperature (°C)	TOF[b]	Conversion of glycerol (%)	Selectivity ($\%_{13PD}$)	Selectivity 13PD/12PD	Yield ($\%_{13PD}$)	Reference
Batch operation										
Pt/sulfated ZrO_2	DMI[c]		73	170	6.8	67	84	19	56	[5]
Ir-ReO_x/SiO_2	H_2O	H_2SO_4	80	120	12.0	50	49	4.9	25	[6]
Pt/WO_3/ZrO_2	DMI[c]		80	170	4.0	86	28	1.9	24	[7]
Pt/WO_3/ZrO_2	DMI[c]-EtOH[d]		55	170	4.6	46	29	1.6	13	[8]
Pt-Re/C	H_2O		40	170	5.7	45	29	1.1	13	[9]
Rh-ReO_x/SiO_2	H_2O		80	120	17.3	79	14	0.3	11	[10,11]
Pt/WO_3/TiO_2/SiO_2	H_2O		55	180	2.8	15	51	5.5	7.7	[12]
Rh/C	Sulfolane	H_2WO_4	80	180	0.1	32	12	2.0	3.8	[13]
Rh/SiO_2	H_2O	Amberlyst 15	80	120	1.1	14	10	0.4	1.4	[14]
Continuous operation										
Pt/WO_3/ZrO_2	H_2O		40	130	4.0	70	46	18	32	[15]
Cu-STA/SiO_2[e]	-		5.4	210	0.2	83	32	1.4	27	[16]

a) applied H_2 pressure; b) Turnover frequency ($mmol_{13PD}mmol_{metal}^{-1}h^{-1}$); c) dimethyl imidazolinone (DMI); d) ethanol (EtOH); e) silicotungstic acid (STA).

What is often indicated as hydrogenolysis is in most instances an elimination of water followed by a hydrogenation of the formed double bond on a metallic surface. [17,18] The catalytic role of the acidic components in the catalytic systems listed in Table 1 is the initial dehydration of glycerol. This is the key

step defining the selectivity of the catalyst. When one of the two primary hydroxyl groups is eliminated, 12PD will be obtained. Only when the secondary alcohol is eliminated 13PD will be formed (Scheme 1).

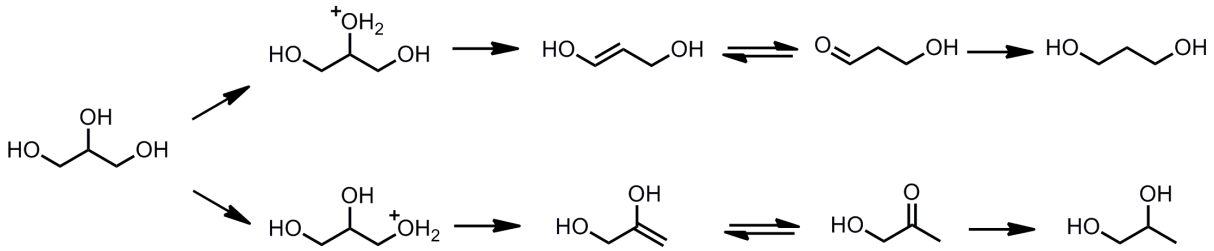

Scheme 1. Formation routes of 1,2-propanediol and 1,3-propanediol from glycerol.

The initial dehydration to form acetol is thermodynamically favored over the formation of 3-hydroxypropanal (Scheme 2). [15] This exemplifies the difficulties in achieving high 13PD selectivities and it follows that the formation of 13PD is kinetically controlled. The formation of a relatively stable secondary carbocation as an intermediate during the formation of 13PD, resulting from the acid catalyzed alcohol elimination is at the heart of kinetic control. [17,19]

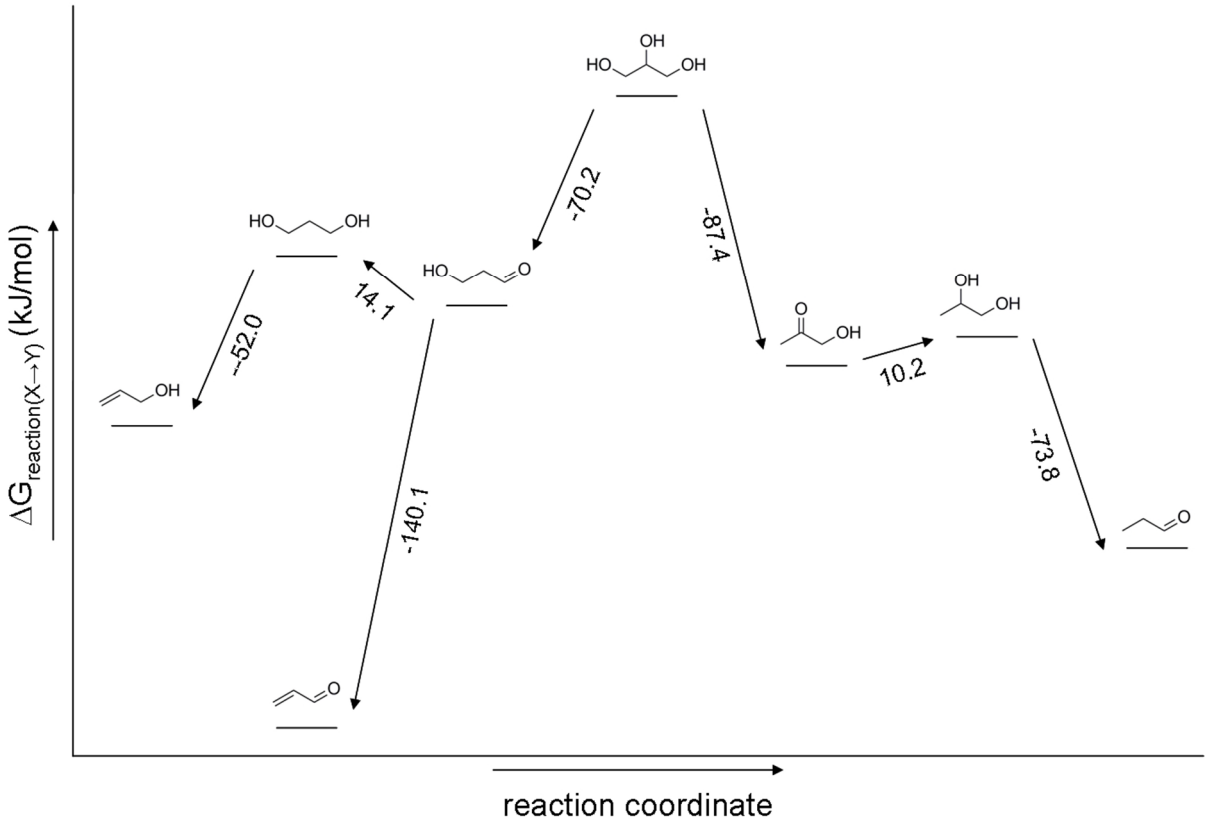

Scheme 2. Reaction energies for glycerol to 12PD and 13PD and their intermediates and degradation products.

Good conversions and 13PD selectivities have been obtained by using either water or 1,3-dimethyl-2-imidazolidinone (DMI) as a solvent (Table 1). However, from an environmental point of view, the use of water is clearly preferred.

Amongst the catalytic systems that display the highest 13PD selectivity several tungsten containing species are present (Table 1). Tungsten has been used as tungsten oxide, tungstic acid and immobilized silicotungstic acid. [7,8,12,13,15,16] However, the role of the tungsten species has not yet been elucidated. Apparently, tungsten plays a yet not understood role in 13PD selectivity.

These two conclusions from Table 1 prompted us to investigate in more detail the role of several tungsten containing acids in the conversion of aqueous glycerol.

2 EXPERIMENTAL SECTION

2.1 MATERIALS

The catalysts used in this work were purchased from Acros Organics (5% Pt/Al_2O_3, 5% Pd/Al_2O_3), Sigma Aldrich (1% Pt/SiO_2) and Strem (5% Pd/SiO_2). 12PD 99%, n-propanol 99.7% (n-PrOH), ethylene glycol 99.8% (EG), silicotungstic acid ≥99.9% (STA), phosphotungstic acid (PTA) and tungstic acid ≥99.0% were purchased from Sigma Aldrich, glycerol 99+% and 1,3-propanediol 98% (13PD) were purchased from Acros Organics, ethanol 99.8% (EtOH) was purchased from Merck and methanol 99.8% (MeOH) and hydrochloric acid 36-38% was purchased from J.T. Baker. All chemicals were used as received and the catalysts were not pretreated before reaction.

2.2 REACTION PROCEDURE

2.2.1 PREPARATION OF REACTION MIXTURE

Aqueous reaction mixtures were prepared by dissolving appropriate amounts of glycerol and acid in demineralized water in a volumetric flask. [4] The hydrogenolysis of glycerol was performed in a HEL PolyBLOCK 8, a parallel autoclave reactor system consisting of eight 16 mL vessels. The appropriate amount of catalyst (25 μmol active metal, relative to glycerol) was added to 5 mL of aqueous reaction mixture. Reactors were purged 3 times with N_2 (20 bar) and 3 times with H_2 (40 bar). Then they were pressurized to the appropriate pressure, stirred at 800 rpm and heated to the reaction temperature within 20 min. Stirring was stopped after the indicated reaction time and the reactors were allowed to cool down to room temperature. The reaction mixture was filtered over a nylon micro filter (Rotilabo, 0.2 μm). An HPLC sample was prepared by diluting filtered reaction mixture using 5 mM H_2SO_4. The liquid products were analyzed by HPLC. Products detected by HPLC were 13PD, 12PD, ethylene glycol (EG), n-propanol (n-PrOH) and ethanol (EtOH). [4,20]

2.2.2 CATALYST RECYCLING

After a standard reaction procedure, the reaction mixture was centrifuged at 900 G using a Heraeus Megafuge 2.0R centrifuge. The supernatant was removed for sampling and 5.5 mL fresh reaction mixture was added to the centrifuged catalyst. 0.5 mL reaction mixture was taken for t = 0 h HPLC sample and the remaining reaction mixture was submitted to a second run, using the standard reaction procedure.

2.3 ANALYSIS

2.3.1 NITROGEN PHYSISORPTION

Porosity and surface area were determined by nitrogen physisorption measurements (Table 2) on a Quantachrome Autosorb-6B at 77 K. Prior to the measurements, the samples were degassed overnight under vacuum at 230 °C using a Quantachrome Autosorb degasser.

Table 2. Porosity and BET surface area of catalysts.

Catalyst	Metal loading (wt.%)	V_{pore} (mL/g)	S_{BET} (m^2/g)
Pt/Al_2O_3	5	0.44	212
Pt/SiO_2	1	1.03	236
Pd/SiO_2	5	1.00	221
Pd/Al_2O_3	5	0.24	171

2.3.2 TEM

Transmission electron microscopy (TEM) was performed using a FEI Tecnai TF20 electron microscope with a field emission gun as the source of electrons operated at 200 kV. Samples were mounted on Quantifoil® carbon polymer supported on a copper grid by placing a few droplets of a suspension of ground sample in ethanol on the grid, followed by drying at ambient conditions.

2.3.3 HPLC ANALYSIS

Samples were analyzed on a CARBOSep COREGEL-87H3 column using a Waters 515 HPLC pump (0.8 mL·min-1) equipped with a Shodex RI SE-61 detector, a Perkin Elmer Series 200 Autosampler (10 μL injection) and a Chrompack HPLC column thermostat SpH 99 (70 °C). 5 mM H2SO4 (pH 1.5) in demineralized water was used as eluent. This resulted in the following retention times: 9.9 (glycerol), 11.9 (EG), 12.7 (12PD), 13.0 (13PD), 14.2 (methanol (MeOH)), 16.2 (EtOH) and 19.8 (n-PrOH). [4,20] Calibration curves of these analytes were constructed to analyze the product concentrations. Products detected by HPLC were 12PD, 13PD, EG, n-PrOH and EtOH. Gaseous degradation and condensation

products were not detected by HPLC. Conversion (C) and selectivity (Sanalyte) were calculated by equations (1) and (2), respectively.

$$C = \frac{[glycerol]_0 - [glycerol]_x}{[glycerol]_0} \cdot 100 \qquad \textbf{(1)}$$

$$S_{analyte} = \frac{\left([analyte]_x / [glycerol]_0\right) \cdot 100}{C} \cdot 100 \qquad \textbf{(2)}$$

where [glycerol]x and [analyte]x stand for glycerol and analyte concentration at reaction time x in hours. Degradation accounts for the formation of gaseous products and is calculated using equation (3). In this case it is assumed that

$$degradation = 100 - \sum_{analyte} S_{analyte} \qquad \textbf{(3)}$$

2.4 Design of Experiment

Using Design Expert software (version 8.0.1) a five-level-five-factor half fraction Central Composite Design (CCD) with 8 center points was designed to investigate the influence of the parameters on both glycerol conversion and 13PD selectivity. The selected factors were pressure, silicotungstic acid concentration, glycerol concentration, reaction time and temperature. Experiments were performed in a randomized order.

3 RESULTS AND DISCUSSION

3.1 Catalyst selection

Hydrogenolysis of glycerol can be considered as a two-step process in which an acid promotes glycerol dehydration, while the resulting double bonds are hydrogenated over a heterogeneous catalyst (Scheme 1). Selectivity towards 13PD can be enhanced by selecting an appropriate acid and hydrogenation catalyst. The acid plays a decisive role in which a hydroxyl group is eliminated, while a swift consecutive hydrogenation prevents further dehydration. [17,18] Three types of tungsten additives (tungstic acid, phosphotungstic acid and silicotungstic acid) were tested in combination with four commercially available hydrogenation catalysts (Pd/SiO_2, Pd/Al_2O_3, Pt/SiO_2 and Pt/Al_2O_3) to investigate their influence on aqueous glycerol conversion and 13PD selectivity. The platinum and palladium catalysts were chosen for their hydrogenation capabilities, while tungsten components were shown to result in 13PD selectivity before, [7,8,12,13,15,16]. The tungsten heteropolyacids are known for their relative thermal instability, however, these kind of catalysts have been successfully applied at similar conditions, [21] even on an industrial scale. [22]

3.2 ACIDS

The performance of the additives tungstic acid, phosphotungstic acid and silicotungstic acid was tested in combination with four hydrogenation catalysts. In order to be able to make a proper comparison, the four catalysts were also tested in absence of any additional acid and in the presence of a non-tungsten containing acid, hydrochloric acid. In absence of acid, glycerol was selectively converted into 12PD, while considerable amounts of degradation products were observed as well (Figure 1a). The activity and selectivity of the four catalysts was comparable, when hydrochloric acid pH 1.5 (similar to the pH of the silicotungstic and phosphotungstic acid) was used (Figure 1b); although small amounts of 13PD were now observed, mainly n-PrOH and other degradation products were formed. Apparently, dehydration was so favourable that either the intermediate 3-hydroxypropanal could not be hydrogenated in time, or that the initially formed propanediols are not stable under reaction conditions and are subsequently dehydrated and degraded. This points towards a stabilizing effect of the tungsten in the different tungsten containing acids. Possibly a glycerol tungstic acid ester is formed as an intermediate, which in combination with tungsten's favourable acidic properties leads to 13PD selectivity. [23-25]

Interestingly, 20 to 40% 13PD formation is observed when a tungsten containing acidic additive is used (Figure 1c-e) in combination with a Pt based catalyst. Moreover, only very small amounts of 12PD were observed. In case heterogeneous tungstic acid is added (Figure 1c), the platinum catalysts selectively produce 13PD, while the palladium catalysts yield 12PD. When phosphotungstic acid is used as a homogeneous additive, 13PD is formed on the platinum catalysts. Fascinatingly, very little to no 13PD or 12PD is formed on the palladium catalysts. Instead higher amounts of n-PrOH and degradation products were observed (Figure 1d).

Silicotungstic acid, another homogeneous tungsten containing acid, gave similar results as phosphotungstic acid, although higher amounts of 13PD are formed with palladium catalysts (Figure 1e).

3.3 PLATINUM VERSUS PALLADIUM

The four tested heterogeneous catalysts contained either palladium or platinum metal on silica or alumina. The conversion of glycerol on these four catalysts was similar when hydrochloric acid was used (Figure 1b), while in the other examples the Pt catalysts showed both higher conversion of glycerol and higher 13PD selectivity. Apparently, platinum is a more active hydrogenation metal to hydrogenate the intermediate 3-hydroxypropanal before it can be further dehydroxylated. This observation is supported by the fact that the 13PD selectivity over the platinum catalysts is higher than over the palladium catalysts (Figure 1c-e). The 12PD selectivity observed with Pd and tungstic acid (Figure 1c) indicates that it is not only the acid that directs the elimination. Although a tungsten additive was used, no 13PD selectivity was observed. This is probably due to the fact that the solid and heterogeneous tungsten acid has less

possibilities for glycerol coordination compared to the homogeneous silico- and phosphotungstic acid. This, in combination with the lower hydrogenation activity of palladium resulted in 12PD formation.

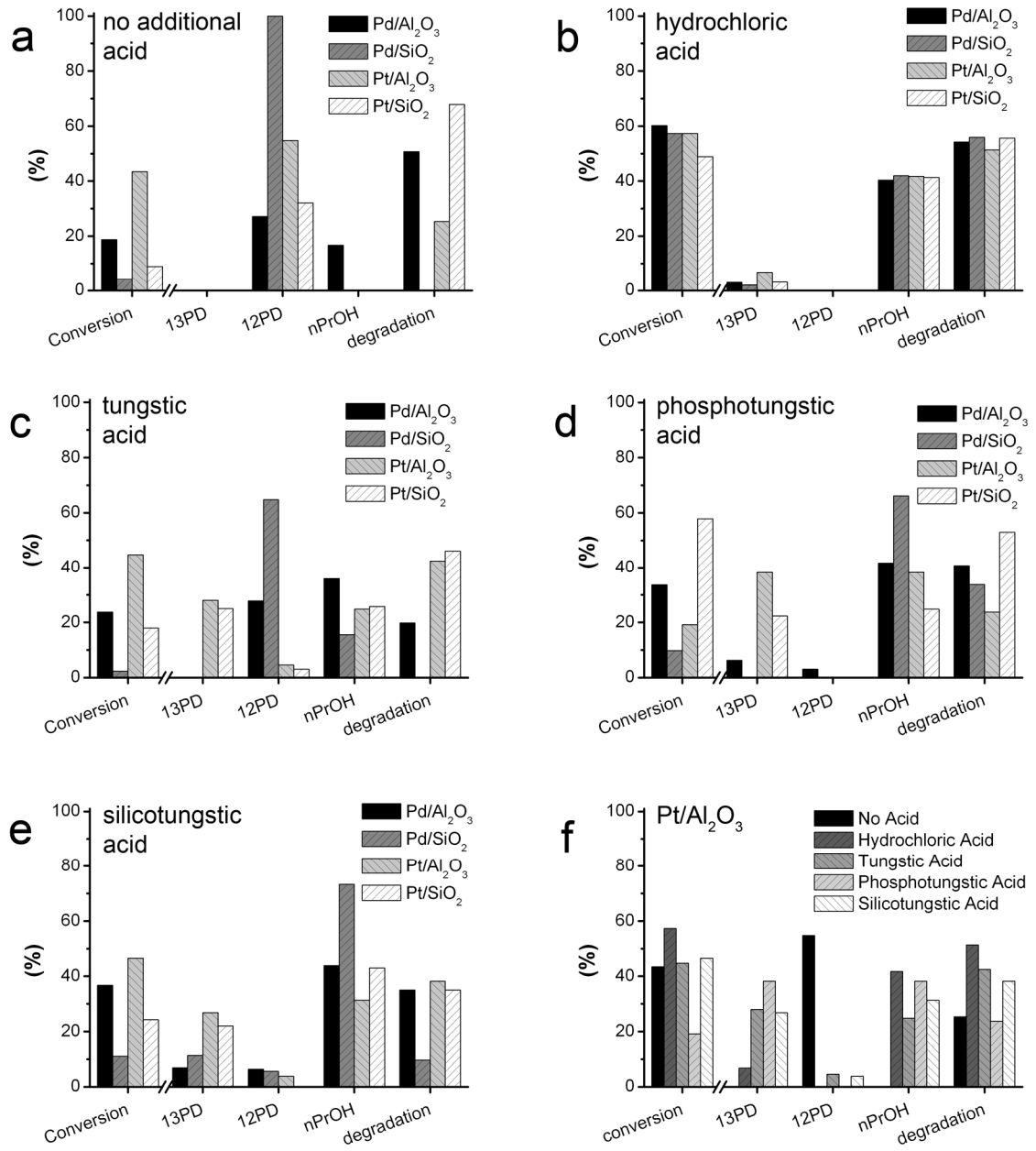

Figure 1. Reaction conditions: 25 μmol active metal; 5 mL 100 mM aqueous glycerol; indicated acidic additive; 200 °C; 40 bar H_2; 18 hours; 800 rpm; a) without additional acid; b) hydrochloric acid (pH 1.5); c) 40 mM tungstic acid; d) 3.5 mM phosphotungstic acid; e) 3.5 mM silicotungstic acid; f) Pt/Al_2O_3.

3.4 Silica versus Alumina

A comparison of the activity and selectivity between SiO_2 and Al_2O_3 based catalysts shows that the support has limited influence on the selectivity. However, the Al_2O_3 supported catalysts generally have a

higher activity than their SiO_2 counterpart. The only exception is Pt/Al_2O_3 vs. Pt/SiO_2 when phosphotungstic acid is used as an additive (Figure 1d). In this case the activity of Pt/SiO_2 exceeds that of Pt/Al_2O_3, but with a poor selectivity.

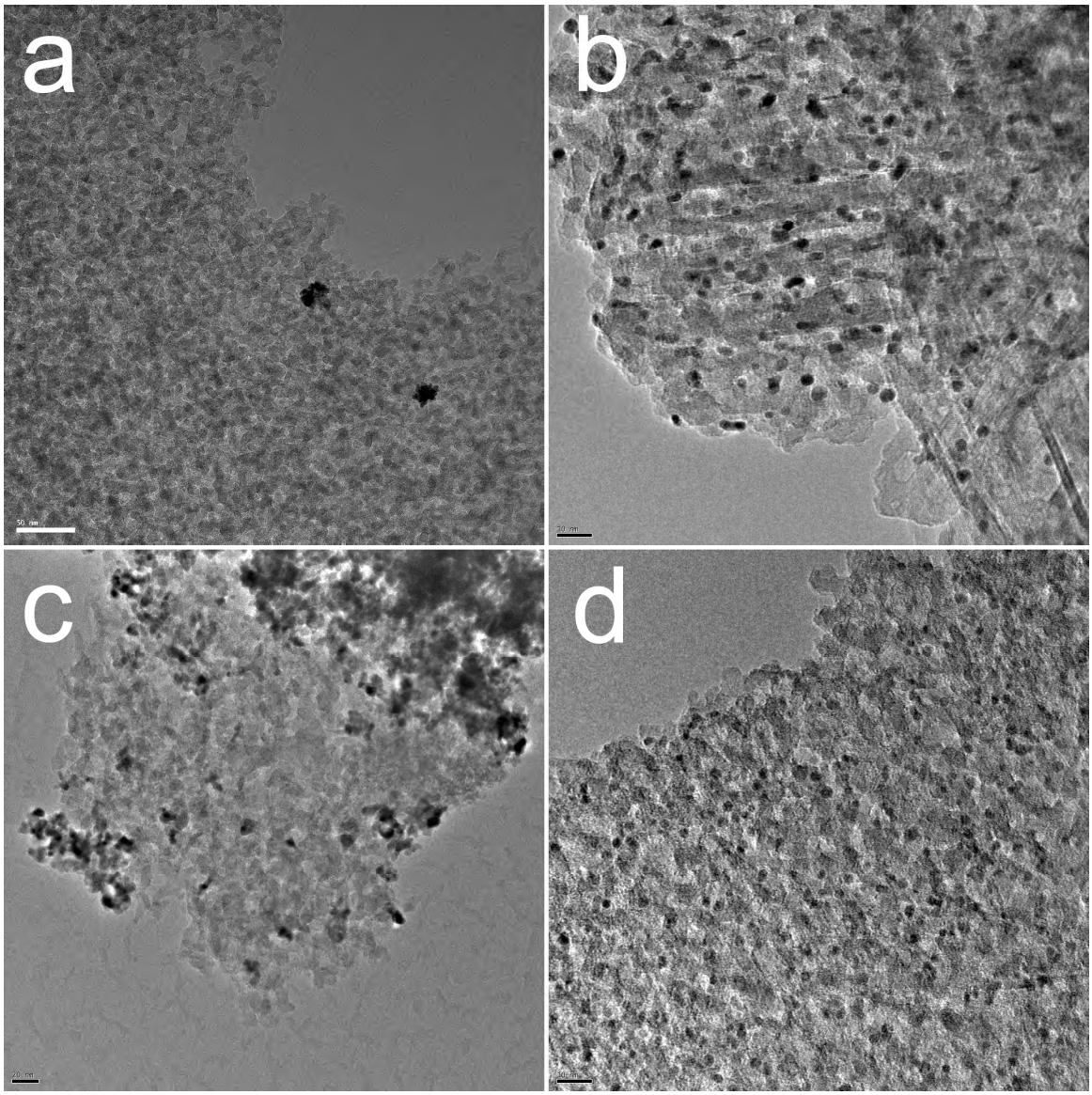

Figure 2. TEM images; a) 1 wt.% Pt/SiO2, bar is 50 nm; b) 5 wt.% Pt/Al2O3, bar is 10 nm; c) 5 wt.% Pd/SiO2, bar is 20 nm; d) 5 wt.% Pd/Al2O3, bar is 10 nm.

The influence of the support on the activity might be explained by the basicity of the Al_2O_3 support. The basic sites on the surface can provide additional dehydration and condensation opportunities, whereas the weak acid sites of the SiO_2 surface are irrelevant in comparison to the acidity of the additive.

Furthermore, the higher metal dispersion on the alumina support, compared to silica (Figure 2), explains the higher conversion over the alumina supports.

3.5 CENTRAL COMPOSITE DESIGN

The catalytic performance tests of the previous section showed that the Pt/Al_2O_3 catalyst gave highest 13PD selectivity in combination with high catalytic activity. The combination of Pt/Al_2O_3 with silicotungstic acid as an additive was chosen as the catalytic system for further optimization. Silicotungstic acid was preferred over phosphotungstic acid because of its superior activity, while the homogeneous silicotungstic acid was considered as a better defined system than the heterogeneous tungstic acid (Figure 1f).

The effects of reaction time (3.5-23.5 h), aqueous glycerol concentration (10-1380 mM), silicotungstic acid concentration (0-12.5 mM), pressure (20-50 bar) and temperature (150-220 °C) on the conversion of glycerol and the selectivity towards 13PD over the Pt/ Al_2O_3 catalyst were investigated through a five-level-five-factor half fraction Central Composite Design (CCD), consisting of 34 experiments (16 factorial points, 10 star points and 8 centre points). The centre point was reproduced eight times in order to obtain a good estimate for the standard deviation of the system and to warrant reproducibility of the reaction over time.

In this design procedure the experimental results of the CCD (Supplementary Information, Table S1, Appendix 3) were correlated by a second order polynomial (equation 4), capturing both the linear and nonlinear effects of the individual variables and the effect of the interaction between variables.

$$y = \beta_0 + \beta_{1i}x_i + \beta_{ij}x_i x_j + \beta_{2i}x_i^2 + \varepsilon \quad (4)$$

Here, y is the response (in this case glycerol conversion or 13PD selectivity), xi is variable i, β0 is the intercept and βni is the coefficient of variable i, βij is the coefficient of the interaction between variable xi and xj and ε includes the experimental error and the effects of any uncontrolled variable present. The polynomial is represented in insightful Response Surface Model (RSM) plots (Figure 3) which readily visualize the influence of the variables.

The correlation model for the conversion of glycerol indicated that temperature and reaction time have the most significant effect (Figure 3a and 3b). Other variables like pressure and silicotungstic acid concentration have an effect on glycerol conversion as well, but to a lesser extent (Figure 3a, 3c and 3d). Interestingly, the glycerol concentration did not influence the glycerol conversion. This means that, since in all experiments 25 μmol platinum was used, Pt/Al_2O_3 was most active at high glycerol concentration.

The model for the 13PD selectivity shows that temperature and silicotungstic acid concentration are the most important variables influencing the selectivity (Figure 3e and 3f).

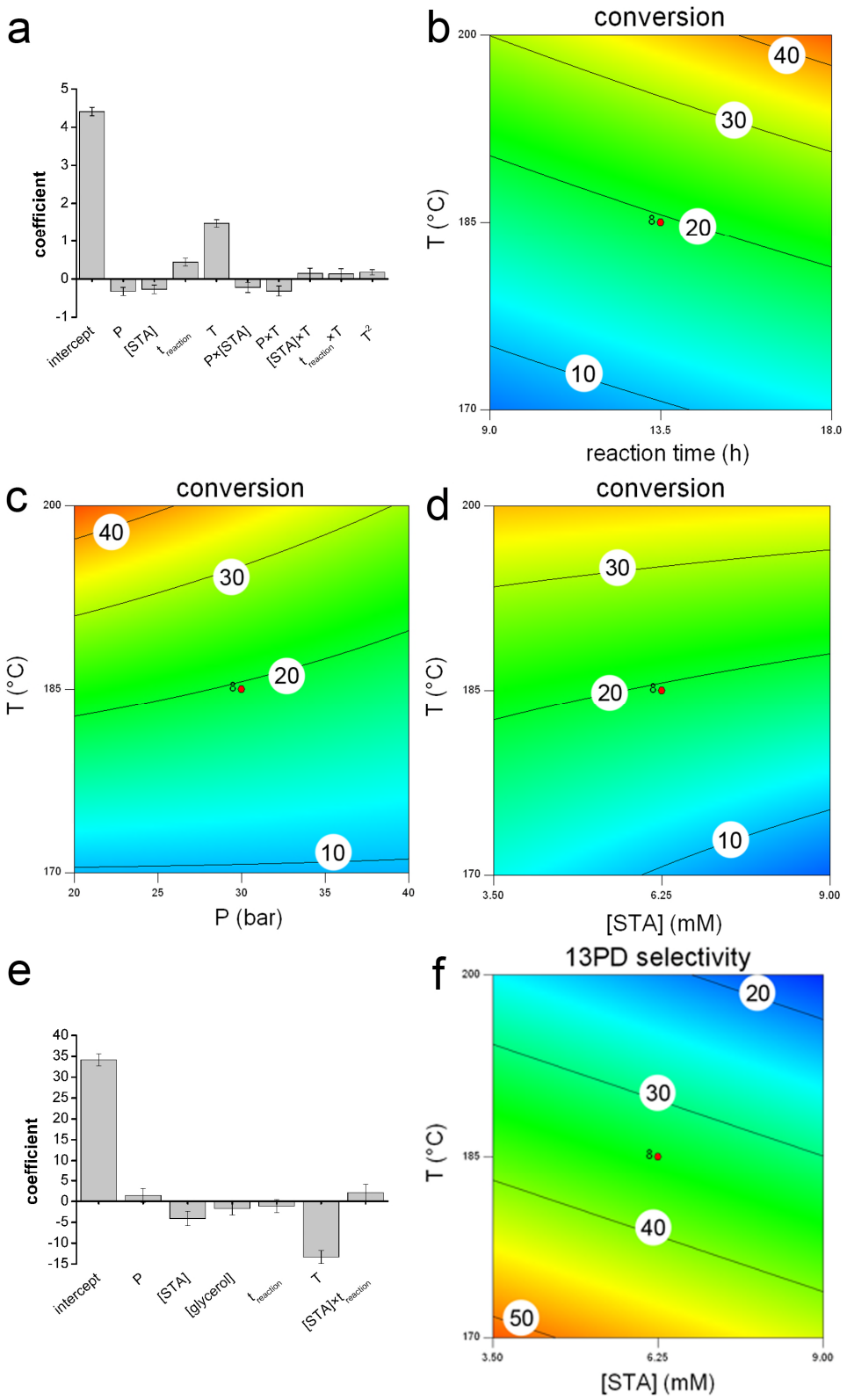

Figure 3. a) Coefficient plot glycerol conversion; b) RSM plot glycerol conversion (reaction time vs. temperature); c) RSM plot glycerol conversion (pressure vs. temperature); d) RSM plot glycerol conversion (silicotungstic acid concentration vs. temperature); e) Coefficient plot 13PD selectivity; f) RSM plot 13PD selectivity (silicotungstic acid concentration vs. temperature).

The Response Surface Graphs ('RSM plots') analysis reveals that highest glycerol conversions are obtained at long reaction time and high temperature, whereas the highest 13PD selectivity is obtained at lower temperatures and low silicotungstic acid concentration. As a result, the activity and selectivity cannot be optimized simultaneously. This result can be rationalized by considering the reaction mechanism of 13PD formation (Scheme 1). The high temperatures will positively influence the initial endothermal dehydration of glycerol, thereby increasing the glycerol conversion. However, it will have an opposite effect on the subsequent hydrogenation of the formed double bond, since this is an exothermal process. The high temperatures will also promote degradation of the formed products.

3.6 SILICOTUNGSTIC ACID CONCENTRATION

Although it was established that silicotungstic acid had a positive effect on 13PD selectivity, high silicotungstic acid concentrations influenced the 13PD selectivity negatively. Apparently, a minimal silicotungstic acid concentration is required to achieve 13PD selectivity at all, while too much acid will promote further dehydration, thereby decreasing the 13PD selectivity.

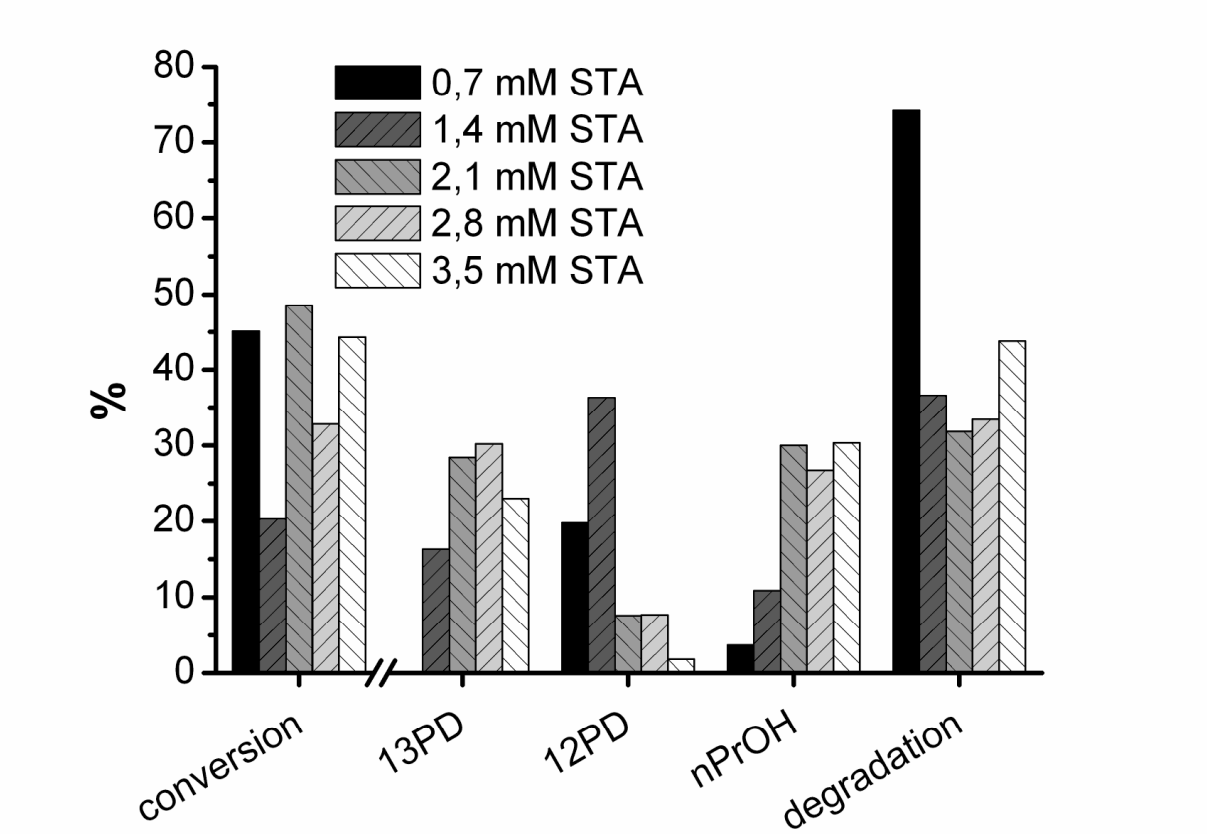

Figure 4. Reduction of glycerol using various STA concentrations. Reaction conditions: 25 μmolPt/Al_2O_3; 5 mL 1000 mM aqueous glycerol; 40 bar H_2; 200 °C; 18 h; 800 rpm.

Indeed, no 13PD is formed when 0.7 mM silicotungstic acid is used and only 12PD and degradation products are observed (Figure 4). Gradually increasing the acid concentration leads to an optimal 13PD selectivity around 2.1 to 2.8 mM, while suppressing the 12PD selectivity, thereby inverting the product selectivity. A further increase of the acid concentration results in lower propanediol selectivities in favor of degradation. Therefore, it can be concluded that 2.1 mM is the optimal silicotungstic acid concentration, with a glycerol conversion of 49% and a 13PD selectivity of 28%.

The differences in selectivity, as described above, can be explained when different mechanisms are considered, at different acid concentrations. The first is the reforming of glycerol, which results in the formation of degradation products and is catalyzed by platinum at low acid concentration. This reaction pathway is inhibited by acid. [26] When more acid is present, a dehydration – hydrogenation mechanism is at play, resulting in the formation of propanediols. Depending on the amount of acid present, either 12PD is formed (low acid concentration) or 13PD is formed (higher acid concentration). When too much acid is present, the propanediols are subsequently degraded and propanol and degradation products are obtained.

3.7 HIGH GLYCEROL CONCENTRATIONS

The glycerol concentration did not have a significant influence on glycerol conversion. Since in all the experiments 25 μmol platinum was used, the Pt/Al_2O_3 apparently converted more glycerol, so displayed a higher activity at higher glycerol concentrations.

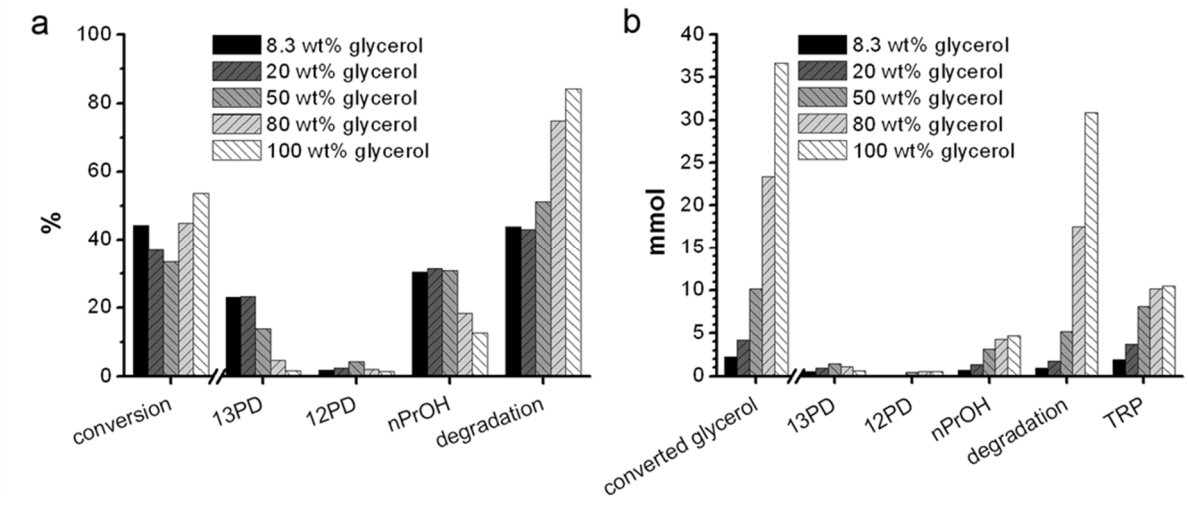

Figure 5. Reduction of concentrated aqueous glycerol solutions. Reaction conditions: 97.5 mg Pt/Al_2O_3; 3.5 mM silicotungstic acid; 40 bar H_2; 200 °C; 18 h; 800 rpm.

This effect was investigated in more detail by increasing glycerol concentrations, from 8.3 wt.% (1000 mM) up to 100 wt.% glycerol (Figure 5), while maintaining the platinum loading at 25 μmol. When comparing the relative conversions and selectivities (Figure 5a) it can be seen that the conversion initially

decreases, while at high glycerol concentrations the conversion shows an upward trend. However, the selectivities towards 13PD, 12PD and n-PrOH show a downward trend in favor of degradation products. This is most apparent when regarding the absolute conversion and production (Figure 5b). The amount of glycerol converted per amount of platinum and acid is increased tremendously, although glycerol is mostly converted into degradation products. One has to bear in mind that three processes take place over the platinum catalyst: glycerol hydrogenolysis, glycerol degradation to gaseous products and glycerol condensation (aldol condensation). The calculated Total Reduction Product (TRP, 13PD + 12PD + 2×n-PrOH) levels off at ~10 mmol. This can be considered the maximum hydrogenation capacity of Pt/Al_2O_3 under these conditions. Any surplus of glycerol will therefore automatically be converted into gaseous and condensed product, which explains the high increase of conversion at high glycerol concentrations. This will be promoted by the acid, which is clearly not a limiting factor.

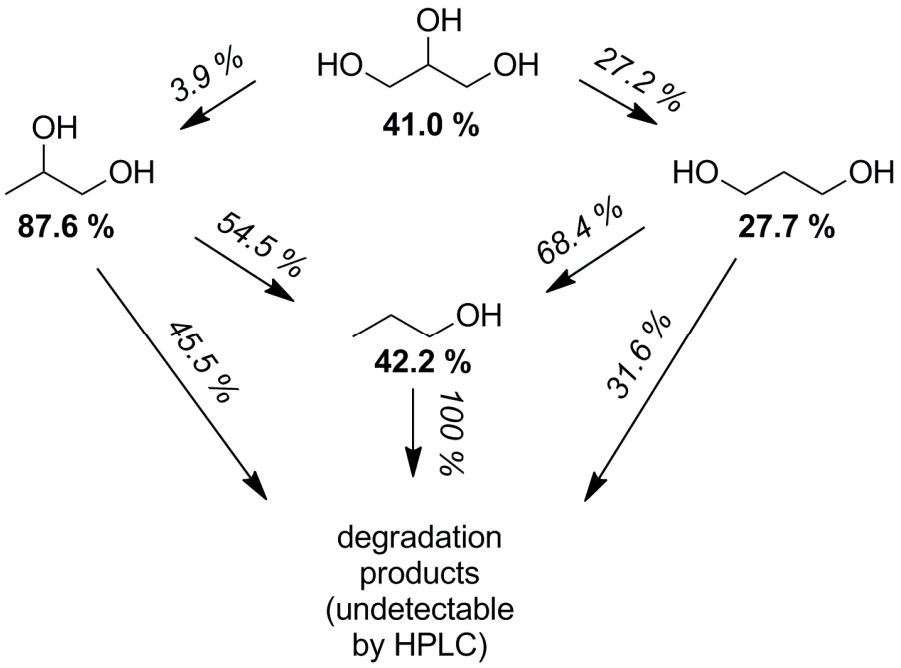

Scheme 3. Glycerol degradation scheme and relative contributions. Reaction conditions: 100 mM aqueous alcohol, 97.5 mg Pt/Al_2O_3; 3.5 mM silicotungstic acid; 40 bar H_2; 200 °C; 18 h; 800 rpm. Bold numbers: conversion of that component as reactant, italics: selectivity.

3.8 Degradation study

To obtain a better understanding of the degradation process of glycerol, the stability of its primary and secondary metabolites was studied using HPLC analysis. This was done by exposing glycerol and its degradation products to the same reaction conditions, and following both conversion and selectivities of all reactions. This resulted in the network given by Scheme 3, where the conversion of the starting materials and the selectivity are shown. Glycerol is selectively converted to 13PD, rather than 12PD. This is attributed to the higher stability of 13PD (28% conversion) compared to 12PD (88% conversion) under

these reaction conditions. This provides, in addition to the selectivity enhancing properties of silicotungstic acid, a supporting explanation for the high 13PD selectivities and high 13PD/12PD ratios obtained using the Pt/Al_2O_3 and silicotungstic acid catalytic system.

3.9 KINETICS

The consequences of the relative stabilities of the glycerol metabolites for the product formation can be visualized by a time dependent experiment. Figure 6 shows that during the course of 72 hours glycerol is steadily converted. However, the amount of 13PD, 12PD and n-PrOH is stabilized after approximately 18 h reaction time, while the amount of degradation products is building up continuously during the 72 hours. Obviously, part of the 13PD, 12PD and n-PrOH produced, is subsequently degraded. The rates of production and degradation of 13PD, 12PD and n-PrOH are in balance, thereby stabilizing their respective yields in the period from 18 to 72 hours.

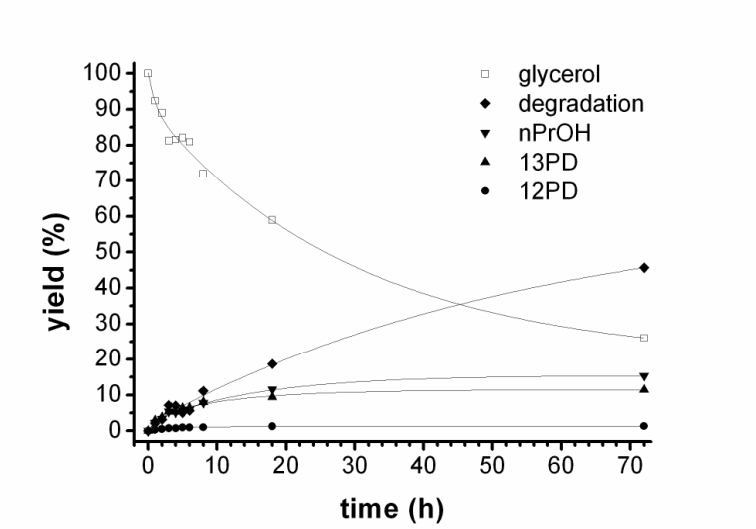

Figure 6. Kinetics of glycerol conversion – Concentration profiles versus time; Reaction conditions: 97.5 mg (0.5 mol%) Pt/Al_2O_3; 3.5 mM STA; 1000 mM glycerol; 40 bar H_2; 200 °C; 800 rpm.

3.10 CATALYST RECYCLING

Two catalyst recycling studies were performed, using different glycerol concentrations (Figure 7). The activity of the catalyst remained the same when 1000 mM glycerol was used. However, the 13PD selectivity decreased in the consecutive recycling run. Both activity and selectivity were reduced in a subsequent run at 100 mM glycerol.

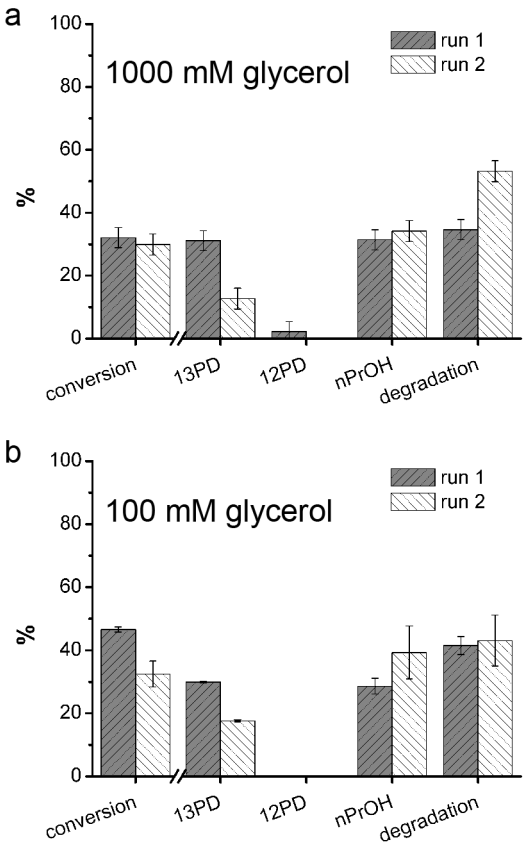

Figure 7. Catalyst recycling study. Reaction conditions: 5 mL RMX containing aqueous glycerol and 3.5 mM STA; ~97.5 mg of 5 wt.% Pt/Al_2O_3; stirring speed 800 rpm; 200 °C; 40 bar H_2; 18 h; a) 1000 mM glycerol; b) 100 mM glycerol.

The decreased 13PD selectivity after recycling is attributed to the sintering of the Pt particles, visible in the TEM pictures in Figure 8c and 8d. Increased Pt particle sizes result in slower hydrogenation, which increases the risk of dehydroxylation of the intermediate 3-hydroxypropanal into acrolein. This ultimately results in increased amounts of n-PrOH and degradation products.

The observation that degradation is only increased when 1000 mM glycerol is used, while the activity of the catalyst remained the same, might be explained by the higher probability of condensation products at elevated glycerol concentrations, since acid catalyzed condensation does not require small Pt particles. I.e. the competing reaction has a higher probability to occur.

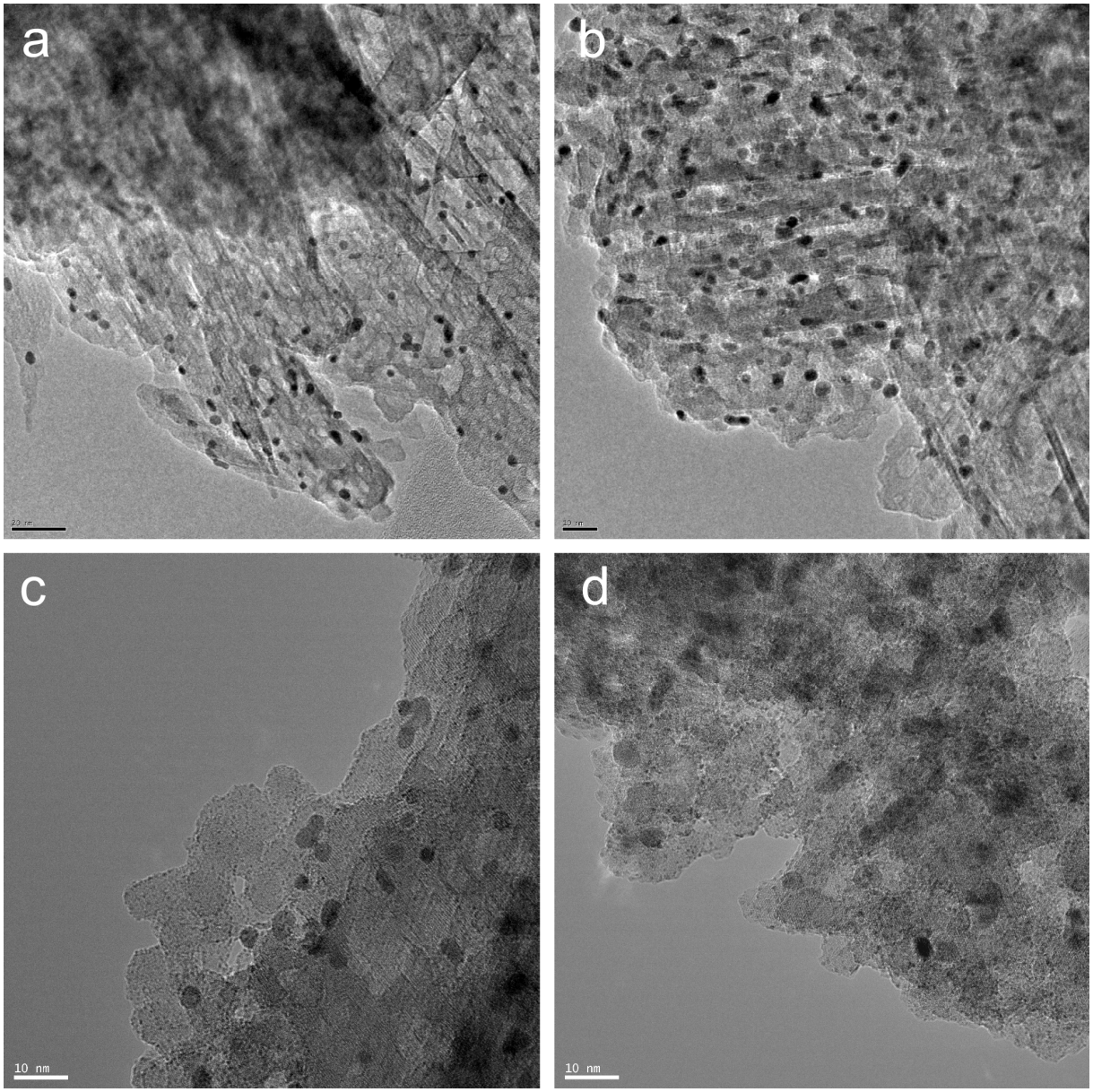

Figure 8. TEM pictures of fresh Pt/Al_2O_3 and spent Pt/Al_2O_3 after reaction in 1000 mM aqueous glycerol a) fresh Pt/Al_2O_3, bar is 20 nm; b) fresh Pt/Al_2O_3, bar is 10 nm; c) spent Pt/Al_2O_3, bar is 10 nm; d) spent Pt/Al_2O_3, bar is 10 nm.

4 DISCUSSION

Pt/Al_2O_3 in combination with silicotungstic acid additive is an excellent system to selectively convert glycerol into 13PD. Both the use of tungsten containing additives and platinum are critical for high 13PD selectivity. A more detailed study of the reaction parameters showed that silicotungstic acid concentration and temperature had the strongest influence on 13PD selectivity. A minimal amount of silicotungstic acid is required to obtain 13PD selectivity, while high concentrations result in degradation. Temperature was

also the parameter that positively influenced glycerol conversion, which made optimization of both glycerol conversion and 13PD selectivity rather difficult.

These results regarding both glycerol conversion and 13PD selectivity can be explained when hydrogenolysis is considered as an acid catalyzed dehydration followed by a hydrogenation over a metallic surface (Scheme 1). [17]

The initial acid catalyzed dehydration is the selectivity controlling step. The formation of a relatively stable secondary carbocation intermediate results in the formation of 13PD. The reaction is therefore kinetically controlled. Following this mechanism, it is the acid that controls the final selectivity. Indeed, there is a clear distinction in selectivity using hydrochloric acid or a tungsten containing acid (Figure 1). Apparently, the tungsten containing acids possess favourable 13PD selectivity inducing properties. This could be through coordination of tungsten to glycerol, as has already been described for ReOx and MoOx and a similar 13PD favoring coordination is envisaged for tungsten compounds. [17,18,27,28]

However, the subsequent hydrogenation plays a major role for the yield of 13PD as well. A swift hydrogenation of 3-hydroxypropanal to 13PD prevents the further dehydration of 3-hydroxypropanal. This explains the higher 13PD selectivities over the more active platinum catalysts compared to the palladium catalysts.

Due to the contradictory temperature requirement for the endothermic dehydration versus the exothermic hydrogenation and increased elimination products at higher temperatures it is difficult to obtain both high glycerol conversion and 13PD selectivity. Moreover, 13PD is relatively stable compared to 12PD, resulting in excellent 13PD/12PD ratios. Nonetheless, it is still prone to degradation. Therefore, it would be beneficial to merge the tungsten and hydrogenation metal in a bifunctional catalyst where both functionalities are in close proximity.

5 CONCLUSIONS

The catalytic system Pt/Al_2O_3 with silicotungstic acid additive converted glycerol selectively into 13PD (49% conversion and 28% 13PD selectivity) with an excellent 13PD/12PD ratio, making this commercially available catalytic system one of the best performing in batch operated processes to date. This was obtained using water instead of the environmentally and technically unattractive 1,3-dimethyl-2-imidazolidinone. The use of both tungsten containing additives and platinum was critical for high 13PD selectivity. 13PD is more stable than 12PD under reaction conditions with this combination, explaining the excellent 13PD/12PD ratio.

The effect of hydrogenation metal, acid concentration, temperature and reaction time on glycerol hydrogenolysis and 13PD selectivity can be rationalized when glycerol hydrogenolysis is regarded as a two-step dehydration-hydrogenation reaction. The optimal reaction conditions for dehydration and

hydrogenation are not compatible, which makes it extremely difficult to obtain both a high conversion of glycerol and a high 13PD selectivity. However, this could be improved when the acidic sites and hydrogenation metal are in close proximity as in a bifunctional catalyst.

ACKNOWLEDGEMENTS

Jeroen ten Dam gratefully acknowledges financial support from NWO ASPECT (053.62.020).

REFERENCES

[1] C. H. C. Zhou, J. N. Beltramini, Y. X. Fan, G. Q. M. Lu, Chem. Soc. Rev., 2008, 37, 527-549.

[2] M. Akiyama, S. Sato, R. Takahashi, K. Inui, M. Yokota, Appl. Catal., A, 2009, 371, 60-66.

[3] S. Sato, M. Akiyama, K. Inui, M. Yokota, Chem. Lett., 2009, 38, 560-561.

[4] J. ten Dam, F. Kapteijn, K. Djanashvili, U. Hanefeld, Catal. Commun., 2011, 13, 1-5.

[5] J. Oh, S. Dash, H. Lee, Green Chem., 2011, 13, 2004-2007.

[6] Y. Nakagawa, Y. Shinmi, S. Koso, K. Tomishige, J. Catal., 2010, 272, 191-194.

[7] T. Kurosaka, H. Maruyama, I. Naribayashi, Y. Sasaki, Catal. Commun., 2008, 9, 1360-1363.

[8] L. F. Gong, Y. Lu, Y. J. Ding, R. H. Lin, J. W. Li, W. D. Dong, T. Wang, W. M. Chen, Chin. J. Catal., 2009, 30, 1189-1191.

[9] O. M. Daniel, A. DeLaRiva, E. L. Kunkes, A. K. Datye, J. A. Dumesic, R. J. Davis, ChemCatChem, 2010, 2, 1107-1114.

[10] Y. Shinmi, S. Koso, T. Kubota, Y. Nakagawa, K. Tomishige, Appl. Catal., B, 2010, 94, 318-326.

[11] A. Shimao, S. Koso, N. Ueda, Y. Shinmi, I. Furikado, K. Tomishige, Chem. Lett., 2009, 38, 540-541.

[12] L. F. Gong, Y. A. Lu, Y. J. Ding, R. H. Lin, J. W. Li, W. D. Dong, T. Wang, W. M. Chen, Appl. Catal., A, 2010, 390, 119-126.

[13] J. Chaminand, L. Djakovitch, P. Gallezot, P. Marion, C. Pinel, C. Rosier, Green Chem., 2004, 6, 359-361.

[14] I. Furikado, T. Miyazawa, S. Koso, A. Shimao, K. Kunimori, K. Tomishige, Green Chem., 2007, 9, 582-588.

[15] L. Huang, Y. L. Zhu, H. Y. Zheng, G. Q. Ding, Y. W. Li, Catal. Lett., 2009, 131, 312-320.

[16] L.-Z. Qin, M.-J. Song, C.-L. Chen, Green Chem., 2010, 12, 1466-1472.

[17] J. ten Dam, U. Hanefeld, ChemSusChem, 2011, 4, 1017-1034.

[18] Y. Nakagawa, K. Tomishige, Catal. Sci. Technol., 2011, 1, 179-190.

[19] F. Auneau, C. Michel, F. Delbecq, C. Pinel, P. Sautet, Chem.–Eur. J., 2011, 17, 14288-14299.

[20] M. Besson, L. Djakovitch, P. Gallezot, C. Pinel, A. Salameh, M. Vospernik, in Catalysis of organic reactions, Vol. 123 (Ed: M. L. Prunier), CRC Press, Boca Raton, FL, 2009.

[21] C. Ramesh Kumar, K. Jagadeeswaraiah, P. S. Sai Prasad, N. Lingaiah, ChemCatChem, 2012, 4, 1360-1367.

[22] M. Misono, N. Nojiri, Applied Catalysis, 1990, 64, 1-30.

[23] D. R. Moberg, T. J. Thibodeau, F. o. G. Amar, B. G. Frederick, J. Phys. Chem. C., 2010, 114, 13782-13795.

[24] S. Li, D. A. Dixon, J. Phys. Chem. A, 2006, 110, 6231-6244.

[25] A. Gervasini, A. Auroux, J. Catal., 1991, 131, 190-198.

[26] G. W. Huber, J. A. Dumesic, Catal., Today 2006, 111, 119-132.

[27] S. Koso, Y. Nakagawa, K. Tomishige, J. Catal., 2011, 280, 221-229.

[28] Y. Amada, Y. Shinmi, S. Koso, T. Kubota, Y. Nakagawa, K. Tomishige, Appl. Catal., B, 2011, 105, 117-127.

APPENDIX 3

Table S1. Experimental results of Central Composite Design.

# Entry	Time (h)	[glycerol] (mM)	[STA] (mM)	Pressure (bar)	Temperature (°C)	Conversion %	13PD selectivity %	Regio-selectivity 13PD/12PD	Turnover Frequency ($mmol_{13PD}mmol_{metal}^{-1}h^{-1}$)	13PD yield %
1	9	390	3.5	20	200	37.0	26.5	4.6	0.8	9.8
2	9	390	3.5	40	170	11.3	56.5	25.7	0.6	6.4
3	9	390	9	20	170	7.2	44.2	16.4	0.3	3.2
4	9	390	9	40	200	21.5	19.0	23.8	0.4	4.1
5	9	1000	3.5	20	170	11.9	49.7	18.4	1.3	5.9
6	9	1000	3.5	40	200	26.7	33.0	11.8	2.0	8.8
7	9	1000	9	20	200	39.5	13.6	10.5	1.2	5.4
8	9	1000	9	40	170	5.8	39.6	19.8	0.5	2.3
9	18	390	3.5	20	170	12.5	51.9	7.5	0.3	6.5
10	18	390	3.5	40	200	41.1	27.1	7.5	0.5	11.1
11	18	390	9	20	200	53.8	14.2	71.0	0.3	7.6
12	18	390	9	40	170	7.2	53.8	26.9	0.2	3.9
13	18	1000	3.5	20	200	53.1	18.9	3.5	1.1	10.0
14	18	1000	3.5	40	170	19.5	40.8	19.4	0.9	8.0
15	18	1000	9	20	170	11.8	42.2	18.3	0.6	5.0
16	18	1000	9	40	200	30.2	14.7	49.0	0.5	4.4
17	13.5	695	6.25	10	185	23.5	32.5	4.2	0.8	7.6
18	13.5	695	6.25	50	185	13.4	37.2	21.9	0.5	5.0
19	13.5	695	0	30	185	3.5	0.0	0.0	0.0	0.0
20	13.5	695	12.5	30	185	15.8	23.7	18.2	0.4	3.7
21	13.5	10	6.25	30	185	21.8	39.3	26.2	0.0	8.6
22	13.5	1380	6.25	30	185	15.5	36.9	10.5	1.2	5.7
23	3.5	695	6.25	30	185	9.8	34.0	13.1	1.3	3.3
24	23.5	695	6.25	30	185	28.1	28.5	15.8	0.5	8.0
25	13.5	695	6.25	30	150	2.6	68.1	85.1	0.2	1.8
26	13.5	695	6.25	30	220	78.8	6.3	7.0	0.5	5.0
27	13.5	695	6.25	30	185	20.4	31.7	12.7	0.7	6.5
28	13.5	695	6.25	30	185	17.9	33.9	12.6	0.6	6.1
29	13.5	695	6.25	30	185	20.9	28.3	14.2	0.6	5.9
30	13.5	695	6.25	30	185	21.6	27.7	14.0	0.6	6.0
31	13.5	695	6.25	30	185	19.3	32.4	14.7	0.6	6.3
32	13.5	695	6.25	30	185	19.5	37.0	15.4	0.7	7.2
33	13.5	695	6.25	30	185	16.6	40.3	14.4	0.7	6.7
34	13.5	695	6.25	30	185	17.0	39.0	20.5	0.7	6.6

Additional reaction conditions: 25 μmol Pt/Al_2O_3 (97.5 mg); 800 rpm.

CHAPTER 3

SYNTHESIS, CHARACTERISATION AND CATALYTIC PERFORMANCE OF A MESOPOROUS TUNGSTEN SILICATE: W-TUD-1

This chapter is based on the publication "J. ten Dam, D. Badloe, A. Ramanathan, K. Djanashvili, F. Kapteijn and U. Hanefeld, Applied Catalysis A: General 468 (2013) 150-159."

ABSTRACT

Tungsten containing TUD-1 catalysts were synthesised by a two-step impregnation method and a direct one-step sol-gel method. The one-step method yielded finely dispersed catalytically active tungsten oxide nano-particles (< 1 nm) (at Si/W ratio above 20), while the two-step method yielded both tungsten oxide nano-particles and bulk tungsten oxide. This was established using INAA, N_2 physisorption, powder XRD, Raman spectroscopy, TEM, Diffuse Reflectance UV-Vis, FT-IR, H_2-TPR and NH_3-TPD analysis. Both types of catalyst preparation resulted in active acidic catalysts for the Prins cyclisation of citronellal. It was demonstrated that the finely dispersed tungsten oxide nano-particles were responsible for the catalytic activity.

Keywords: Tungsten; TUD-1; Mesoporous Material; Prins Reaction; Acidity.

1. INTRODUCTION

The incorporation of metal oxides into the silica framework of mesoporous or microporous materials leads to a wide variety of catalytically active materials and has attracted extensive research interest. Depending on the chosen metal, these catalysts provide hydration/dehydration, redox or acid-base activity. [1-7]

By variation of the synthesis method, different silica structures can be prepared: [8] MCM-41, [1,2,9] MCM-48, [3,10-12] SBA-15 [4,5,13-15] or TUD-1 [6,7] to name just a few. For the production of relatively large (in terms of molecular size) fine chemicals, mesoporous silicates are the catalyst materials of choice, because of their beneficial mass transfer properties. In this respect, TUD-1 is especially attractive, because of its high stability and straightforward, adjustable, environmentally benign synthesis. [16,17]

TUD-1 has a mesoporous and amorphous sponge-like structure. It has been used as a carrier material for incipient wetness impregnation. In addition, numerous metals i.e. Al, Ti, Zr, V, Cr, Mn, Fe, Co, Cu and Ga have been incorporated into its silica framework. [16-18]

Tungsten is catalytically very active and its heteropoly acids have been employed for many purposes. To increase surface area and accessibility of the tungsten it is desirable to incorporate it into or on mesoporous silicates. This is, however, not a trivial task since tungsten is considerably larger than silicon, with an ionic radius of 0.42 Å relative to 0.26 Å. [19] Consequently, relatively few tungsten containing mesoporous silicates are known to date. [20] Recently, a study was published where phosphotungstic acid, a heteropoly acid, was added to the synthesis mix of TUD-1. This resulted in the inclusion of the heteropoly acid in the mesoporous TUD-1 matrix. [21]

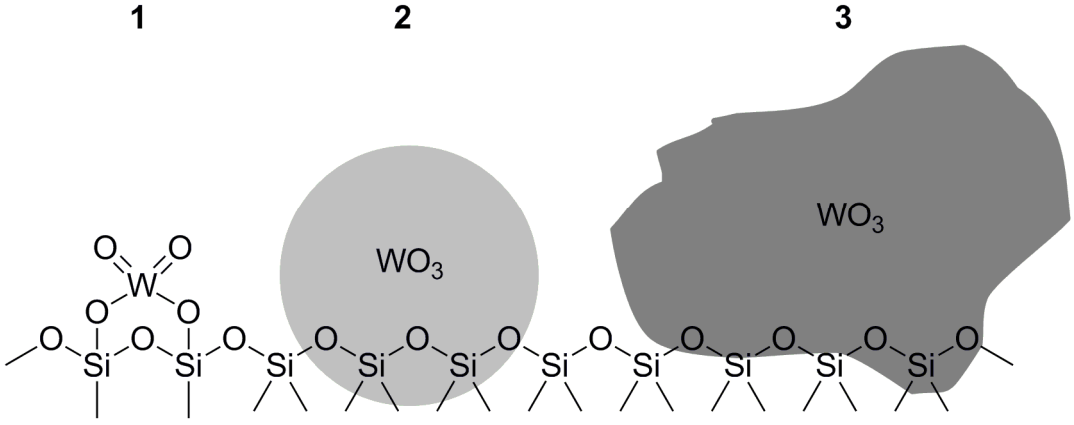

Scheme 1. Three types of tungsten on silica: 1) incorporated tungsten (isolated tungsten species); [20] 2) WO_3 nano-particle (~1 nm); 3) bulk WO_3 particles (up to 100 nm).

The incorporation (Scheme 1, **1**) or fine dispersion of tungsten oxide nanoparticles (Scheme 1, **2**) on the TUD-1 material, which is different from the inclusion of heteropoly acid, would be highly interesting

because of its enhanced catalytic properties in acid catalysed reactions. However, agglomeration of tungsten into bulk WO_3 (Scheme 1, **3**) during the synthesis results in catalytically less active tungsten species.

In this paper we describe the nature of the tungsten particles derived from both incipient wetness impregnation of TUD-1 and a direct sol-gel synthesis of W-TUD-1. This is achieved by using several analysis methods like Instrumental Neutron Activation Analysis, nitrogen physisorption, XRD, Raman spectroscopy, Diffuse Reflectance UV-Vis spectroscopy, TEM, H_2-TPR and NH_3-TPD. The acidic properties of the catalysts are tested in the industrially relevant Prins cyclisation of citronellal. [6,7,22-24] This acid catalysed reaction is part of commercial menthol synthesis. [25-27] Industrially it is catalysed by a homogeneous Lewis acid that cannot be recycled. A stable heterogeneous catalyst would therefore be highly desirable.

2. EXPERIMENTAL

2.1. MATERIALS

Tetraethoxysilane (TEOS, Aldrich, 98%), triethanolamine (TEA, Acros, 97%), tetraethylammonium hydroxide (TEAOH, Aldrich, 35 wt-% aqueous solution), tungstic acid (Aldrich, >99%), ammonium hydroxide (J.T. Baker, 25 wt-% aqueous solution), tungsten(VI) ethoxide (Alfa Aesar), dry ethanol (Merck), dry *i*-propanol (Merck), (-)-citronellal (Janssen Chimica, 97%), dry toluene (sure seal, Aldrich).

2.2. CATALYST PREPARATION

2.2.1. WO_3/TUD-1

TUD-1 was synthesised according to Heikkila *et al.*, [28] using 20.0 g tetraethoxysilane (TEOS, Aldrich, 98%), 14.8 g triethanolamine (TEA, Acros, 97%), 5.1 g demineralised H_2O and 20.1 g tetraethylammonium hydroxide (TEAOH, Aldrich, 35 wt-% aqueous solution). The final molar gel composition was SiO_2/TEA/H_2O/TEAOH (1:1:11:0.5). Three samples of WO_3/TUD-1 (10, 20 and 30 wt-%) were prepared by incipient wetness impregnation of TUD-1 (pore volume = 0.897 $cm^3 \cdot g^{-1}$) using solutions of appropriate amounts of tungstic acid (Aldrich) in aqueous ammonium hydroxide (J.T. Baker, 25 wt-% aqueous solution). The material was dried overnight at 95 °C and calcined at 600 °C for 10 hours with a temperature ramp of 1 $°C \cdot min^{-1}$ in a flow of dry air.

These materials are named WO_3/TUD-1_x, where x (10, 20 or 30) represents the wt-% of WO_3 on the TUD-1 support.

2.2.2. W-TUD-1

A series of W-TUD-1 (Si/W = 50, 40, 30, 20 and 10) was synthesised using tungsten(VI) ethoxide ($W(OEt)_6$, Alfa Aesar) as tungsten precursor. Initially, tungsten(VI) ethoxide was dissolved in a mixture of TEA, dry ethanol (8.0 g) and dry *i*-propanol (8.0 g) in a 250 mL polyethylene bottle. Under vigorous stirring 20.0 g TEOS (Aldrich, 98%) was slowly added with a dropping funnel. After stirring for 2-3 h a solution of TEAOH (20.1 g, Aldrich, 35 wt-% aqueous solution) with additional demineralised H_2O was added drop-wise and the vigorous stirring was continued for another 1-2 h. The amounts of $W(OEt)_6$, TEA and demineralised H_2O were chosen so that the final molar gel composition was Si/W/TEA/H_2O/TEAOH (1: n: 1+2n: 11: 0.5). The resulting liquid was poured into a porcelain dish and aged at room temperature for at least 24 h. The resulting thickened gel was dried in an oven at 98 °C for at least 12 h. The dried sample was ground and hydrothermally treated at 180 °C for 5 h in a stainless steel Teflon-lined autoclave. Finally, calcination was performed at 600 °C for 10 h with a temperature ramp of 1 °C·min^{-1} in a flow of dry air.

These materials are named W-TUD-1_x, where x (10, 20, 30, 40 or 50) represents the Si/W ratio in the catalyst.

If the same synthesis was performed with $W(OEt)_5$ or WCl_6, the synthesis was not successful.

2.3. CATALYST CHARACTERISATION

2.3.1. INAA

Elemental analysis for Si and W was established by Instrumental Neutron Activation Analysis (INAA) and was performed at the Reactor Institute Delft (RID). The sample was irradiated with neutrons (neutron flux of $1.6 \cdot 10^{17}$ neutrons s^{-1}·cm^{-2}) in the Hoger Onderwijs Reactor. In this process, stable isotopes were converted into radioactive isotopes. These isotopes radiate gamma radiation which was measured with semi-conductor gamma-ray spectrometers equipped with a germanium semiconductor. The wavelength is specific for each element. The amount of each element was determined from the signal area of the sample and a calibration standard.

2.3.2. N_2 PHYSISORPTION

Specific surface areas and pore characteristics of the materials were determined using the BET and BJH models from nitrogen sorption measurements on a Quantachrome Autosorb-6B at -196 °C. Prior to the measurements, the samples were degassed overnight under vacuum at 350 °C using a Quantachrome Autosorb degasser.

2.3.3. X-RAY DIFFRACTION

X-ray diffraction patterns of the W-TUD-1 samples were recorded on a Bruker-AXS D8 Advance diffractometer with Cu-Kα radiation, which was operated at 25 mA and 45 kV. The measuring step size was 0.0387 ° with a step time of 1 s^{-1}. The diffraction spectrum was taken over a range from 5 ° to 90 ° 2θ.

X-ray diffraction patterns of the WO_3/TUD-1 samples were measured using a Bruker D8 Advance diffractometer with a Lynxeye detector and CuKα radiation. Measuring range from 5 ° to 95 ° 2θ with a step size of 0.02 ° and a scan speed of 0.15 s^{-1}.

Low angle XRD spectra were obtained from a Bruker AXS D5000 with Cu-Kα radiation, which was operated at 36 mA and 36 kV. The measuring step size was 0.01 ° with a step time of 2 s^{-1}. The diffraction pattern was recorded over a range from 0.5 ° to 3.5 ° 2θ.

2.3.4. FT-IR SPECTROSCOPY

The FT-IR spectra were measured on a Perkin Elmer Spectrum ONE instrument. A KBr wafer was prepared containing a particular amount of the calcined sample that allowed for a transmission of minimally 50% (< 1 mg). The spectrum was taken over a range of 450-4000 cm^{-1} with a resolution of 1 cm^{-1}.

2.3.5. RAMAN SPECTROSCOPY

Raman analysis was performed using a Renishaw Ramascope System 2000 instrument linked to a Leica microscope. 20 mW Ar^+ laser (laser line of 514 nm) was used as excitation source. The backscattered light was filtered for Rayleigh scattering using a holographic notch filter. The spectrograph uses a grating to disperse the light over the detector, which recorded the Raman spectra with a resolution of 4 cm^{-1}. The beam position was determined by focusing on the magnified powder sample.

2.3.6. DR UV-VIS SPECTROSCOPY

UV-Vis spectra were obtained from a Perkin Elmer lambda 900 diffuse reflectance spectrometer with a SUPRASIL quartz glass sample holder, using $BaSO_4$ as reference. Measuring range from 190 to 600 nm with a scan speed of 2.5 $nm \cdot s^{-1}$.

The Kubelka-Munk relation was used to analyse the diffuse reflectance spectra, to determine the absorbance from the UV-Vis reflectance spectra, and the band gap energy (see Appendix 4).

2.3.7. ELECTRON MICROSCOPY

High-resolution transmission electron microscopy (HR-TEM) was performed on a Philips CM30UT electron microscope with a LaB6 filament as the source of electrons operated at 300 kV. Samples were prepared by placing a few droplets of a suspension of ground sample in ethanol on the grid, followed by drying at ambient conditions.

2.3.8. NH_3-TEMPERATURE PROGRAMMED DESORPTION

A calcined sample was pretreated in a continuous stream of He (10 mL·min^{-1}) at 250 °C (ramping at 10 °C·min^{-1} from room temperature). After returning to 100 °C, the sample was flushed for 30 min with ammonia (9.982 mol% ammonia in He, 10 mL·min^{-1}). Subsequently the physically adsorbed ammonia was removed by flushing with He (10 mL·min^{-1}) for 30 min at the same temperature. Subsequently the temperature was ramped (1 °C·min^{-1}) from 100 °C to 600 °C and ammonia desorption was recorded on a Micromeritics Autochem 2910 equipped with a Thermal Conductivity Detector.

2.3.9. TEMPERATURE PROGRAMMED REDUCTION

A glass tube containing a bed of the calcined sample and silicon carbide was continuously flushed with 25 mL·min^{-1} Ar. After a stable Ar flow was established, H_2 (2.6 mL·min^{-1}) was added and the temperature was kept constant for 5 minutes at 30 ºC. Subsequently the temperature was linearly increased to 1000 °C with a ramp of 5 °C·min^{-1}. Finally, the temperature of 1000 °C was maintained for 30 min before cooling down. The hydrogen consumption was measured over time by means of a thermal conductivity detector (TCD).

2.3.10. X-RAY PHOTOELECTRON SPECTROSCOPY

To analyse each powdered catalyst sample with XPS, it was pressed into clean indium foil (Alfa Products, 99.9975 %) with a thickness of 0.5 mm and subsequently placed on a flat specimen holder. The XPS measurements were performed with a PHI 5400 ESCA provided with a dual Mg/Al anode X-ray source, a hemispherical capacitor analyser and a 5 keV ion-gun. The input lens to the analyser was set at a take-off angle with respect to the normal of the sample surface of 45 °. The input lens aperture used was 3.5×1.0 mm. All spectra were recorded using an unmonochromatised Al-Kα (1486.6 eV) radiation. The X-ray source was operated at an acceleration voltage of 13 kV and power of 200 W. During the spectrum acquisition the background pressure of the ultra-high vacuum system was 5·10^{-9} mbar or less. Prior to the measurement a survey was recorded between 0 – 1000 eV using 0.5 eV step size and pass energy of 89.45 eV.

The spectral features of the C $1s_{1/2}$, O $1s_{1/2}$, Si 2p and W $4f_{7/2}$ photoelectron regions (Table 1) were recorded with pass energy of 44.75 eV and step size of 0.20 eV. The total acquisition time per data point was 4 seconds for C 1s and O 1s and 8 seconds for Si 2p and W 4f.

The spectra were evaluated with Multipak 8.0 software (Physical Electronics). At the beginning the satellite peak subtraction was performed. The background intensity of the spectra was described with an Iterated-Sherley except for the O $1s_{1/2}$ area where a linear background was required. [29,30] Next, the position of the photoelectron spectral lines was determined. Using the sensitivity factor presented below in Table 1, the elemental composition was calculated. The charging up of the specimens was corrected adopting a value of 103.5 ± 0.2 eV for the Si 2p binding energy. [7]

Table 1. Acquisition region and area sensitivity factors are presented for the photoelectron lines analysed.

Spectral lines	Region (eV)	Sensitivity factor
C $1s_{1/2}$	280- 300	0.314
O $1s_{1/2}$	525- 545	0.733
Si 2p	95- 115	0.368
W $4f_{7/2}$	29- 49	3.863

2.4. CATALYTIC TESTING

2.4.1. CATALYTIC EXPERIMENTS

For the Prins cyclisation, (-)-citronellal (Janssen Chimica, 97%) was distilled prior to use and dry toluene (sure seal, Aldrich) was used as a solvent. WO_3/TUD-1 and W-TUD-1 catalysts were activated in the presence of air by heating at 1 °C·min^{-1} up to 600 °C. This temperature was held for 10 h. The reaction was carried out under a nitrogen atmosphere.

The Prins reactions were performed by adding 50 mg catalyst to a Schlenk tube. The toluene (5 mL), (-)-citronellal (617 mg, 4 mmol) and 1,3,5-trimethylbenzene (100 μL, internal standard) were subsequently added and the mixture was heated to 80 °C.

A 20 μL sample was taken every 10 minutes during the first 60 minutes, after which additional samples were collected after 90, 120 and 180 minutes. These samples were diluted with 980 μL toluene and analysed by GC.

The samples were analysed on a Shimadzu GC-17A gas chromatograph equipped with an injector at 250 °C, a Cyclodex-B column (60 m × 0.25 mm × 0.25 μm) and using a FID detector at 270 °C. The retention times observed (16 min 140 °C isotherm, then a ramp of 50 °C·min^{-1} to 250 °C, then an

isotherm for 1 min) are: 7.9 min 1,3,5-trimethylbenzene, 13.1 min (-)-citronellal, 14.4 min (+)-isopulegol, 14.8 min (-)-neo-isopulegol, 16.1 min (-)-iso-isopulegol, 16.2 min (-)-neoiso-isopulegol. [6,7,23]

2.4.2. RECYCLING EXPERIMENT

The recycling experiment was performed using the procedure described above. W-TUD-1 (Si/W = 20) was used as catalyst. After 180 minutes of reaction, the reaction mixture was removed and fresh reaction mixture was added to the spent catalyst. This mixture was then again allowed to react for 180 minutes, while taking samples at previous described time intervals. The samples were analysed using the same GC method.

3. RESULTS

3.1. CATALYSTS CHARACTERISATION

The chemical composition and the pore structure of the materials are summarised in Table 2 and the nitrogen isotherms and pore size distributions are presented in Figure 1. All samples show a type IV isotherm, typical for mesoporous materials where capillary condensation in mesopores occurs in a relative pressure range of 0.4-0.8. All materials show a H2 type hysteresis loop. [31] The sloping adsorption and steep desorption is an indication of interconnected pores. The sloping is decreased with increasing tungsten content, which can be explained by the formation of extra-framework tungsten oxide that can block part of the pores (Figure 1a).

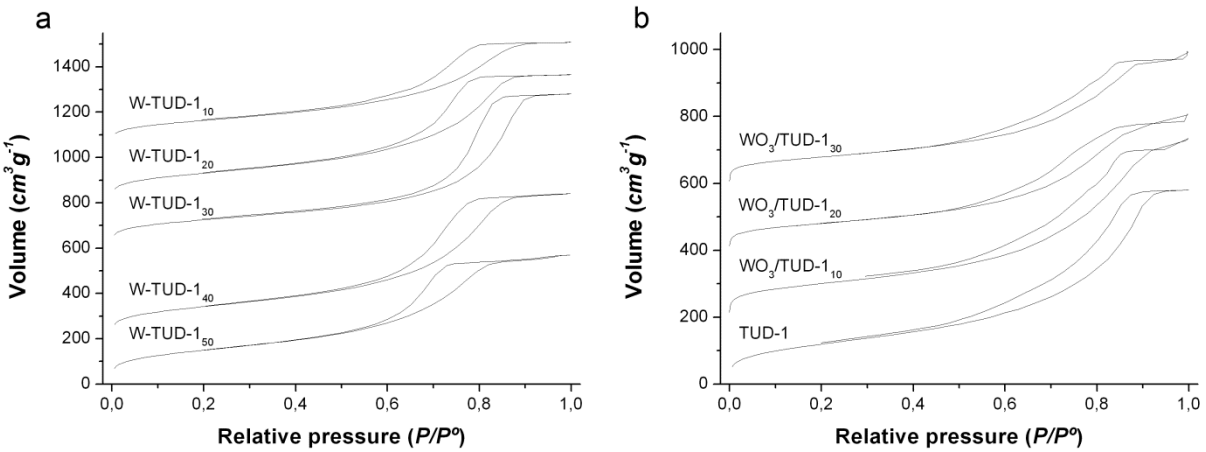

Figure 1. Nitrogen physisorption isotherms for a) W-TUD-1 and b) WO_3/TUD-1 samples and pore size distribution for c) W-TUD-1 and d) WO_3/TUD-1 samples.

This is also reflected in the decrease of pore volume for especially the high loading sample W-TUD-1 (Si/W = 10) (Table 2, entry 9). This loss in pore volume due to the presence of extra-framework tungsten

oxide is more pronounced for the impregnated materials (Table 2, entries 1-4). The desorption slope of the hysteresis loop is more parallel to the adsorption slope when increasing the tungsten content. This can be characterised by a shift towards a H3 hysteresis type, typically caused by disorder of the pores (e.g. blocking of branches in the pore network). Capillary condensation of nitrogen in empty pores proceeds at lower pressures compared to condensation on flat surfaces. For this reason, the pore size distributions were determined from the desorption slope.

Table 2. Chemical composition and pore structure parameters for WO_3/TUD-1 and W-TUD-1 materials.

Entry	Sample	Si/W[a]	BET Area ($m^2 \cdot g^{-1}$)	Pore Volume ($mL \cdot g^{-1}$)	Average Pore Diameter (nm)
1	TUD-1	-	437.8	0.897	8.2
2	WO_3/TUD-1_{10}	38.6 (40.0)	365.0	0.789	8.6
3	WO_3/TUD-1_{20}	19.3 (17.4)	292.5	0.622	8.5
4	WO_3/TUD-1_{30}	12.9 (12.6)	277.8	0.613	8.8
5	W-TUD-1_{50}	50 (43.9)	542.2	0.878	6.5
6	W-TUD-1_{40}	40 (36.3)	518.7	0.986	7.6
7	W-TUD-1_{30}	30 (27.6)	450.8	1.052	9.3
8	W-TUD-1_{20}	20 (18.9)	475.5	0.873	7.3
9	W-TUD-1_{10}	10 (8.6)	414.8	0.708	6.8

[a] Molar ratio Si/W in synthesis mixture, between brackets is Si/W determined by INAA analysis.

Because of the tuneability of the pore size of TUD-1 materials, it was expected to have average pore sizes between 7-10 nm for a hydrothermal treatment of 5 h. [17] Where other metal TUD-1 materials show a general increase in surface area when increasing the metal loading and a steeper decrease in average pore diameter, the W-TUD-1 shows a more similar pore diameter and a slight decrease in surface area (Table 2). [17]

XPS spectra were recorded for WO_3/TUD-1 (20 wt% WO_3), W-TUD-1 (Si/W = 10 and 50). The different samples showed signals at identical energies. The binding energies of tungsten (W $4f_{7/2}$) are 35.0 ± 0.2 eV and 36.8 ± 0.2 eV. These binding energies are attributed to WO_3, so tungsten is present as W^{6+}. [32] The oxygen peaks (O $1s_{1/2}$) found at binding energies of 530 eV and lower point to metal oxides. The binding energy of WO_3 is located around 530 ± 1 eV. From these observations it can be concluded that tungsten is present as WO_3 in both W-TUD-1 and WO_3/TUD-1 samples.

Figure 2 shows the XRD patterns of the W-TUD-1 and WO_3/TUD-1 materials. The W-TUD-1 samples show no crystallinity at low tungsten loadings. The W-TUD-1 (Si/W = 20) material only shows a minimal diffraction at 23 ° and 33 ° 2θ from crystalline tungsten oxide, while the W-TUD-1 (Si/W = 10) material

shows sharp reflections. This transition of observing crystalline metal oxide between a ratio of Si/M = 20 and Si/M = 10 is general for many different metal TUD-1 materials. [17] In addition, the reported limit of achieving tungsten incorporation without the presence of extra framework tungsten oxide for different types of tungsten silicates (e.g. W-MCM-41), lies between these ratios. [3,12-14,20,33,34] In Figure 2b the WO_3/Si-TUD-1 samples show a clear increase in intensity of crystalline tungsten oxide peaks. An important observation is that WO_3/TUD-1 (10 wt-% WO_3), which has similar tungsten content as W-TUD-1 (Si/W = 40), already shows diffraction patters for crystalline tungsten oxide. In comparison the W-TUD-1 samples having higher tungsten loadings do not exhibit WO_3 reflections, even though the signal to noise ratio of these measurements is superior.

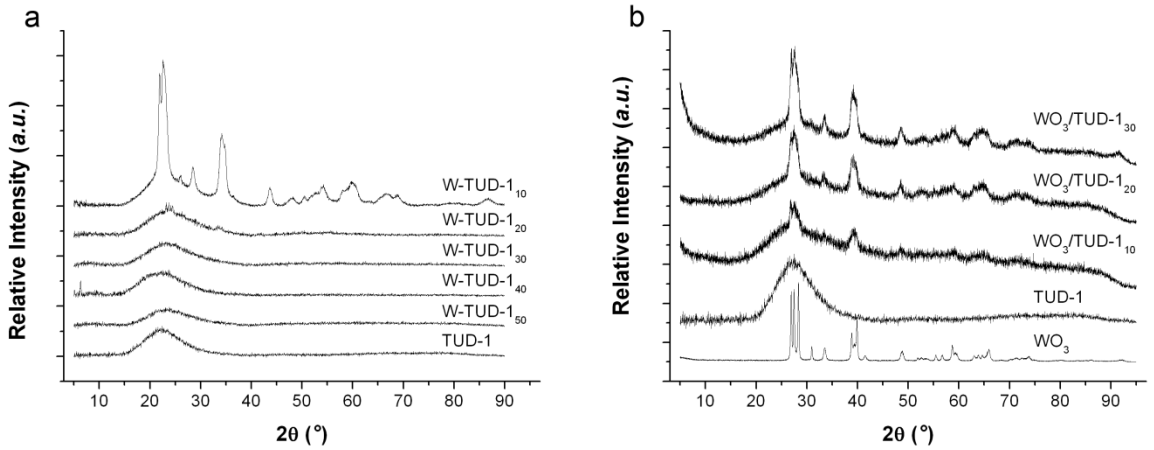

Figure 2. XRD patterns of a) W-TUD-1 and b) WO_3/TUD-1 samples.

The Raman spectra of the W-TUD-1 samples synthesised from $W(OEt)_6$ and bulk WO_3 are presented in Figure 3a. The spectra of WO_3/TUD-1 samples, the references TUD-1 and WO_3 are presented in Figure 3b. Raman spectroscopy is widely applied for characterising transition metals, where the symmetry of the metal oxide framework give strong Raman activity. [9]

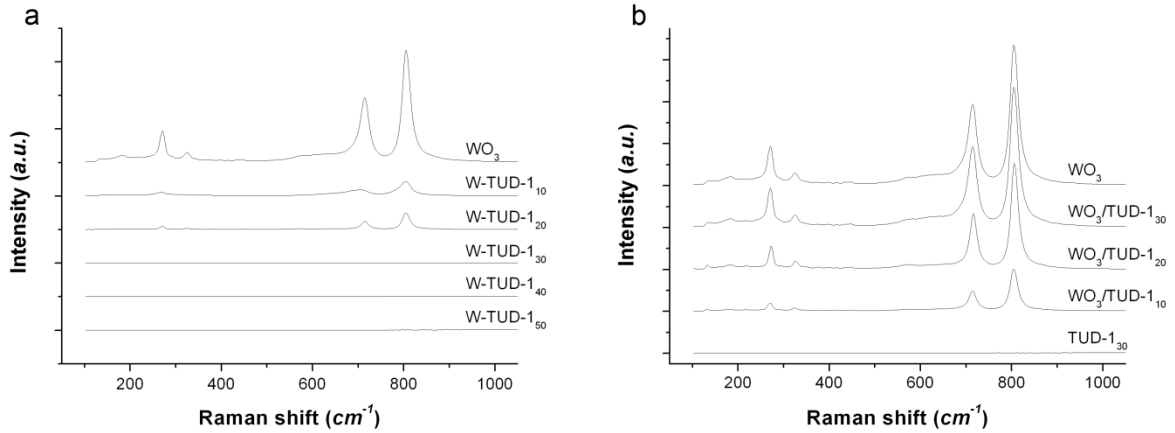

Figure 3. Raman spectra of a) W-TUD-1 and b) WO3/TUD-1 samples.

Typical Raman bands of WO_3 can be found at 267, 327, 714 and 804 cm^{-1}. [35] Low intensity signals of these bands are observed for Si/W ratios ≤ 20, indicating the presence of extra framework WO_3 (Figure 3a). These bands are absent for the W-TUD-1 samples with Si/W ratios higher than 20, indicating isolated or highly dispersed tungsten oxide, confirming the observations made by XRD analysis. [3,9,12,33,34]

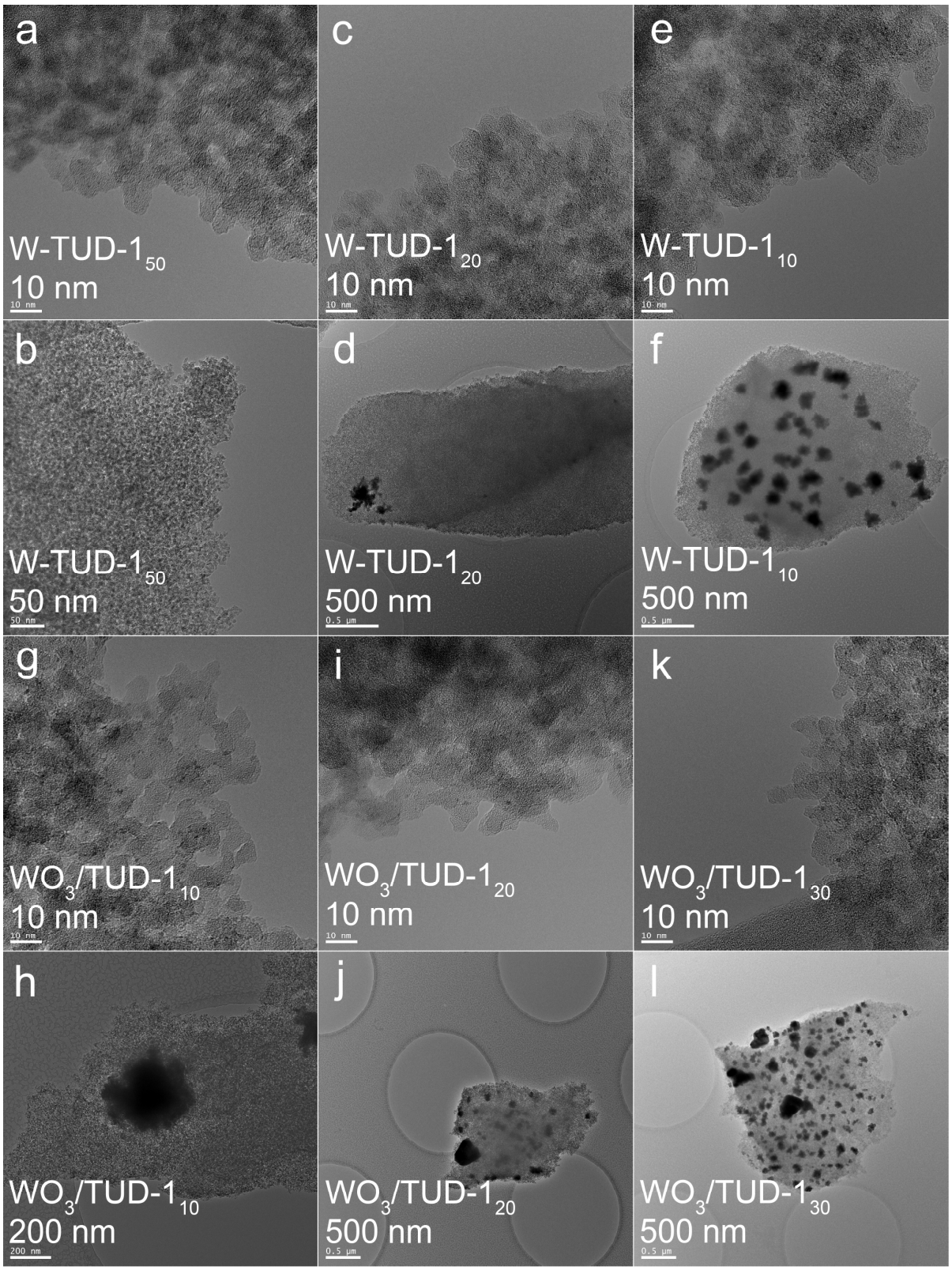

Figure 4. TEM images of W-TUD-1 and WO_3/TUD-1 samples.

The impregnated TUD-1 samples (Figure 3b) show a clear intensity increase of 267, 327, 714 and 804 cm^{-1} as the WO_3 loading is increased. This is in agreement with the observations by XRD, which supports highly dispersed or isolated framework incorporated tungsten for these W-TUD-1 materials from the absence of crystalline WO_3 peaks in the spectra even more strongly.

Figure 4 shows TEM images of W-TUD-1 (Si/W = 50, 20 and 10) and all WO_3/TUD-1's. The images at high amplification (Figure 4a, c, e, g, i, k) are all comparable. Highly dispersed sub-nanometer WO_3 particles are visible. Differences become apparent in the overview images at lower amplification (Figure 4b, d, f, h, j, l). Dependent on the tungsten loading, different amounts of bulk WO_3 are observed. The W-TUD-1 (Si/W = 50) sample does not show any bulk WO_3 (Figure 4b), W-TUD-1 (Si/W = 20) shows some bulk WO_3 (Figure 4d) and W-TUD-1 (Si/W = 10) is covered with bulk WO_3 particles. The same trend is observed for the WO_3/TUD-1 materials (Figure 4h, j, l), with the difference that WO_3/TUD-1 (10 wt-% WO_3), having the lowest WO_3 loading of the impregnated samples, already shows regions with bulk WO_3.

DR UV-Vis was employed to further investigate local structures of tungsten present in the material. The observation of ligand-to-metal charge transfer, only possible for isolated transition metals, would give direct evidence of tetrahedral incorporation of tungsten. [15] The DR UV-Vis spectra of the W-TUD-1 materials, WO_3/TUD-1 samples, TUD-1 and bulk WO_3 are presented in Figure 5. All spectra show a broad absorption band ranging from 220 to 450 nm. The reported sharp absorption bands at 230 nm and from 250 to 350 nm, which are assigned to isolated tetrahedral incorporated tungsten and isolated low oligomeric tungsten species respectively are not obtained in any of the samples. [3,5,11,15,33,34] Instead the broad band shifts from 380 nm to 450 nm with increasing tungsten content (Si/W ratio decreases from 50 to 10; Figure 5a).

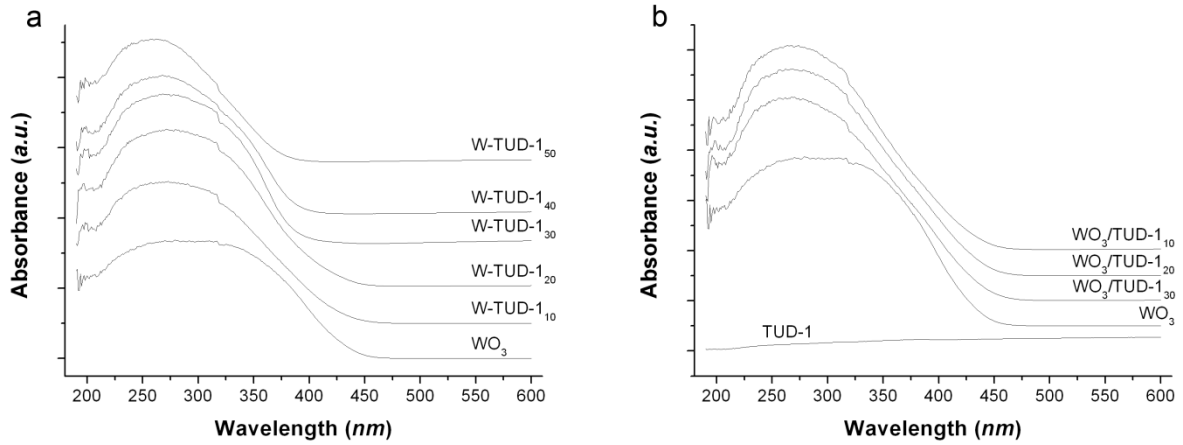

Figure 5. DR UV-Vis spectra of a) W-TUD-1 and b) WO_3/TUD-1 samples.

DR UV-Vis is widely used to determine the band gap E_g (magnitude of the energy gap separating the valence and conduction band) of semiconductors and insulators. [36] Previous studies revealed that the

different local structures of tungsten oxide have specific band gap energies. [37] The band gap energies obtained from Tauc-plots (see Appendix 4) are reported in Table 3.

Table 3. Band gap energy and average number of W-O-W Bonds in a WO_3 particle determined from DR UV-Vis spectra.

Sample	E_g (eV)[a]	$N_{W\text{-}O\text{-}W}$[b]
WO_3	2.8	5.25[c]
WO_3/TUD-1_{10}	3.2	4.31
WO_3/TUD-1_{20}	3.2	4.31
WO_3/TUD-1_{30}	3.2	4.31
W-TUD-1_{50}	3.65	3.24
W-TUD-1_{40}	3.40	3.83
W-TUD-1_{30}	3.30	4.07
W-TUD-1_{20}	3.25	4.19
W-TUD-1_{10}	3.20	4.31

[a]Band gap energy; [b]Number of W-O-W bonds per W determined according to $N_{W-O-W} = 11.89 - 2.37E_g \; with \; R^2 = 0.9496$; [37] [c]Calculated from relation *b*. Note however that the number of W-O-W bonds per W in bulk WO_3 is 6.

The W-TUD-1 samples show a decrease in band gap energy from 3.65 to 3.2 eV for an increase in tungsten loading. According to Ross-Medgaarden et al. this range of band gap energies is typical for tungsten(VI) oxide (WO_3) clusters. [37] Bulk tungsten oxide has a band gap energy of 2.8 eV and isolated tetrahedrally coordinated tungsten (WO_4) around 5.2-5.6 eV. As the tungsten structure present in the TUD-1 materials comprises clusters of WO_3, estimation of the cluster size was made (Table 3). A linear correlation was assumed to enable estimation of the degree of aggregation/polymerisation (average number of W-O-W bonds per W ($N_{W\text{-}O\text{-}W}$)) from DR UV-Vis band gap energies compared to reference compounds. [37] The $N_{W\text{-}O\text{-}W}$ of 5.25 for bulk WO_3 is referred to as infinite WO_3 3D structure, band gap energy E_g around 4 eV are Keggin type clusters (XW_nO_y, where n = 9; 12; 17 and y = 34; 40; 61) in the nano-size range, and *Eg* around 3 eV are polymeric chains of tungsten oxide. [37]

The FT-IR spectra of the W-TUD-1 and WO_3/TUD-1 materials are presented in Figure 6. All samples exhibit absorption bands at 460, 810, 960, 1070 and 1200 cm^{-1}. The absorption bands at 460, 810 and 1070 with a shoulder at 1200 cm^{-1} can be assigned to the symmetric and asymmetric stretching of Si-O-Si vibrations of tetrahedral SiO_2 units. The absorption band at 960 cm^{-1} has been widely used to characterise the incorporation of transition metal atoms in the silica framework. The stretching vibration of Si–O is affected by the neighbouring metal atoms. This indicates incorporation of the metal elements into the silica framework. As the metal (tungsten) loading is increased an increase in the 960 cm^{-1} intensity is observed. However, the WO_3/TUD-1 samples (Figure 6b), where no isolated incorporation of tungsten is

expected, also show a minimal absorbance around 960 cm^{-1}, compared to the blank. Impregnated tungsten oxide particles establish interaction with the silica support during calcination, therefore the presence of the 960 cm-1 absorbance does not allow an unambiguous conclusion.

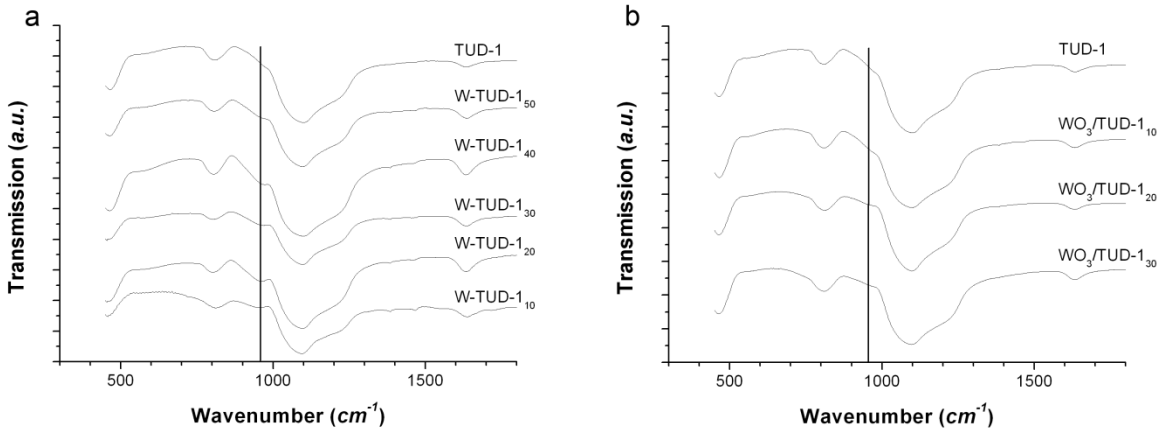

Figure 6. FT-IR spectra of a) W-TUD-1 and b) WO_3/TUD-1 samples.

Figure 7 shows the TPR profiles of the W-TUD-1 and WO3/TUD-1 samples and WO_3. WO_3 shows three main reduction peaks, with a maximum located at 650, 875 and 930 ºC, due to the three step reduction of WO_3.

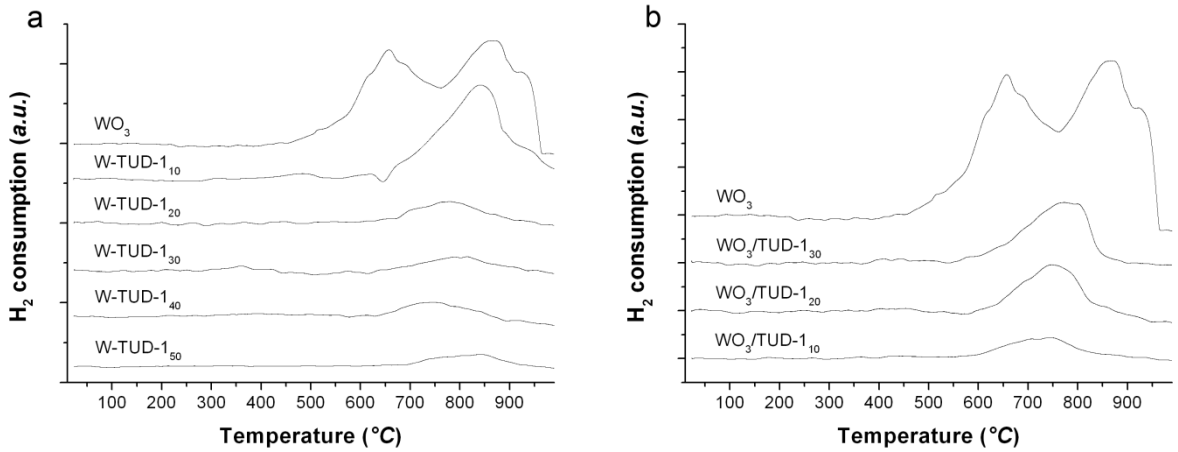

Figure 7. H_2-TPR profiles of a) W-TUD-1 and b) WO_3/TUD-1 samples.

The reduction stages at 650 ºC is the reduction stage of W(VI) and at 875 ºC and 930 ºC are the reduction stages of W(IV). [5] Similar to the XRD results where crystalline tungsten oxide was present in WO_3/TUD-1's and W-TUD-1 (Si/W = 10) materials, the TPR profiles show a defined reduction peak. As a result of interactions with the support the temperature of reduction shifted towards higher temperatures (700-800 ºC) making the three stage reduction behaviour of WO_3 less pronounced. Reduction of metal oxides becomes more difficult when the interactions of the metal oxides with the support increase. [5] The shift in reduction starting temperature from 650 ºC for W-TUD-1 (Si/W = 20) to 700 ºC for W-TUD-1

(Si/W = 50), and reduction peak temperature of around 750 ºC to 825 ºC, indicates a higher dispersion of the tungsten species when decreasing the tungsten loading.

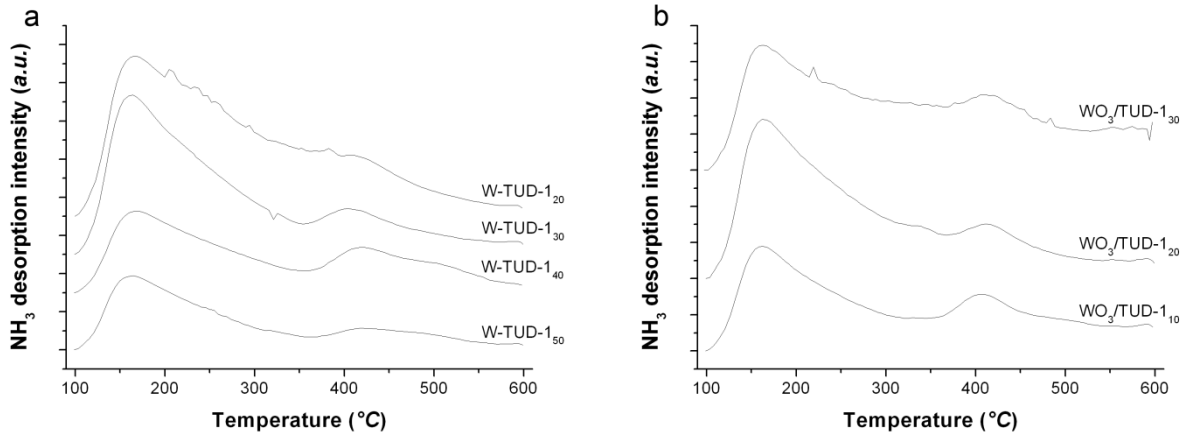

Figure 8. NH_3-TPD spectra of a) W-TUD-1 and b) WO_3/TUD-1 materials.

NH_3-TPD was used to investigate the acidic characteristics of the different tungsten catalysts. Figures 8a and b show the NH_3-TPD profiles of the W-TUD-1 and WO_3/TUD-1 samples, respectively. All TPD profiles show ammonia desorption effects created by the acid sites of tungsten oxide species. [5] The desorption profiles of all the samples consist of two broad overlapping peaks, indicating acid sites with different acid strengths. The peak at low temperatures (100-350 ºC) is assigned to weak acid sites. This is because chemisorbed ammonia with weak interactions is desorbed at low temperatures.

Table 4. Quantitative analysis of NH_3-TPD data.

Catalyst	Total Acidity ($mmolg^{-1}$)[a]	Weak Acid Sites ($mmolg^{-1}$)[b]	% Weak Acid Sites	Strong Acid Sites ($mmolg^{-1}$)[c]	% Strong Acid Sites
TUD-1	0.02	0.014	70	0.006	30
WO_3[38]	0.0	0.0	n.a.	0.0	n.a.
WO_3/TUD-1_{10}	0.34	0.21	61	0.13	39
WO_3/TUD-1_{20}	0.45	0.33	73	0.12	27
WO_3/TUD-1_{30}	0.49	0.29	59	0.20	41
W-TUD-1_{50}	0.38	0.28	74	0.10	26
W-TUD-1_{40}	0.52	0.33	63	0.19	37
W-TUD-1_{30}	0.78	0.59	76	0.19	24
W-TUD-1_{20}	0.99	0.73	74	0.26	26
W-TUD-1_{10}	0.47	0.44	94	0.03	6

[a]Total catalyst acidity determined over a temperature range of 100-600 °C; [b]Weak acid sites determined from 100-350 °C; [c]Strong acid sites determined from 350-600 °C.

The smaller high temperature desorption peak is attributed to ammonia desorption from stronger acid sites. With increasing tungsten loading, an optimum in the total acidity is obtained for the W-TUD-1_{20}

sample (Table 4), . Deconvolution of the total acid sites into the two types does not indicate a clear trend in the distribution of these acid sites (Table 4). W-TUD-1 and WO_3/TUD-1 materials only differ in the total amount of acid sites rather than in type of acid, e.g. in structural differences. An exception is W-TUD-1_{10} which mainly consists of weak acidic sites.

3.2. CATALYTIC RESULTS

The prepared catalysts were tested in the Prins cyclisation of (-)-citronellal. This acid catalysed reaction produces isopulegol, thereby introducing two additional stereocenters. This can lead to four possible diastereoisomers, but only two major products are expected, (+)-isopulegol and (-)-neo-isopulegol (Table 5). These products are the result of the transition state where the methyl group is in the equatorial position of the chair conformation. (+)-Isopulegol is the major product, since all substituents are in the equatorial position, while (-)-neo-isopulegol has the hydroxyl group, which is relatively smaller than the propylene group, in the axial position (Table 5).

Table 5. Catalytic results of the Prins cyclisation of (-)-citronellal.

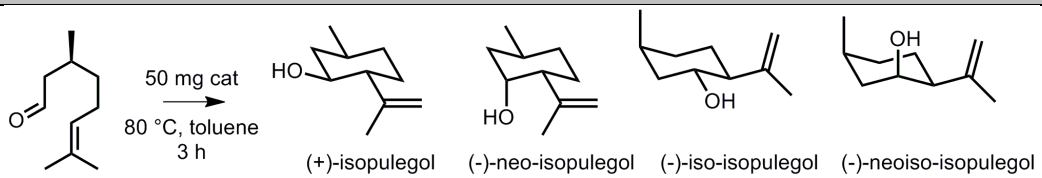

Entry	Catalyst	Conversion	Selectivity				*TOF*[a]
			(+)-isopulegol	(-)-neo-isopulegol	(-)-iso-isopulegol	(-)-neoiso- isopulegol	
		(%)	(%)	(%)	(%)	(%)	($mol \cdot mol^{-1} \cdot h^{-1}$)
1	W-TUD-1_{10}	95.5	61.4	32.2	4.6	1.9	123.5
2	W-TUD-1_{20}	100.0	59.7	34.0	4.5	1.8	329.7
3	W-TUD-1_{30}	95.7	60.1	32.9	5.0	2.0	355.5
4	W-TUD-1_{40}	76.3	61.0	32.1	4.9	2.0	401.7
5	W-TUD-1_{50}	60.2	61.3	31.7	4.9	2.1	335.6
6	WO_3/TUD-1_5	27.3	62.7	31.5	4.0	1.8	95.0
7	WO_3/TUD-1_{10}	32.9	62.9	32.8	4.3	0	59.0
8	WO_3/TUD-1_{20}	19.9	65.4	30.4	4.2	0	8.4
9	WO_3	1.3	100	0	0	0	0.0
10	TUD-1	3.0	100	0	0	0	n.a.

[a] initial turnover frequency (TOF) in mol converted citronellal per mol tungsten per hour (calculated over the first 10 minutes of reaction).

The catalytic test results are presented in Table 5 and the kinetic profile of the most active catalyst (W-TUD-1 (Si/W = 20)) is shown in Figure 9. Bulk tungsten oxide (entry 9) and siliceous TUD-1 (entry 10) are inactive in the Prins cyclisation of (-)-citronellal. The W-TUD-1 catalysts (entries 1 to 5) are more active than the WO_3/TUD-1 catalysts (entries 6-8). This is emphasised in Figure 10, where the turnover frequency (TOF) of the W-TUD-1 and WO_3/TUD-1 catalysts is plotted against tungsten loading. Lower

tungsten loadings result in higher TOF's, indicating better dispersed particles on the catalysts. The selectivity is the same for all the catalysts, giving roughly a 2 to 1 ratio for (+)-isopulegol and (-)-neo-isopulegol. This result was also found in by using other TUD-1 catalysts and was expected, since the pores in mesoporous TUD-1 are too spacious to have any kinetic control through steric influence on the transitional chair conformation.

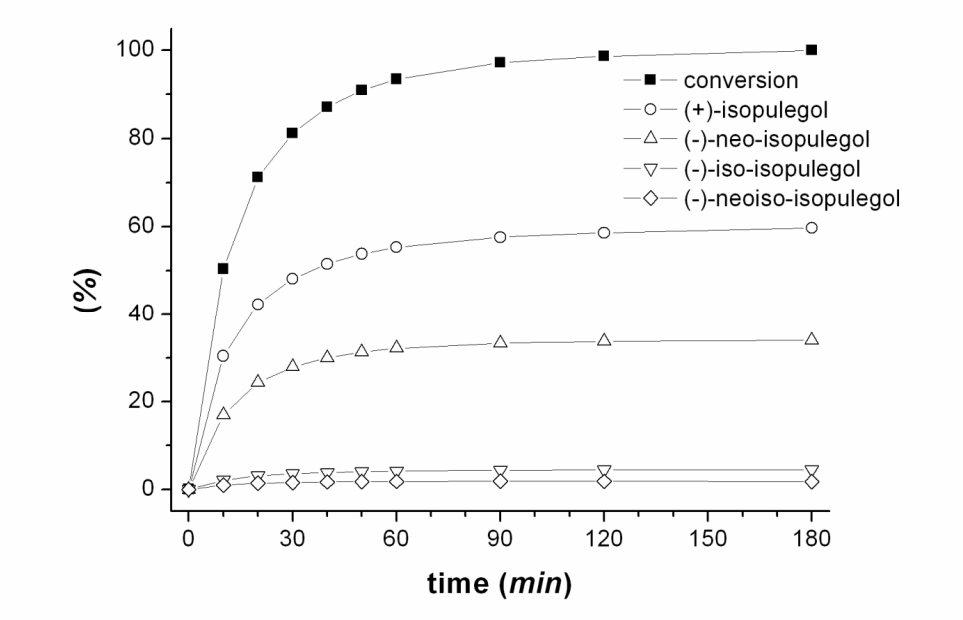

Figure 9. Kinetic profile of Prins cyclisation of (-)-citronellal using W-TUD-1 (Si/W = 20) at 80 °C.

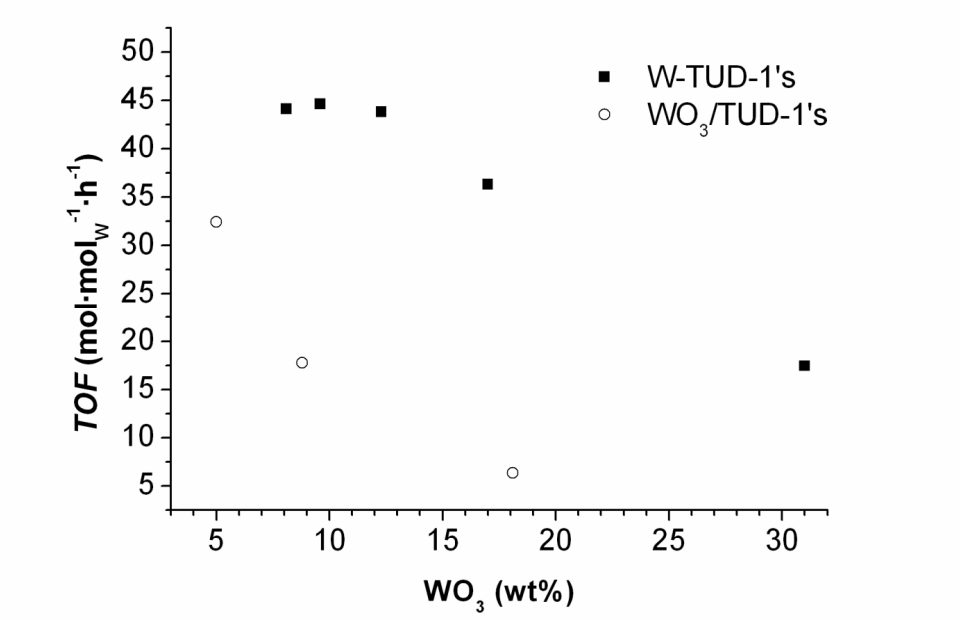

Figure 10. Turnover frequencies of the W-TUD-1 and WO_3/TUD-1 catalysts (calculated over the first 10 minutes of reaction).

3.3. RECYCLING EXPERIMENT

The recyclability of the W-TUD-1 (Si/W = 20) catalyst was tested. While the fresh catalyst gave 100 % conversion within 3 hours, the recycled catalyst was able to convert only 23.2 % (-)-citronellal. The recycling of the catalyst did not influence the selectivity. The decrease in catalyst activity can be explained by the differences in the TEM images taken from both fresh and spent catalyst (Figure 11).

The WO_3-particles sintered over the course of the reaction. This resulted in larger WO_3 nano-particles (compare Figure 11a and 11c) and more, inactive bulk WO_3 (compare Figure 11b and 11d).

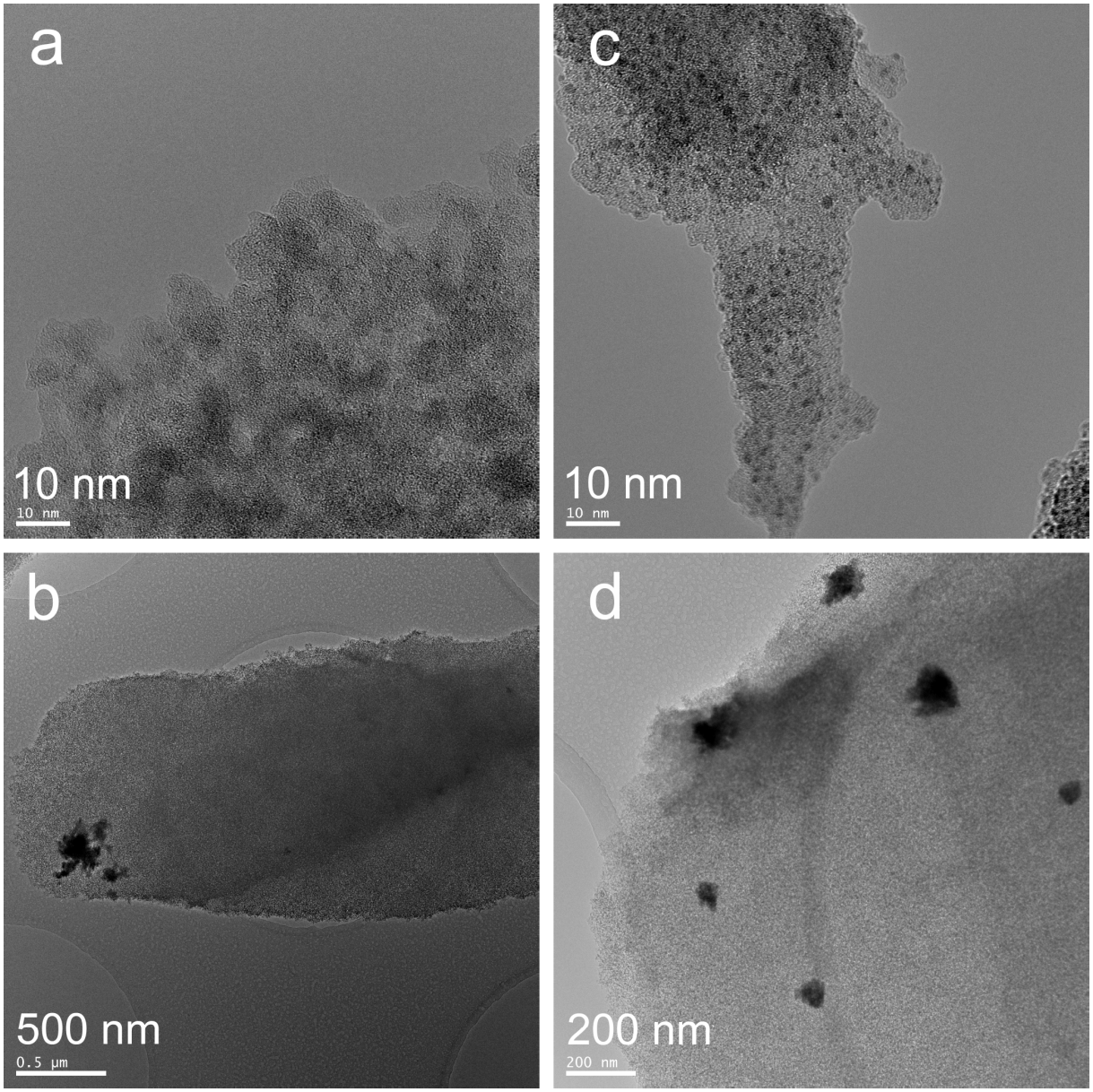

Figure 11. TEM images of (a and b) fresh W-TUD-1 (Si/W = 20) and (c and d) spent W-TUD-1 (Si/W = 20).

4. DISCUSSION

The objective of this research was to form mesoporous silica structures with finely dispersed or incorporated acidic tungsten oxide sites. The two synthesis methods allowed a comparison and critical analysis of the catalyst characterisation data.

Physisorption experiments showed that the typical sponge-like structure of TUD-1 is formed and the chemical analysis established the high predictability of the synthesis.

XPS analysis showed that all materials contain WO_3 and no isolated tungsten was observed. XRD revealed that the WO_3/TUD-1 materials all contained bulk WO_3, while WO_3 signals were only observed for the high loading W-TUD-1 samples (Si/W = 10 and 20). Consequently, the samples with lower tungsten loadings (i.e. W-TUD-1 (Si/W = 30, 40 and 50)) seem to contain supported nano-particles below the detection limit of XRD (approximately 2-3 nm).

The XRD results are confirmed by Raman spectroscopy. The same materials showed Raman signals for WO_3, whereas these signals were absent in the W-TUD-1 materials with lower tungsten loading.

TEM analysis reveals that all the materials contain finely dispersed sub-nano WO_3 particles. In the W-TUD-1 samples with Si/W ratios 30, 40 and 50 the sub-nano WO_3 particles were the only observed tungsten species, whereas the higher loading W-TUD-1 samples (Si/W = 10 and 20) and all the WO_3/TUD-1 showed additional larger bulk WO_3 particles.

The question remains whether the tungsten species are incorporated or that there is a mixture of structures present in the sample. For the WO_3/TUD-1 materials, framework incorporated tungsten can be excluded, based on the synthesis method. However, UV absorption at 230 nm is observed making it difficult to determine the nature of the tungsten species. Using XPS analysis it could be concluded that tungsten was only present in its WO_3 form.

An estimation of the average particle sizes could be made from DR UV-Vis measurements. Using the Kubelka-Munk equation and a Tauc-plot the band gap energy (E_g) of the WO_3 particles could be determined. In this case smaller WO_3 particles will result in higher band gap energies. Indeed, the E_g is increasing from W-TUD-1 (Si/W = 10) to W-TUD-1 (Si/W = 50). This shows that the average WO_3 particle size is increasing with increased tungsten loading.

Using FT-IR it was possible to investigate the interaction of the WO_3 particles with the silica support by inspection of the absorption band at 960 cm^{-1}. This signal originates from a Si-O-W bond, signifying the interaction of the WO_3 phase with the support. This band is more pronounced in the W-TUD-1 materials compared to the WO_3/TUD-1 materials, since the smaller particles in these materials show more interaction with the support.

The reduction temperature, observed from TPR measurements, is shifted to higher temperatures as a result of the interaction of the WO_3 particles with the support.

Although previous analyses showed that no optimal dispersion of the tungsten via framework incorporation was achieved, excellent dispersion in the form of nano-particles occurred. The objective was to form either isolated incorporated tungsten species or finely dispersed nano-particles on the silica surface. The previous analyses show that in fact finely dispersed nano-particles were formed.

This raises the question of why, in the case of the W-TUD-1 materials, no framework incorporation took place. To obtain incorporated tungsten tungstatranes should be formed during the sol-gel synthesis of W-TUD-1. [17] This proved successful with titanium, zirconium and numerous other metal precursors before. Stable atranes are formed from tungsten(IV) sources, which are not stable in the presence of water. [39] The formation of the nano-particles when $W(OEt)_6$ is used as the tungsten precursor and formation of bulk WO_3 when $W(OEt)_5$ and WCl_6 are used can be explained by the hydrolysis rate of these compounds. Where $W(OEt)_5$ and WCl_6 are rapidly hydrolysed in the presence of water, forming bulk WO_3 particles, the hydrolysis of $W(OEt)_6$ is sufficiently slow to form the nano-particles.

The acidic properties of the WO_3 particles were investigated using NH_3-TPD. It was shown that W-TUD-1 and WO_3/TUD-1 materials did not differ in acid type, but only in amount of acid sites. The W-TUD-1 materials were more acidic then the WO_3/TUD-1 materials. The higher amount of acid sites for W-TUD-1 samples when comparing with similar tungsten loadings for the impregnated samples is explained by previously observed results (e.g. XRD). Higher dispersed tungsten particles, means that more acid sites are exposed compared to the more bulky tungsten particles. [3,5] For the same reason a slight decrease of acidity when increasing the WO_3 loading for the impregnated samples was obtained.

Ultimately, the materials were tested in the acid catalysed Prins cyclisation. It was shown that WO_3 is only active as small particles, since the bulk WO_3 did not show any activity and the sintered spent catalyst is less active then fresh catalyst. The selectivity of all the catalysts was comparable, while W-TUD-1 (Si/W = 20) showed highest conversion.

The selectivity is thermodynamically controlled, with (+)-isopulegol being the product with all the substituents in the six-membered ring in the more stable equatorial position. Given the large pore size of the TUD-1's no steric induction was achieved, as observed earlier with Zr-TUD-1 and Al-TUD-1.

On a tungsten basis, W-TUD-1 (Si/W = 50), W-TUD-1 (Si/W = 40) and W-TUD-1 (Si/W = 30) showed the highest turnover frequency. This can be explained by the fact that these catalysts contain the best dispersed and therefore most active WO_3 particles. When tungsten loading exceeds Si/W ratio of 30, larger tungsten particles are formed, which negatively influences the activity.

The increase in turnover frequency at lower tungsten loading is levelled off. This can be explained by the fact that at these metal loadings the tungsten is finely dispersed and the W-TUD-1 samples contain

identical tungsten oxide nano-particles of a minimal size. These nano-particles are converting substrate at their highest rate, underlining the absence of diffusion limitation in mesoporous TUD-1 materials. [17]

5. CONCLUSIONS

TUD-1 supported WO_3 catalysts were synthesised using two different methods. The first method was a subsequent sol-gel synthesis of TUD-1 followed by impregnation of WO_3 (WO_3/TUD-1 catalysts). The second was the one-step sol-gel synthesis of W-TUD-1 catalysts. The impregnation method resulted in mainly bulk WO_3 particles in addition to sub-nano WO_3 particles, while the latter method resulted in finely dispersed sub-nano WO_3 particles on the TUD-1 material, without the formation of bulk WO3 (for Si/W ratios higher than 20).

The recycling of the catalyst affects its activity, while selectivity is maintained. The decrease in activity can be explained by the sintering of the tungsten nano-particles during the reaction.

The acid catalysed Prins cyclisation showed that the sub-nano WO_3 particles were the active phase on the catalyst. This explains why the W-TUD-1 catalysts were more active than the bulk WO_3 containing WO_3/TUD-1.

ACKNOWLEDGEMENTS

Jeroen ten Dam gratefully acknowledges financial support from NWO ASPECT (053.62.020).

NOTES AND REFERENCES

[1] P. Trens, V. Stathopoulos, M.J. Hudson and P. Pomonis, Appl. Catal. A-Gen., 2004, 263, 103-108.

[2] Z.R. Zhang, J.S. Sue, X.M. Zhang and S.B. Li, Appl. Catal. A-Gen., 1999, 179, 11-19.

[3] X.L. Yang, W.L. Dai, R.H. Gao, H. Chen, H.X. Li, Y. Cao and K.N. Fan, J. Mol. Cat. A, 2005, 241, 205-214.

[4] C.Y. Cheng, K.J. Lin, M.R. Prasad, S.J. Fu, S.Y. Chang, S.G. Shyu, H.S. Sheu, C.H. Chen, C.H. Chuang and M.T. Lin, Catal. Commun., 2007, 8, 1060-1064.

[5] X.L. Yang, R.H. Gao, W.L. Dai and K.N. Fan, J. Phys. Chem. C, 2008, 112, 3819-3826.

[6] A. Ramanathan, M.C.C. Villalobos, C. Kwakernaak, S. Telalovic and U. Hanefeld, Chem.-Eur. J., 2008, 14, 961-972.

[7] S. Telalovic, A. Ramanathan, J.F. Ng, R. Maheswari, C. Kwakernaak, F. Soulimani, H.C. Brouwer, G.K. Chuah, B.M. Weckhuysen and U. Hanefeld, Chem.-Eur. J., 2011, 17, 2077-2088.

[8] V. Meynen, P. Cool and E.F. Vansant, Microporous Mesoporous Mater., 2009, 125, 170-223.

[9] Z.R. Zhang, J.S. Sue, X.M. Zhang and S.B. Li, Chem. Commun., 1998, 241-242.

[10] M.S. Morey, J.D. Bryan, S. Schwarz and G.D. Stucky, Chem. Mater., 2000, 12, 3435-3444.

[11] D. Hua, S. Chen, G. Yuan and Y. Wang, J. Porous Mater., 2011, 18, 729-734.

[12] D. Zhao, A. Rodriguez, N.M. Dimitrijevic, T. Rajh and R.T. Koodali, J. Phys. Chem. C, 2010, 114, 15728-15734.

[13] L.H. Hu, S.F. Ji, Z. Jiang, H.L. Song, P.Y. Wu and Q.Q. Lint, J. Phys. Chem. C, 2007, 111, 15173-15184.

[14] X.L. Zhang, C.Y. Yuan, M.Y. Li, B.A. Gao, X.Y. Wang and X.C. Zheng, J. Non-Cryst. Solids, 2009, 355, 2209-2215.

[15] J.C. Hu, Y.D. Wang, L.F. Chen, R. Richards, W.M. Yang, Z.C. Liu and W. Xu, Microporous Mesoporous Mater., 2006, 93, 158-163.

[16] J.C. Jansen, Z. Shan, L. Marchese, W. Zhou, N. van der Puil and T. Maschmeyer, Chem. Commun., 2001, 713-714.

[17] S. Telalovic, A. Ramanathan, G. Mul and U. Hanefeld, J. Mater. Chem., 2010, 20, 642-658.

[18] B. Karmakar, A. Sinhamahapatra, A.B. Panda, J. Banerji and B. Chowdhury, Appl. Catal. A, 2011, 392, 111-117.

[19] CRC Handbook of Chemistry and Physics, CRC Press, 1993.

[20] A. Ramanathan, B. Subramaniam, D. Badloe, U. Hanefeld and R. Maheswari, J. Porous Mater., 2012, 19, 961-968.

[21] L. Tang, G. Luo, M. Zhu, L. Kang and B. Dai, J. Ind. Eng. Chem., 2013, 19, 620-626.

[22] K.A. da Silva, P.A. Robles-Dutenhefner, E.M.B. Sousa, E.F. Kozhevnikova, I.V. Kozhevnikov and E.V. Gusevskaya, Catal. Commun., 2004, 5, 425-429.

[23] P. Mäki-Arvela, N. Kumar, V. Nieminen, R. Sjoholm, T. Salmi and D.Y. Murzin, J. Catal., 2004, 225, 155-169.

[24] R.G. Jacob, G. Perin, L.N. Loi, C.S. Pinno and E.J. Lenardao, Tetrahedron Lett., 2003, 44, 3605-3608.

[25] C.B. Cortes, V.T. Galvan, S.S. Pedro and T.V. Garcia, Catal. Today, 2011, 172, 21-26.

[26] F. Neatu, S. Coman, V.I. Parvulescu, G. Poncelet, D. De Vos and P. Jacobs, Top. Catal., 2009, 52, 1292-1300.

[27] A.F. Trasarti, A.J. Marchi and C.R. Apesteguia, J. Catal., 2007, 247, 155-165.

[28] T. Heikkilä, J. Salonen, J. Tuura, M.S. Hamdy, G. Mul, N. Kumar, T. Salmi, D.Y. Murzin, L. Laitinen, A.M. Kaukonen, J. Hirvonen and V.P. Lehto, Int. J. Pharm., 2007, 331, 133-138.

[29] D.A. Shirley, Physical Review B, 1972, 5, 4709-4714.

[30] Surf. Interface Anal., 1991, 17, 889-892.

[31] K.S.W. Sing, D.H. Everett, R.A.W. Haul, L. Moscou, R.A. Pierotti, J. Rouquérol and T. Siemieniewska, Pure Appl. Chem., 1985, 57, 603-619.

[32] NIST Standard Reference Database 20, http://srdata.nist.gov/xps/.

[33] O. Klepel, W. Böhlmann, E.B. Ivanov, V. Riede and H. Papp, Microporous Mesoporous Mater., 2004, 76, 105-112.

[34] Y. Su, Y.M. Liu, L.C. Wang, M. Chen, Y. Cao, W.L. Dai, H.Y. He and K.N. Fan, Appl. Catal. A, 2006, 315, 91-100.

[35] J.G. Graselli and B.J. Bulkin, in: Analytical Raman Spectroscopy, Wiley, New York, 1991, pp. 352.

[36] B. G. Yakobi, Semiconductor Materials: an Introduction to Basic Principles (Microdevices), Springer, 2002.

[37] E.I. Ross-Medgaarden and I.E. Wachs, J. Phys. Chem. C, 2007, 111, 15089-15099.

[38] D. Hua, S.-L. Chen, G. Yuan, Y. Wang, Q. Zhao, X. Wang and B. Fu, Microporous Mesoporous Mater., 2011, 143, 320-325.

[39] A.K. Phukan and A.K. Guha, Inorg. Chem., 2010, 49, 9884-9890.

APPENDIX 4

SMALL-ANGLE XRD

Small-angle XRD spectra of WO_3/TUD-1 and W-TUD-1 materials are presented in Figure SI 1. This Figure shows no small angle diffraction on the mesopores of W-TUD-1. Where TUD-1 materials in general show an intense diffraction peak at 0.5-2.5 ° *2θ* indicating a meso-structural pore arrangement. However, in order to obtain this a couple of conditions should be satisfied; highly uniform pore sizes, regular spacing between pores and regular arrangement of pores. These properties are characteristic for surfactant templated mesoporous materals (e.g. MCM and SBA) in contrast to the random interconnecting "sponge-like" pore structure of the TUD-1.

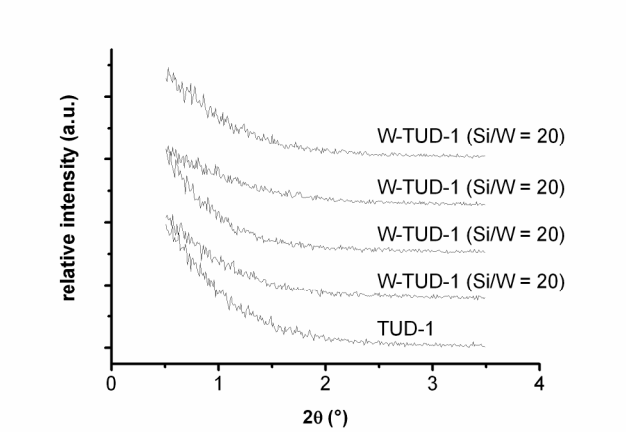

Figure S1. Small-angle XRD spectra.

KUBELKA-MUNK RELATION AND THE BAND GAP ENERGY FROM DR UV-VIS SPECTRA

The Kubelka-Munk relation is presented in equation S1.

$$F(R_\infty) = \frac{(1-R_\infty)^2}{2R_\infty} \qquad \textbf{(S1)}$$

Where $F(R_\infty)$ is called remission or Kubelka-Munk function.

This relation is an empirical analogue of the Lambert Beer relation for transmittance spectroscopy. Here the ratio of transmittance intensity and the intensity of the incident beam is used to determine absorbance which is linearly related to the concentration of the absorbing species. In the same fashion the remittance of a diffuse reflecting sample is the ratio of reflected and incident intensities. To achieve a high accuracy, the sample has to be infinitely thick, so the light beam does not penetrate to the sample holder. This is

unpractical, therefore the relative remittance (R_∞) is the ratio of remittance of the sample to that of a standard according to equation S2.

$$\textbf{(S2)} \qquad R_\infty = \frac{R_{\text{sample}}}{R_{\text{standard}}}$$

The relation between absorption coefficient and the band gap is given by equation (S3)

$$\textbf{(S3)} \qquad \alpha h\nu = c_1\left(h\nu - E_g\right)^{1/2}$$

Where α is the absorption coefficient, E_g is the edge energy or band gap and c_1 is a proportionality constant. Here $h\nu$ is the photon energy, h is Planck's' constant and the frequency is $\nu = c/\lambda$, where c is the speed of light and λ the wavelength. This results in equation S4 when applying the calculated absorbance of a sample from equation S3.

$$\textbf{(S4)} \qquad \left[F(R_\infty)h\nu\right]^2 = c_2\left(h\nu - E_g\right)$$

A Tauc-plot was constructed by plotting $\left[F(R_\infty)h\nu\right]^2$ against $h\nu$, E_g was obtained at the intersection with the x-axis. Note that determining E_g from diffuse reflectance spectra can only be used as an approximation as it is based on empirical relations.

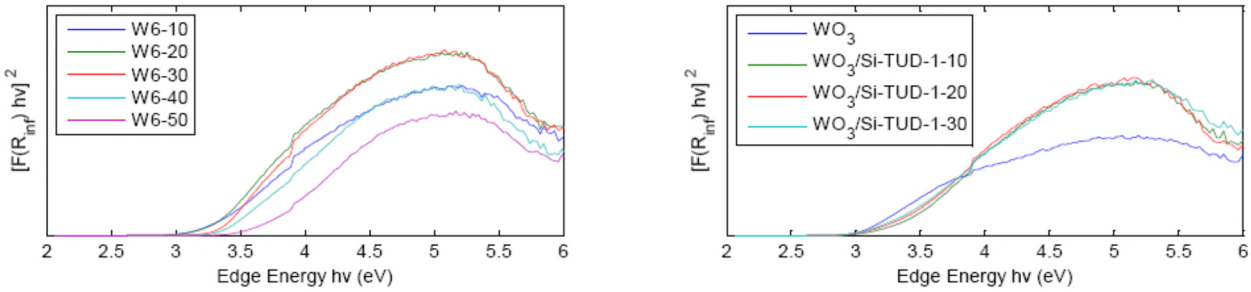

Figure S2. UV-vis DR spectra and Tauc-plots of the W-TUD-1 and WO_3/TUD-1 materials.

X-RAY PHOTOELECTRON SPECTROSCOPY

Table S1. XPS analysis data W-TUD-1 (Si/W = 10).

Spectral line	Peak position (eV)	Area	Area fraction (%)	Sensitivity factor (area)	Atomic fraction (%)	ID
C $1s_{1/2}$	± 285	-	100	0.314	4.6	adventitious C
Si 2p	103.5	17396	100	0.368	25.5	SiO_2
O $1s_{1/2}$	530.1	10883	11.49	0.733	66.5	metal oxides
O $1s_{1/2}$	532.2	25096	26.49			TUD-1
O $1s_{1/2}$	533.3	48312	51.01			TUD-1
O $1s_{1/2}$	534.6	10429	11.01			TUD-1
W $4f_{7/2}$	34.9	11159	48.10	3.863	3.3	W(VI)
W $4f_{7/2}$	37.0	8369	36.08			W(VI)
W $4f_{5/2}$	37.3	2097	9.04			W(VI)
W $4f_{5/2}$	39.4	1537	6.78			W(VI)

Table S2. XPS analysis data W-TUD-1 (Si/W = 50).

Spectral line	Peak position (eV)	Area	Area fraction (%)	Sensitivity factor (area)	Atomic fraction (%)	ID
C $1s_{1/2}$	± 285	-	100	0.314	7.9	adventitious C
Si 2p	103.5	21477	100	0.368	26.6	SiO_2
O $1s_{1/2}$	527.3	3889	3.39	0.733	65.1	metal oxides
O $1s_{1/2}$	529.8	3611	3.15			metal oxides
O $1s_{1/2}$	532.2	30235	26.36			TUD-1
O $1s_{1/2}$	533.3	61978	54.04			TUD-1
O $1s_{1/2}$	534.6	14985	13.06			TUD-1
W $4f_{7/2}$	35.2	788	21.24	3.863	0.5	W(VI)
W $4f_{7/2}$	36.8	1332	35.91			W(VI)
W $4f_{5/2}$	37.3	591	15.93			W(VI)
W $4f_{5/2}$	38.9	999	26.93			W(VI)

Table S3. XPS analysis data WO_3/TUD-1 (20 wt% WO_3)

Spectral line	Peak position (eV)	Area	Area fraction (%)	Sensitivity factor (area)	Atomic fraction (%)	ID
C $1s_{1/2}$	± 285	-	100	0.314	3.9	adventitious C
Si 2p	103.5	22527	100	0.368	29.8	SiO_2
O $1s_{1/2}$	530.3	1537	3.08	0.733	65.6	metal oxides
O $1s_{1/2}$	532.4	16296	32.66			TUD-1
O $1s_{1/2}$	533.4	28001	56.12			TUD-1
O $1s_{1/2}$	534.7	4060	8.14			TUD-1
W $4f_{7/2}$	34.9	2111	37.20	3.863	0.7	W(VI)
W $4f_{7/2}$	36.8	1132	19.94			W(VI)
W $4f_{5/2}$	37.0	1584	27.90			W(VI)
W $4f_{5/2}$	38.9	849	14.95			W(VI)

CHAPTER 4

SYNTHESIS, CHARACTERIZATION AND PERFORMANCE OF BIFUNCTIONAL CATALYSTS FOR THE SYNTHESIS OF MENTHOL FROM CITRONELLAL

This chapter is based on the publication "J. ten Dam, A. Ramanathan, K. Djanashvili, F. Kapteijn and U. Hanefeld, RSC Advances, susbmitted."

ABSTRACT

A The synthesis of a series of bifunctional catalysts (1 wt.% Pt/W-TUD-1 (Technische Universiteit Delft-1) and 1 wt.% Pt/WO_3/TUD-1) with different tungsten loadings (5 - 30 wt.% WO_3) is described. They were characterized using ICP-OES, INAA, N_2 physisorption, XRD and TEM. Their catalytic performance (activity and selectivity) was evaluated in the two-step catalytic synthesis of menthol from citronellal using kinetic analysis. Introducing tungsten during the TUD-1 synthesis results in a high WO_3 dispersion, essential for the acidity of the catalyst. High tungsten dispersion is also critical for the Pt hydrogenation activity. Therefore, high dispersion combined with optimal tungsten loading resulted in the highest catalytic activity. The best performing catalyst was 1 wt.% Pt/W-TUD-1 (silicon to tungsten ratio of 30), with the highest yields of menthol (96%).

Keywords: Bifunctional Catalyst; Prins Cyclisation; Hydrogenation; Menthol Synthesis; Kinetic Analysis.

1. INTRODUCTION

The conversion of biomass to chemicals has attracted a lot of attention in recent years. An advantage of biomass is that nature already invested energy in the production of carbon-carbon bonds through photosynthesis. Ideally, this carbon backbone is used as a scaffold for the synthesis of chemicals, by manipulating the chemical groups that are connected to this scaffold. As a drawback of this approach, the majority of naturally occurring chemicals are over-functionalized, implying that some chemical groups need to be removed to provide chemicals that can substitute the current fossil oil derived chemicals. Therefore, a major challenge in the research field of biomass to chemicals is the development of catalysts that can selectively remove unwanted functionalities, while leaving the desired groups intact. [1-4]

Biomass consists of almost 50% oxygen that is observed in functional groups including alcohols, ketones, aldehydes and carboxylic acids. One can remove these groups through different mechanisms in which both a hydrogenation centre and an acidic site are important active sites. Combining these catalytic functionalities in a single material is key in the development of biomass conversion catalysts. [5-8]

Citronellal can be obtained from the fractional distillation of natural citronella oil. This monoterpenoid is a versatile building block for a series of organic syntheses. [9] One extensively researched process, is the one pot, 2-step synthesis of menthol. [10-15] This sequence relies on the Prins cyclisation that converts citronellal into isopulegol. [16-20] This olefin is subsequently hydrogenated to form menthol. [10-15]

The process needs both an acid and a hydrogenation catalyst function. Bifunctional acidic hydrogenation catalysts can be obtained in various ways. They can be prepared by impregnating acidic supports/catalysts like zeolites, acidic carbons, Al-TUD-1, B-TUD-1, SAPOs and acidic resins with a hydrogenation metal precursor (Pt, Pd, Rh, Ru, Ir, Cu, Ni and Co. [10-13,21-24]

Another option is to consecutively impregnate an inert carrier with an acid and a hydrogenation metal precursor solution (or vice versa). Ferrari *et al.* studied the influence of the order of impregnation on the activity of a CoMo catalyst in a hydrodeoxygenation and decarboxylation. They showed that acid impregnation (Mo) followed by hydrogenation metal (Co) produced a more active catalyst. [25]

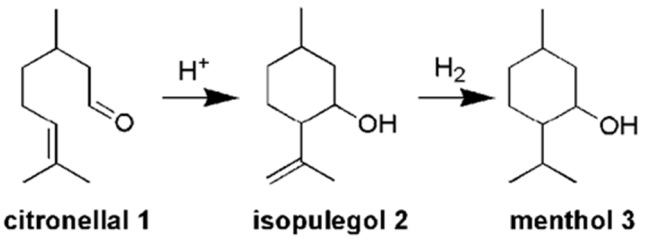

Scheme 1. Menthol synthesis from citronellal.

This chapter describes the synthesis of two series of bifunctional acidic hydrogenation catalysts. The acidity is derived from tungsten, while platinum is the hydrogenation centre. [26-29] The first series is

based on the direct synthesis of W-TUD-1, which is subsequently impregnated with a platinum precursor solution. The second series is based on the consecutive impregnation of TUD-1 with WO_3 and with platinum precursor solutions. Their catalytic activity is evaluated in the two-step synthesis of menthol from citronellal (Scheme 1). [10-15] In this example the selectivity revolves around the acidic sites: they should be acidic enough to catalyse the Prins cyclisation of citronellal, but they should not be able to remove the formed hydroxyl group through elimination. [16-20]

TUD-1 was chosen as a support because of its amorphous structure and relatively large pore size. These characteristics aid in overcoming diffusion limitations, which is particularly important in liquid phase fine chemical synthesis because of the molecular sizes involved. [21,30] Previous work showed that direct synthesis of W-TUD-1 resulted in smaller WO_3 particles (below XRD detection limit, i.e. 2-3 nm) leading to a more acidic catalyst than the impregnation method (WO_3/TUD-1). [31] Pt was chosen for its high hydrogenation activity.

The menthol synthesis from citronellal was chosen as model reaction to establish the catalytic activity and selectivity of the synthesized catalysts. The advantage of this model reaction is that both the acid and hydrogenation catalysis can be tested individually: the conversion of citronellal to isopulegol is acid catalysed and hydrogenation of isopulegol yields menthol. [10-20]

2. EXPERIMENTAL

2.1. MATERIALS

Tetraethoxysilane (TEOS, Aldrich, 98%), triethanolamine (TEA, Acros, 97%), tetraethylammonium hydroxide (TEAOH, Aldrich, 35 wt.% aqueous solution), tungstic acid (Aldrich, >99%), ammonium hydroxide (J.T. Baker, 25 wt.% aqueous solution), tungsten(VI) ethoxide (Alfa Aesar), dry ethanol (Merck), dry *i*-propanol (Merck), chloroplatinic acid ($H_2PtCl_6 \cdot 6H_2O$, Aldrich, ≥37.50% Pt basis), isopulegol (Acros, technical), (*rac*)-citronellal (Acros, ≥95%), dry toluene (sure seal, Aldrich), trimethylbenzene (Acros, 99%).

2.2. CATALYST PREPARATION

2.2.1. WO_3/TUD-1

TUD-1 was synthesized according to Heikkila *et al.*, [32] using 20.0 g tetraethoxysilane (TEOS, Aldrich, 98%), 14.8 g triethanolamine (TEA, Acros, 97%), 5.1 g demineralized H_2O and 20.1 g tetraethylammonium hydroxide (TEAOH, Aldrich, 35 wt.% aqueous solution). The final molar gel composition was SiO_2/TEA/H_2O/TEAOH = 1:1:11:0.5. Three samples of WO_3/TUD-1 (5, 10 and 20

wt.%) were prepared by incipient wetness impregnation of TUD-1 (pore volume = 0.897 $cm^3 \cdot g^{-1}$) using solutions of appropriate amounts of tungstic acid (Aldrich) in aqueous ammonium hydroxide (J.T. Baker, 25 wt.% aqueous solution). The material was dried overnight at 95 °C and calcined at 600 °C for 10 h with a temperature ramp of 1 $°C \cdot min^{-1}$ in a flow of dry air.

These materials are denoted by $WO_3/TUD\text{-}1_x$, where *x* (5, 10 or 20) represents the wt.% of WO_3 on the TUD-1 support.

2.2.2. Pt/WO_3/TUD-1

$WO_3/TUD\text{-}1_x$ samples (5, 10 and 20 wt.%) were synthesized as described above. The incorporation of 1 wt.% platinum was performed by incipient wetness impregnation (pore volume determined by nitrogen physisorption) using solutions containing appropriate amounts of aqueous chloroplatinic hexahydrate ($H_2PtCl_6 \cdot 6H_2O$, Aldrich, ≥ 37.50 wt.% Pt basis). The material was dried overnight at 95 °C and calcined at 600 °C for 2 h with a heating rate of 1 $°C \cdot min^{-1}$ in a flow of dry air. These materials were then stored in a drying oven at 80 °C to prevent water adsorption from air, thereby avoiding potential sintering upon recalcination.

Catalysts are not specifically pre-reduced before reaction, but PtO_x is readily reduced at reaction conditions (20 bar hydrogen pressure and 80°C).

These materials are denoted by $Pt/WO_3/TUD\text{-}1_x$ where *x* (5, 10 or 20) represents the wt.% of WO_3 on the TUD-1 support.

2.2.3. W-TUD-1

A series of W-TUD-1 (Si/W = 50, 40, 30, 20 and 10) was synthesized using tungsten(VI) ethoxide ($W(OEt)_6$, Alfa Aesar) as tungsten precursor. Initially, tungsten(VI) ethoxide was dissolved in a mixture of TEA, dry ethanol (8.0 g) and dry *i*-propanol (8.0 g) in a 250 mL polyethylene bottle. Under vigorous stirring 20.0 g TEOS (Aldrich, 98%) was slowly added with a dropping funnel. After stirring for 2-3 h a solution of TEAOH (20.1 g, Aldrich, 35 wt.% aqueous solution) with additional demineralized H_2O was added drop-wise and the vigorous stirring was continued for another 1-2 h. The amounts of $W(OEt)_6$, TEA and demineralized H_2O were chosen so that the final molar gel composition was Si/W/TEA/H_2O/TEAOH = 1: *n*: 1+2*n*: 11: 0.5. The resulting liquid was poured into a porcelain dish and aged at room temperature for at least 24 h. The resulting thickened gel was dried in an oven at 98 °C for at least 12 h. The dried sample was ground and hydrothermally treated at 180 °C for 5 h in a stainless steel Teflon-lined autoclave. Finally, calcination was performed at 600 °C for 10 h with a heating rate of 1 $°C \cdot min^{-1}$ in a flow of dry air.

These materials are denoted by $W\text{-}TUD\text{-}1_x$, where *x* (28, 16, 11, 9 or 7) represents the WO_3-loading in wt.%, which is equivalent to the following Si/W ratios, respectively: 10, 20, 30, 40 or 50.

2.2.4. Pt/W-TUD-1

W-TUD-1 samples (Si/W = 50, 40, 30, 20 and 10) were synthesized as described above. The incorporation of 1 wt.% platinum was performed by incipient wetness impregnation (pore volume determined by nitrogen physisorption) using solutions containing appropriate amounts of aqueous chloroplatinic hexahydrate ($H_2PtCl_6 \cdot 6H_2O$, Aldrich, ≥37.50 wt.% Pt basis). The impregnated material was dried overnight at 95 °C and calcined at 600 °C for 2 h with a heating rate of 1 °C·min^{-1} in a flow of dry air. These materials were then stored in a drying oven at 80 °C to prevent water adsorption from air, thereby avoiding potential sintering upon recalcination.

Catalysts are not specifically pre-reduced before reaction, but PtO_x is readily reduced at reaction conditions (20 bar hydrogen pressure and 80°C).

These materials are denoted by Pt/W-TUD-1$_x$, where x (28, 16, 11, 9 or 7) represents the WO_3-loading in wt.%, which is equivalent to the following Si/W ratios, respectively: 10, 20, 30, 40 or 50.

2.3. CATALYST CHARACTERIZATION

2.3.1. ICP-OES

Elemental analysis for Pt was performed using Inductively Coupled Plasma – Optical Emission Spectrometry ICP-OES (Optima 4300DV, Perkin Elmer USA). Samples were prepared by adding 5 to 10 mg catalyst to 1 mL concentrated hydrochloric acid. This dispersion was left overnight. The dispersion was diluted using 50 mL 1.0% hydrofluoric and 1.5% sulfuric acid. Agitation for 24 h led to a homogenous solution.

2.3.2. INAA

Elemental analysis for Si and W was established by Instrumental Neutron Activation Analysis (INAA) and was performed at the Reactor Institute Delft (RID). The sample was irradiated with neutrons (neutron flux of 1.6·1017 neutrons s^{-1}·cm^{-2}) in the Hoger Onderwijs Reactor, Delft. In this process, stable isotopes were converted into radioactive isotopes. These isotopes emit gamma radiation, which was measured with semi-conductor gamma-ray spectrometers equipped with a germanium semiconductor. The wavelength is specific for each element. The amount of this element was determined from the signal area of the sample and a calibration standard.

2.3.3. N_2 PHYSISORPTION

Specific surface areas and pore characteristics of the materials were determined using the BET and BJH models from nitrogen sorption measurements on a Quantachrome Autosorb-6B at -196 °C. [33] Prior to

the measurements, the samples were degassed overnight under vacuum at 350 °C using a Quantachrome Autosorb degasser.

Table 1. Chemical composition and pore structure.

Catalyst	WO_3 wt.%	Pt (ICP) wt.%	S_{BET} m^2g^{-1}	V_{pore} cm^3g^{-1}	D_{pore} Å
TUD-1	-	-	655	0.58	35
WO_3/TUD-1_{20}	18.2[a]	-	210	0.33	60
WO_3/TUD-1_{10}	8.8[a]	-	225	0.36	65
WO_3/TUD-1_5	5.3[c]	-	245	0.42	70
W-TUD-1_{28}	31.0[a]	-	420	0.48	45
W-TUD-1_{16}	17.0[a]	-	635	0.83	50
W-TUD-1_{11}	12.3[a]	-	710	0.81	45
W-TUD-1_9	9.6[a]	-	635	0.90	55
W-TUD-1_7	8.1[a]	-	720	0.91	50
Pt/WO_3/TUD-1_{20}	14.3[b]	1.01	220	0.33	60
Pt/WO_3/TUD-1_{10}	10.6[b]	1.01	200	0.33	65
Pt/WO_3/TUD-1_5	5.3[b]	0.84	255	0.44	70
Pt/W-TUD-1_{28}	17.0[b]	1.06	415	0.49	50
Pt/W-TUD-1_{16}	13.8[b]	0.89	605	0.72	45
Pt/W-TUD-1_{11}	10.6[b]	0.72	655	0.72	45
Pt/W-TUD-1_9	9.4[b]	0.74	590	0.84	55
Pt/W-TUD-1_7	7.5[b]	0.61	670	0.74	45

[a]INAA; [b]ICP; [c]ICP on Pt/WO_3/TUD-1_5.

2.3.4. X-RAY DIFFRACTION

X-ray diffraction patterns of the W-TUD-1 samples were recorded on a Bruker-AXS D8 Advance diffractometer with Cu-Kα radiation, which was operated at 25 mA and 45 kV. The measuring step size was 0.0387º with a step time of 1 s^{-1}. The diffraction spectrum was taken over a range from 5 ° to 90 ° *2θ*. X-ray diffraction patterns of the WO_3/TUD-1, Pt/W-TUD-1 and Pt/WO_3/TUD-1 samples were measured using a Bruker D8 Advance diffractometer with a Lynxeye detector and Cu*Ka* radiation. Measuring range from 5 ° to 95 ° *2θ* with a step size of 0.02º and a scan speed of 0.15 s^{-1}.

2.3.5. ELECTRON MICROSCOPY

High-resolution transmission electron microscopy (HR-TEM) was performed on a Philips CM30UT electron microscope with a LaB_6 filament as the source of electrons operated at 300 kV. Samples were

prepared by placing a few droplets of a suspension of ground sample in ethanol on the grid, followed by drying at ambient conditions.

2.3.6. NH_3-Temperature Programmed Desorption

A calcined sample was pretreated in a continuous stream of He (10 mL·min^{-1}) at 250 °C (ramping at 10 °C·min^{-1} from room temperature). After returning to 100 °C, the sample was flushed for 30 min with ammonia (9.982 mol.% ammonia in He, 10 mL·min^{-1}). Subsequently the physically adsorbed ammonia was removed by flushing with He (10 mL·min^{-1}) for 30 min at the same temperature. Subsequently the temperature was ramped (1 °C·min^{-1}) from 100 °C to 600 °C and ammonia desorption was recorded on a Micromeritics Autochem 2910 equipped with a Thermal Conductivity Detector.

2.4. Catalytic performance testing

2.4.1. Isopulegol Hydrogenation

Isopulegol hydrogenation was performed in a PolyBLOCK 8 (HEL group), a parallel autoclave reactor system consisting of eight 16 mL vessels. Technical isopulegol (308.5 mg, 2.0 mmol), dry toluene (4.0 mL) and catalyst (powder, 50 mg) were added to the reactor. The autoclave was purged three times with nitrogen (20 bar) and three times with hydrogen (20 bar) and then pressurized with hydrogen (20 bar). The reactor was magnetically stirred (800 rpm) and heated to 80 °C within 10 minutes and kept at this temperature for 16 h. Stirring was stopped and the reactors were allowed to cool down to room temperature. 1,3,5-trimethylbenzene (100 μL, 0.716 mmol) was added to the reaction mixture as internal standard. A GC sample was prepared by diluting 40 μL reaction mixture with 960 μL dry toluene.

The apparent turnover frequency (*TOF*) for hydrogenation is defined as mol isopulegol converted per mol Pt present per hour, based on a rate constant k that is derived from a first order rate approximation (Appendix 5).

2.4.2. Isopulegol Hydrogenation – Kinetic profile

A kinetic profile was obtained by using the isopulegol hydrogenation procedure that is described above by operating 8 parallel reactions in the PolyBLOCK 8. Pt/W-TUD-1_{11} (50 mg) was used as a catalyst and the reactions were individually stopped at the indicated reaction times.

2.4.3. Menthol Synthesis

Menthol synthesis was performed in two stages in a PolyBLOCK 8. In the first stage (*rac*)-Citronellal (308.5 mg, 2.0 mmol), dry toluene (4.0 mL) and catalyst (powder, 50 mg) were added to the reactor. The autoclave was purged three times with nitrogen (20 bar) and then pressurized with nitrogen (20 bar). The

reactor was magnetically stirred (800 rpm) and heated to 80 °C within 10 minutes and kept at this temperature for 5 h. Stirring was stopped and the reactors were allowed to cool down to room temperature. A GC sample was prepared by diluting 40 μL reaction mixture with 960 μL dry toluene and 1,3,5-trimethylbenzene (1.0 μL, 7.16 μmol) was added to the GC sample as an internal standard).

The apparent turnover frequency (TOF_w) for the Prins cyclisation is defined as mmol citronellal converted per mol W per hour, based on a rate constant k that is derived from a first order rate approximation (Appendix 5).

For stage 2 the reactor was closed again and the same procedure as described for isopulegol hydrogenation was followed.

2.4.4. Recycling Experiment

After the menthol synthesis the reaction mixture was filtered off and the catalyst was rinsed using dry toluene. Then (*rac*)-citronellal (308.5, 2.0 mmol) and dry toluene (4.0 mL) were added and the reaction procedure for menthol synthesis was repeated.

2.4.5. GC analysis

The GC samples were analyzed on a Shimadzu GC-17A gas chromatograph (16 min at 140 °C isothermal, followed by a ramp of 50 °C·min^{-1} to 250 °C, and 1 min isothermal) equipped with an injector at 250 °C, a Cyclodex-B column (60 m × 0.25 mm × 0.25 μm) and using a FID detector at 270 °C. The retention times observed are: 8.0 min 1,3,5-trimethylbenzene, 13.4 and 13.5 min (*rac*)-citronellal, 14.8, 15.0, 15.1, 15.2, 16.4 and 16.6 min (*rac*)-isopulegol, 16.3, 16.3, 16.8 and 16.8 min (*rac*)-menthol, 12.0 and 16.6 min 3,7-dimethyloctan-1-ol, 17.7 min 3,7-dimethyl-6-octen-1-ol. [17,19,30] The Prins cyclisation of citronellal in this study is not stereoselective due to the relatively large pores of TUD-1 and forms a thermodynamic distribution of isomers. [21,30] Moreover, this study utilizes (*rac*)-citronellal and was therefore not focused on stereoisomeric distribution of reaction products.

3. RESULTS AND DISCUSSION

3.1. Catalysts Characterization

The chemical composition of the samples is determined by a combination of INAA and ICP-OES. It shows a good correlation between the amounts of tungsten and platinum (0.9 ± 0.2 wt.%) used for the synthesis of the catalysts and the amounts that were present in the materials (Table 1).

The pore structures of the materials are summarized in Table 1 and the nitrogen isotherms and pore size distributions are presented in Figure 1. All samples show a type IV isotherm, typical for mesoporous

materials where capillary condensation in mesopores occurs in a relative pressure range of 0.4-0.8. All materials show a H2 type hysteresis loop (Figure 1). [34]

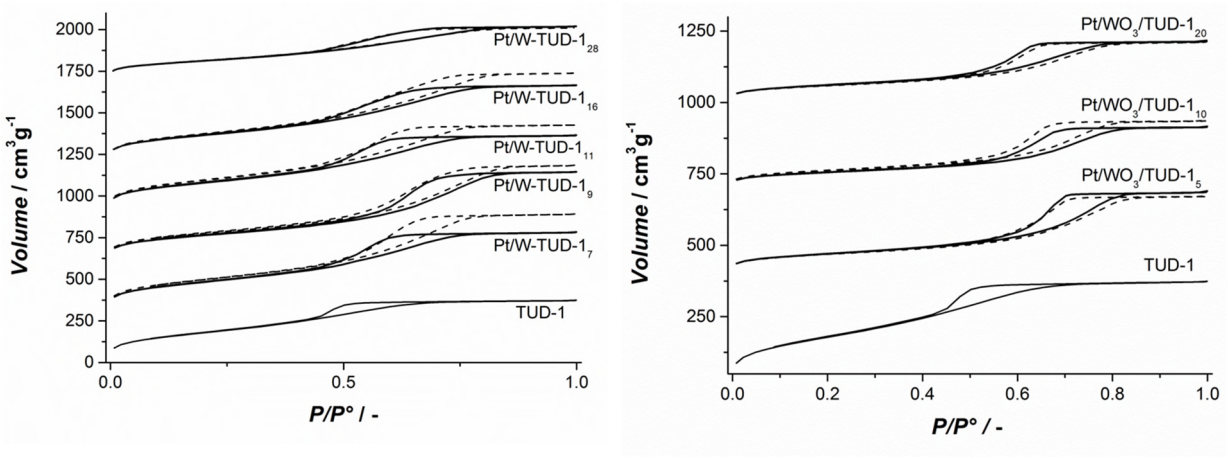

Figure 1. (*left)* Isotherms of Pt/W-TUD-1 samples (*bold*) and W-TUD-1 samples (*dashed*); (*right)* Isotherms of Pt/WO_3/TUD-1 samples (*bold*) and WO_3/TUD-1 samples (*dashed*).

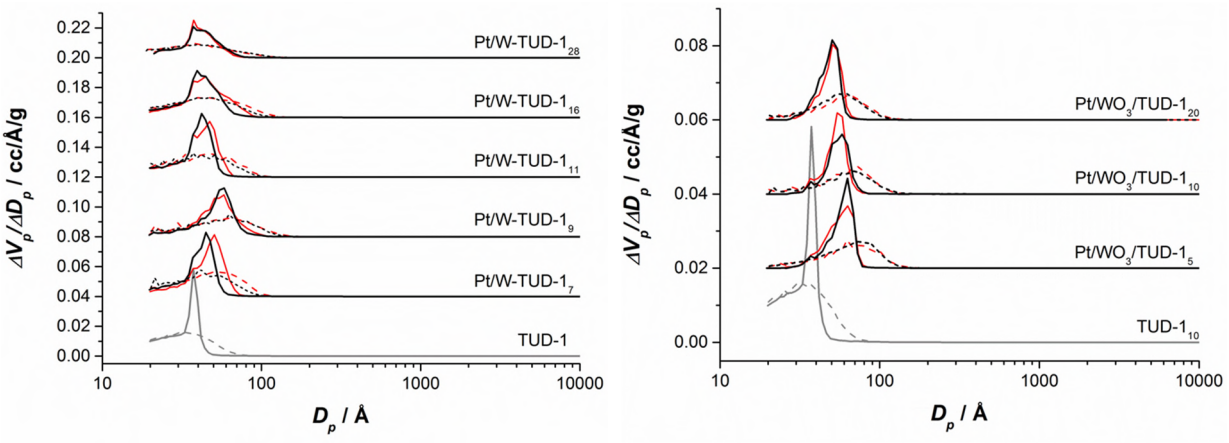

Figure 2. Pore size distribution of Pt/W-TUD-1 samples (*left*). (*dashed*) adsorption (*solid*) desorption. Red lines are samples without Pt. Pore size distribution of Pt/WO_3/TUD-1 samples (*right*). (*dash*) adsorption (*solid*) desorption. Red lines are samples without Pt. (distribution of different samples shifted by +0.02 units).

The W-TUD-1 samples have a larger pore volume and larger BET area than the WO_3/TUD-1 samples. Impregnation of the W-TUD-1 samples with platinum precursor resulted in slightly lower pore volumes and BET areas, while impregnation of the WO_3/TUD-1 samples did not affect the physical properties of this material (Table 1). It is noted that in some cases the adsorption-desorption hysteresis closes at 0.42 relative pressure, which indicates the influence of the tensile strength effect, indicating that the distinct pore size visible for e.g. TUD-1 at ~ 3-4 nm is an artefact of this phenomenon. [35]

The XRD results show that the tungsten is better dispersed on the Pt/W-TUD-1 samples. WO_3 reflections start only appearing at Pt/W-TUD-1_{16}, whereas WO_3 reflections are already visible in

$Pt/WO_3/TUD\text{-}1_5$. Addition of Pt to both the W-TUD-1 and the WO_3/TUD-1 materials results in barely visible Pt reflections around 45 and 55°, indicating that the Pt particles on the material are well dispersed and close to the detection limit of XRD (Figure 3).

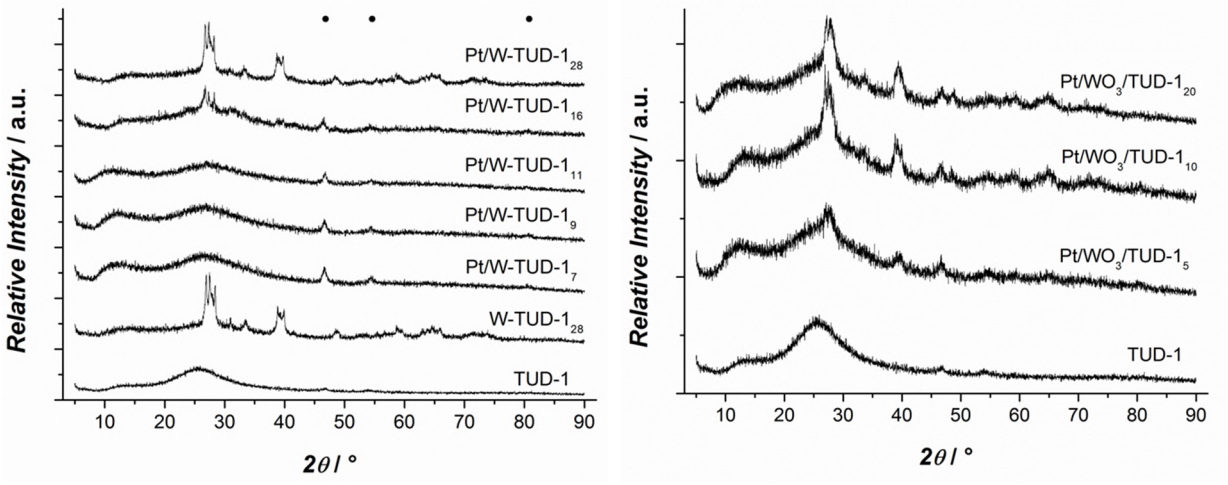

Figure 3. XRD patterns of Pt/W-TUD-1 samples (*left*); XRD patterns of Pt/WO_3/TUD-1 samples (*right*).

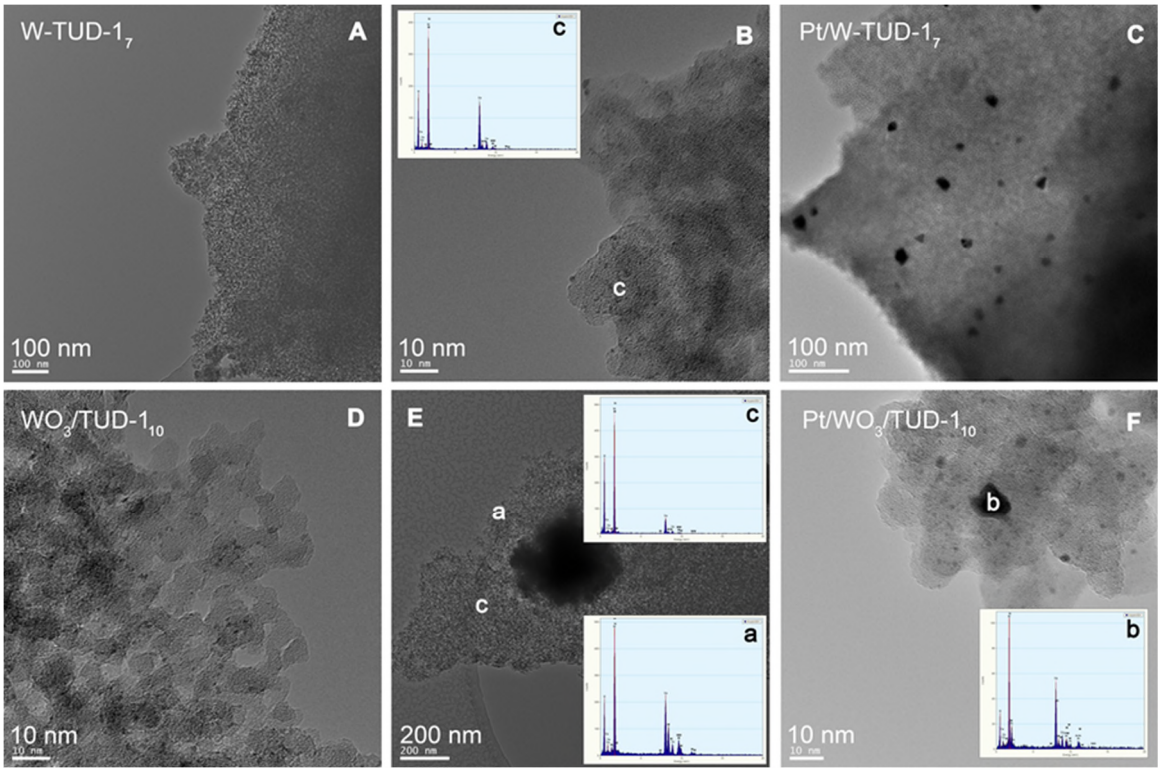

Figure 4. TEM images of W-TUD-1_7 (A and B) and Pt/W-TUD-1_7 (C) and WO_3/TUD-1_{10} (D and E) and Pt/WO_3/TUD-1_{10} (F).

The TEM images before and after Pt addition show that the supports are not affected by the impregnation procedure (Figure 4). Platinum has been well dispersed on the W-TUD-1_7 support and is

present in < 25 nm particles. The Pt/WO_3/TUD-1_{10} material shows a typical Pt particle size of 10 nm diameter. Figure 5 shows more detailed TEM images and EDX analyses of Pt loaded WO_3/TUD-1 samples, and shows the differences between Pt and WO_3 particles. Pt particles are identified by an EDX signal at 2.0 keV and can be recognized by their dark colour and sharp edges. [36] The WO_3 particles are identified by EDX through the W signal at 1.8 keV and are generally more vague than the sharply outlined Pt particles.

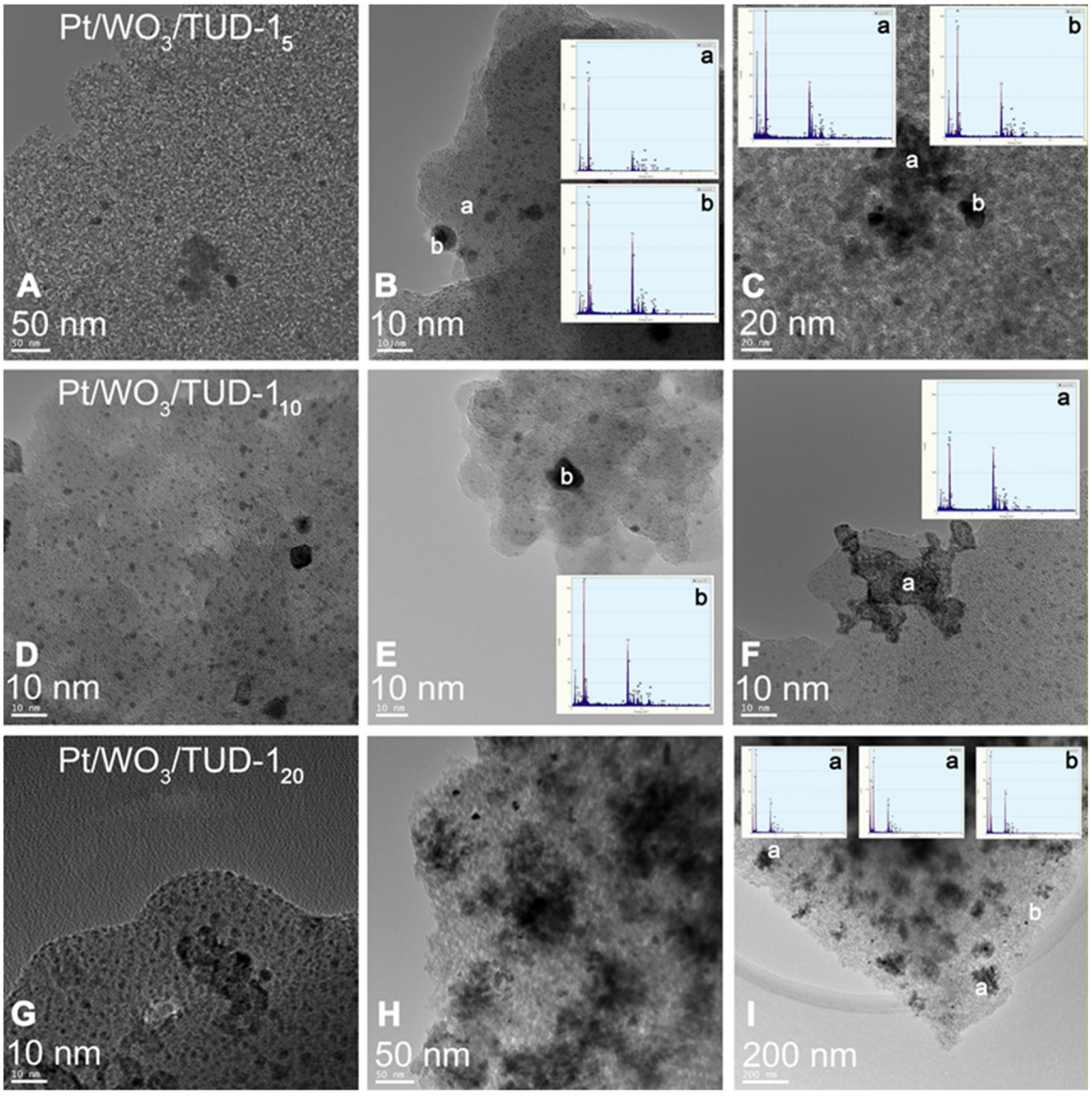

Figure 5. TEM images of Pt impregnated WO_3/TUD-1 and corresponding EDX analysis. Pt/WO_3/TUD-1_5 (A, B and C); Pt/WO_3/TUD-1_{10} (D, E and F); *Bottom*: Pt/WO_3/TUD-1_{20} (G, H and I).

The particles on Pt/WO_3/TUD-1_5 that were assigned with an '*a*' in the top row of Figure 5 were identified as WO_3 particles by EDX. The Pt particles, which tend to be smaller than the WO_3 particles, were tagged with a '*b*'. The Pt particle in the middle image in the middle row of Figure 5 can be clearly distinguished from the WO_3 particle in the image on the right hand side.

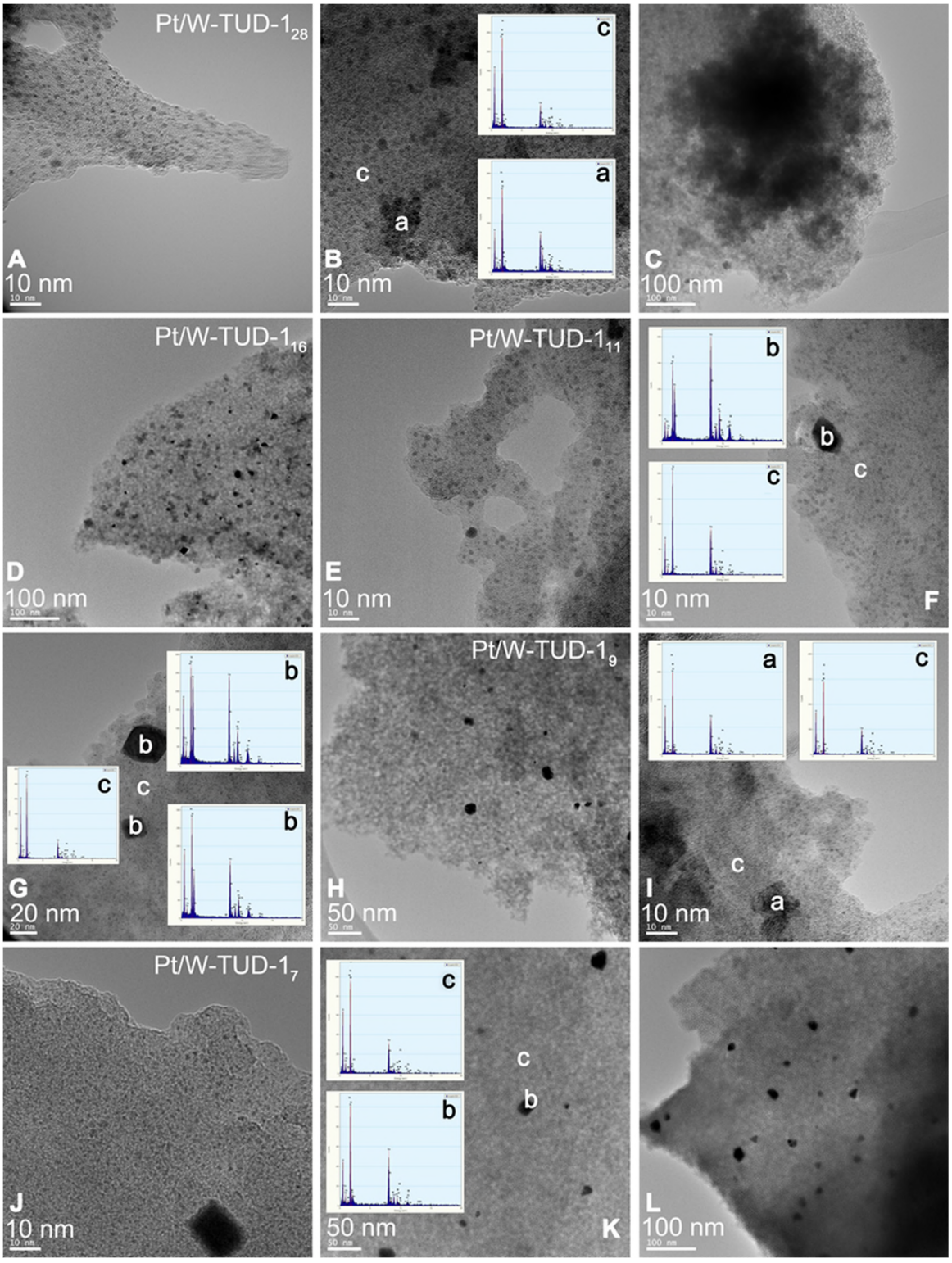

Figure 6. TEM images of Pt impregnated W-TUD-1 and corresponding EDX analysis. Pt/W-TUD-1_{28} (A, B and C); Pt/W-TUD-1_{16} (D), Pt/W-TUD-1_{11} (E, F and G); Pt/W-TUD-1_{9} (H and I); Pt/W-TUD-1_{7} (J, K and L).

The TEM images of Pt/WO_3/TUD-1_{20} show relatively more agglomerations of WO_3, as a result of the higher tungsten loading. The irregularly shaped forms ('*a*') were identified as WO_3, while the sharp dark

dot proved to be a Pt particle ('*b*'), which shows that the tungsten loading has no effect on the Pt particle size or shape. All of the Pt/WO_3/TUD-1 materials, irrespective of the tungsten loading, show relatively large agglomerates of WO_3. The higher the tungsten loading, the larger these agglomerates become.

As a direct result of the high tungsten loading, the Pt/W-TUD-1_{28} material shows the largest WO_3 agglomerations (Figure 6, 'a') of all the Pt/W-TUD-1 samples. This is also recognized from the XRD results, which show a clear WO_3 reflection for this material. Interestingly, there are not as much Pt particles (Figure 6, 'b') visible on the Pt/W-TUD-1_{28} (Figure 6, 100 nm scale bar) as in the image of Pt/W-TUD-1_{16} with the same scaling. On the other hand, the observed WO_3 agglomerations in this image are much smaller than in the Pt/W-TUD-1_{28} material and become scarce when the tungsten loading is lowered even more (Pt/W-TUD-$1_{11,\ 9\ \text{and}\ 7}$). The Pt particles on these materials do not seem to change much in size and shape over the range of tungsten loadings. Some EDX spectra of the TUD-1 background are added as comparison (Figure 6, 'c').

3.2. CATALYST PERFORMANCE

3.2.1. ISOPULEGOL HYDROGENATION

A hydrogenation rate constant k was calculated for the conversion of isopulegol to menthol (Table 2), assuming a first order dependence on isopulegol concentration (vide infra). These rate constants are used to calculate initial rates r_0, which serve to compare the hydrogenation activity of the individual catalysts (Figure 7). Both the Carberry number (extraparticle mass transfer) and the Weisz modulus (intraparticle mass transfer) proved to be sufficiently low to assure that the reactions proceeded without any mass transfer limitations (Appendix 6). The different Pt loadings are taken into account by calculating a turnover frequency (*TOF*), which is calculated by normalizing the initial rate for the Pt content (Table 2). The only observed trend is that the Pt/W-TUD-1 catalysts are more active hydrogenation catalysts than the Pt/WO_3/TUD-1 materials, with Pt/W-TUD-1_{28} and Pt/W-TUD-1_9 being the most active in the series. However, there is no observable trend for the hydrogenation activity and the WO_3 content of the catalysts themselves. This could indicate that the particle size of the WO_3 that is present on the catalyst contributes to the hydrogenation activity.

It is important to note that WO_3 by itself is not an active hydrogenation catalyst and the activity of the individual catalysts is likely to be dependent on the Pt metal surface and its environment. This relates to the Pt dispersion on the catalyst, but is difficult to quantify based on the XRD and TEM data. The incipient wetness impregnation of the different catalysts must have led to a varying Pt dispersion, resulting in a wide range of hydrogenation activities.

Interestingly, no deoxygenated products are observed during the reaction, showing that under these reaction conditions the material is not acidic enough to remove the hydroxyl group that is present in both isopulegol and menthol.

Table 2. Conversion of isopulegol after 16 h hydrogenation over Pt/W-TUD-1 and Pt/WO_3/TUD-1 catalysts and derived kinetic parameters. Reaction conditions: 2.0 mmol isopulegol, 4.0 mL toluene, 50 mg catalyst, 20 bar H_2, 80 °C, 800 rpm.

Catalyst	Conversion (%)	Pt (wt.%)	k (10^{-7} mL·mg_{cat}^{-1}·s^{-1})	r_0 (10^{-7} mol·g_{cat}^{-1}·s^{-1})	TOF_{Pt} (10^{-3} mol·mol_{Pt}^{-1}·s^{-1})
Pt/W-TUD-1_{28}	95.1	1.06	41	21	38
Pt/W-TUD-1_{16}	6.8	0.89	0.9	0.5	1.1
Pt/W-TUD-1_{11}	31.6	0.72	5.3	2.8	7.7
Pt/W-TUD-1_9	83.9	0.74	23	12	31
Pt/W-TUD-1_7	47.6	0.61	8.6	4.3	14
Pt/WO_3/TUD-1_5	16.7	0.84	2.4	1.2	2.8
Pt/WO_3/TUD-1_{10}	13.7	1.01	2.0	1.0	2.0
Pt/WO_3/TUD-1_{20}	24.8	1.01	3.6	1.8	3.4

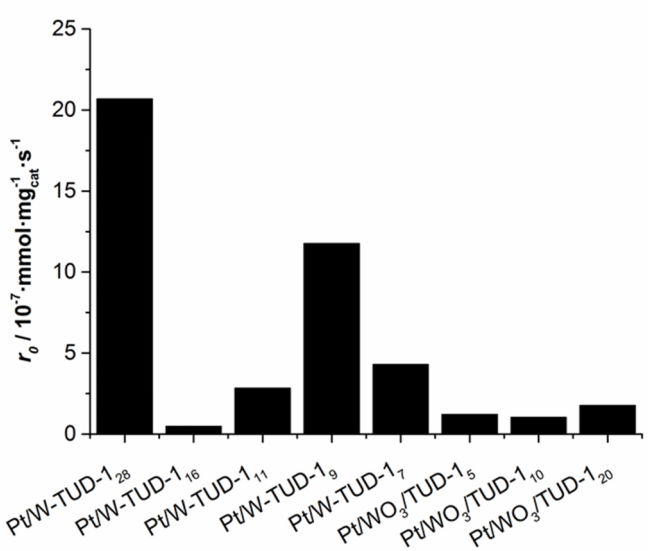

Figure 7. Initial hydrogenation rate r_0 of isopulegol over Pt/W-TUD-1 and Pt/WO_3/TUD-1 catalysts. Reaction conditions: 2.0 mmol isopulegol, 4.0 mL toluene, 50 mg catalyst, 20 bar H_2, 80 °C, 800 rpm.

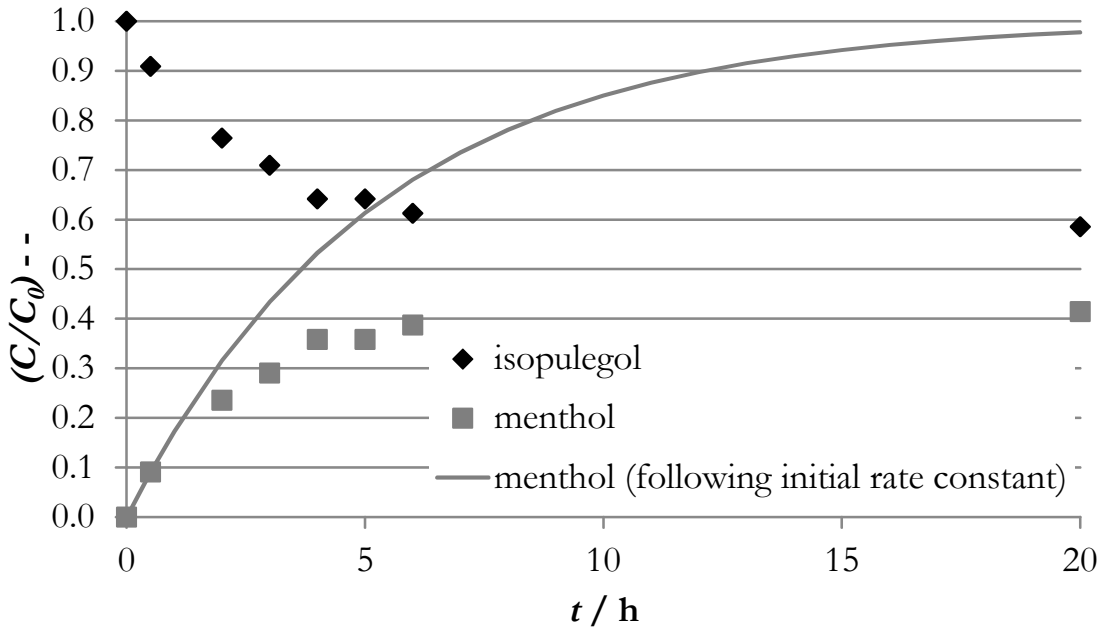

Figure 8. Kinetic profiles of isopulegol hydrogenation using Pt/W-TUD-1_{11} as catalyst. Reaction conditions: 2.0 mmol isopulegol, 4.0 mL toluene, 50 mg catalyst, 20 bar H_2, 80°C. The line indicates the menthol concentration development predicted based on the initial rate constant k.

3.2.2. Kinetic Profile

The kinetic profile of Pt/W-TUD-1_{11} shows that the conversion of isopulegol stabilizes around 40% (Figure 8). This is attributed to catalyst deactivation, as other catalysts have shown higher conversions before (Figure 7), [37] so product inhibition is excluded as a cause. The deactivation starts in an early stage of the reaction and becomes progressively worse. This is visualized by the curve that predicts the menthol concentration in case the initial rate constant k_0 would be maintained throughout the reaction. Since the mass balance is around 95%, some polymerization and coking could be possible deactivation mechanisms. Other possible deactivation mechanisms are sintering and poisoning. [37]

Poisoning is not expected by using these clean feeds, and product inhibition was not observed in previous studies of isopulegol hydrogenation. [11] Agglomeration of the Pt particles is observed by TEM after reaction, as can be seen in Figure 9.

Obviously, the observed catalyst deactivation has an effect on the accuracy of our assumption of first order rate dependence. However, this is still the best assumption that we can make.

3.2.3. Menthol Synthesis

Hydrogenation of isopulegol only probed the hydrogenation activity of the bifunctional Pt/W-TUD-1 and Pt/WO_3/TUD-1 catalysts. However, the acidic supports also allow for the Prins cyclisation of citronellal

to isopulegol. This implies that menthol can be produced directly from citronellal, thereby fully utilizing the capabilities of these bifunctional catalysts (Table 3).

Table 3. Menthol synthesis in two stages. Stage 1 Prins cyclisation for 5 h, stage 2 consecutive hydrogenation for 16 h.

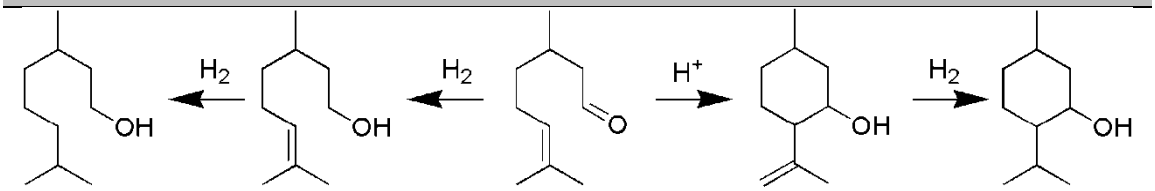

5 **4** **citronellal 1** **isopulegol 2** **menthol 3**

	Stage 1	Stage 1 + stage 2					5 h Prins cyclisation		16 h Hydrogenation	
	Yield (%) t = 5 h	Yield (%) t = 21 h					k ($\mu L \cdot g_{cat}^{-1} \cdot s^{-1}$) [a]	TOF_{Pr} ($mmol \cdot mol_W^{-1} \cdot s^{-1}$) [b]	k ($\mu L \cdot mg_{cat}^{-1} \cdot s^{-1}$) [c]	TOF_{Pt} ($mmol \cdot mol_{Pt}^{-1} \cdot s^{-1}$)[d]
Catalyst	**2**	**1**	**2**	**3**	**5**	**4**				
Pt/W-TUD-1_{28}	85.2	0	0	83.3	16.7	0	8.4	3.0	5.3	3.9
Pt/W-TUD-1_{16}	90.6	0	23.2	73.8	2.0	1.0	10.1	7.1	2.2	22.9
Pt/W-TUD-1_{11}	99.5	0	0	96.4	3.6	0	22.8	22.6	4.6	65.2
Pt/W-TUD-1_{9}	93.6	0	0	90.9	9.1	0	12.0	14.3	4.9	59.3
Pt/W-TUD-1_{7}	93.4	0	0	91.3	8.7	0	11.5	17.0	5.0	77.2
Pt/WO_3/TUD-1_{5}	30.6	30.8	19.2	22.0	20.9	7.2	1.6	3.5	0.6 [e]	4.8 [f]
Pt/WO_3/TUD-1_{10}	24.5	24.3	20.2	12.8	21.0	21.7	1.3	1.7	0.8 [e]	5.6 [f]
Pt/WO_3/TUD-1_{20}	24.0	23.7	16.2	14.9	36.4	8.7	1.2	0.8	1.0 [e]	7.6 [f]

Reaction conditions Prins cyclisation: 2.0 mmol citronellal, 4.0 mL toluene, 50 mg catalyst, 80°C, 20 bar N_2, 5 h; Reaction conditions Hydrogenation: Reaction mixture (including catalyst) of Prins cyclisation is used, 80°C, 20 bar H_2, 16 h.

[a] Prins cyclisation rate constant k is calculated from citronellal conversion after 5 h by assuming a first order in citronellal concentration

[b] Prins cyclisation TOF_{Pr} is calculated from the initial rate r_0, and accounts for the amount of W in the catalyst, defined as mol converted citronellal per mol W per s

[c] Isopulegol hydrogenation rate constant k is calculated assuming a first order in isopulegol concentration, and assuming no additional isopulegol is formed during hydrogenation (t > 5h) (therefore rate constants for Pt/WO_3/TUD-1 catalysts cannot be calculated)

[d] Isopulegol hydrogenation TOF_{Pt} is calculated from the initial rate r_0, and accounts for the amount of Pt in the catalyst, defined as mol converted isopulegol per mol Pt per s

[e] Citronellal double bond hydrogenation rate constant k is calculated for the Pt/WO_3/TUD-1 catalysts, assuming a first order in citronellal double bond concentration, and assuming no additional Prins cyclisation occurs during hydrogenation

[f] Citronellal double bond hydrogenation TOF_{Pt} is calculated from the initial rate r_0, and accounts for the amount of Pt in the catalyst, defined as mol converted double bond per mol Pt per s

The highest menthol yield was achieved over Pt/W-TUD-1_{11}. Overall, 96% citronellal could be converted into menthol by sequential operation. The remaining 4% was retrieved as 3,7-dimethyloctan-1-ol, resulting from the direct hydrogenation of citronellal. This clearly shows that the acidity of these materials does not lead to unwanted oxygen elimination.

Table 4. NH_3-TPD acidity. [31]

Catalyst	Total Acidity ($mmol \cdot g_{cat}^{-1}$)[a]	Acidity/W ($mol_{H+} \cdot mol_W^{-1}$)	ρ_{WO3} (WO_3 units·nm^{-2})
TUD-1	0.02	n.a.	n.a.
WO_3 [40]	0.0	n.a.	n.a.
WO_3/TUD-1_{10}	0.34	0.90	0.38
WO_3/TUD-1_{20}	0.45	0.57	0.88
W-TUD-1_7	0.38	1.09	0.29
W-TUD-1_9	0.52	1.26	0.39
W-TUD-1_{11}	0.78	1.47	0.45
W-TUD-1_{16}	0.99	1.35	0.70
W-TUD-1_{28}	0.47	0.35	1.92

[a] Total catalyst acidity determined over a temperature range of 100-600 °C.

The Prins cyclisation is performed under a nitrogen atmosphere in the first stage, as the hydrogenation of the carbonyl and alkene by the platinum catalyst would reduce the menthol selectivity significantly (converting citronellal into dimethyloctenol and dimethyloctanol (Table 3, **4** and **5**), thereby preventing the formation of menthol). Overall, the Pt/W-TUD-1 catalysts show a higher conversion of citronellal compared to the Pt/WO_3/TUD-1 catalysts. In this series, the catalysts with a low tungsten loading (Pt/W-TUD-$1_{7, 9 \text{ and } 11}$) have a far higher TOF_w than a higher tungsten loading catalysts (Pt/W-TUD-$1_{16 \text{ and } 28}$). In fact, Pt/W-TUD-1_{28} has a TOF_w that is comparable to the TOF_w of the Pt/WO_3/TUD-1 catalysts. The Pt/WO_3/TUD-1 catalysts show an increasing TOF_w with decreasing tungsten loading. This is in agreement with earlier work with the W-TUD-1 and WO_3/TUD-1 materials without Pt and is the result of the better dispersion of tungsten (Table 4). [31] The highest TOF_w was observed for the Pt/W-TUD-1_{11} catalyst, because this material contains an optimal amount of small WO_3 particles (Table 1), without forming large, relatively non-acidic, WO_3 particles. It exhibits the highest number of acid sites per tungsten (Table 4).

The surface coverage of tungsten on an alumina support was recently reported by García-Fernández *et al.* [38]. They evaluated the tungsten surface density (ρ_W, expressed in W atoms per nm^2) according to the Kerkhof-Moulijn model. [39] It was found that this model was valid for a tungsten loading up to 9 wt.%. At higher tungsten loadings the tungsten starts forming three-dimensional clusters. This is somewhat in agreement with our observation that at higher WO_3-loadings our catalysts are becoming less acidic per tungsten atom (Table 4). Obviously, the WO_3 surface density (ρ_{WO3}, expressed in WO_3 molecules per nm^2) at which three-dimensional clusters are formed is different for alumina and TUD-1 (a silica material). It is expected that these clusters start to form at lower ρ_{WO3} because of the weaker interaction of a silica surface compared to an alumina surface. A strong indication for this is the decrease in surface area of the WO_3/TUD-1 and Pt/WO_3/TUD-1 materials and W/TUD-1_{28} Pt/W-TUD-1_{28} (Table 1). After 5 h the

second stage, the hydrogenation of isopulegol to menthol, was started by replacing the nitrogen atmosphere by the reducing hydrogen atmosphere. From this point on, the Prins cyclisation and hydrogenation proceed simultaneously. After 21 h, the citronellal is completely converted over the Pt/W-TUD-1 catalysts (except for Pt/W-TUD-1_{16}) into menthol **3** and dimethyloctanol **5**. When Pt/W-TUD-1_{16} was used, some isopulegol and **4** remained. This illustrates that hydrogenation over this catalyst is not so efficient, as was also shown for the neat hydrogenation (Table 3). Isopulegol and **4** are also observed when the Pt/WO_3/TUD-1 catalyst samples were used, which is in agreement with the low TOF_{Pt} for these catalysts that were determined for the hydrogenation (Table 3).

The TOF_{Pt}'s for the isopulegol conversion experiment (Table 2) are lower than the TOF_{Pt}'s were observed during the menthol synthesis experiment (Table 3). It was assumed that the PtO_x on the catalyst would readily reduce to the active metallic Pt under 20 bar of pure hydrogen at reaction temperature but it seems that this was not the case. The 5 hours under nitrogen atmosphere might have pre-reduced the PtO_x on the catalyst, resulting in a higher activity.

In this experiment, a direct comparison of the hydrogenation efficiency of the eight acidic hydrogenation catalysts is difficult, as the different catalysts are subjected to different substrate concentrations, which is a direct result from the preceding Prins cyclisation.

The five Pt/W-TUD-1 catalysts can be compared, as the initial Prins cyclisation over these catalysts was almost complete, which resulted in comparable starting concentrations of isopulegol. Using a first order rate approximation an isopulegol hydrogenation rate constant can then be derived for these catalysts. This is used to calculate initial rates r_0 and TOF_{Pt}. This shows that the Pt/W-TUD-1 catalysts have TOF_{Pt} values that are in the same order of magnitude ($2.3\text{-}7.7 \cdot 10^{-2}$ $mol \cdot mol_{Pt}^{-1} \cdot s^{-1}$) and also comparable to those in Table 2, which is to be expected when conversions are close to 100% and Pt concentrations in the different experiments are comparable.

However, this approach cannot be applied to analysis of the Pt/WO_3/TUD-1 samples, as after the initial Prins cyclisation stage only 25-30% isopulegol was produced. In order to be able to compare the hydrogenation activity under these conditions, the concentration of double bonds in citronellal that is left after Prins cyclisation was defined. A double bond hydrogenation (both carbon-carbon and carbon-oxygen double bonds) rate constant k was then calculated, assuming a first order rate approximation and similar reactivity. From these k values, initial rates r_0 were calculated. These were normalized for Pt content to get TOF_{Pt} values.

3.2.4. Recycling Experiment

The catalysts were separated from the reaction mixture and subjected to another round of menthol synthesis to investigate their recyclability (Table 5). The initial Prins cyclisation clearly shows that the solid acid's activity is greatly reduced after one cycle. Obviously, a deactivation mechanism is at play for all

catalysts. TEM analysis shows that agglomeration of WO_3 particles occurred, resulting in larger, less active particles (Figure 9). This was previously shown for the materials without Pt. [31]

The recycled Pt/WO_3/TUD-1 catalysts all show a one order of magnitude lower Prins cyclisation activity, independent of the tungsten loading. This is likely due to relatively large particles of similar size WO_3 present in these catalysts that agglomerate at comparable rates. The recycled Pt/WO_3/TUD-1 catalysts are again outperformed by the Pt/W-TUD-1 catalysts in this acid catalyzed citronellal conversion. However,

Table 5. Menthol synthesis with recycled catalyst samples in two stages. Stage 1 Prins cyclisation for 5 h, stage 2 consecutive hydrogenation for 16 h.

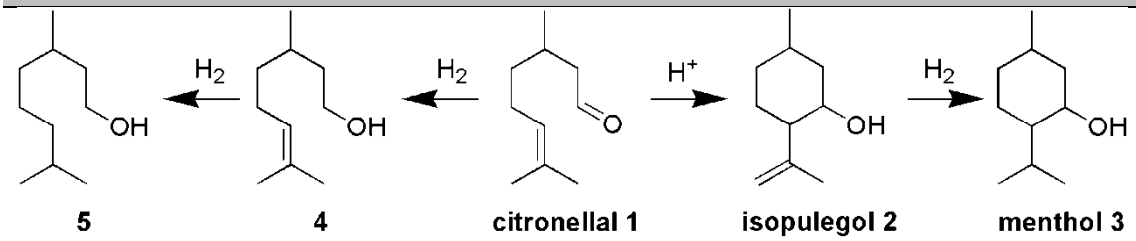

	Stage 1						5 h Prins cyclisation			16 h Hydrogenation		
	Yield (%) t = 5 h	Yield (%) t = 21 h					k_c ($\mu L \cdot g_{cat}^{-1} \cdot s^{-1}$) [a]	TOF_{ir} ($mmol \cdot mol_W^{-1} \cdot s^{-1}$) [b]	TOF_{fresh}/TOF_{spent}	k_c ($\mu L \cdot g_{cat}^{-1} \cdot s^{-1}$) [c]	TOF_{Pt} ($mmol \cdot mol_{Pt}^{-1} \cdot s^{-1}$) [d]	TOF_{fresh}/TOF_{spent}
Catalyst	**2**	**1**	**2**	**3**	**5**	**4**						
Pt/W-TUD-1_{28}	16.5	18.1	9.0	19.1	42.6	11.2	0.6	0.3	10	0.9	9.1	n.a. [e]
Pt/W-TUD-1_{16}	20.8	26.8	22.2	19.1	26.1	5.8	0.9	0.7	11	0.5	5.3	n.a. [e]
Pt/W-TUD-1_{11}	16.0	19.6	11.3	17.3	45.2	6.7	0.7	0.7	32	1.0	13.0	n.a. [e]
Pt/W-TUD-1_9												
Pt/W-TUD-1_7	4.0	0	0	3.2	96.8	0	0.2	0.3	63	45.2	701.3	n.a. [e]
Pt/WO_3/TUD-1_5	4.7	72.4	12.7	0	4.2	10.7	0.2	0.5	8	0.1	1.6	3
Pt/WO_3/TUD-1_{10}	4.1	51.1	5.4	-0.7	16.0	28.3	0.2	0.3	7	0.5	4.9	1
Pt/WO_3/TUD-1_{20}	4.9	49.9	4.9	0.9	40.3	3.9	0.2	0.1	6	0.7	7.3	1

Reaction conditions Prins cyclisation: 2.0 mmol citronellal, 4.0 mL toluene, 50 mg recycled catalyst, 80°C, 20 bar N_2, 5 h; Reaction conditions Hydrogenation: Reaction mixture (including catalyst) of Prins cyclisation is used, 80°C, 20 bar H_2, 16 h.

[a] Prins cyclisation rate constant k_c is calculated from citronellal conversion after 5 h by assuming a first order in citronellal concentration

[b] Prins cyclisation *TOF* is calculated from the initial rate r_0, and accounts for the amount of W in the catalyst, defined as mol converted citronellal per mol W per s

[c] Citronellal double bond hydrogenation rate constant k_c is calculated for the Pt/WO_3/TUD-1 catalysts, assuming a first order in citronellal double bond concentration, and assuming no additional Prins cyclisation occurs during hydrogenation

[d] Citronellal double bond hydrogenation *TOF* is calculated from the initial rate r_0, and accounts for the amount of Pt in the catalyst, defined as mol converted double bond per mol Pt per s

[e] fresh TOF_{Pt} is calculated in a differently than spent TOF_{Pt}, therefore the two cannot be directly compared

the TOF_W's of the two types of recycled catalyst are now of the same order of magnitude. Interestingly, the recycled Pt/W-TUD-1 catalysts with higher tungsten loadings (Pt/W-TUD-$1_{28,\ 16\ and\ 11}$) now exhibit higher citronellal conversion than the catalyst with the lowest tungsten loading, which in this recycle experiment only shows minimal Prins cyclisation activity. The TOF_W of the Pt/W-TUD-$1_{11\ and\ 7}$ catalysts had decreased by a factor 33 and 63, respectively, while the TOF_W of the Pt/W-TUD-$1_{28\ and\ 16}$ only decreased by a factor 10. This indicates that the small WO_3 particles that were present on the original Pt/W-TUD-$1_{11\ and\ 7}$ materials are prone to agglomeration, resulting in decreased catalytic activity. So, the decrease in Prins cyclisation activity is attributed to the agglomeration of the finely dispersed small WO_3 particles. The agglomeration of small WO_3 particles has a relatively larger effect on the acidity of the material, and hence the acidic activity of the catalyst, than agglomeration of larger WO_3 particles.

The reduced acidic activity of the bifunctional catalysts impacts the overall menthol synthesis. As less isopulegol is formed, less menthol is produced. The citronellal that is still present after 5 h of Prins cyclisation can continue to be converted into isopulegol during the hydrogenation stage. This is observed for Pt/W-TUD$_{28,\ 16\ and\ 11}$ and Pt/WO_3/TUD-1_5. However, larger amounts of **4** and **5** are now observed as citronellal can also be hydrogenated before it is converted into isopulegol. This shows that all eight catalysts still exhibit hydrogenation activity.

As the hydrogenation TOF_{Pt} with regards to menthol cannot be calculated for these recycled catalysts, it is difficult to compare the hydrogenation activities of the Pt/W-TUD-1 catalysts. However, due to the lack of acid activity for these recycled catalysts, the hydrogenation activity can still be evaluated using the same approach that was used to determine the TOF_{Pt} in the fresh Pt/WO_3/TUD-1 samples in Table 4. The concentration of double bonds in citronellal that is still present after Prins cyclisation was defined and a first order rate approximation was assumed with respect to the hydrogenated products **4** and **5** to calculate a hydrogenation rate constant k for the different catalysts. Initial rates r_0 were calculated from these rate constants and normalizing them on Pt content provides TOF_{Pt} values.

These TOF_{Pt} values can only be compared to the TOF_{Pt} values of the fresh Pt/WO_3/TUD-1 catalysts, as they are calculated in the same way. This shows that the hydrogenation TOF_{Pt} for the Pt/WO_3/TUD-1 is maintained after the recycle for Pt/WO_3/TUD-1_{20} and Pt/WO_3/TUD-1_{10}, while the TOF_W for Pt/WO_3/TUD$_5$ has slightly decreased, but still has the same order of magnitude.

On the other hand, the TOF_W's of Pt/W-TUD-$1_{28,\ 16\ and\ 11}$ have decreased by a factor of 5. This is in agreement with Figure 9A, where an increase in Pt particle size can be seen in comparison with the fresh catalyst.

Initially, the higher WO_3 dispersion on the fresh Pt/W-TUD-1 catalysts compared to the fresh Pt/WO_3/TUD-1 catalysts resulted in increased isopulegol formation and TOF_W. It is also clear that the reaction conditions influence the catalytic activity of the WO_3 phase for both types of catalyst. However, catalysts that contain small WO_3 particles, which are responsible for initial high activity (Pt/W-TUD-1),

are more affected by particle agglomeration than the bulk WO_3 phase that is present in the Pt/WO_3/TUD-1 catalysts. As a result, the TOF_w for catalysts that contained these small WO_3 particles decreased more than the catalysts that contained more bulk WO_3.

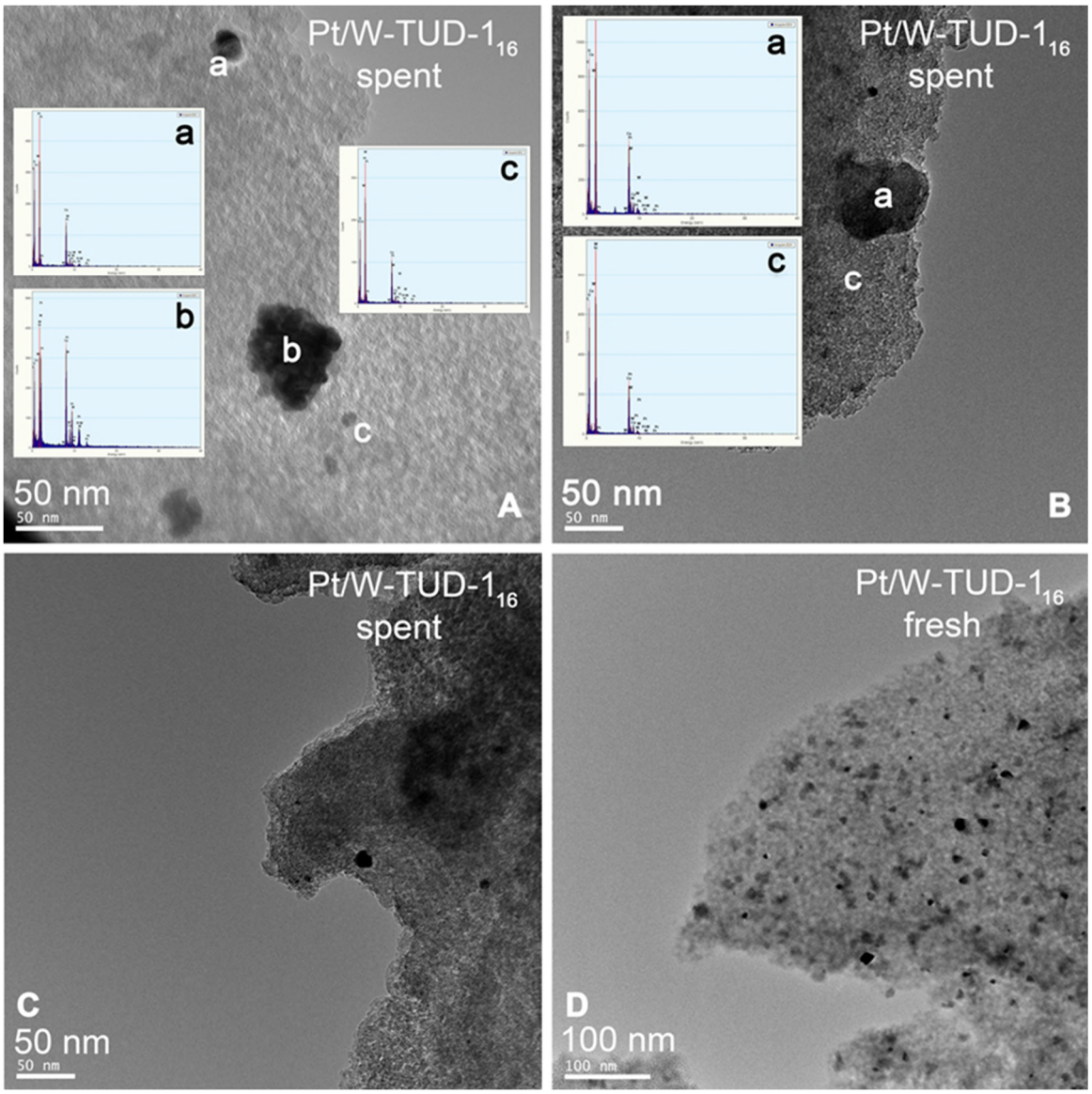

Figure 9. TEM images and EDX analysis of spent (A, B and D) and fresh (D) Pt/W-TUD-1_{16}. WO_3, Pt and background are labelled as a, b and c, respectively.

The hydrogenation TOF_{Pt} is higher for the catalysts containing finely dispersed WO_3 particles, i.e. Pt/W-TUD-1, than for the bulk WO_3 containing Pt/WO_3/TUD-1 catalysts. However, recycling of the catalysts showed that the hydrogenation activity only decreased for the spent Pt/W-TUD-1 catalysts. This indicates that the Pt on the Pt/W-TUD-1 catalysts differs from the Pt on the Pt/WO_3/TUD-1 samples and that the Pt on the Pt/WO_3/TUD-1 is relatively stable, but less active.

As a hypothesis, this could be due to the Pt being located on the finely dispersed WO_3, resulting in a more active Pt phase, but one that is deactivated more readily upon agglomeration of the small WO_3 particles during reaction. [38,41]

3.2.5. GLYCEROL CONVERSION

The catalytic performance of the Pt/W-TUD and Pt/WO_3 catalysts in the hydrogenolysis of glycerol was investigated using conditions similar to the ones used in Chapter 1 and 2 (100 mg catalyst, 100 mM aqueous glycerol, 200 °C, 18 h, 20 bar H_2). Unfortunately, only very low glycerol conversion were observed, and no 1,3-propanediol was detected. This suggests that the WO_3 particles present on the Pt/W-TUD-1 catalyst are not acidic enough for glycerol deoxygenation. Interestingly, a recent paper described the conversion of glycerol over a Pt/WO_3/Al_2O_3 catalyst using similar conditions (350 mg catalyst, 543 mM aqueous glycerol (5 wt.%), 220 °C, 24 h, 45 bar H_2). [38] This provided an impressive 1,3-propanediol yield of 28 % (53 % glycerol conversion, 52 % 1,3-propanediol selectivity). The catalyst that was used contained 9 wt.% Pt and 8 wt.% WO_3. The WO_3 loading of this catalyst is reasonably close to the Pt/W-TUD-1_7, Pt/W-TUD-1_9 and Pt/W-TUD-1_{11}. However, the WO_3 dispersion on the Al_2O_3 catalyst is expected to be higher than the WO_3 dispersion on the SiO_2 surface of the TUD-1 support. Moreover, the Pt loading on the successful catalyst was 9 times higher. This indicates that besides high WO_3 dispersion, swift hydrogenation after initial dehydration is critical to obtain high 1,3-propanediol selectivity.

4. CONCLUSIONS

A series of bifunctional heterogeneous catalysts was prepared through platinum impregnation of two different types of acidic tungsten oxide containing supports with different tungsten oxide loadings. A kinetic analysis was performed to compare the catalytic activities of the synthesized catalysts. These catalysts have proven to be effective in the acid catalyzed Prins cyclisation of citronellal and the subsequent hydrogenation of isopulegol into menthol. The unwanted acid catalyzed dehydroxylation was not observed for any of these catalysts.

Pt/W-TUD-1 materials are more active in the Prins cyclisation of citronellal than their Pt/WO_3/TUD-1 counterparts. A good dispersion of WO_3 is critical for high acidity and introducing the tungsten during the TUD-1 synthesis results in a higher WO_3 dispersion than after impregnation of TUD-1. Unfortunately, these small WO_3 particles are more sensitive to agglomeration during the reaction and the recycled Pt/W-TUD-1 catalysts have TOF_{in}'s that are more resembling the activity of the less active bulk WO_3. The highest activity was observed for the fresh Pt/W-TUD-1_{11} catalyst, attributed to an optimum between dispersion and WO_3 loading, *i.e.* higher WO_3 loading resulted in a lower dispersion, whereas a lower loading implies less available active tungsten.

The Pt/W-TUD-1 materials are also more active hydrogenation catalysts than the Pt/WO_3/TUD-1 materials. No correlation between tungsten loading and hydrogenation activity exists, but there is a correlation between hydrogenation activity and the presence of small WO_3 particles. The hydrogenation activity of the catalysts remains after recycling for the Pt/WO_3/TUD-1 catalysts, while it decreased for the Pt/W-TUD-1 catalysts. This suggests that initially the Pt is present on the small WO_3 particles in the Pt/W-TUD-1 catalysts, but this activity is lost during reaction due to agglomeration of the small WO_3 particles.

REFERENCES

[1] T.J. Benson, P.R. Daggolu, R.A. Hernandez, S. Liu and M.G. White, Adv. Catal., 2013, 56, 187-353.

[2] J.C. Serrano-Ruiz, R.M. West and J.A. Dumesic, Chem. Biomol. Eng., 2010, 1, 79-100.

[3] J. ten Dam and U. Hanefeld, ChemSusChem, 2011, 4, 1017-1034.

[4] J.S. Kruger, V. Nikolakis and D.G. Vlachos, Curr. Opin. Chem. Eng., 2012, 1, 312-320.

[5] I. Fechete, Y. Wang and J.C. Védrine, Catal. Today, 2012, 189, 2-27.

[6] J. ten Dam, F. Kapteijn, K. Djanashvili and U. Hanefeld, Catal. Commun., 2011, 13, 1-5.

[7] J. ten Dam, K. Djanashvili, F. Kapteijn and U. Hanefeld, ChemCatChem, 2012, 5, 497-505.

[8] M. Shiramizu and F.D. Toste, Angew. Chem. Int. Ed., 2012, 51, 8082-8086.

[9] E.J. Lenardao, G.V. Botteselle, F. de Azambuja, G. Perin and R.G. Jacob, Tetrahedron, 2007, 63, 6671-6712.

[10] C. Barrales Cortés, V. Tamayo Galván, S. Santiago Pedro and T. Viveros García, Catal. Today, 2011, 172, 21-26.

[11] Y. Nie, W. Niah, S. Jaenicke and G-K. Chuah, J. Catal., 2007, 248, 1-10.

[12] K.A. da Silvia Rocha, P.A. Robles-Dutenhefner, E.M.B. Sousa, E.F. Kozhevnikova, I.V. Kozhevnikov and I.V. Gusevskaya, Appl. Catal. A: Gen., 2007, 317, 171-174.

[13] J. Plößer, M. Lucas and P. Claus, J. Catal., 2014, 320, 189-197.

[14] A. Negoi, S. Wuttke, E. Kemnitz, D. Macovei, V.I. Parvulescu, C.M. Teodorescu and S.M. Coman, Angew. Chem. Int. Ed., 2010, 49, 8134-8138.

[15] F.G. Cirujano, F.X. Llabrés I Xamena and A. Corma, Dalton Trans., 2012, 41, 4249-4254.

[16] G-K. Chuah, S.H. Liu, S. Jaenicke and L.J. Harrison, J. Catal., 2001, 200, 352-359.

[17] Z. Yongzhong, N. Yuntong, S. Jaenicke and G-K. Chuah, J. Catal., 2005, 229, 404-413.

[18] M. Vandichel, F. Vermoortele, S. Cottenie, D.E. De Vos, M. Waroquier and V. Van Speybroeck, J. Catal., 2013, 305, 118-129.

[19] P. Mäki-Arvela, N. Kumar, V. Nieminen, R. Sjöholm, T. Salmi and D.Y. Murzin, J. Catal., 2004, 225, 155-169.

[20] M. Fuentes, J. Magraner, C. de las Pozas and R. Roque-Malherbe, Appl. Catal., 1989, 47, 367-374.

[21] S. Telalović, A. Ramanathan, J.F. Ng, R. Maheswari, C. Kwakernaak, F. Soulimani, H.C. Brouwer, G.K. Chuah, B.M. Weckhuysen and U. Hanefeld, Chem. Eur. J., 2011, 17, 2077-2088.

[22] A. Ranoux, K. Djanashvili, I.W.C.E. Arends and U. Hanefeld, RSC Adv., 2013, 3, 21524-21534.

[23] R. Nieguth, J. ten Dam, A. Petrenz, A. Ramanathan, U. Hanefeld and M.B. Ansorge-Schumacher, RSC Adv., 2014, 4, 45495-45503.

[24] Y. Chen, Z. Guo, T. Chen and Y. Yang, J. Catal., 2010, 275, 11-24.

[25] M. Ferrari, B. Delmon and P. Grange, Carbon, 2002, 40, 471-640.

[26] D. Liu, X-Y. Quek, S. Hu, L. Li, H.M. Lim and Y. Yang, Catal. Today, 2009, 147S, S51-S57.

[27] L. Tang, G. Luo, M. Zhy, L. Kang and B. Dai, J. Indus. Eng. Chem., 2013, 19, 620-626.

[28] S.K. Wilkinson, I. McManus, H. Daly, J.M. Thompson, C. Hardacre, N. Sedaie Bonab, J. ten Dam, M.J.H. Simmons, C. D'Agostino, J. McGregor, L.F. Gladden and E.H. Stitt, J. Catal., 2015, 330, 362-373.

[29] I. McManus, H. Daly, J.M. Thompson, E. Connor, C. Hardacre, S.K. Wilkinson, N. Sedaie Bonab, J. ten Dam, M.J.H. Simmons, E.H. Stitt, C. D'Agostino, J. McGregor, L.F. Gladden and J.J. Delgado, J. Catal., 2015, 330, 344-353.

[30] A. Ramanathan, M.C.C. Villalobos, C. Kwakernaak, S. Telalović and U. Hanefeld, Chem. Eur. J., 2008, 14, 961-972.

[31] J. ten Dam, D. Badloe, A. Ramanatan, K. Djanashvili, F. Kapteijn and U. Hanefeld, Appl. Catal. A: Gen., 2013, 468, 150-159.

[32] T. Heikkilä, J. Salonen, J. Tuura, M.S. Hamdy, G. Mul, N. Kumar, T. Salmi, D.Y. Murzin, L. Laitinen, A.M. Kaukonen, J. Hirvonen and V.P. Lehto, Int. J. Pharm. 331 (2007) 133-138.

[33] M. F. de Lange, T. J. H Vlugt, J. Gascon and F. Kapteijn, Microporous Mesoporous Mater., 2014, 200, 199-215.

[34] K.S.W. Sing, D.H. Everett, R.A.W. Haul, L. Moscou, R.A. Pierotti, J. Rouquérol and T. Siemieniewska, Pure Appl. Chem., 1985, 57, 603-619.

[35] J.C. Groen and J. Perez-Ramirez, Appl. Catal. A: Gen., 2005, 268, 121-125.

[36] NIST Standard Reference Database 20, http://srdata.nist.gov/xps

[37] J. A. Moulijn, A. E. van Diepen and F. Kapteijn, Appl.Catal.A: Gen., 2001, 212, 3-16.

[38] S. García-Fernández, I. Gandarias, J. Requies, M.B. Güemez, S. Bennici, A. Auroux and P.L. Arias, J. Catal., 2015, 323, 65-75.

[39] F.P.J.M. Kerkhof, J.A. Moulijn, J. Phys. Chem., 1979, 83, 1612-1619.

[40] D. Hua, S.-L. Chen, G. Yuan, Y. Wang, Q. Zhao, X. Wang and B. Fu, Microporous Mesoporous Mater., 2011, 143, 320-325.

[41] E.V. Ramos-Fernandez, C.J.M. Pieters, B.J. van der Linden, J. Juan Alcaniz, P. Serra Crespo, M.W.G.M. Verhoeven, J.W. Niemantsverdriet, J. Gascon and F. Kapteijn, J. Catal., 2012, 289, 42-52.

APPENDIX 5

Semi-batch reactor (constant hydrogen pressure) design equation:

A.1 $$\frac{dc_i}{dt} = -\left(\frac{W_{cat}}{V}\right) k \cdot c_i$$

A.2 $$\frac{dc_i}{c_i} = -\hat{c}_{cat} \cdot k \cdot dt$$

Separation of variables and integration:

A.3 $$ln\left(\frac{c_i}{c_{i0}}\right) = \ln(1 - x_i) = -\hat{c}_{cat} \cdot k \cdot t$$

A.4 $$\hat{c}_{cat} = \left(\frac{W_{cat}}{V}\right) \left[\mathrm{mg_{cat}mL^{-1}}\right]$$

So for the first order rate constant, the initial rate and *TOF* we have, including dimensions:

A.5 $$k = -\frac{\ln(1-x_i)}{\hat{c}_{cat} \cdot t} \left[\mathrm{mL \cdot mg_{cat}^{-1} \cdot s^{-1}}\right]$$

A.6 $$r_0 = k \cdot c_{i0} \left[\mathrm{mmol \cdot mg_{cat}^{-1} \cdot s^{-1}}\right] \text{ with } c_{i0} \text{ in } \mathrm{mmol \cdot mL^{-1}}$$

A.7 $$TOF = \frac{r_0}{\hat{c}_{Pt}} \left[\mathrm{mmol \cdot mmol_{Pt}^{-1} \cdot s^{-1}}\right] \text{ with } \hat{c}_{Pt} \text{ in } \mathrm{mmol_{Pt} \cdot mg_{cat}^{-1}}$$

Where:

c_i	concentration of component i	$[\mathrm{mmol \cdot mL^{-1}}]$
c_{i0}	concentration of component i at t = 0	$[\mathrm{mmol \cdot mL^{-1}}]$
W_{cat}	catalyst mass	$[\mathrm{mg}]$
V	reaction volume	$[\mathrm{mL}]$
$\hat{c}_{cat}$	catalyst on basis of concentration	$[\mathrm{mg_{cat}mL^{-1}}]$
k	rate constant	$[\mathrm{mL \cdot mg_{cat}^{-1} \cdot s^{-1}}]$
t	time	$[\mathrm{s}]$
x_i	conversion of component i	$[\mathrm{n.a.}]$
r_0	initial rate	$[\mathrm{mmol \cdot mg_{cat}^{-1} \cdot s^{-1}}]$
TOF	turnover frequency	$\left[\mathrm{mmol \cdot mmol_{Pt}^{-1} \cdot s^{-1}}\right]$
$\hat{c}_{Pt}$	catalyst on basis of platinum concentration	$[\mathrm{mmol_{Pt} \cdot mg_{cat}^{-1}}]$

APPENDIX 6

Mass transfer considerations utilising Carberry numbers and WW-criteria

Carberry number

The Carberry number is used to estimate extraparticle mass transfer, which can be neglected when Ca < 0.05.

$$Ca = \frac{r_{v,obs}}{a^{'}\ k_f c_b} < \frac{0.05}{|n|}$$

Where:

Ca Carberry number $[-]$

$r_{v,obs}$ observed reaction rate per unit particle volume $[mol \cdot s^{-1} \cdot m_p^{-3}]$

a' specific external surface of the catalyst particle ($a' = 6/d_p$) $[m^2 \cdot m^{-3}]$

k_f mass transfer coefficient ($k_f = Sh \cdot D/d_p$) $[m \cdot s^{-1}]$

c_b concentration in the bulk $[mol \cdot m^{-3}]$

n reaction order $[-]$ – in these examples $n = 1$

d_p particle diameter $[m]$ – in these examples $d_p = 200\mu m$

Sh Sherwood correlation $[m]$ – in these examples $Sh = 2$, which is valid for a sphere in a stagnant fluid

D diffusion coefficient of the reactant in the liquid phase ($D = D_{eff}/{\sim}0.1$) $[m^2 \cdot s^{-1}]$ – D was taken from the thesis of Martijn Zieverink: $D = 1.8 \cdot 10^{-9}$ for the substrates and $D = 1.8 \cdot 10^{-8}$ for hydrogen

Weisz criterion

The Weisz modulus is used to estimate the influence of pore diffusion on reaction rates in heterogeneously catalysed reactions. pore diffusion limitations are insignificant if the modulus satisfies the criterion.

$$M_W = \eta\varphi^2 = \left(\frac{r_{v,obs}L^2}{D_{eff}c_s}\right)\left(\frac{n+1}{2}\right) < 0.15$$

Where:

M_W Weisz Modulus

φ Thiele modulus: $\varphi = L\sqrt{k_v/D_{eff}}$

k_v rate constant per unit volume $[s^{-1}]$

η effectiveness factor

D_{eff} effective diffusivity in particle $[m^2 \cdot s^{-1}]$ – D_{eff} was taken from the thesis of Martijn Zieverink: $D_{eff} = 1.8 \cdot 10^{-10}$ for the substrates and $D = 1.8 \cdot 10^{-9}$ for hydrogen

$r_{v,obs}$ observed reaction rate per unit particle volume $[mol \cdot s^{-1} \cdot m_p^{-3}]$

L characteristic catalyst dimension $L = d_p/6\ [m]$

c_s concentration at the external particle surface $[mol \cdot m^{-3}]$

n reaction order $[-]$ – in these examples $n = 1$

d_p particle diameter $[m]$ – in these examples $d_p = 200\mu m$

Table A1. Carberry numbers and WW-criteria for catalytic data Table 2 – isopulegol hydrogenation

	concentration bulk		rate constant	initial rate	observed reaction rate	Carberry number		WW-criterion	
	$Cb_{isopulegol}$	Cb_{H2}	k	r_0	$r_{v,obs}$	$Ca_{isopulegol}$	Ca_{H2}	$\Phi_{isopulegol}$	Φ_{H2}
	(mol·m^{-3})	(mol·m^{-3})	(mL·mg$_{cat}^{-1}$·s^{-1})	(mmol·mg$_{cat}^{-1}$·s^{-1})	(mol·s^{-1}·m$_p^{-3}$)	-	-	-	-
Pt/W-TUD-1$_{28}$	509.1	92.9	4.1E-06	2.1E-06	2.07	7.5E-03	4.0E-03	2.5E-02	1.4E-02
Pt/W-TUD-1$_{16}$	518.2	92.9	9.3E-08	4.8E-08	0.05	1.7E-04	9.6E-05	5.7E-04	3.2E-04
Pt/W-TUD-1$_{11}$	532.1	92.9	5.3E-07	2.8E-07	0.28	9.9E-04	5.7E-04	3.3E-03	1.9E-03
Pt/W-TUD-1$_9$	507.8	92.9	2.3E-06	1.2E-06	1.18	4.3E-03	2.3E-03	1.4E-02	7.8E-03
Pt/W-TUD-1$_7$	497.4	92.9	8.6E-07	4.3E-07	0.43	1.6E-03	8.6E-04	5.3E-03	2.9E-03
Pt/WO3/TUD-1$_5$	508.4	92.9	2.4E-07	1.2E-07	0.12	4.4E-04	2.4E-04	1.5E-03	8.0E-04
Pt/WO3/TUD-1$_{10}$	508.6	92.9	2.0E-07	1.0E-07	0.10	3.8E-04	2.1E-04	1.3E-03	6.8E-04
Pt/WO3/TUD-1$_{20}$	490.6	92.9	3.6E-07	1.8E-07	0.18	6.7E-04	3.5E-04	2.2E-03	1.2E-03

Table A2. Carberry numbers and WW-criteria for catalytic data figure 8 – isopulegol hydrogenation

	concentration bulk		rate constant	initial rate	observed reaction rate	Carberry number		WW-criterion	
	$Cb_{isopulegol}$	Cb_{H2}	k	r_0	$r_{v,obs}$	$Ca_{isopulegol}$	Ca_{H2}	$\Phi_{isopulegol}$	Φ_{H2}
	(mol·m^{-3})	(mol·m^{-3})	(mL·mg$_{cat}^{-1}$·s^{-1})	(mmol·mg$_{cat}^{-1}$·s^{-1})	(mol·s^{-1}·m$_p^{-3}$)	-	-	-	-
Pt/W-TUD-1$_{11}$	466.6	92.9	4.3E-06	2.0E-06	1.99	7.9E-03	4.0E-03	2.6E-02	1.3E-02

Table A3. Carberry numbers and WW-criteria for catalytic data table 4 – Prins cyclisation

	concentration bulk	rate constant	initial rate	observed reaction rate	Carberry number	WW-criterion
	$Cb_{citronellal}$	k	r	$r_{v,obs}$	$Ca_{citronellal}$	$\Phi_{citronellal}$
	mol·m^{-3}	(mL·mg$_{cat}^{-1}$·s^{-1})	(mmol·mg$_{cat}^{-1}$·s^{-1})	(mol·s^{-1}·m$_p^{-3}$)	-	-
Pt/W-TUD-1$_{28}$	468.7	8.4E-06	4.0E-06	3.95	1.6E-02	5.2E-02
Pt/W-TUD-1$_{16}$	515.1	1.0E-05	5.2E-06	5.18	1.9E-02	6.2E-02
Pt/W-TUD-1$_{11}$	525.0	2.3E-05	1.2E-05	11.98	**4.2E-02**	**1.4E-01**
Pt/W-TUD-1$_9$	493.0	1.2E-05	5.9E-06	5.92	2.2E-02	7.4E-02
Pt/W-TUD-1$_7$	516.2	1.2E-05	6.0E-06	5.95	2.1E-02	7.1E-02
Pt/WO3/TUD-1$_5$	497.2	1.6E-06	7.9E-07	0.79	2.9E-03	9.8E-03
Pt/WO3/TUD-1$_{10}$	527.1	1.3E-06	6.6E-07	0.66	2.3E-03	7.8E-03
Pt/WO3/TUD-1$_{20}$	511.5	1.2E-06	6.1E-07	0.61	2.2E-03	7.3E-03

Table A4. Carberry numbers and WW-criteria for catalytic data table 4 - hydrogenation

	concentration bulk	rate constant	initial rate	observed	Carberry number	WW-criterion

	$Cb_{isopulegol}$ (mol·m^{-3})	Cb_{H2} (mol·m^{-3})	k (mL·mg$_{cat}^{-1}$·s^{-1})	r (mmol·mg$_{cat}^{-1}$·s^{-1})	reaction rate $r_{y,obs}$ (mol·s^{-1}·m$_p^{-3}$)	$Ca_{isopulegol}$ -	Ca_{H2} -	$\Phi_{isopulegol}$ -	Φ_{H2} -
Pt/W-TUD-1$_{28}$	399.3	92.9	5.3E-06	2.1E-06	2.10	9.7E-03	4.2E-03	3.2E-02	1.4E-02
Pt/W-TUD-1$_{16}$	466.8	92.9	2.2E-06	1.0E-06	1.04	4.1E-03	2.1E-03	1.4E-02	6.9E-03
Pt/W-TUD-1$_{11}$	522.5	92.9	4.6E-06	2.4E-06	2.41	8.5E-03	4.8E-03	2.8E-02	1.6E-02
Pt/W-TUD-1$_{9}$	461.4	92.9	4.9E-06	2.2E-06	2.25	9.0E-03	4.5E-03	3.0E-02	1.5E-02
Pt/W-TUD-1$_{7}$	482.4	92.9	5.0E-06	2.4E-06	2.41	9.3E-03	4.8E-03	3.1E-02	1.6E-02
Pt/WO3/TUD-1$_{5}$	152.3	92.9	5.9E-07	2.1E-07	0.21	2.5E-03	4.1E-04	8.3E-03	1.4E-03
Pt/WO3/TUD-1$_{10}$	129.1	92.9	7.7E-07	2.9E-07	0.29	4.1E-03	5.8E-04	1.4E-02	1.9E-03
Pt/WO3/TUD-1$_{20}$	122.6	92.9	1.0E-06	4.0E-07	0.40	6.0E-03	7.9E-04	2.0E-02	2.6E-03

Table A5. Carberry numbers and WW-criteria for catalytic data table 5 – Prins cyclisation

	concentration bulk $Cb_{citronellal}$ mol·m^{-3}	rate constant k (mL·mg$_{cat}^{-1}$·s^{-1})	initial rate r (mmol·mg$_{cat}^{-1}$·s^{-1})	observed reaction rate $r_{y,obs}$ (mol·s^{-1}·m$_p^{-3}$)	Carberry number $Ca_{citronellal}$ -	WW-criterion $\Phi_{citronellal}$ -
Pt/W-TUD-1$_{28}$	694.0	5.9E-07	4.1E-07	0.41	1.1E-03	3.6E-03
Pt/W-TUD-1$_{16}$	576.8	8.6E-07	5.0E-07	0.50	1.6E-03	5.3E-03
Pt/W-TUD-1$_{11}$	551.8	6.7E-07	3.7E-07	0.37	1.2E-03	4.2E-03
Pt/W-TUD-1$_{9}$	-	-	-	-	-	-
Pt/W-TUD-1$_{7}$	551.1	1.7E-07	9.4E-08	0.09	3.2E-04	1.1E-03
Pt/WO3/TUD-1$_{5}$	553.6	1.9E-07	1.0E-07	0.10	3.5E-04	1.2E-03
Pt/WO3/TUD-1$_{10}$	523.1	1.8E-07	9.4E-08	0.09	3.3E-04	1.1E-03
Pt/WO3/TUD-1$_{20}$	532.0	1.9E-07	1.0E-07	0.10	3.6E-04	1.2E-03

Table A6. Carberry numbers and WW-criteria for catalytic data table 5 - hydrogenation

	concentration bulk $Cb_{isopulegol}$ (mol·m-3)	Cb_{H2} (mol·m-3)	rate constant k (mL·mg$_{cat}^{-1}$·s^{-1})	initial rate r (mmol·mg$_{cat}^{-1}$·s^{-1})	observed reaction rate $r_{y,obs}$ (mol·s^{-1}·m$_p^{-3}$)	Carberry number $Ca_{isopulegol}$ -	Ca_{H2} -	WW-criterion $\Phi_{isopulegol}$ -	Φ_{H2} -
Pt/W-TUD-1$_{28}$	562.2	92.9	8.8E-07	5.0E-07	0.50	1.6E-03	9.9E-04	5.4E-03	3.3E-03
Pt/W-TUD-1$_{16}$	455.5	92.9	5.3E-07	2.4E-07	0.24	9.7E-04	4.8E-04	3.2E-03	1.6E-03
Pt/W-TUD-1$_{11}$	462.3	92.9	1.0E-06	4.8E-07	0.48	1.9E-03	9.6E-04	6.4E-03	3.2E-03
Pt/W-TUD-1$_{9}$									
Pt/W-TUD-1$_{7}$	485.4	92.9	4.5E-05	2.2E-05	21.93	**8.4E-02**	**4.4E-02**	**2.8E-01**	**1.5E-01**
Pt/WO3/TUD-1$_{5}$	532.9	92.9	1.3E-07	6.8E-08	0.07	2.4E-04	1.4E-04	7.9E-04	4.5E-04
Pt/WO3/TUD-1$_{10}$	497.8	92.9	5.1E-07	2.5E-07	0.25	9.4E-04	5.0E-04	3.1E-03	1.7E-03
Pt/WO3/TUD-1$_{20}$	528.3	92.9	7.2E-07	3.8E-07	0.38	1.3E-03	7.5E-04	4.4E-03	2.5E-03

Reference

Martijn Zieverink, 2006, "A catalysis engineering approach to selective hydrogenation", TU Delft, Delft, pp 1-166.

SUMMARY AND CONCLUSION

SUMMARY

The overall topic in this thesis is the formation of 1,3-propanediol from glycerol. The link to this topic might not be obvious in every chapter. In this summary the main conclusions of the individual chapters will be summarized and the link to 1,3-propanediol formation will be addressed.

The initial idea of the thesis was to use bor(on)ic acid as an additive in the hydrogenolysis of glycerol, with the aim to increase 1,3-propanediol selectivity. Bor(on)ic acids form bor(on)ate esters from diols and polyols. The thought was that this interaction could influence the selectivity of glycerol hydrogenolysis. This hypothesis was studied and tested in Chapter 1. The appendix of the first chapter studied the formation of the bor(on)ate esters of glycerol and its dehydrated and hydrogenated reaction products. The pK_a of a series of different bor(on)ic acids was established using NMR titrations. It was confirmed that the pK_a of these acids is decreased in the presence of electron withdrawing groups. This is in line with the fact that Lewis acidic boron gets more acidic in the absence of electrons. NMR titrations of bor(on)ic acid in the presence of diols and glycerol showed that bor(on)ate esters are formed at alkaline pH. Boronate ester association constants are linearly dependent on pK_a, i.e. higher pK_a results in more borate ester formation. Highest ester concentrations were observed for using boric acid. The ratio of 1,2-/1,3-glycerol ester is highest for boric acid. The association constant of bor(on)ate esters is not just dependent on the bor(on)ic acid, but the diol has an influence as well. The association constants for the bor(on)ate esters of glycerol and its hydrogenolysis products show the following trend: glycerol > 1,2-propanediol > ethylene glycol ~ 1,3-propanediol. The high association constant of glycerol compared to the other diols could be due to chance. There are simply more possibilities to form a glycerol (a polyol) ester than there are possibilities to form a diol ester. However, it was found that the association constant of 1,2-diol esters increases with an increasing tail: ethylene glycol > 1,2-propanediol > 1,2-butanediol > 3-fluoro-1,2-propanediol. This cannot be explained by chance. Additional temperature dependent NMR titrations showed that this trend can be explained by an entropy effect. This effect means that more borate ester is formed if the resulting ester has a free-moving tail. This free moving tail results in higher remaining entropy and has thus a positive effect on ΔG and hence the association constant. Based on the borate ester study it was decided to opt for boric acid as an additive in glycerol hydrogenolysis. This is based on the fact that boric acid forms highest amounts of borate esters, its water solubility and its stability under hydrogenolysis conditions.

Chapter 1 investigated the influence of boric acid on the hydrogenolysis of glycerol. Initially Design of Experiment was used as a technique to select variables that are significant in glycerol hydrogenolysis. This allowed selecting the most promising catalyst from 19 candidates in a minimum amount of experiments. A first D-optimal design tested 15 different catalysts and was employed to investigate the influence of the variables temperature (150-200°C), pH (10-12), sulfolane (0-5 v/v%), metal (Ni, Pd, Pt, Rh and Ru) and support (Al_2O_3, SiO_2 and C). This showed that only temperature, metal and support were significantly

influencing glycerol conversion. An increased temperature has a positive effect on glycerol conversion, while Pd and Pt lead to highest conversions, although Pd resulted in more glycerol degradation. Al_2O_3 and C are the preferred supports for high glycerol conversions. A second D-optimal design evaluated the remaining four catalysts ($Pd/BaSO_4$, $Pd/CaCO_3$, $Pt/CaCO_3$ and Ir/C) and the same variables as in the first design. This again showed that increased temperature leads to higher glycerol conversion. Sulfolane turned out to have a detrimental effect on conversion, while $Pd/BaSO_4$ and $Pt/CaCO_3$ emerged as the most promising catalysts.

The six catalysts that resulted in the highest conversions of glycerol were chosen from the set of reactions from the two D-optimal designs. These reactions were repeated in the absence of boric acid, to study the effect of this additive on glycerol conversion and selectivity. It showed that boric acid can have an effect on both. In the case of $Pt/CaCO_3$, which already emerged as an active catalyst, the selectivity was completely inverted from 1,2-propanediol to lactic acid selectivity upon the addition of boric acid.

The hydrogenolysis of glycerol using $Pt/CaCO_3$ as a catalyst was studied in more detail by constructing a response surface model through a Central Composite Design. This evaluated the influence of boric acid concentration (0-125 mM), temperature (130-220°C) and pH (8-13) on catalyst activity and selectivity. This showed that glycerol conversion is mainly influenced by temperature with a small contribution of pH. No 1,3-propanediol was observed during these experiments and lactic acid was the main product besides 1,2-propanediol. The selectivity towards 1,2-propanediol is highest at low boric acid concentrations, low pH and low temperature. However, this coincides with low glycerol conversions as well. The lactic acid selectivity is highest at high pH and boric acid concentration and remains high at higher temperatures, which means that lactic acid can be produced at high glycerol conversions.

Boric acid concentration does not have an effect on glycerol hydrogenolysis activity, but it does affect the selectivity. It mainly influences the formation of lactic acid, the formation of which under hydrogenolysis conditions initially seems surprising as it requires the oxidation of one of the carbon centres. However, it can be explained by the base catalysed Cannizarro reaction, which involves a nucleophilic attack of an intermediate aldehyde by a hydroxide group, followed by a hydride shift to the alpha carbon. This means that lactic acid can only be formed under alkaline conditions and hence the selectivity towards lactic acid is highest at high pH.

As shown in the introduction acidic conditions are necessary to form 1,3-propanediol from glycerol. At these conditions boric acid is not useful, as it does not form borate esters at acidic pH. Therefore, another additive was chosen in Chapter 2. Literature suggested that tungsten-containing compounds improved the 1,3-propanediol selectivity, so a series of these co-catalysts (tungstic acid, phosphotungstic acid and silicotungstic acid) were tested together with some hydrogenation catalysts (Pt/SiO_2, Pd/SiO_2, Pt/Al_2O_3 and Pd/Al_2O_3) in glycerol hydrogenolysis.

Initial tests indeed showed the superior 1,3-propanediol selectivity of the tungsten containing acids compared to hydrochloric acid and in the absence of acid. Interestingly, Pt proved to be more selective towards 1,3-propanediol than Pd-based hydrogenation catalysts. This was attributed to the higher hydrogenation activity of Pt, that results in the faster hydrogenation of intermediate 3-hydroxypropanal, preventing the subsequent elimination of the hydroxyl group. The alumina support was beneficial for activity, while catalyst support proved to have little effect on selectivity. Based on these initial findings, Pt/Al_2O_3 and silicotungstic acid were chosen as a catalytic system and were further optimised for 1,3-propanediol formation.

The application of a Central Composite Design allowed constructing a surface model that evaluated the effect of hydrogen pressure, silicotungstic acid concentration, reaction time, temperature, and glycerol concentration. Reaction temperature and reaction time proved to have most effect on glycerol conversion. Highest conversions were obtained at high temperature (200°C) and long reaction time (18 h). Interestingly, glycerol conversion was not influenced by initial glycerol concentration. This shows that the catalytic system was most active at high glycerol concentrations (1000 mM). 1,3-Propanediol selectivity was mostly influenced by reaction temperature and silicotungstic acid concentration, but unfortunately in a negative sense, meaning that the highest selectivities were obtained at low temperature (170 °C) and low acid concentration (3.5 mM). This makes sense, as too much acid can result in too much dehydration. On the other hand, a minimal amount of acid is necessary to obtain 1,3-propanediol selectivity. Experimentally this turned out to be at 2.1 mM silicotungstic acid, resulting in 49% glycerol conversion at 28% 1,3-propanediol selectivity. Unfortunately, the opposite effect of temperature on activity and selectivity means that the conversion cannot be increased too much, without negatively affecting 1,3-propanediol selectivity.

A study of the degradation of glycerol and its primary hydrogenolysis products showed that the 1,3-propanediol selectivity could partly be explained by its relative stability at reaction conditions. It was shown to be more stable than glycerol, *n*-propanol and 1,2-propanediol. This relative stability is very relevant, as this could point towards the development of more selective catalyst systems. For instance, if a catalyst was better able to hydrogenate the intermediate 3-hydroxylpropanal, more relatively stable 1,3-propanediol could be formed. Moreover, the dehydration of 3-hydroxylpropanal to acrolein, forming *n*-propanol would be suppressed at the same time. This can be achieved when the dehydration (tungsten additive) and hydrogenation functionalities (Pt metal) are in close proximity. To achieve this using homogeneous silicotungstic acid is not straightforward. An easier method would be the development of a heterogeneous acidic tungsten catalyst, to which a hydrogenation function such as Pt was added. This was the focus in the last two chapters of this thesis.

The process of producing a Pt loaded heterogeneous tungsten containing acid started with the synthesis of tungsten containing TUD-1 in Chapter 3. TUD-1 is an amorphous mesoporous silica, that lends itself for the incorporation of a variety of metals. It was chosen for its mesoporosity, as this enhances mass

transport, which is critical in the liquid phase conversion of relatively large biomass derived molecules, while tungsten will provide the acidity. Tungsten containing TUD-1 materials were synthesised using two different methods. The first method was a straightforward impregnation of tungstic acid, yielding WO_3/TUD-1. The second method introduced the tungsten during the sol-gel synthesis of W-TUD-1, using tungsten(VI) ethoxide as the tungsten source.

Detailed characterisation of the materials (INAA, N_2 physisorption, powder XRD, Raman spectroscopy, TEM, Diffuse Reflectance UV-Vis, FT-IR, H_2-TPR and NH_3-TPD) has shown that straightforward impregnation resulted in relatively large WO_3 particles, while the sol-gel synthesis of W-TUD-1 (Si/W >20) yielded very small finely dispersed WO_3 particles, resulting in superior acidity of the latter material. This was confirmed by the catalytic testing, where the Prins cyclisation of citronellal to isopulegol was used as a model reaction.

The final step in producing a hydrodeoxygenation catalyst suitable for converting biomass-derived components was the introduction of the hydrogenation metal. This was the focus of Chapter 4, where the WO_3/TUD-1 and W-TUD-1 catalysts were loaded with 1 wt% platinum. The addition of platinum did not affect the activity of the acid catalysts. The Pt/W-TUD-1 was still most active in the Prins cyclisation of citronellal. With a hydrogenation metal present, the hydrogenation activity could be investigated by converting the isopulegol into menthol. This showed that the hydrogenation activity of the Pt/W-TUD-1 was superior to the Pt/WO_3/TUD-1 catalyst.

Catalytic tests in which citronellal was converted into menthol showed that the produced systems were indeed bifunctional catalysts, having both active acidic and hydrogenation functionalities. Unfortunately, the catalysts were only able to convert a minimal amount of glycerol and no 1,3-propanediol was observed. This suggests that the WO_3 particles present on the Pt/W-TUD-1 catalyst are not acidic enough for glycerol deoxygenation.

CONCLUSION

Glycerol can be converted selectively into lactic acid and 1,2-propanediol under alkaline conditions using boric acid as an additive. 1,3-Propanediol was formed at good conversion (49%) and selectivity (28%) using silicotungstic acid as a co-catalyst with 5 wt% Pt/Al_2O_3. Unfortunately, the heterogeneous Pt/W-TUD-1 catalyst that was synthesised with the aim of converting glycerol into 1,3-propanediol was not active in that system.

The production of 1,3-propanediol will need an acidic catalyst. Unfortunately, glycerol, as a by-product from biodiesel production, is available as an aqueous alkaline feed. This means that feed and catalytic system are incompatible. Distilling the feed, an ion-exchange or another sort of purification is not cost-effective. Therefore it will be better to convert this alkaline waste stream into another valuable chemical,

or to use a different technology (biocatalysis or direct hydrogenolysis). Although most glycerol research is focusing on the production of propanediols, lactic acid (Chapter 1) could be an interesting alternative, as this chemical depends on the hydroxide catalysed Cannizzaro reaction, which would be provided by the alkaline feed, turning a fundamental issue into an advantage.

SAMENVATTING EN CONCLUSIE

SAMENVATTING

Het onderwerp van dit proefschrift is de vorming van 1,3-propaandiol uit glycerol. De link naar dit onderwerp zal niet altijd even duidelijk zijn in ieder hoofdstuk. In deze samenvatting zullen de belangrijkste conclusies uit de verschillende hoofdstukken worden samengevat en zal de link naar 1,3-propaandiol worden verduidelijkt.

Het oorspronkelijke idee van het proefschrift was om boorzuur en zijn derivaten als additief te gebruiken voor de hydrogenolyse van glycerol, met als doel om de 1,3-propaandiol selectiviteit te vergroten. Mengsels van boorzuur en di- en polyolen vormen boraat esters. In het geval van glycerol (een polyol) kan zowel 1,2-glycerol boraat ester, als 1,3-glycerol boraat ester gevormd worden. Het beïnvloeden van deze interactie werd geacht de selectiviteit van de glycerol hydrogenolyse te beïnvloeden. Deze hypothese is in Hoofdstuk 1 onderzocht. De appendix van het eerste hoofdstuk bestudeert de vorming van boraat esters van glycerol en zijn gedehydrateerde en gehydrogeneerde reactieproducten. De pK_a's van een serie verschillende boorzuur derivaten is bepaald met behulp van NMR (Nucleaire Magnetische Resonantie) titraties. Het is bevestigd dat de pK_a van deze zuren afneemt wanneer er elektronen-zuigende groepen aanwezig zijn. Dit is in overeenstemming met het feit dat het Lewis zure boor zuurder wordt in de afwezigheid van elektronen. NMR-titraties van boorzuur (derivaten) en de aanwezigheid van diolen en glycerol lieten zien dat boorzuur esters worden gevormd in een basische oplossing. De associatie constanten van boraat esters zijn lineair afhankelijk van de pK_a van het boorzuur – een hogere pK_a zal resulteren in een verhoogde boraat ester concentratie. De hoogste boraat ester concentraties zijn waargenomen voor boorzuur, bovendien heeft boorzuur eveneens de hoogste 1,2-/1,3-glycerol ester ratio. De associatie constante van boraat esters van glycerol is niet alleen afhankelijk van het boorzuur, maar eveneens van het gebruikte diol. De associatie constanten van de (derivaten van) boraat esters van glycerol en zijn hydrogenolyse producten laten de volgende trend zien: glycerol > 1,2-propaandiol > ethyleen glycol > ~ 1,3-propaandiol. De hoge associatie constanten van glycerol vergeleken met de andere diolen kan gedeeltelijk worden toegeschreven aan een kansverdeling. Er zijn simpelweg meerdere mogelijkheden om een glycerol ester te vormen, terwijl een diol maar een enkele ester kan vormen. Maar dit is niet het volledige verhaal. Het is aangetoond dat de associatie constante van een 1,2-diol ester toeneemt wanneer dit diol een langere staart heeft: ethyleen glycol > 1,2-propaandiol > 1,2-butaandiol > 3-fluoro-1,2-propanediol. Dit kan niet worden toegeschreven aan een kansverdeling. Aanvullende temperatuur-afhankelijke NMR-titraties stelden vast dat deze trend kan worden toegeschreven aan een entropisch effect. Dit effect houdt in dat meer boraat ester wordt gevormd wanneer de resulterende ester een vrij-bewegende staart heeft. Deze vrij-bewegende staart resulteert in een hogere entropie en heeft hierdoor een positief effect op ΔG (Gibbs vrije energie) en hierdoor ook op de associatie constante. Met bovenstaande boraat ester studie in het achterhoofd werd besloten om boorzuur te gebruiken als een additief voor

glycerol hydrogenolyse. Dit is gebaseerd op het feit dat boorzuur de hoogste concentraties boraat esters vormt, het wateroplosbaar is en dat het stabiel is onder hydrogenolyse condities.

De invloed van boorzuur op de hydrogenolyse van glycerol werd onderzocht in Hoofdstuk 1. In eerste instantie werd een Ontwerp van Experimenten methode gebruikt om een serie significante variabelen in de hydrogenolyse van glycerol te selecteren. Deze aanpak stond toe dat de katalysatoren met de hoogste potentie konden worden geselecteerd uit 19 kandidaten door middel van een minimaal aantal experimenten. Een eerste D-optimal ontwerp omvatte 15 verschillende katalysatoren en werd eveneens gebruikt om de invloed van de variabelen temperatuur (150-200 °C), pH (10-12), sulfolaan (0-5 v/v.%), metaal (Ni, Pd, Pt, Rh en Ru) en drager (Al_2O_3, SiO_2 and C) te testen. Dit liet zien dat alleen temperatuur, metaal en drager een significante invloed hebben op glycerol conversie. Een hogere temperatuur had een positief effect op glycerol conversie. Hoewel Pd en Pt leidden tot de hoogste conversies, resulteerde Pd vooral in de afbraak van glycerol. Al_2O_3 en C zijn de beste dragers wat betreft glycerol conversie. Een tweede D-optimal ontwerp evalueerde de overgebleven vier katalysatoren ($Pd/BaSO_4$, $Pd/CaCO_3$, $Pt/CaCO_3$ en Ir/C) en dezelfde variabelen als in het eerste D-optimal ontwerp. Dit toonde wederom aan dat een verhoogde temperatuur leidt tot verhoogde glycerol conversie. Het bleek dat sulfolaan een negatief effect had op glycerol conversie. $Pd/BaSO_4$ en $Pt/CaCO_3$ kwamen naar voren als de meest veelbelovende katalysatoren.

De zes katalysatoren die resulteerden in de hoogste conversie van glycerol werden geselecteerd uit de reactie set van de twee D-optimal ontwerpen. Deze reacties werden herhaald in de afwezigheid van boorzuur, om het effect van dit additief op de conversie en selectiviteit van de omzetting van glycerol te bestuderen. Het bleek dat boorzuur een effect kan hebben op beide. In het geval van $Pt/CaCO_3$, dat al een actieve katalysator bleek te zijn, werd de selectiviteit volledig omgedraaid. In de aanwezigheid van boorzuur werd vooral melkzuur gevormd, terwijl wanneer er geen boorzuur aanwezig is vooral 1,2-propaandiol gevormd wordt.

De $Pt/CaCO_3$ gekatalyseerde hydrogenolyse van glycerol is nauwkeuriger bestudeerd door het opstellen van een respons oppervlak model met behulp van een Central Composite Design. Dit onderzocht het effect van boorzuur concentratie (0-125 mM), temperatuur (130-220°C) en pH (8-13) op zowel katalysator activiteit als selectiviteit. Het bleek dat glycerol conversie vooral wordt beïnvloed door de reactietemperatuur en een kleine bijdrage van pH. Geen enkel spoor van 1,3-propaandiol werd aangetroffen in deze experimenten en de meest voorkomende producten waren melkzuur en 1,2-propaandiol. De 1,2-propaandiol selectiviteit is het grootst bij een lage boorzuur concentratie, lage pH en lage temperatuur. Deze reactiecondities komen overeen met een lage glycerol conversie. De melkzuur selectiviteit is het hoogst bij een hoge pH en hoge boorzuur concentratie en blijft hoog bij een hoge temperatuur, waardoor melkzuur geproduceerd kan worden bij hoge glycerol conversies.

De boorzuur concentratie heeft geen effect op de glycerol hydrogenolyse activiteit, maar het heeft wel degelijk invloed op de selectiviteit. Het heeft vooral invloed op de vorming van melkzuur. De productie van melkzuur onder hydrogenolyse reactie condities was verrassend, omdat een van de koolstofatomen van glycerol geoxideerd dient te worden. De vorming van melkzuur kan worden verklaard door de base gekatalyseerde Cannizarro reactie, wat inhoudt dat een hydride een nucleofiele aanval uitvoert op een halffabricaat (aldehyde), gevolgd door een hydride sprong naar het alfa koolstofatoom. Dit houdt in dat melkzuur alleen gevormd kan worden onder basische omstandigheden en hierdoor is de selectiviteit voor melkzuur het hoogst bij hoge pH.

De introductie heeft laten zien dat 1,3-propaandiol alleen gevormd kan worden uit glycerol onder zure reactie condities. Onder deze condities is boorzuur niet geschikt, omdat het geen boraat esters vormt onder zure omstandigheden. Daarom werd in Hoofdstuk 2 voor een ander additief gekozen. De wetenschappelijke literatuur suggereerde dat wolfraam-bevattende stoffen de 1,3-propaandiol selectiviteit kunnen bevorderen. Daarom werd een serie wolfraam-bevattende co-katalysatoren (wolfraamzuur, fosfowolfraamzuur, silicowolfraamzuur) getest in combinatie met een serie hydrogenerings katalysatoren (Pt/SiO_2, Pd/SiO_2, Pt/Al_2O_3 en Pd/Al_2O_3) voor glycerol hydrogenolyse.

De eerste tests toonden inderdaad aan dat de wolfraam-bevattende zuren een superieure 1,3-propaandiol selectiviteit vertoonden, in vergelijking met de blanco reacties met zoutzuur en de afwezigheid van zuur. Deze tests lieten tevens zien dat Pt een hogere 1,3-propaandiol selectiviteit vertoonde dan de Pd bevattende hydrogenerings katalysatoren. Dit werd toegeschreven aan de hogere hydrogenerings activiteit van Pt, wat resulteert in een snellere hydrogenering van het halffabricaat 3-hydroxypropanal, wat voorkomt dat de hydroxylgroep vervolgens wordt geëlimineerd. De alumina drager droeg bij aan een verhoogde activiteit, terwijl de drager weinig effect had op de selectiviteit. Aan de hand van deze inleidende resultaten werden Pt/Al_2O_3 en silicowolfraamzuur gekozen als katalytisch systeem en werden de reactie condities verder geoptimaliseerd voor 1,3-propaandiol formatie.

Het gebruik van een Central Composite Design leidde tot een respons oppervlak model dat de effecten van waterstof druk, silicowolfraamzuur concentratie, reactietijd, temperatuur, en glycerol concentratie op de Pt/Al_2O_3 en silicowolfraamzuur gekatalyseerde omzetting van glycerol naar 1,3-propaandiol beschreef. De reactie temperatuur en reactietijd hadden de grootste invloed op de glycerol conversie. De hoogste conversies werden bereikt bij een hoge temperatuur (200°C) en lange reactietijd (18 h). Verrassend genoeg had de initiële glycerol concentratie geen effect op de glycerol conversie. Dit toont aan dat het katalytisch systeem het meest actief is bij hoge glycerol concentraties (1000 mM). 1,3-propaandiol selectiviteit werd vooral bepaald door de reactie temperatuur en silicowolfraamzuur concentratie, maar helaas in negatieve zin. Dit houdt in dat de hoogste selectiviteiten werden behaald bij een lage temperatuur (170°) en een lage silicowolfraamzuur concentratie (35 mM). Dit is niet verrassend, omdat te veel zuur kan leiden tot de dehydratie. Aan de andere kant was een minimale hoeveelheid silicowolfraamzuur nodig om überhaupt 1,3-propaandiol te vormen. Experimenten toonden aan dat de optimale zuur concentratie 2.1 mM

silicowolfraamzuur is, wat leidde tot 49% glycerol conversie en 28% 1,3-propaandiol selectiviteit. Helaas betekent dit dat door het tegengestelde effect dat de reactie temperatuur heeft op conversie en selectiviteit de conversie niet verhoogd kan worden, zonder de 1,3-propaandiol selectiviteit negatief te beïnvloeden.

Een studie naar de degradatie van glycerol en zijn primaire hydrogenolyse producten toonde aan dat de 1,3-propaandiol selectiviteit gedeeltelijk kan worden verklaard aan de hand van zijn relatieve stabiliteit onder reactiecondities. 1,3-Propaandiol is stabieler dan glycerol, *n*-propanol en 1,2-propaandiol. Deze stabiliteit is relevant, omdat dit gegeven gebruikt kan worden om selectievere katalytische systemen te ontwikkelen. Bijvoorbeeld, wanneer een katalysator beter in staat is om het halffabricaat 3-hydroxylpropanal te hydrogeneren, dan wordt meer relatief stabiel 1,3-propaandiol gevormd. Bovendien voorkomt deze hydrogenering dat 3-hydroxylpropanal wordt omgezet naar acroleine, dat vervolgens kan worden gehydrogeneerd tot *n*-propanol – wat dus ook de vorming van *n*-propanol onderdrukt. Dit kan worden bereikt wanneer de dehydratatie- (wolfraam-additief) en hydrogeneringsfunctionaliteit (Pt metaal) dicht bij elkaar zitten. Dit is moeilijk te bewerkstelligen met het homogene silicowolfraamzuur. Het is gemakkelijker om een heterogene zure wolfraam katalysator te ontwikkelen, waaraan een hydrogeneringsfunctionaliteit zoals Pt wordt toegevoegd. De ontwikkeling van een dergelijke katalysator wordt beschreven in de laatste twee hoofdstukken van dit proefschrift.

De ontwikkeling van een Pt bevattende heterogene wolfraamzuur katalysator startte met de synthese van een wolfraamzuur bevattende TUD-1 drager in Hoofdstuk 3. TUD-1 is een amorf mesoporeuse silica drager, dat zich uitstekend leent voor de incorporatie van verschillende metalen. Het is gekozen om zijn mesoporeuse eigenschappen, omdat dit het massatransport in de katalysator bespoedigt, wat cruciaal is in de conversie van relatief grote biomassa-afgeleide moleculen in de vloeistoffase. Wolfraam zal zorgen voor de zure functionaliteit in dit materiaal. Wolfraam bevattende TUD-1 materialen werden gesynthetiseerd volgens twee verschillende methodes. De eerste methode was een directe impregnatie van wolfraamzuur, resulterend in WO_3/TUD-1. De tweede methode introduceerde het wolfraam in de vorm van wolfraam(VI) ethoxide tijdens de vloeistof-gel synthese van TUD-1, wat resulteerde in W-TUD-1.

Gedetailleerde karakterisatie van deze materialen (INAA, N_2 physisorptie, poeder Röntgendiffractie, Raman spectroscopie, Transmissie Elektronen Microscopie, Diffuse Reflectie UV-Vis, FT-IR, H_2 Temperatuur Geprogrammeerde Reductie en NH_3 Temperatuur Geprogrammeerde Desorptie) toonden aan dat de impregnatie resulteerde in relatief grote WO_3 deeltjes, terwijl de vloeistof-gel synthese van W-TUD-1 (Si/W>20) resulteerde in een goede spreiding van hele kleine WO_3 deeltjes, wat het laatstgenoemde materiaal goede zure eigenschappen gaf. Dit werd bevestigd door middel van katalytische tests, waar de Prins cyclisatie van citronellal tot isopulegol werd gebruikt als een model reactie.

De laatste stap in de ontwikkeling van een hydrodeoxygenatie katalysator die geschikt is voor de conversie van biomassa-afgeleide moleculen was de introductie van het hydrogeneringsmetaal. Dit was het onderwerp van Hoofdstuk 4, waar de WO_3/TUD-1 en W-TUD-1 katalysatoren werden geïmpregneerd

met 1 wt% platina. De toevoeging van platina had geen effect op de activiteit van de wolfraamzuur bevattende dragers. De Pt/W-TUD-1 was nog steeds de meest actieve katalysator voor de Prins cyclisatie van citronellal. De activiteit van het geïntroduceerde hydrogeneringsmetaal werd vastgesteld door middel van de conversie van isopulegol naar menthol. Dit toonde aan dat de hydrogeneringsactiviteit van de Pt/W-TUD-1 beter was dan de Pt/WO_3/TUD-1 katalysator.

Katalytische tests waarin citronellal werd omgezet in menthol toonden aan dat de geproduceerde katalysatoren inderdaad bifunctionele katalysatoren waren, met zowel actieve zure als hydrogeneringsactiviteit. Wanneer deze katalysatoren werden getest voor de conversie van glycerol bleek dat enkel een kleine hoeveelheid glycerol werd omgezet en er werd geen 1,3-propaandiol waargenomen. Dit suggereert dat de WO_3-deeltjes die aanwezig zijn op het oppervlak van de Pt/W-TUD-1 katalysator niet zuur genoeg zijn voor glycerol deoxygenatie.

CONCLUSIE

Door middel van boorzuur als additief kan glycerol onder basische omstandigheden selectief worden omgezet in melkzuur en 1,2-propaandiol. 1,3-Propaandiol werd gevormd met een goede conversie (49%) en selectiviteit (28%), met behulp van silicowolfraamzuur als co-katalysator en 5 wt% Pt/Al_2O_3. Helaas was de gesynthetiseerde heterogene Pt/W-TUD-1 katalysator – met als doel om glycerol om te zetten in 1,3-propaandiol – niet actief in dat systeem.

De productie van 1,3-propaandiol vereist een zure katalysator. Helaas is glycerol, als een bijproduct van de biodiesel productie, beschikbaar als een substraat in een waterige basische oplossing. Dit betekent dat een substraat en katalytisch systeem onverenigbaar zijn. Destillatie van glycerol, een ionenwisselaar of een andere vorm van zuivering is niet kosteneffectief. Daarom zou het beter zijn om deze alkalische afvalstroom om te zetten met behulp van een andere technologie (biokatalyse of directe hydrogenolyse), of om deze glycerol stroom om te zetten in een ander waardevol product. Hoewel het merendeel van het glycerol onderzoek zich richt op de productie van propaandiolen, zou melkzuur (Hoofdstuk 1) een interessant alternatief kunnen zijn. De vorming van dit product is namelijk afhankelijk van de hydroxide gekatalyseerde Cannizzaro reactie, dat reeds aanwezig is in de waterige basische oplossing, waardoor deze fundamentele complicatie wordt omgezet in een voordeel.

LIST OF PUBLICATIONS

[1] B.H.M. Kuijpers, S. Groothuys, C. Hawner, **J. ten Dam**, P.J.L.M. Quaedflieg, H.E. Schoemaker, F.L. van Delft and F.P.J.T Rutjes, Org. Process Res. Dev., 2008, 12, 503-511: Cu-Catalyzed Formation of Triazole-Linked Glycoamino Acids and Application in Chemoenzymatic Peptide Synthesis.

[2] **J. ten Dam**, F. Kapteijn, K. Djanashvili and U. Hanefeld, Catal. Commun., 2011, 13, 1-5: Tuning selectivity of $Pt/CaCO_3$ in glycerol hydrogenolysis – A Design of Experiments approach.

[3] **J. ten Dam** and U. Hanefeld, ChemSusChem, 2011, 4, 1017-1034: Renewable Chemicals: Dehydroxylation of Glycerol and Polyols.

[4] **J. ten Dam**, K. Djanashvili, F. Kapteijn and U. Hanefeld, ChemCatChem, 2013, 5, 497-505: Pt/Al_2O_3 Catalyzed 1,3-Propanediol Formation from Glycerol using Tungsten Additives.

[5] **J. ten Dam**, D. Badloe, A. Ramanathan, K. Djanashvili, F. Kapteijn and U. Hanefeld, Appl. Catal. A: Gen., 2013, 468, 150-159: Synthesis, characterisation and catalytic performance of a mesoporous tungsten silicate: W-TUD-1.

[6] A.G. Denkova, B.E. Terpstra, O.M. Steinbach, **J. ten Dam** and H.Th. Wolterbeek, Sep. Sci. Technol., 2013, 48, 1331-1338: Adsorption of Molybdenum on Mesoporous Aluminum Oxides for Potential Application in Nuclear Medicine.

[7] C. Mukarakate, M.J. Watson, **J. ten Dam**, X. Baucherel, S. Budhi, M.M. Yung, H. Ben, K. Iisa, R.M. Baldwin and M.R. Nimlos, Green Chem., 2014, 16, 4891-4905: Upgrading biomass pyrolysis vapors over β-zeolites: role of silica-to-alumina ratio.

[8] R. Nieguth, **J. ten Dam**, A. Petrenz, A. Ramanathan, U. Hanefeld and M.B. Ansorge-Schumacher, RSC Adv., 2014, 4, 45495-45503: Combined heterogeneous bio- and chemo-catalysis for dynamic kinetic resolution of (*rac*)-benzoin.

[9] C. Mukarakate, J.D. McBrayer, T.J. Evans, S. Budhi, D.J. Robichaud, K. Iisa, **J. ten Dam**, M.J. Watson, R.M. Watson, R.M. Baldwin and M.R. Nimlos, Green Chem., 2015, 17, 4217-4227: Catalytic fast pyrolysis of biomass: the reactions of water and aromatic intermediates produces phenols.

[10] McManus, H. Daly, J.M. Thompson, E. Connor, C. Hardacre, S.K. Wilkinson, N. Sedaie Bonab, **J. ten Dam**, M.J.H. Simmons, E.H. Stitt, C. D'Agostino, J. McGregor, L.F. Gladden and J.J. Delgado, J. Catal., 2015, 330, 344-353: Effect of solvent on the hydrogenation of 4-phenyl-2-butanone over Pt based catalysts.

[11] S.K. Wilkinson, I. McManus, H. Daly, J.M. Thompson, C. Hardacre, N. Sedaie Bonab, **J. ten Dam**, M.J.H. Simmons, C. D'Agostino, J. McGregor, L.F. Gladden and E.H. Stitt, J. Catal., 2015, 330, 362-373: A kinetic analysis methodology to elucidate the roles of metal, support and solvent for the hydrogenation of 4-phenyl-2-butanone over Pt/TiO_2.

[12] K. Iisa, R.J. French, K.A. Orton, M.M. Yung, D.K. Johnson, **J. ten Dam**, M.J. Watson and M.R. Nimlos, Energy&Fuels, 2016, 30, 2144-2157: In Situ and ex Situ Catalytic Pyrolysis of Pine in a Bench-Scale Fluidized Bed Reactor System.

[13] **J. ten Dam**, A. Ramanathan, K. Djanashvili, F. Kapteijn, U. Hanefeld, RSC Adv., Submitted: Synthesis, Characterization and Performance of Bifunctional Catalysts for the Synthesis of Menthol from Citronellal.

ACKNOWLEDGEMENTS

I've thoroughly enjoyed my time in Delft. Not just the science but the social aspects as well. It has been incredible to be in such an internationally oriented environment within the Netherlands. To put it into perspective – I have got more Dutch colleagues in the UK!

Ulf, hartelijk dank voor onze wetenschappelijke discussies en je vertrouwen tijdens en na mijn tijd in Delft. Ik kan je niet genoeg bedanken voor je 'suggestie' om een tweemaandelijks rapport bij te houden tijdens mijn eerste jaar. Deze documenten hebben me enorm geholpen bij het schrijven van de appendix over NMR-titraties, door mijn geheugen wat op te frissen, nadat deze verslagen enkele jaren lagen te versloffen in de krochten van mijn harde schijf.

Freek, bedankt voor de bijdrage van je inzichten in catalysis engineering. Deze complementaire opvattingen ten opzichte van Ulf hebben menig publicatie tot een hoger niveau getild. In mijn derde jaar had ik beter naar je moeten luisteren en eens wat met Athena visual studio moeten gaan spelen. Dit zou me behoorlijk wat tijd hebben bespaard tijdens mijn eerste jaren bij Johnson Matthey.

Kristina, jouw kennis en kunde van NMR is ongekend. De boraatchemietitraties in mijn eerste jaar waren misschien niet de meest enerverende experimenten tijdens mijn promotie, maar de prettige conversaties met jou, Daniel en Joop deden dat snel vergeten.

Joop, samen met jou hebben we de NMR-experimenten tot een samenhangend geheel weten te smeden. Hartelijk dank voor het delen van je gedetailleerde kennis en je jarenlange ervaring in de boraatchemie.

Mieke, jij bent het cement van de BOC-groep. Buiten je ongelooflijke administratieve en organisatorische behendigheid, ben je altijd betrokken met alle leden van de groep. Ik vond het fijn om af en toe een update mailtje uit Delft te ontvangen. Samen met Els heb je me door de administratieve rondslomp dat een proefschrift heet weten te loodsen. Hier wil ik jullie beiden voor bedanken.

Dinesh, hartelijk dank voor je inzet tijdens je werk aan W-TUD-1. Dit heeft geleid tot hoofdstuk 3 en vormde de basis voor hoofdstuk 4.

I have had too many colleagues during my four years in Delft to mention them all. So instead, I will revisit a series of unforgettable moments. Waldorf en Statler, aka John and Sander, het 'naambordje' begon als een grap, maar jullie consultancy activiteiten waren wel degelijk nuttig. Het is fijn voor een beginnende promovendus om enkele tips en trucs uit de eerste hand mee te krijgen. Frank, Daniel and Maria – together we have perfected 'the very very very last one'. It needed repeated polishing in the oldest pub of Delft, but we have done it in the end. Broodje Leo was one of the weekly activities that brought the group together and I am proud to know that this tradition is still honoured within the team. Talking about food – Monica's baking skills and love of chocolate were unrivalled. Toby, Paul and Bart, I still think that our re-enactment

of the Reservoir Dogs was better than the original. Luigi, thank you for preparing a fantastic pizza in my kitchen. The new tenant of that place is probably still wondering where all that flour comes from. Remco, voor een verstandig man heb je verbazingwekkend weinig verstand van voetbal. De problem solving skills van Maarten hebben een labstandaard gekost, maar mijn fiets gered van de Delftse gracht. Sander en Daniela, jullie bruiloft in Rome was onvergetelijk. Het was alleen fijn geweest als ik van tevoren had geweten dat ik een van de zeven gangen beleefd af had kunnen slaan. Sometimes you need to break away from the lab and what better way to spend the sunny afternoon cycling to the beach together with Adeline and Julie? De E-cast was een goede afsluiting van de donderdag samen met de BOC en SAS-groep. Chris en Patrick, jullie hebben het concept bier en bitterballen tot een hoger niveau getild. Ik vraag me af of er nog steeds een SAS te bestellen is in Delft. Florian, I enjoyed playing Guitar Hero with you – being my colleague and neighbour also ensured that we didn't have any complaints regarding the sound.

One short word of thanks to my JM colleagues from JMTC Chilton, and Catalyst Research in particular. Even more specifically my office mates, who would not mention the completion of my thesis at every opportunity (I am looking at you Xavier).

As an extension to that, I'd like to thank Sam, Peter and Canan for being my Thesis Weekend buddies. If it did not speed up the writing, at least it has improved my cooking skills. Canan, thank you for waiting for me to finish.

Leon, bedankt voor de cover foto. Een voorbeeld van de schoonheid van Teesside, als je maar de moeite neemt om de velden en de heuvels in te trekken.

Javier, I really appreciate your offer to draw the pictures for my laymen's presentation – they are not done at the time of writing, but I am sure it will be amazing!

Sjuppe Ellef uit Meijel kan niet onvermeld blijven. Jullie zijn een geweldige vriendengroep en maken mijn weekendtripjes naar Limburg extra bijzonder. Het is fijn om af en toe mijn zinnen te verzetten en na een eerste vraag of het goed gaat met de chemie hebben we het gelukkig alweer snel over voetbal.

Thijs, je bent mijn favoriete broer. Ik geniet ervan om met jou activiteiten te ondernemen en van gedachten te wisselen over van alles en nog wat; wetenschap-gerelateerd en stukken minder hoogdravend.

Pap en Mam, bedankt voor jullie steun en interesse door de jaren heen. Jullie aanmoediging van mijn nieuwsgierigheid heeft mij aangezet tot een carrière in de chemie. Ik hou van jullie.

En tot slot Anique. Jij was onmisbaar tijdens het schrijven van mijn proefschrift. Je gaf de juiste zetjes op de juiste momenten. I love you.